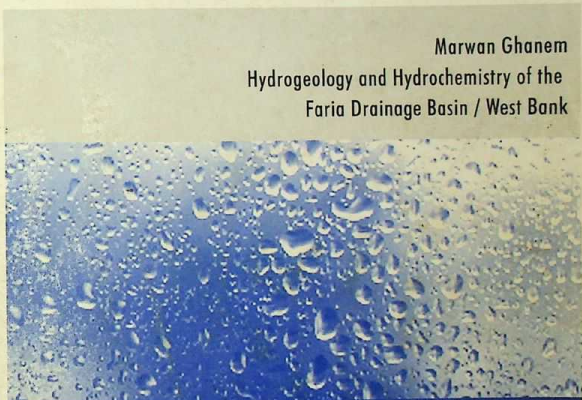Marwan Ghanem
Hydrogeology and Hydrochemistry of the
Faria Drainage Basin / West Bank

Wissenschaftliche Mitteilungen

INSTITUT FÜR GEOLOGIE

TECHNISCHE UNIVERSITÄT BERGAKADEMIE FREIBERG
Institut für Geologie

Wissenschaftliche Mitteilungen

11

Freiberg
1999

Marwan Ghanem

Hydrogeology and Hydrochemistry of the
Faria Drainage Basin / West Bank

143 Seiten, 62 Abbildungen, 26 Tabellen,
135 Literaturstellen, 32 Anlagen

To my father Ghaleb and to my mother Zuhreihe

To my wife " Naheda"

To my children " Ghaleb, Rawan, Razan and Ghandy"

ACKNOWLEDGEMENT

ABSTRACT

Hydrogeological and hydrochemical studies were conducted in the Faria drainage basin in the north eastern part of the West Bank. Stratigraphical and structural maps were compiled using the GIS software package TNT-mips in order to define the recharge zones of the aquifer system in the area. A hydrological study was conducted to determine the recharge to the groundwater. Thirty years records of precipitation, wind, humidity and surface runoff were used to determine the recharge rate in the semi-arid to arid regions. Using global and hydrometeorological groundwater-balance equations as well as the salt-balance method and a numerical model, the recharge was estimated to be about 60 million cubic meters (Mill. m^3) per year.

The aquifer system consists of a upper phreatic and a lower confined aquifers. The phreatic aquifer consists of Pleistocene, Neogene and Eocene sub-aquifers with a saturated thickness of 3 to 82.9 m; while the thickness of the lower aquifer ranges from 131 to 440 m and consists of lower and upper Cenomanian sub-aquifers. A total of three step-drawdown tests, five constant rate-pumping tests and two recovery tests were carried out to determine the hydraulic characteristics of the sub-aquifers and to evaluate their potentials. Using the methods of Jacob, Theis and recovery, transmissivities were obtained.

A hydrochemical study was conducted to define water types in the study area and to determine hydrochemical parameters of the aquifer system. More than 150 water samples were analysed within two water sampling campaigns (before and after recharge), which covered all springs and groundwater wells as well as surface waters (wadies) in the area. The physical, chemical and microbiological properties were determined. Statistical analyses of all hydrochemical elements were used to compute statistics at the 0.01 significance level using the software SPSS. Indicators for water quality were determined using salinity and soluble sodium percentage. Graphs and compositional diagrams of hydrochemical analyses were plotted to show ion distribution and water type. Hydrogeochemical modelling was used to determine distribution of species and saturation indices.

Environmental isotope analyses of ^2H, ^{18}O and ^3H were carried out in the phreatic and confined aquifers in order to determine the origin of groundwater bodies. The values of ^2H and ^{18}O are used to identify the local meteoric water line in the area.

A digital elevation model and an rainfall distribution model were constructed for the Faria basin. A 3-dimensional numerical groundwater flow model was built using the visual Modflow modelling software. The aquifer system was represented by two layers of phreatic and confined aquifers and one aquiclude. 400 runs were performed within the steady state calibration procedure. A fairly good agreement between measured and calculated heads were found.

7

TABLE OF CONTENTS   Page

8

LIST OF FIGURES

14

LIST OF TABLES

16

17

LIST OF APPENDIXES

18

LIST OF SYMBOLS

A	cross-sectional area
A_o	average runoff in the area of study(mg/liter)
AAS	atomic absorbance spectrometry
Al	Holocene
ANOVA	The analysis of variance
Ar	Argon
B	saturated thickness
Br^-	Bromide
C1, Lc1	lower Cenomanian
C2	upper Cenomanian
C3t	upper Cenomanian
Ca^{2+}	Calcium
Cd	cadmium
C_g	average chloride content of groundwater (mg/liter)
Cl^-	Chloride
cm	centimeter
C_p	average chloride content of rainwater (mg/liter)
Cu	cupper
^{14}C	carbon-14
°C	degree centigrade
DEM	digital elevation model
DO	dissolved oxygen
DTM	digital terrain model
ΔS	drawdown
δ	delta
Δv	volume of the cell
Δh	change in head over a time interval of length Δt.
$\dfrac{\delta_h}{\delta_l}$	hydraulic gradient
E	Eocene
E	east
Ea	evaporation
EC	electric conductivity
Eh	redox potential
ENE	east north eastern
ET	evapotranspiration,
ETP	potential evapotranspiration
F^-	fluoride
Fc	fecal coliform
F_d	average annual dry fallout of chloride (g/m²/year)
Fe	iron
F_{err}	distribution error
F_{tab}	tabulated distribution
G	average annual replenishment
G.S.I	geological Israeli classification

21

List of symbols

GWW	Groundwater for Windows
h	potentiometric head
HCO_3^-	Bicarbonate
hr	hour
^2H	Deuterium
^3H	Tritium
IN	israeli nomenclature
I	interception
I^-	iodine
IAP	ion active product
IS	ion strength
K	conductivity
K^{1+}	potassium or Kalium
Kcb	Bethlehem formation
Kch	Hebron formation
Kclbk	Lower Beit Kahel formation
Kcubk	Upper Beit Kahel formation
Kcy	Yatta formation
K_h	horizontal hydraulic conductivity
Kj	kilo Joule
km	kilometers
Kr	Ramali formation
K/T-C	Chalk undifferentiated formation
K/tj	Jerusalem formation
K_{sp}	solubility of product
K_x, K_y & K_z	values of hydraulic conductivity along the x, y and z coordinate axes
K_v	vertical hydraulic conductivity
L	liter
L	length of the river
Lc2	Neocomian
L &U. Ce	lower and upper Cenomanian
m	meters
M	change in soil moisture
m^3	cubic meter
Max(x)	maximum (x)
mcm	Mill. m^3
m^2/d	meter square per day
meq/L	milli equivalent pro liter
MF	membrane filter
mg	milligram
Mg^{2+}	magnesium
mg/L	milligram pro
Mill. m^3	million cubic meters
Min(x)	minimum (x)
mL	milliliter
mm	millimeters
mmol/L	millimole pro liter
Mn	manganese
mol/L	mole pro liter

22

mS	millisiemens
mV	millivolt
µg/L	microgram pro liter
µm	micrometer
µS/cm	microsemens pro centimeter
N	rainfall
N	north
Na^{1+}	sodium
NK	number of groups
NM	nanometer
NNE	north north east
NNW	north north west
NO_3^-	Nitrate
NP	Neogene - Pleistocene
NW	northwest
^{16}O	oxygen - 16
^{18}O	Oxygen - 18
P	precipitation
Pb	lead
pE	16.9 redox potential
$PO4^{3-}$	phosphate
Pt	Platinum
Q	discharge (L^3/t)
Q	natural replenishment
Qha	Alluvium formation
Qhg	Gravels and fans formation
Q_i	a flow rate into the cell
Q+N	Quaternary and Neogene sub-aquifers
Qpl, QpII	Lisan formation
R	Albian
R	storm water runoff,
R	water crop (runoff & replenishment)
R	recharge
R	resistivity
r	correlation coefficient
R_g	replenishment
RMS	square root of the standard deviations
R_x	isotopic ratio $^{18}O / ^{16}O$ or $^2H/ ^1H$ in the substance x
R_s	runoff
S	Senonian
S	south
S	storativity
S_0	specific storage coefficient
S_s	specific storativity
S_s	specific storage of a porous material
S_s	specific storage in the finite difference formulation
SD	standard deviations
SE	southeast
sec	second

List of symbols

SI	saturation indices
SiO_2	Silica
s.l.	sea level
SMOW	Standard Mean Ocean Water
SO_4^2	Sulfate
SSW	south south west
s.w.l.	static water level
Sy	specific yield
T	transmissivity,
t	Turonian
t	time.
Tc	Total coliform
T (°C)	temperature
TDI	total dissolved ions
TDS	total dissolved solids
Te-L	Bedded Limestone formation
Te-Lc	Limestone with chalk formation
Te-Lu	Undifferentiated Limestone with chalk formation
Te-Cl	Chalk with limestone and chert formation
Te-c/l	chalk with nummulitic limestone formation
Te-l/c	nummelitic limestone with chalk formation
Te-lr	reef limestone formation
TH	total hardness
Tpb	Beida formation
TU	tritium unit
UTM	Universal Mercator Transverse
UV	ultraviolet
W	west
W	wide of the river
w	a volumetric flux per unit
WSERU	water and Soil Environmental Research Unit
WSW	west south western
y	year
Zn	zinc
< d.t	lower than detection limit
$^0/_{00}$	promille
%	percent

24

1 INTRODUCTION

Water resources in the West Bank (Fig.1.1) are scarce. This is due to the fact that the West bank as well as the Jordan river basin are lying within an arid region. Groundwater is considered to be the main fresh water resource in the West Bank. There are three main aquifers in the West Bank, i.e. the northeastern, the western and eastern (Fig.1.2).

1.1 Geography

The area of the study is the Faria drainage basin which is situated in the northeastern part of the West Bank (Fig. 1.2). It lies within the eastern aquifers and it has an area of 320 km². It lies within the following coordinates:

Latitude   (Y0, Y1) national 160000 - 195000 m N (international 32° 2` - 32° 12`N)
Longitude (X0, X1) national 175000 - 200000 m E (international 35° 12`- 35° 35` E)

The Faria drainage basin borders to the: North Jordan and Fassayel - Auja drainage basins from the north and south respectively, Alexander, Yarkon and Hadera drainage basins from the west and the Jordan river from the east (Fig 1.3). The western boundary of the study area lies at the main watershed between the Mediterranean and the Jordan river. It lies on the eastern flank of Judean anticline, between the Nablus city and the Jordan valley. The eastern part of the basin lies within the Jordan Rift, which is the major structure in the area. The study area rises to 704 m (above sea level) in the western parts and drops gradually to -320 m (below sea level) in the Jordan Rift valley. Geographically, it lies in the Nablus District, where twenty Arabian villages are located within this region with about 90000 inhabitants. The major town is Tubas with 20000 inhabitants. The inhabitants in the area represent 10% of the total population of the West Bank. Five Israeli settlements Elon More, Baracha, Ireet, Hamra and Itmar were built in the area after 1967. Faria basin could be subdivided according to the north national coordinates (Y) into Lower (from 160000 to 176000m N), Middle (176000m to 184000 m N) and Upper (from 184000 to 190000 m N) Faria.

1.2 Geomorphology

In general, the West Bank is divided into two main topographic units: a hilly region in the western and the Jordan Rift valley in the eastern parts. The study area is subdivided into three physiographic regions: the mountain regions in the west and the hills of the Judean desert in the middle and Jordan Rift in the east. The basin of Faria is like a fan with a length of 36 km and an area of 320 square km. This basin is named after Wadi El Faria, which is located within the area and crosses the area from the NW to SE. This Wadi Faria starts from the eastern sides of Dier Al Hateb village towards western and turned to the north and then northeastern forming a funnel shape named Wadi Al Bathan. It reaches after three kilometers Wadi El Malaki which is carrying the wastewater of the Nablus city as well as the settlements and mixes with the water of Faria springs, keeping the name Wadi El Faria till Jiftlik village. After that, it has the name of Wadi El Jawzeli in Faria graben and then Wadi Karantine and passes a path parallel to Jordan river for a long of 7 km before reaching the Jordan river at an altitude of - 320 m below sea level (ABU SAFAT 1990). Along this Wadi, many river terraces

25
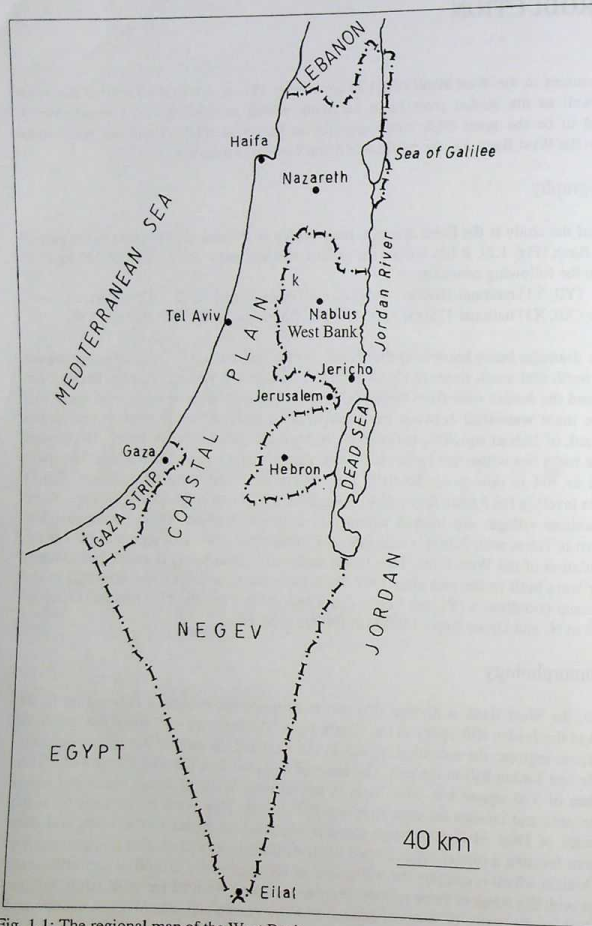
Fig. 1.1: The regional map of the West Bank .

are formed; they are narrow in the middle part and wide in the lower part. In the lower part it is difficult to differentiate between the terraces because of the large scale interaction between them (ABU SAFAT 1990). The overall slope of the eastern parts are of three times steeper than that of as in the western parts (SHWARTZ 1980). Eastwards, the runoff has cut steeply the sides of the Wadies from the mountain region to the Jordan valley. All Wadies and streams drain eastwards and are seasonal; they are considered as a part of the greater Jordan river drainage basins. Appendix 1.1 shows the drainage pattern of the Faria basin computed using GIS software package TNT – mips.
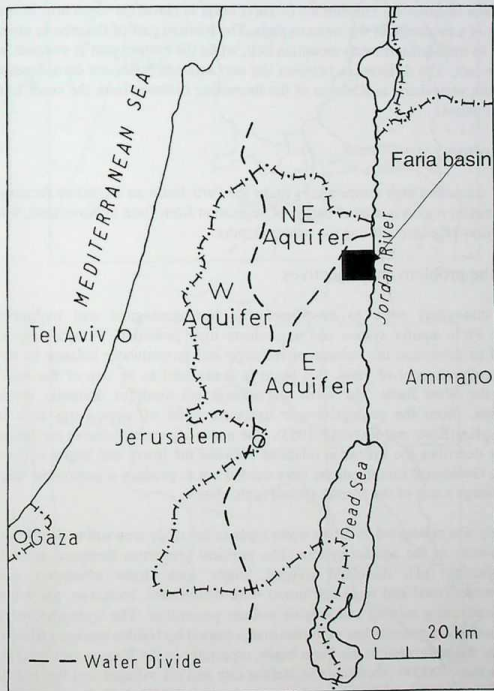
Fig. 1.2: The major groundwater basins of the West Bank and the location map
     of the study area.

1.3 Climate

Climatologically, the West Bank is part of the subtropical zone, which has two climate seasons with a short period of transition: the warm and dry season (summer) and the cool and wet season (winter). The climate of the West Bank constitutes a transition region from subtropical arid (south) to subtropical wet (north). The western slopes have an annual rainfall of 500 - 700 mm per year and the eastern slopes 100 - 500 mm per year. The rainy season is winter, occurring from November to May with a maximum rainfall in January. There is an abundance of sunshine with an average radiation of 5000 to 7500 kJ per square meter every day on a horizontal area in summer. The climate of Faria basin is classified as an arid in the eastern parts; while it is a moderate in the western parts. The western part of the area is more elevated and belongs to the Mediterranean mountain belt, while the eastern part is situated in the rift valley climate belt. The differences between the two adjacent zones are considerable and their transitions are very sharp as a reason of the increasing distance from the coast line within an orographic control.

1.4 Soil and agriculture

Fertile soil, plenty of water and high temperatures make the Faria basin an important farming area. The Judean mountain region is almost barren of vegetation from June to November, but is covered by a thin grass vegetation during the winter months.

1.5 Statement of the problem and objectives

The objectives of this study were to investigate the hydrogeological and hydraulic characteristics of the Faria aquifer system and to evaluate their potentials. A hydrological study was conducted to determine the volume of recharge and groundwater balance in the basin. From the agricultural point of view, this basin is considered to be one of the most important basins in the West Bank. The wells and springs are used for domestic water supplies and irrigation. From the geological and structural point of view Faria area is considered to be complex (ROFE and RAFFETY 1963). The major structural features are faults and folds. This study describes the hydraulic relations between the lower and upper aquifer systems in this basin. Geological investigations were carried out to produce a geological map in order to define recharge zones of the aquifer system in this basin.

A hydrochemical study was conducted to define water types in the study area and to determine hydrochemical parameters of the aquifer system. The physical properties (temperature and EC), chemical properties (pH, dissolved oxygen, major ions, trace elements) and microbiological properties (total and fecal coliforms) were determined. Indicators for water quality were determined using salinity and soluble sodium percentage. The hydrochemistry part of the study evaluates the groundwater pollution that is caused by Nablus sewage effluent, which is pumped over the watershed in the Faria basin, especially in the Eocene sub-aquifer. The effluent of more than 200000 inhabitants in Nablus city and it's villages and the Israeli settlements mixes with the water of Faria and Badan springs in the Wadi Faria area. More than 27 wells of Eocene formations are affected by this sewage. The owners of more than 70 wells in the Faria basin will benefit from this study. The study covers water management and planning (including groundwater modeling) of the Faria basin.

28
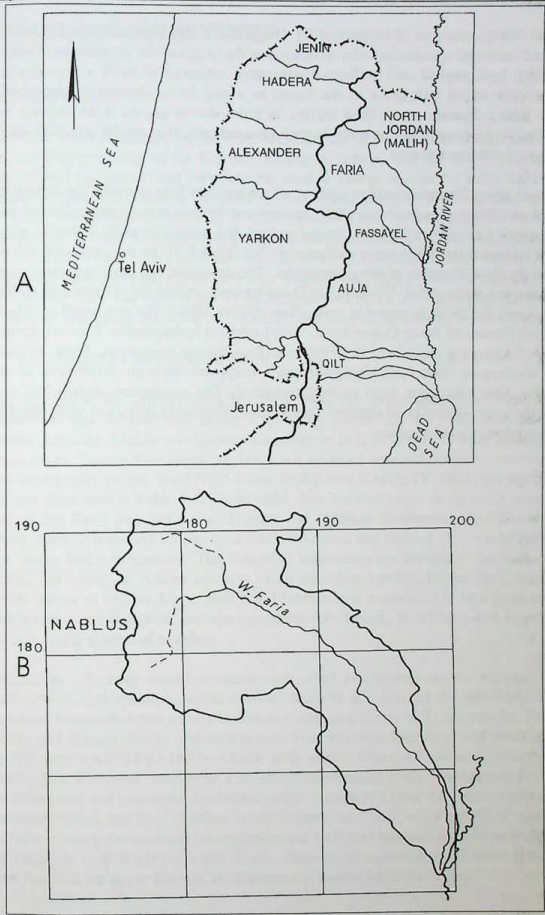
Fig. 1.3: The major drainage basins in the West Bank (A) and the Faria basin (B).

29

Environmental isotope analyses of Deuterium ^{2}H, Oxygen - 18 and Tritium ^{3}H were done for the phreatic and confined aquifers in order to determine the origin of the groundwater bodies. Hydrogeological, hydrological and geological data were collected to build a groundwater model for the area which will serve in the future as a tool for examining hydrogeologic operation and their influence on the flow regime. In order also to get the water balance for steady state (before production in this basin began) a groundwater flow model was built using Visual Modflow modeling software.

Pumping tests of about 20 representative wells to all sub aquifers help to define the storativity of these aquifers. Water samples from wells, springs and surface water were collected and analysed chemically (major cations and major anions and trace elements). Twenty water samples were collected for the isotopic analyses of ^{18}O, ^{2}H and ^{3}H to determine the age of this water and the flow direction of the groundwater. The directions and rates of groundwater flow were measured through ^{3}H, ^{18}O and ^{2}H. These isotopes, especially ^{3}H serve as tracers and could be used for defining regional water flow (TODD 1980). The sub-aquifers, which their range from Eocene to lower Cenomanian, were identified hydraulically. Thirteen springs were recorded discharging in the area from recent to Cenomanian formations. Some of these springs are discharging from one formation and disappears through infiltration to be discharged after few kilometers from another formation. The occurrence, distribution and movement of the groundwater in all aquifers were studied. This study defines as well, whether leakage from other basins takes place.

2 GEOLOGICAL SETTING

2.1 Introduction

The West Bank is situated on the north-western side of the Arabian shield. Depending upon the sea floor spreading of the Red sea, geologists believe, that the Afro Arabian Shield has been drifted northwards and narrowed the ancient Tethys sea. At the same time the Arabian Shield became detached from the great African Shield along the line Red Sea - Gulf of Suez. A strike - slip fault occurred at a line Aqaba - Dead Sea- Jordan Rift and continued northwards in Syria, Lebanon and Turkey. Geological studies in the area date back to 1880 (TRISTRAM 1865; LARTET 1869; HULL 1889; BLANCKENHORN 1896). A geological map was published of the region on a large scale by PICARD (1928). Geological mapping on a 1: 20 000 scale was carried out by ROFE and RAFFETY (1963). Appendix 2.1 shows the geological map of the West Bank after ROFE and RAFFETY (1965).

2.1.1 Stratigraphy of the West Bank

The majority of the formations in the West Bank are composed of carbonate sediments of Cretaceous age. Jurassic and Lower Cretaceous formations are located at the core of the Judean Anticline. Middle and Upper Cretaceous as well as Lower Tertiary forming Ajlun and Belqa series. Eocene formations are Jenin sub series of nummulitic reef limestone and chalk. The stratigraphy of the West Bank (after ROFE and RAFFETY 1963) are described below and are illustrated in Table 2.1. Rocks older than Jurassic occur in an small area, only in the east of the Dead Sea and are of Triassic age (Nubian Sandstone) (ROFE and RAFFETY 1965). Jurassic rocks are limestone of 242m thickness and divided into two formations: Lower and Upper Malih formations. The following formations are located in the Cretaceous rocks: Ramali formation of Albian age acts as an excellent aquifer, Lower Beit Kahil formation which acts as an aquifer, Upper Beit Kahil formation is considered to be a good aquifer, Yatta which acts as an aquiclude and the formations of Hebron, Bethlehem and Jerusalem, which act as a united system of aquifers.

Cretaceous - Tertiary transition chalk with chert are located on the western limb of the Nablus-Beit Qad syncline, while narrow outcrops are located on the flank of the Faria anticline. Jenin sub-series covers Senonian chalks and cherts of Tertiary rocks, Paleocene soft chalks and Eocene chalks and limestones. Five different limestone and chalk are recorded (ROFE and RAFFETY, 1965): Chalk with minor Chert, Chalk with minor interbedded Nummulitic limestone, limestone with minor interbedded chalk, bedded massive nummulitic limestone and reef limestone. Quaternary rocks consist of Lisan, Alluvium, Outwash Fans and Piedmont Cones and Nari (Surface crust) formations. There was a period of relatively minor volcanic activity documented by agglomerates, tuffs and basaltic lava. Some small exposures are found in both Wadi Faria and Malih. Four minor occurrences of basic lava flows have been found in the upper Hebron, Bethlehem and Lower Jerusalem.

Table 2.1: The classifications of geological formations of the West Bank and the hydrogeological connections in formation terms of ROFE and RAFFETY (1965) and the corresponding Israelian classifications (G.S.I. 1996).

Geological time scale			group		formation terminology		lithology	thickness range (m)	aquifer potentiality
Era	System	Epoch	Roff & Raffety	G.S.I.	Roff & Raffety	G.S.I.			
Cenozoic	Quaternary	Holocene	Recent	Kurkar	Alluvium	Alluvium,soil & sand dunes	marl, alluvium gravel	variable	good aquifer
					Gravels &fans	River gravels			
		Pleistocene	Lisan	Dead Sea	Lisan	Lisan	laminated marl and gypsum	200+	good with soluble mineral content
	Tertiary Neogene	Pliocene Miocene	Beida	Saqiye	Beida	Conglomerate Bit Mir, Zig lag rocks	conglomerate	200+	good aquifer
	Paleogene	Middle Miocene - Paleocene	Belqa	Jenin sub Series	Avedat — Reef limestone, Numulitic limestone with chalk, chalk with numulitic limestone	Reef Limestone Zora, Numulitic limestone Zora, Numulitic limestone with chalk - Taqiya, chalk with numulitic - Gareeb	Reef limestone, bedded limestone, chalk with limestone undifferentiated	0 - 100 / 15 - 200 / 0 - 170 / 0 - 125 (0470m)	aquifer in limestone zones and aquiclude in chalk zones
Mesozoic		Senonian Campanian		Mt. Scoups	chalk	Mishash	chalk	0 - 450	leaky aquifer
		Santonian			chert	Menula	chert	0 - 40	
		Turonian			Jerusalem	Bin'a	Limestone and dolomite	50 - 110	good aquifer
		Cenomanian Upper	Judea	Judea	Bethlehem	Weradim	dolomitic lime - stone, dolomite	30 -115	good aquifer
						Kefar Sha'ul	chalk		poor aquifer
		middle			Hebron	Aminadav	l.s, dolomite, chert, chalk	105-260	Excellent aquifer
	Cretaceous	lower			Yatta	Moza Marl Beit Meir	dolomitic limestone, marl chalky	50-150	leaky aquifer
					Upper Beit kahil	Dolomite Kesalon	interbedded limestone, marl and chalk	110-190	very good aquifer
		lower				Soreq	interbedded limestone,dolo-mite and chalky limestone		
					Lower Beit Kahil	Giva't Ye'arim	limestone	250-290	aquifer
		Albian				Kefirah	shale, interbedded chalky limestone		aquiclude
		Neocomian-Albian	Kurnab	Kurnov	Ramali	Qatana Ein Kenvah	sandstone, sandy limestone	260-290	aquiclude aquifer
	Jurassic	Bajocian - Bathonian	Zerqa		Upper Malih	Tamon	marl, chalky limestone and marl	190	leaky aquifer
					Lower Malih		limestone, oolitic limestone	55	good aquifer
						Igneous	basic igneous	variable	

2.1.3 Geological structure of the West Bank

2.1.3 Geological structure of the West Bank

The West Bank is tectonically variable with the dominant fold, the Faria anticline. The flanks of this structure are complicated by minor folds in parallel and at right angles. The Nablus Beit Qad syncline and the Faria anticline together with the Jordan Rift are the dominating structures in the West Bank. Nearly all folds have a general strike of 5 - 30 degree E and are usually asymmetrical. The steeper southeast flank may become vertical or change into a fault. Figure 2.1 shows the tectonic map (fault pattern) of the West Bank after ROFE and RAFFETY (1965). Two major folds in the West Bank are Ein Qinya (southwest) and Faria (northeast) which are termed Judean Anticline. The major folds in the northern West Bank are Anabta Anticline, Faria Anticline, Nablus - Beit Qad Syncline, Ein Quiniya anticline and Ein Samia Syncline. In the western sides of the West Bank the Rujeib monocline, which lies along Jerusalem - Nablus road becomes more steeper in the north while in the eastern sides Ein Fara- Fassyil monocline (in the northern of Wadi Faria named Khalit Es Samra monocline) it becomes less steeper.

The northern end of Judean anticline is broken by a large number of faults trending NW-SE. The main depressed areas, boarded by complex fault system, are the Faria, Tubas and Tayasir Grabens. Many faults trending N-S, swinging 90 degree and becoming WSW-ENE. The NW-SE block faults occur in the east through Eocene formations and forming the strongest set of faults, the Bardala group, which swings northwest from the Rift compared to Faria graben. The majority of them are normal faults and most of them are dipping close to the vertical.

Joints are often up to one meter wide at the surface and filled with soil in some cases (ROFE and RAFFETY 1965). Some joints are due to competency of individual beds within a formation. Dolomitization has associated with well developed joints in the dolomite and limestone rocks (PETTIJOHN 1956). Certain formations are highly jointed like Jerusalem, Hebron, Yatta and Bethlehem. The limestone are of low primary porosity and all the joints are important to provide for water movement to the development of solution channels (karstification).

2.2 Geology of the Faria drainage basin

2.2.1 Introduction

A sequence of sedimentary and volcanic rocks of Jurassic to recent age outcrops at the core and along the flanks of the Faria anticline in eastern West Bank. This area is of a special interest because a series of unconformable contacts occur over an extremely short distance within the Upper Cretaceous - Upper Tertiary sequence associated with sharp facies and thickness changes. Geological studies in the study area date back to ROFE and RAFFETY (1963). SHALIV (1972) mapped geologically part of the area, along the Wadi El Faria of a scale 1: 20000. A geological map of the region, including the southern part of the Faria basin was published by the geological Survey of Israel (1996) at a scale of 1: 100000 (southern Shomeron).
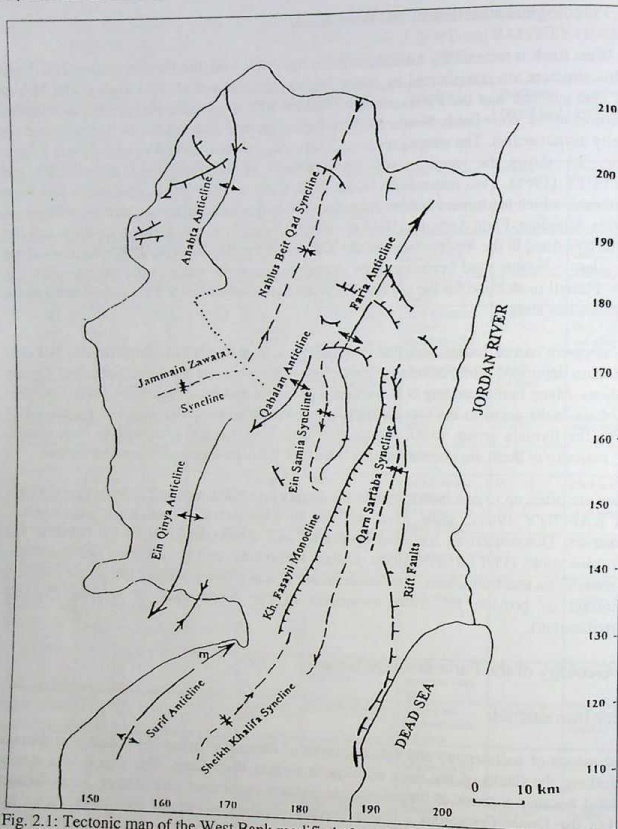
Fig. 2.1: Tectonic map of the West Bank modified after ROFE and RAFFETY (1965).

A geologic map of the area was drawn in terms of formations named after ROFE and RAFFETY (Appendix 2.2). This geological map was drawn as a mosaic map from 4 maps of a scale at 1: 50 000. Geological fieldwork during the water sampling campaign was carried out to check and correct some formations. It was scanned and treated with TNT mips GIS software.

34

2.2.2 Stratigraphy

The majority of the rocks are composed of limestone and dolomite. A composite columnar section in the area of study modified after SHALIV (1972) is illustrated in Fig. 2.2.

2.2.2.1 Cretaceous rocks

The formations outcropping along the Faria anticline are of Cretaceous age. Strata of Cenomanian and Turonian age mainly dolomite and limestone predominate in the Judean mountains. Senonian chalks and flints form most of the eastern part of the area. The western parts are confined to a narrow strip near to the flexure zone. The rock sequence, that is exposed in the Faria anticline was deposited throughout a shallow shelf of a warm sea, and consist essentially of carbonates.

2.2.2.1.1 Kurnub (Kurnov) group

The Ramali formation (kr), the only one in the Kurnub group, is composed of ferrugineous, mainly unconsolidated, brown to white and bedded sandstone. It's thickness is 220m and it is an excellent aquifer. It is equivalent to Aptian age and from the Israeli nomenclature (IN) it is equivalent to Qatana (70-80m), Ein Kenvah and Tammun formations.

2.2.2.1.2 Ajlun (Judea) group

The Lower Beit Kahil formation (kclbk) is defined in an lower and upper part. The upper part consists of thick bedded limestone and marly limestone with shales. In some places limestones are dolomitic and karstic; while in the lower part it is interbedded with chalky limestones and yellow shale. It's main outcrops is in the north of Faria anticlinal axes. It represents the lower Cenomanian of the world stratigraphy. According to Israeli classifications, this formation consist of four formations Ein Qinya (50m), Kefira (100-120m) and Giv'at Ye'arim - dolomite (65-90m).

The Upper Beit Kahil formation (kcubk) represents the lower part of Cenomanian, the northern outcrops are on the deeply eroded flanks of the Faria anticline. It's thickness ranges from 65 to 145m and it is composed of well bedded chalky limestone and dolomite with clastic massive limestone. Dolomite is massive, blocky and weathered with fine chert. Chalky limestones are thin bedded with thin laminated marl. This formation represents Soreq and Kesalon formations (IN). It is a well fractured aquifer. The Yatta formation (kcy) is related to the lower part of the middle Cenomanian and is composed of thin interbedded limestone, marl and chalky limestone and thin bedded, laminated dolomite. It represents Bet Meir (40 - 80m) and Moza marl (0-9m) (IN). This formation acts as an aquiclude.

The Hebron formation (kch) represents the upper part of the middle Cenomanian and equivalent to Amminadav formation (IN). The thickness ranges from 110 to 130m and is composed of dolomite and limestone.

SERIES	STAGE	LITHOSTRATIGRAPHY	LITHOLOGY
HOLOCENE		Alluvium	
NEOGENE		Neogene - Pleistocene	
	EOCENE	Eocene Formations	
SENON-PALEOC.		Mt. Scopus Group	
UPPER CRETACEOUS	TURONIAN	Nezer Fm.	
		Shivta Fm.	
		Derorim Fm.	
		Weradim Fm.	
	CENOMANIAN	Kefar Shaul Fm.	
		Amminadav Fm.	
		Moza Fm.	
		Bet Meir Fm.	
		Keslan Fm.	
		Soreq Fm.	
		Giv'aT Yearim Dol.	
		Kefira Fm.	
LOWER CRETACEOUS	ALBIAN	Qatana Fm.	
		Ein-Qinya Fm.	
		Tammun Fm.	
	APTIAN	Ein-El-Assab Lst.	
		Mabi Sa'id Fm.	
	NEOCOMIAN	Matira Fm.	
		Tayasir Volcanics	

Legend:
- Alluvium
- Conglomerate
- Shales
- Dolomite (Brecciated)
- Dolomite (Crystline)
- Quartzolite
- Flint (Bedded)
- Flint (Brecciated)
- Flint (Concre. Tabular)
- Dolomite (Fine cryst.)
- Calcareous Dolomite
- Marly Limestone
- Marl
- Limestone (fine Cryst.)
- Sandstone (cross bedded)
- Shales & Tuff
- Basalt
- Unconformity

Fig. 2.2: Composite columnar section modified after SHALIV (1972).

The dolomite is brown, weathered, thin bedded and brecciated at the base. It consists of coarsely or poorly bedded, non-fossiliferous, hard dolomite and limestone. In the western part

36

of Faria anticline and in the northeastern of Tubas, the outcrops of high altitude in a relatively high rain fall area, exhibit weathering characteristics. The majority of the rocks have undergone karstification, thus being a good aquifer.

The Bethlehem formation (kcb) is equivalent to the upper Cenomanian with a thickness of 30-100m. It is composed of recrystalised, dolomitised limestone and dolomite with calcitic bands. Dolomites are brown, weathered with cream marl. It is well jointed and equivalent to Kefar Sha'ul or Avnon (lower) from the Israeli classifications, which consists of well bedded and finely crystalline dolomite. The upper part is Veradim (IN) and consists of well bedded hard dolomite and limestone. It is considered to be an aquifer .

The Jerusalem formation (ktj) is composed of bedded - massive limestone and marl and is considered to be a good aquifer. The upper part is composed of limestone, which is rich of macrofossils and of 30-60m thickness, while the lower part is composed of marly limestone of 20 - 30m thickness. It represents Turonian and it consists of three formations (IN): Derorim, Shivta and Nezar (Bin'a formation). The Derorim formation consists of yellow, red or grey thin bedded limestone and chalk with some Chert concretions. The Shiva Formation consists of limestone and dolomite and forms a typical cliff morphology. Nezar formation consists of limestone, dolomite, marl and some chert. The three formations Hebron, Bethlehem and Jerusalem are connected hydraulically.

2.2.2.2 Cretaceous - Tertiary transition chalk with chert
2.2.2.2.1 Belqa series (Mount Scoups)

Chert formation (k/t-c) has a Santonian age and represents Menuha (IN). It has a thickness of 25-82m. The chert is brown to orange, weathered , tabular - nodular with interbedded chalk. Chalk formation (ct) represents Santonian- Campanian (Senonian) from world stratigraphy and Mishash (IN). Chalk is the predominant rock with a maximum thickness of 30m and it is massive, bedded in the lower part, soft and unbedded in the upper part. A 30 meter thick phosphatic layer along 15km in the direction N-S of this formation is subdivided into lower calcitic dolomitic phosphatic rock, an intermediate dolomite limestone and upper nodular phosphorite (MIMRAN 1984).

2.2.2.3 Tertiary Rocks

The series of this age named Jenin subseries (Avedat formation IN) and cover Senonian chalks and cherts, Palaeocene soft chalks and Eocene chalks and limestones of 100 -180m thickness. Four different limestones and chalks formations are found in the area:
1- Chalk with nummulitic limestone (Te-c/l): Chalk is cream, white, soft and weathered with iron staining. The nummulitic limestone is bituminous.
2- Nummulitic limestone with chalk (Te-l/c): Limestones are thin bedded, pink with chalk and marl intercalation.
3- Nummulitic bedded limestone (Te-L): The nummulitic limestone is thick and thin bedded, weathered and karstified.
4- Reef limestone (Te-lr): The limestone is unbedded and weathered.

They represent Gareb for the fourth, Taqiya for the third and Zora formations for the first and the second subformations (IN). Jenin subseries form good aquifers, but in some areas, where a

large thickness of marl act as an aquiclude.

2.2.2.4 Tertiary - Quaternary (Neogene) rocks

The Beida (Saqiye) group consists of Beida formation (Tpb). A coarse and immature conglomerate is the major constituent of this formation. It represents Miocene - Pliocene from the world stratigraphy and equivalent to Samra formation (IN). Lisan (Dead Sea) group consists of Lisan formation (QpII). Evaporate, weathered marl with grey colour, gypsum and thin limestones are the constituents of this formation. It's thickness is about 50m and is composed of laminated chalk, gypsum, and clay with some sandstones. Recent (Kerker) group consists of Gravel and fans (Qhg) and Alluvium formations. The gravel and fans is composed of unconsolidated gravel and conglomerate of variable thickness. The Alluvium (Qha) consists of unconsolidated sand, marl and gravel.

In the northern neighbouring catchment Bet Shean area, K-Ar dating indicate an establishment of a six stage model of the geological history of the area (MIMRAN 1969). In Wadi Faria thin basaltic layers are interbedded with ferrous sandstone in the lower part of Ramali formation. There are two separated masses of igneous materials phonolites and basalts with agglomerates and tuffs (BLAKE 1939).

2.2.2.5 The area of formations

According to the geological map of the study area, the area of each formation and the corresponding area (relative to the total area of Faria basin) were estimated using TNT-mips. Results are shown Table 2.2. The Eocene outcrops covers 78 km^2 and represent 23% of the Faria basin, while the Pleistocene and Quaternary outcrops equal 75 km^2 and represent 22% of the basin. The Senonian outcrops represent 10% of the area. The upper and lower Cenomanian cover an area of 154 Km^2 and represent 36% of the Faria basin.

2.2.3 Karstification

The dominance of carbonate rocks in the West Bank suggests the possible existence of karst caves. Fractures and karsts are common in Eocene and Cretaceous limestone and dolomites in the West Bank (ARKIN 1980). The development of karstification begins after the percolation of rainfall down along the fractures and dissociation and displacement of carbonate materials due to enriched CO_2- contents. The system of interconnecting cavities are enlarged through repetition of this process. The upper erosion surface in the area is heavily karstified in the vadose zone and on the surface. Higher solution rates in the elevated areas keep the erosion surface relatively flat (FRUMKIN 1992).

The erosion surface is developed since Oligocene regression and the Pleistocene uplift (FRUMKIN 1992). The Judean karst erosion surface have started to develop during the Upper Eocene and Oligocene (PICARD 1943). Karst features on the crests of the western hills indicate that at the beginning of the Pleistocene uplift, the Judean erosion surface actively karstified (ARKIN 1980). The extreme ranges in rainfall and temperature influence the solubility of carbonate rocks (ARKIN 1980). The Ajlun group rocks have the characteristics of a mature karst system. Karst terraces are caused by mass dissolution of calcite with associated collapse structures within limestone and dolomite rocks. Huge caverns are

38

observed in the Hebron formation with a few sink holes after a heavily period of rainfall. The present development of karst is immature in some places (ROFE and RAFFETY 1965). Shallow and deeper karst were recognised at depths of 3 - 5 m from the surface (ARKIN 1980). Karst development is recognized along the fracture plane surface forming solution rills that become cavities at depth.

Table 2.2: The area of each geological formation and its percentage.

Formation name	symbol	area (km²)	percentage
Alluvium	Qha	54.0	0.16
Gravels and fans	Qhg	2.5	0.01
Lisan	Qpl	3.6	0.01
Beida	Tpb	14.3	0.04
Bedded Limestone	Te-L	8.0	0.02
Limestone with chalk	Te-Lc	26.0	0.08
Undifferentiated Limestone with chalk	Te-Lu	44.5	0.13
Chalk with limestone and chert	Te-Cl	7.2	0.02
Chalk undifferentiated	K/T-C	26.0	0.08
Jerusalem	Ktj	19.1	0.06
Bethlehem	Kcb	12.1	0.04
Hebron	Kch	65.2	0.19
Yatta	Kcy	21.3	0.06
Lower Beit Kahel	Kclbk	18.2	0.05
Upper Beit Kahel	Kcubk	11.4	0.03
Ramali	Kr	6.7	0.02
Total area		339.9	1.00

2.2.4 Structure and tectonics

The area is characterised by intensive fault systems in a general E-W direction. This fault system creates grabens, horsts and step structures. These faults varies from a few meters to 100 -150 m (GUTTMAN 1995). The main elements which control the geological structure and the flow regime are the anticlinic and synclinic structures which transverse the entire study. The main structural elements are the Jordan Rift valley and Faria anticline. Appendix 2.3 shows the structural map of the area of a scale at 1: 50 000 modified after ROFE and RAFFETY (1965). This map is drawn from 4 structural map sheets of the area and treated with TNT-mips programme.

2.2.4.1 Jordan Rift Valley

The Jordan Rift valley extends for 420 km in a general north south direction, from the southern shores of lake Tiberias (-212m below sea level) to the top of the Gulf of Aqaba (BURDON 1959). It is largely covered by chalky, fine laminated sediments of the Upper Pleistocene brackish Lisan lake (Lisan formation). The base of the valley is composed of marl layers and silt. It has two terraces: Zhor and Ghor. The Jordan valley is part of the Syrio - African Rift valley. In the Neogene and early Pleistocene it was a plateau connecting lake Tiberias with the Dead sea. The base of the valley is composed of saline marls of lacustrine deposits with sand and gravel. The Dead sea rift is the transform plate boundary between the Arabian plate and Sinai block of the African plate. Motion along this transform is thought to

have started in the Middle Miocene, with the end of the main opening phase of the Gulf of Suiz (STECKLER et al. 1988; SHALIV, 1989). The instantaneous rate of motion along the transform is about 0.6 cm/ year (JOFFE and GARFUNKEI 1989). The Dead Sea transform is a left lateral system of faults. A mathematical model of the evolution of the Dead Sea rift suggests that the rift was created as a result of the propagation of two fracture zones at its northern and southern ends toward each other (LYAKHOVSKY ET AL. 1994).

Seismic reflection data show few of the main tectonic characteristics of the Dead sea rift in the Jericho area, in the south of the study area. This study indicated, that the main fault zone dips to the west called strike slip nature (ROTSTEIN et al. 1991). A satellite imagery was used for detecting the active faults and for a digital seismotectonic map in Carmel - Wadi Faria by ABOU KARAKI (1985). There is a recent seismic activity along the transform boundary itself (ABOU KARAKI 1985).

2.2.4.2 Faria anticline

The Faria anticline begins as a minor flexure in the south, then trends to NNW along 10 km (grid N160) and swings to the east to become NNE. The amplitude increases northerly to be symmetrical. It's eastern and western limbs are very steep. It descends and is buried in the Jordan valley. It is cutted by fracture systems perpendicular to the anticline axis, which form horsts and grabens in the Faria valley. The NE - trending anticline is crossed by several major NW - trending faults which form a series of horsts and grabens (BAER et al. 1993). The tilting of the SE-flank of Faria anticline occurred in four stages (MIMRAN 1984). These stages are latest Turonian - early Santonian, late early Eocene, middle Eocene - Pliocene and late Neogene. The oldest faulting stage dates back to the early Cretaceous and is suggested to be associated with volcanic activity in Wadi Malih (MIMRAN 1972). Paleomagnetic techniques and structural studies have indicated that the block rotation of Faria anticline is a none changing stress field and it is stable. This rotation could explain the development of the Bet She'an valley in the north of the study area (BAER et al. 1993).

2.2.4.3 Fractures

The fractures in the study area fall into three main groups: straight, undulating and irregular. The most common trend is NNE to SSW with some irregular fractures showing N-S trend. The irregular fractures are open and show karstic fratures such as solution rills, calcite deposits and soil staining (ARKIN 1980).

3 HYDROLOGY

3.1 Introduction

The hydrological studies were undertaken to determine the recharge to the aquifers, together with other factors that control it. The hydrological parameters rainfall, wind, solar energy, humidity, soil moisture, runoff and discharge are analysed to get a feeling about the hydrological situation in the Faria basin. The major drainage in the West Bank is either eastwards to the Jordan valley and the Dead Sea or westwards to the Mediterranean sea (Fig.1.3). Faria basin lies within the eastern drainage basin.

3.2 Rainfall in the West Bank

The West Bank has a mediterranean type climate. In winter, the predominately low pressure area of the Mediterranean centered between two air masses, the north Atlantic high pressure of north Africa and the Euro-Asian winter high pressure located over Russia, is the primary cause of winter weather in the West Bank (HUSARY et al. 1995). The steep gradient of the Jordan valley produces an effect which reduces the quantity of rainfall in the Jordan Rift area. Rainfall however is the source of the water resources of the West Bank (SCHWARTZ 1980) and the only input parameter in the water budget of the West Bank. This rainfall infiltrates to the subsurface and recharges aquifers which feed the largest springs in the West Bank. It rains in the winter months (November till May) followed by completely dry summer months. Rainfall decreases dramatically from north to south and from west to east. The long term average period from 1931 to 1996 is illustrated in an isohyet map (Fig. 3.1) modified after RABI et al. (1996). The highest rainfall average of 700 mm/year occurs in the locations of high elevations (around Nablus city); the western slopes have an average of 500 - 600 mm/year. The eastern slopes have an average range from 450 to 150 mm/year around Jericho and the average rainfall amounts are decreasing sharply to the east, reflecting the very steep gradient. The total amount of rainfall showed variable ranges from 87.5 million cubic meters (Mill. m³) in the year 88/89 to 153.4 Mill. m³ in the year 91/92 (GTZ 1995).

3.2.1 Rainfall in Faria basin

The historical records of rainfall in the Faria basin are taken from the stations of Beit Dajan, Faria agricultural, Faria police, Toubas, Nablus, Meithlun and Talluza (Table 3.1). Rainfall data for the Faria basin are accessible for these seven stations in the following form: daily data for Beit Dajan, Toubas and Talluza stations; monthly data for the Faria agricultural, Nablus & Meithlun stations and annual data for Faria police, Faria agricultural and Beit Dajan stations (Table 3.2). Precipitation in the Faria area decreases from the west to the east (Fig. 3.2). This is most apparent in the northwestern part of the study area, where the topographic gradient is huge. From the yearly average of 600 mm rainfall in Nablus - Talluza areas, precipitation decreases to an average of 300 to 400 mm in Tammun area, and it is between 150 and 200 mm in the Jiftlik area. Towards the east and southeast, there is a sharp drop in the precipitation amounts over a relatively short distance and reaches 150 mm. The eastern parts of the Faria basin lies within a rain shadow causing the sharply change of precipitation.

Table 3.1: Details about rain gauges: location (grid reference), elevation above sea level (s.l), type of record (daily, monthly or annually) and the period of records.

No. of station	station	coordinates (x,y) in km	altitude m above sea level	period	type of records
1	Beit Dajan	185/177	+500	52/53-62/63 62/63-91/92	annually daily
2	Faria Agricultural	196/172	- 237	52-63 69-80/81	annually monthly
3	Faria Police	196,5/171,75	-225	52-63	annually
4	Toubas	184,75/191	+ 350	69-92	daily
5	Talluza	177,5/186	+ 350	62-93	daily
6	Nablus	178/178		61-90	monthly
7	Meithalun	178/185		61-90	monthly

Table 3.2: Calculated average annual of rainfall (mm/year) of the data available for the study area.

Station	1952/53-92/93	52/53-61/62	62/63-71/72	52/53-81/82	average 61-90	92/93
Talluza	645		666	597	608	674
Nablus					598	
Meithalun					576	
Beit Dajan	377	325	361	411	401	641
Tayasir	321	332	210		333	
Faria agricultural	210	200	208	222	210	
Faria Police	184	192	95		184	
Toubas	415		392	405	424	431

Rainfall decreases also along the north - south gradient. The isohyet map for Faria basin is complex, because of the broken topography and faults and it is illustrated in Fig. 3.3. The average rainfall amounts decrease sharply to the east, caused by a great change in the topographic slopes from the west to east; the isohyet map is generally parallel to the western edge of N-S Jordan Rift valley and increase from 184 mm at Faria police station to 608 mm at Talluza station. The average number of wet to dry days in Beit Dajan and Talluza stations are 11.6 and 14.8 %, respectively.
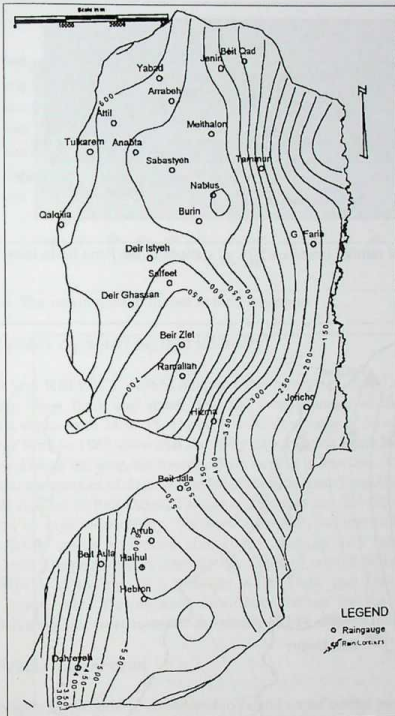
Fig. 3.1: The rainfall isoheyt map in the West Bank modefied after RABI et al.(1996) of rainfall (mm/year) for all stations in the Faria basin from West to East.

The maximum rainfall average is shown at Toubas station at the year 79/80 and 82/83 reaching an amount of 700mm; while the minimum rainfall average is shown at the year 75/76 (440 mm). In Talluza station for the period 62 to 93, a maximum annual average of rainfall is shown at the year 87/88 (1000 mm). The year 76/77 is recorded to be under the average. In Faria Agricultural station a maximum annual average is shown for the year 73/74 (for the period 52-81) of 420 mm, which is more than the average. Two peeks of 800 mm yearly are recorded in Biet Dajan station for the years 79/80 and 82/83 of a period 52-86. The rainfall fluctuations in mm yearly and monthly are illustrated in Figures 3.4, 3.5 and Appendix 3.1.

43
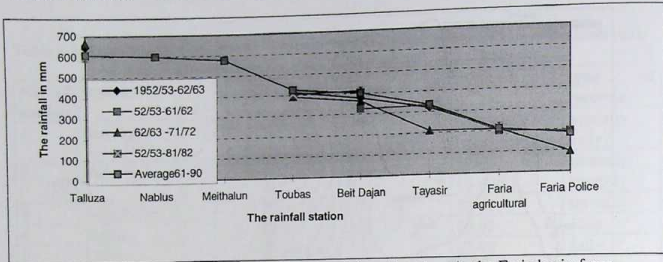
Fig. 3.2: The average annual of rainfall (mm/year) for all stations in the Faria basin from West to East.
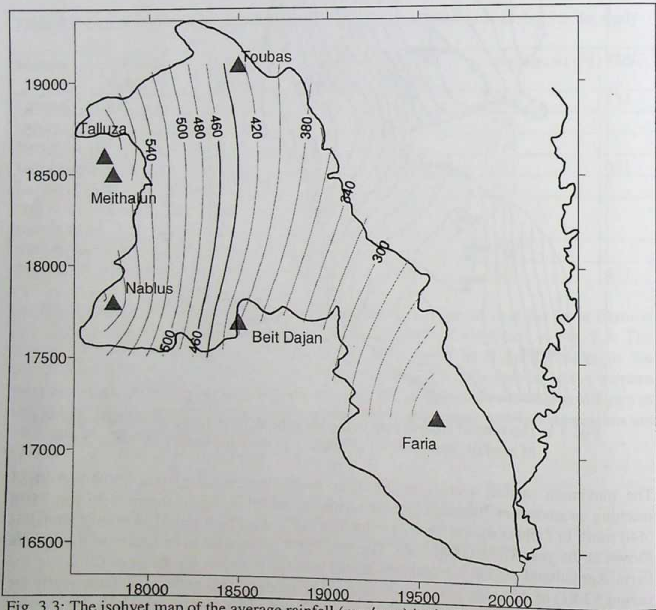
Fig. 3.3: The isohyet map of the average rainfall (mm/year) in the Faria basin (1961-90).

44
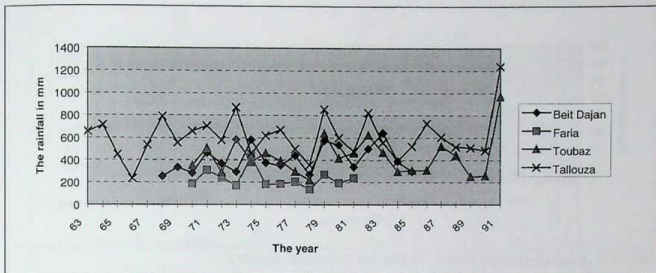
Fig.3.4: The yearly rainfall in mm in the Faria basin.

3.2.2 Rainy days and rainfall intensity

ROFE and RAFFETY (1965) analysed the records of daily rainfall for 18 stations in the northern West Bank and stated, that the mean number of rain days per year at different stations varies from 25 to 55. The daily rainfall records of 30 stations in the West Bank from the year 1952 to 1965 show that the rainy days ranging from 30 to 55. It can be demonstrated that for 87% of the year, the average daily rainfall is less than 0.5 mm (HUSARY et. al 1995). The average number of days of rainfall depth less than 5 mm/day over the recorded period for rainfall stations in Beit Dajan, Talluza and Toubas are 327 (90% of the year), 318 (87%) and 322 (88%) days, respectively. The maximum daily amount in Beit Dajan station is 133 mm (28.1.1979); while in Talluze and Toubas stations 124 mm (16.12.1991) and 116 mm (18.1.1976), respectively. A monthly maximum of rainfall in Talluza station was recorded for Jan./1974 to be 454 mm. It is recorded in Beit Dajan and Toubas stations to be 379 and 306 mm, respectively. The monthly maximum average for the period 68-91 in Nablus and Meithalun stations were recorded in January of 142 and 138 mm.

3.3 Evapotranspiration

The evapotranspiration is considered to be the major output parameter in the water budget of the West Bank. Potential evaporation is high with typical values of 1900 mm per year on the western slopes of the general watershed in the West Bank (western boundary of the study area) and 2600 mm around Jericho in the Jordan Rift valley (eastern boundary of the study area). The highest monthly average is 8 mm/day during July in the western, while being 11 mm/day in the eastern part. Potential evaporation along the Faria valley close to the Rift valley is calculated by SHALIV (1972) to be 2000 mm/ year. The potential evaporation in Faria was estimated to be 2341 mm in the year 63/64 and 2426 mm in the year 64/65. The monthly evaporation of Nablus station is illustrated in Figure 3.6.
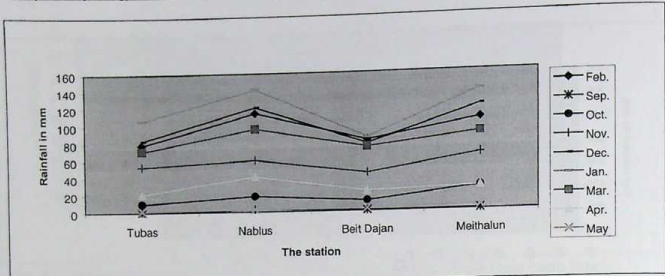
Fig.3.5: Average rainfall heights in mm for individual months.

In the lower Faria (Faria station) evapotranspiration reaches a total of 300 mm monthly in summer and of 120 mm in winter months. Isohyet evapotrasporation map for the period 1962-63 plotted in Figure 3.7 after ROFE and RAFFETY (1965) shows that the values vary from 1250 mm in the southern Nablus to 1950 mm at Faria. The average actual evapotranspiration is estimated to be 345 mm/year for all stations of the area of study using the Turc equation (Table 3.5). Actual evaporation values of the eastern stations are more close to the rainfall values than the values of the western stations (Fig. 3.8).
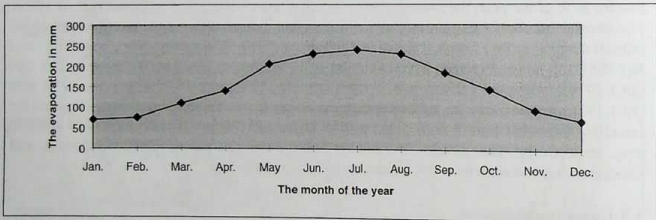
Fig. 3.6: The monthly potential evaporation in Nablus station in mm.

3.3.1 Temperature

The average summer temperature in the West Bank varies between 20 and 23° C, reaching a maximum of 43° C. The average temperature in winter is 10 to 11°C and reaching a minimum of 3°C. August is the warmest; while January is the coldest month. The variations are expected to be from the differences in position, elevation, distance from the coast and the environment around the station. The temperature increases from north to south contrary to the altitude.

46
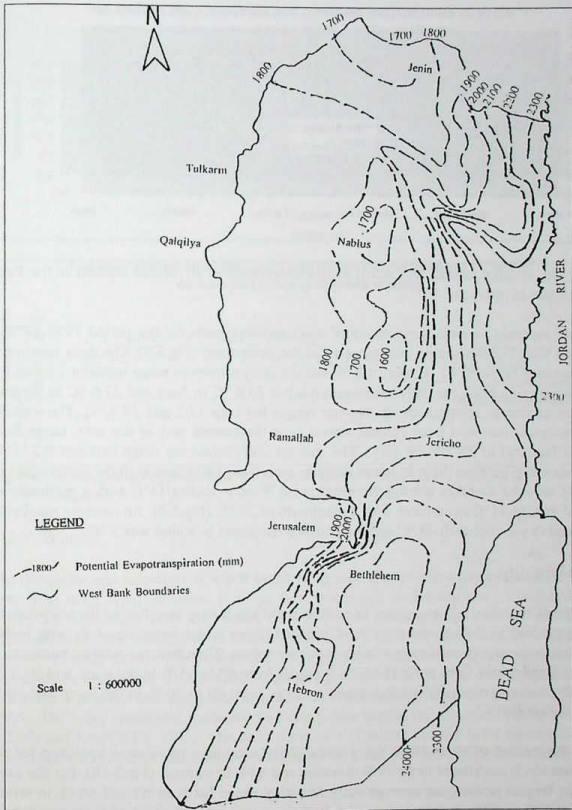
Fig. 3.7: Potential evapotranspiration map in the West Bank modified
         after ROFE and RAFFETY (1965).
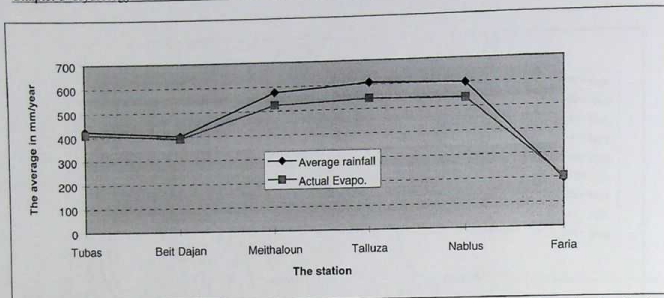
Fig.3.8: The average rainfall and actual evapotranspiration in all rainfall stations in the Faria basin in mm/year.

An actual monthly average temperature of daily measurements for the period 1970-1979 is calculated from Nablus station (western part of the study area) (Fig.3.9). The daily maximum in winter range between 13 °C and 14.8 °C and the daily minimum range between 7.2 and 8.2 °C. In summer months, the daily maximum reaches 26.6 °C in June and 27.8 °C in August. The daily minimum temperature in summer ranges between 17.2 and 19.7 °C. The average daily maximum recorded from Bequot station near the eastern part of the area, range from 16°C (in January) to 35.7°C (in July). The average daily minimum range between 8.2 °C in December and 21.8°C in July. In lower Faria as seen from Faria station in the eastern part of the study area the monthly average temperature in Winter reaches 15°C with a minimum of 9°C; and getting 31°C in summer with a maximum of 39 °C (Fig.3.9). An extreme maximum is recorded in summer with 48 °C and the extreme minimum in winter was 3 °C.

3.3.2 Humidity

Atmospheric moisture e.g. expressed in relative humidity is very sensitive to the temperature. This comparison in the hot and dry site of Jericho shows a high moisture of air with higher dew point temperatures and lower relative humidity values. Therefore, the relative humidity in the West Bank varies from north to south. It ranges from 60 to 65 % in the north and 50 % in the south during summer. While in winter, it ranges from 65 to 70 % in the north and 70 to 75% in the south.

During the period 1970 to 1979, the average daily maximum of relative humidity for the Nablus station is calculated to be 77% in winter and 83% in summer (Fig.3.10). For the same period in Bequot station, an average daily humidity range between 63 and 68 % in winter months and 48 to 57% in summer months. In the eastern part of the area of study as recorded from Faria station, the average maximum yearly is about 60% and the yearly minimum range between 5 to 10 % at the hot days and 80 to 90 % at the rainy days (Fig.3.10).

48

The average daily maximum and minimum temperatures °C in the western parts of Faria basin (Nablus station)

The daily and monthly maximum and minimum temperatures °C in the eastern part of the area (Faria station)
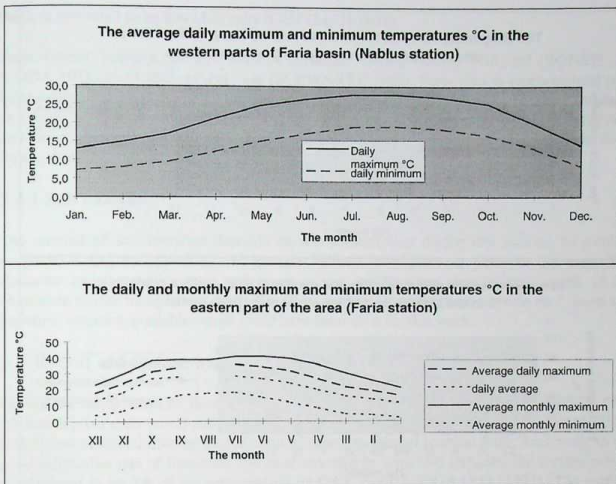
Fig. 3.9: Average daily maximum and minimum temperatures °C at Nablus and Faria stations.

3.3.3 Wind

The directions and velocities of winds in the study area change according to the seasons of the year. The main wind direction is from west, southwest and northwest. Variations during winter are associated with the pattern of depressions passing from west to east over the Mediterranean. The average wind velocity is about 14 knots in winter and 10 - 12 knots in summer (Tahal, 1975). The Jordan Rift valley stations show the highest summer values, especially in wadi Faria. This is due to a greater pressure effect for the cool air coming down to the Faria in order to replace the rising hot air in the Jordan valley (ROFE and RAFFETY 1965). The wind speed was measured by Faria police station for the year 1961 to be 3.8 m/s (ROFE and RAFFETY 1965). The daily reversal N-S winds cause a local movement within the Jordan valley, due to differential heating over the Dead Sea and the Jordan valley.

The daily maximum and minimum of relative humidity in % in the western part of the study area (Nablus station)

The average daily and maximum and minimum daily realtive humidity in % in the eastern part of the study area (Faria station)
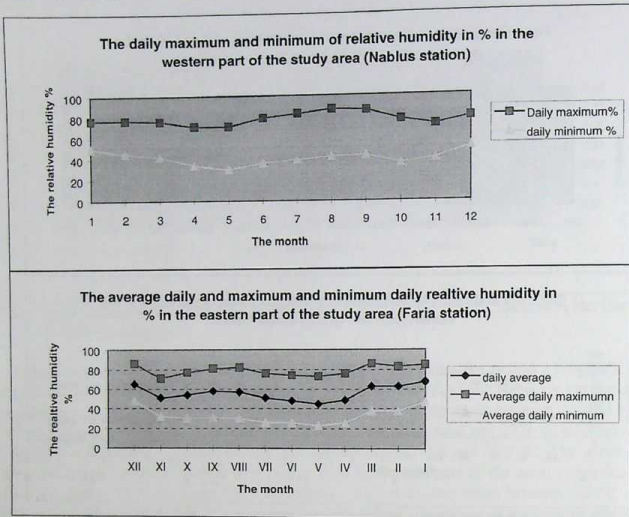
Fig. 3.10: The average daily and minimum and maximum daily relative humidity % at Nablus and Faria station.

3.3.4 Solar energy

The sun is the main source for evatransporation processes. The reduction of radiation varies with the amount of clouds present. A special climatological feature of the West Bank is the intensity of insulation through the year. The summer is almost cloudless, and in winter, even at days of rainfall, there are a few hours of sunshine. The total hours of sunshine sum up to 3200 to 3300 hours per year (METEOROLOGICAL SERVICE 1997). The total energy supplied for the West Bank gains 7.5 millions gram calories per square meter on a summer day and 3 millions in winter season. The sunshine duration in Bequat station (eastern part) shows a total of 7 to 15 hours/day for May and August, respectively. A mildy range is recorded to be 5 hours/day for October and 7 hours/day for August and July. A moderate sunshine duration intensity of 1 to 9 hours/day is recorded for May and July.

3.4 Infiltration and groundwater recharge

The rainfall minus evapotranspiration subdivides into runoff and infiltration; the later includes soil moisture. The total discharge was estimated to be 821 Mill. m³ in the northern West Bank for the year 63/64 and 836 for the year 64/65 (ROFE and RAFFETY 1965). The main source of groundwater recharge in the West Bank is direct infiltration of rainfall through the fractured rocks. The annual renewable water in the eastern aquifers has been estimated to be 125 Mill. m³ per year (GUTTMAN 1995). The main recharge of the groundwater system in the West

50

Bank is estimated to be 800 Mill. m³/y (GUTTMAN 1995).

Faria Eocene aquifers has an estimated recharge ranging from 4 Mill. m³ (BONEH and BAIDA 1978) to 13 Mill. m³ per year (SCHWARTZ 1982). Faria area is characterized by a huge infiltration quantity for the following reasons: the nature of the rocks are very fractured as a result of tectonics in the area, a high discharge of Faria wadi and other springs in the area and steep dipping formations. The recharge of the Pleistocene sub-aquifer occurs from flood flows, local rain and at times, flow from adjacent formations.

3.4.1 Soil moisture

The amount of soil moisture depends on it's consumption during dry seasons by surface evaporation and transpiration, which varies widely from place to place in the area. The character and the thickness of soil cover as well as the type, density, root depth of the vegetation are the main factors controlling this amount. However there were no data about soil moisture variation available which could have been used for this work.

3.5 Runoff and surface water

During the rainy season, flood-flows occur in dry river beds after heavy rainfalls. The relationship between runoff and rainfall is complex. A study was done by ROFE & RAFFETY (1965) and indicated that the overall ratio of runoff to rainfall is about 0.02. According to the good infiltration rate of limestone and sand outcrops in semi-arid climates, the surface runoff is estimated to be 2% of the precipitation by GAT and DANSGAARD (1972). The surface runoff in the West Bank is dominated by flash floods in the wadies. Regarding to the karst nature, the highly solubility of the rock in water is responsible for forming underground features like caverns and sinkholes. The overall runoff percentage was calculated to be 0.2 - 5 % of the rainfall (ROFE and RAFFETY 1965). This average of the flood water runoff represents 30 - 50 Mill. m³/y in the northern West Bank. The actual runoff was estimated to be 21.5 Mill. m³ for the northern West Bank and 60 Mill. m³ for the total West Bank in the year 1964/65. This runoff represents 2.2% of the total rainfall in that year.

There was a flood monitoring station (discharge gauge) at wadi Faria before 1967. In wadi Faria, an average runoff of 4.49 Mill. m³ yearly was estimated by GTZ (1995). Tectonic movements, such as uplifting of the mountains in the region and the deeping of the Jordan Rift valley, would steepen the subsurface flow gradients to the east. In addition to the natural runoff nearly 60 - 100 m³ per hour of wastewater is flowing into wadi Faria from Nablus municipality and as well 50 m³ per hour of industrial wastewater from the Israeli industrial zone in the study area for 2-3 days a week . This yields to a yearly average of 0.85 Mill. m³ of waste water.

3.5.1 Jordan River

The major surface water source in the West Bank is the Jordan river, which is about 260 km long and runs from the source at Banias to the Dead Sea with a total catchment area of 18,300 km². The river system is composed of the Hasbani, Dan and Banias rivers. They flow south in the deep depression from the northern mountains to lake Tiberias at around 200 meters below sea level, finally spilling into the Dead Sea at around -410 meters below sea level. The

discharge of the Jordan river for the year 81/82 was measured to be 267 Mill. m³ at the coordinates X,Y (208,287 km), 380 Mill. m³ (299,271 km) and of 117 Mill. m³ at the station (203,226 km). The later station is the nearest station to the area of study and had a discharge of 98.7 Mill. m³ for the year 86/87 (HYDROLOGICAL YEAR BOOK OF ISRAEL 1987).

3.5.2 Groundwater discharge

The flow from springs fluctuates between winter and summer and in wet and dry years. The average amount of discharge for all springs in the West Bank was measured to be 75 Mill. m³/y. Four spring groups are located in the Faria basin, Nablus (partly), Faria, Badan and Miska (ROFE and RAFFETY 1965). The discharge of all spring-groups in the Faria basin during the period 71-94 is illustrated in Appendix 3.2. These spring groups are discharging into wadi Faria and are classified according to their geographic locations into upper and lower springs. The upper springs consist of Faria and Badan groups and the lower springs consist of Miska group springs. Badan group drains from Jenin sub series limestones and are recharged from the south- and northwestern parts of the study area. It contains the springs of Hamad & Beida, Qudeira, Jiser, Sedreh, Taban and Subyan. Faria group springs contain of two major springs; Ein Faria and Ein Duleib. The yield of Faria spring was measured with 7 Mill. m³ in the year 1962/63. The Faria group is located at the eastern margin of the Jenin limestone sub series of the western sides of the study area. Miska group is the name given to seven springs in the area with considerable flow fluctuations. Ein Miska is the largest and the water emerges through a thin alluvial cover of the upper Beida formation and marls of Faria wadi. Its discharge ranges from 0.4 cubic meter/sec to 0.7 cubic meter/sec.

The average yearly discharge of the springs in Faria basin is calculated to be 14.1 Mill. m³ (NUSEIBEH and NASSER 1996). The flow from springs is directly affected by the total amount of rainfall and it's distribution as well as it's intensity (Appendix 3.3); while the groundwater is indirectly affected due to the time needed for infiltration. Seventy wells are located in the Faria basin, 61 wells are of active use. The average discharge of all wells in the Faria basin is calculated to be 18 Mill. m³. The pumpage from the lower aquifer (lower and upper Cenomanian sub-aquifers) is larger than from the upper aquifer (Eocene and Neogene sub-aquifers) (Fig.3.11).

3.6 Water balance

In the West Bank, a rainfall average of 450 mm/y is recorded giving an average total of 2600 Mill. m³/y. Around 650 Mill. m³ of this amount is estimated to be infiltrating in the soil in order to replenish the aquifer annually. The remainder is lost either through surface runoff or evapotranspiration. Annual potential evaporation averages between 1800 to 2600 mm/y. An overall water balance conducted by ROFE and RAFFETY (1965) shows that runoff and surface flow, evaporation and recharge represent 6.3%, 66.9% and 26.8%, respectively.
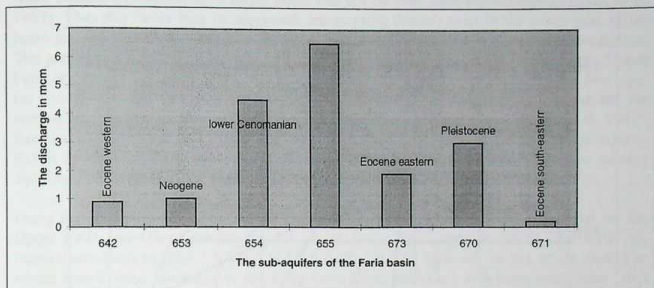
Fig.3.11: The yearly average discharge of all sub-aquifers in Mill. m³ (mcm).

3.6.1 Water balance of the Faria basin

The water balance in the western parts of the area of study was computed for the year 1962 and 1963 after ROFE and RAFFETY and showed that the recharge is 4.8 Mill. m³ yearly representing 17% of the rainfall. A groundwater recharge was estimated for the year 62/63 for some sub-aquifers (Table 3.3) after ROFE & RAFFETY (1965).

Table 3.3: The groundwater recharge in Mill. m³ from Jenin to Ajlun groups in the western parts of the Faria basin for the year 62/63 (ROFE and RAFFETY 1965).

Formation	area (km²)	rainfall 62/63 in Mill. m³				recharge/Rainfall %
		total	evaporation	runoff	recharge	
Jenin	99	4.8	4.5	0	0.3	6.2
Chalks	38.1	1.6	1.3	0	0.3	18.8
Ajlun	220.6	21.7	17.3	0.2	4.2	19.4
Total	357.7	28.1	23.1	0.2	4.8	17.08

The water balance of the Faria basin as well as groundwater balance was computed and estimated using the methods of global Turc formulas, hydrometeorological method and the salt balance method and discussed in the following sections.

3.6.2 Global formulas

Applying Thiessen Polygons method for the area of study (Scenario 1), the Faria basin was subdivided into six categories (Fig. 3.12). Table 3.4 shows the categories A-F, their representative areas, the rainfall gauges and its rainfall average (1961-1991) and the amount of rainfall. Using the global Turc formula, the water crop R (runoff & replenishment) is calculated from precipitation P and temperature T (°C). The following equations are used after Turc (CANSTANCY 1967): $R = P - (P / (0.9 + (P^2/L^2))^{0.5}$
where $L = 300 + 25 * T + 0.05 * T^3$ (T is the average yearly Temperature °C).

53
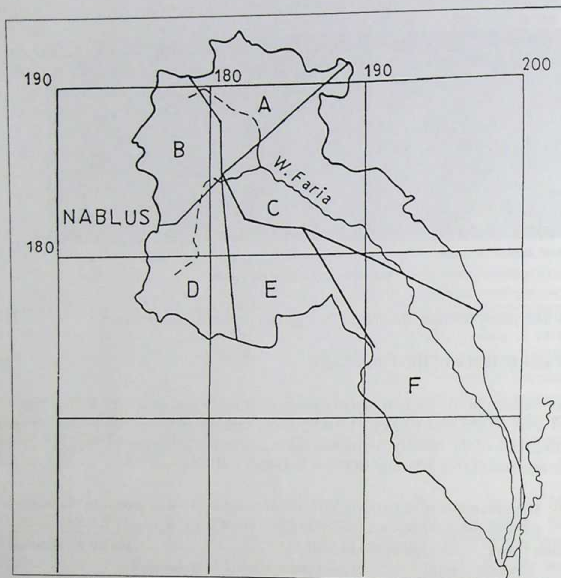
Fig. 3.12: The Faria basin with its rainfall categories after applying Thiessen Polygons
method of the corresponding rainfall stations.

GOLDSCHMIDT (1959) derived the equation R = 0.9 (P - 360) for the Mediterranean areas
with annual precipitation between 450 and 650 mm. The yearly average of rainfall as well as
the average temperature are listed in Table 3.5. According to the yearly average amount of
rainfall (Scenario 2), the Faria area is subdivided into two regions, Upper and Lower Faria.
Upper Faria is lying within an average rainfall of more than 400mm/y. The arithmetric
average rainfall of the upper Faria was calculated to be 521.4 mm/y from Beit Dajan, Tubas,
Talluza, Meithalun and Nablus stations; while the lower Faria was calculated from the Faria
police and agricultural stations with 196 mm/y. The area of the Upper Faria consists 65%,
which is 215 km² and the lower covers 115 km². The water crop for the upper Faria was
calculated to be 161.4 mm/y from the Goldschmidt equation. It was concluded that the
evaporation in the lower Faria is very high and it does not allow the rainfall to infiltrate.

3.6.3 Hydrometeorological method

The general water balance contains the following parameters: P = ET + M + R + I + Q ; with
P - precipitation, ET- evapotranspiration, M - change in soil moisture, R - storm water runoff,
I - interception and Q - natural replenishment. Soil moisture is the factor that influence the

54

water balance calculation for a single storm and not for long term calculations (ARAD, et al. 1967). Thus this factor may be neglected. Interception doesn't exist in the lower part of the basin and the amount that exists in the upper part may be included in the evapotranspiration. The geology in the study area is of two different types: dolomite & limestone in the Upper Faria and chalks and marls of low hydraulic conductivity in the Lower Faria. For the first type, the runoff rates are very low and negligible as compared to the precipitation and for the second type the average annual runoff reaches 10 % of the precipitation (ARAD, et al. 1967). Because no runoff gauge exists in the area of study, it has to be calculated by estimation. ROFE and RAFFETY (1965) estimated the runoff to be 2% of the rainfall for the eastern aquifers. Following this, the amount of runoff would be 128.59 * 0.02 = 2.6 Mill. m³/y.

Using the two estimations of runoff in the Faria basin, the runoff is of 2% of rainfall for the Upper Faria and 1% of rainfall for the Lower Faria. This refers to 2.8 to 13.8 Mill. m³, respectively leads to [(2.8 * 0.65) + (13.8 * 0.35)] = 6.65 Mill. m³ for the whole area. The whole runoff from rainwater in the Faria basin (6.65 Mill. m³) and from wastewater, that drains over wadi Faria (0.85 Mill. m³) was calculated to be 7.5 Mill. m³. Using the Hydrometeorological method of the equation R = R$_s$ + R$_g$ = P - Ea, where R$_s$ is the runoff and R$_g$ is the replenishment, this leads to the same result as the global Turc formula (67.5 Mill. m³ for the whole area and 44 Mill. m³ for the Upper Faria).

Table 3.4: The yearly average rainfall (mm) of Faria basin in categories A-F.

Category	percent %	area (km²)	rainfall station	average rainfall (mm)	amount of rainfall (m³ * 10³)
A	10	33	Tubas	424	13,992
B	9	29.7	Meithalun	576	17,107
C	25	82.5	Talluza	608	50,160
D	11	36.3	Nablus	598	21707
E	10	33	Beit Dajan	401	13,233
F	35	115.5	Faria Police & Agricultural	196	22,638
Total					138 837 000 m³

Table 3.5: The water crop after global and Goldschmidt formulas (local).

Station	P (mm) /year	T °C	actual evaporation (Ea)	P-Ea mm/year	Goldschmidt mm/year	rainfall Mill. m³ (Goldschmidt)
Tubas (A)	424		409,6	14,4	57,6	1,9
Meithalun (B)	576	17.9	523,6	52,4	194,4	5,8
Talluza (C)	608		543,1	64,9	223,2	18,4
Nablus (D)	598	17.6	535,4	62,6	214,2	7,8
Beit Dajan (E)	401		390,7	10,3	36,6	1,3
Faria (F)	196	20.8	205,6	0	n.n*	n.n
Total			345.4mm	204.6 mm/y[***1, 2]		38,1 Mill. m³

* not determined   ***1 for 204.6 mm, the calculation of R is 67518000 cubic meters for the whole area

***2 for 204.6 mm, the calculation of R is 43989000 cubic meters for the Upper Faria

3.6.4 The salt balance method

Two possibilities, using salt balance equations were used to compute the water crop in the study area. In a region, where airborne salts are the only source of chloride in groundwater, the salt balance of the aquifer (eq. 1) is given by the following average annual replenishment R_g:

$$R_g = (P (C_p / C_g)) + (F_d / C_g), \qquad (1)$$

where, R_g is the average annual replenishment (mm/year), P is the average annual precipitation (mm/year), C_p is the average chloride content of rainwater (mg/liter), C_g is the average chloride content of groundwater (mg/liter), F_d is the average annual dry fallout of chloride (g/m²/year). The amount of dissolved solids in the rainwater accounts for only 10% of chloride concentration in the groundwater for the eastern aquifers (SCHWARTZ 1980). Thus the value of F_d / C_g is less than 0.1 and may be neglected. The yearly average of precipitation in the area is taken from the Upper Faria with 521.4 mm, since the Lower Faria has not recharge. The annual average of chloride of the rainwater in the Jordan Rift valley is 10 mg/liter (SCHWARTZ 1980 and Meteorological Service, 1997). The runoff in the area is taken with 2% of the rainfall.

The second possibility is to use the following salt equation (eq. 2):

$$G = ((P - A_o) / C_g) * C_n \qquad (2)$$

where, G is the average annual replenishment, P is the average annual precipitation (mm/year), A_o is the average runoff in the area of study, C_g is the average chloride of groundwater (mg/liter), C_n is the average chloride of rainwater (mg/liter).

The average chloride of each sub-aquifer was taken from two rounds of water sampling before and after groundwater recharge periods 1996 / 1997 as illustrated in Table 3.6. The results of applying equations 1 and 2 (Table 3.6) lead to the same amounts of recharge. Following the results of equation 2 and taking into consideration that the Phreatic sub-aquifers are connected with each other and also the Lower sub-aquifers are hydraulically connected, this leads to the following conclusions:

1- The recharge of the phreatic and confined aquifers comes from the western , northwestern and southwestern regions (Upper Faria)
2- The recharge of the Eocene and Neogene sub-aquifers comes directly from rainfall in western part and flows underground to the eastern part of the Faria basin. The recharge of the confined aquifer was estimated to be the sum of the recharge in the west and east parts.
3- The recharge of the Phreatic aquifer is calculated to be 77.2 mm and 76.2 mm for the confined one. This leads to the amount of 49.1 Mill. 10³ of rain water may infiltrate into the aquifer system.

3.6.5 Goldschmidt equation

GOLDSCHMIDT and JACOB (1958 in Arad et. al 1967) studied the Cenomanian Turonian aquifers in Israel and their recharge (R) and they developed the following equation: R = 0.86 (P - 360), where P is the average annual precipitation in the area. Applying this equation an amount of 138.8 mm will infiltrate within the area of study, which gives an amount of 44.4 Mill. m³. In arid regions, where rainfall is less than 280 mm or 360 mm, there is no recharge.

3.7 Groundwater balance

Assuming the sum of precipitation - evaporation (P - Ea) in the study area to be 204.6 mm, this leads to an amount of 67.5 Mill. m³ of infiltrated water or flowing as runoff. Considering the runoff to be 7.5 Mill. m³, this leads to the recharge estimation in the basin of 67.5 - 7.5 = 60 Mill. m³, which represent 43.2% of the rainfall (138.8 Mill. m³) and 36.3 Mill. m³ for the Upper Faria (26 %) (Fig.3.13). The average discharge of all aquifers (1967-1993) is calculated to be 18 Mill. m³ and the average yearly discharge of the all springs in the area of study is calculated from the year 1970 to 1994 to be 14.1 Mill. m³. That means an amount of
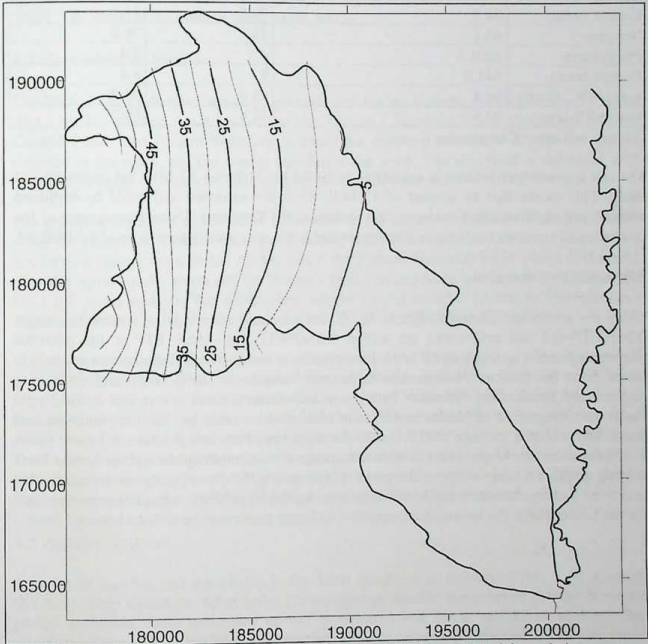
Fig.3.13: The recharge contour map of the Faria basin according to global formula in mm/year.

32.1 Mill. m³ of all aquifers is discharging from this aquifer. Thus an amount of 60 - 32.1 = 27.9 Mill. m³ of all aquifers is not exploited. Applying the above parameters of the groundwater balance in the Upper Faria, leads to an amount of 8 Mill. m³ of groundwater, that

could be exploited there.

Another scenario of runoff is taken from GOLDSCHMIDT et al. (1967) in the Qilt catchment which is in the eastern parts of the Dead Sea; Runoff = 0.237 (P - 252). According to this equation the runoff is calculated to be 13.3 Mill. m³ (9-14% of the P). Following the above procedure, the recharge is calculated to be 51.1 Mill. m³ and the balance is +19.2 Mill. m³.

Table 3.6: The recharge of the salt balance method in Mill. m³ for sub-aquifers of the phreatic and confined aquifers during 1996/ 1997.

Sub-aquifer	average chloride content (mg/l)	recharge (eq. 2)	recharge (eq. 1)
Eocene (west)	64.3	79.5	81.1
Neogene	68.1	75	76.6
Pleistocene	1201.5	4.3	4.4
Eocene (east)	644.9	8	8.4
L & U Ce[*1] (west)	54.4	93.9	95.9
l and u Ce (east)	87.5	58.4	59.7

[*1] lower and upper Cenomanian

The salt groundwater balance is calculated to be 49.1 - 32.1 = + 17 Mill. m³ in the area of study. This means that an amount of 17 Mill. m³ is not exploited and could be exploited without any negative affect to the aquifer system in the Faria area. Using the scenario of the Goldschmidt equation the balance of groundwater in the area is estimated to be +12.3 Mill.m³.

3.8 Aridity of the area

Using the aridity definition (UNESCO 1979), the semi arid zone is lying within this range: 0.2<P/ETP<0.5 and arid zones are within 0.05<P/ETP<0.2, where ETP is the potential evapotranspiration in mm/y and P is the Precipitation in mm/y. The ETP in the area of study is taken from the stations Nablus, Meithalun and Faria to be 1560, 1750 and 1936 mm respectively. Because the difference between recorded temperatures is very low in the Upper Faria, the average ETP of Nablus as well as of Meithalun are taken as a basis for other stations there. The recorded average P/ETP is 0.36 for the Upper Faria and 0.1 for the Lower Faria. This means that the Upper Faria is within the range of semi arid regions and the Lower Faria is lying within the range of the arid regions. Consequently the area of study can be subdivided into three recharge zones: a highly sensitive zone for the Upper Faria and a low sensitive zone for the Lower Faria. An intermediate sensitive recharge zone could be defined between them.

4 HYDROGEOLOGY

4.1 Introduction

The water sources in the West Bank's Faria basin originate from the rain and occasional snow that precipitates during winter seasons over the western parts of the study area. Most of the groundwater in the West Bank occurs in fissures, karstic features and joints of the mostly carbonate Ajlun group of Late Cretaceous age. The upper Cretaceous formations comprise the regional lower and upper Cenomanian aquifer systems (BLAKE AND GOLDSCHMIDT 1947). The range in thickness is from 400 to 900 m.

4.2 Groundwater basins

The West Bank is divided into three groundwater basins western, northeastern and eastern (Fig.1.2). The western basin also called the Yarqon - Tanninim basin, discharges into the Coastal Plain. The eastern boundary includes the northern extension of the Ein Qiniya anticline in the south, and the Anabta anticline in the north. The safe yield is estimated with 340 Mill. m³/year, of which 40 Mill. m³/year is brackish water (SCHWARTZ 1982).

The dominant direction of the water movement in the northeastern basin is northeastwards along the plunge of Nablus - Beit Qad syncline. It is subdivided into two overlying aquifer discharging mainly towards Bet Shean valley; the Nablus (Samaria) basin which is draining from the Ajlun aquifer group and the Nablus - Jenin (Avdat) basin which is draining from the Jenin sub series aquifers. The northeastern aquifer system includes Eocene to Cenomanian - Turonian formations, with a safe yield of 130 Mill. m³/year (SCHWARZ 1982).

All eastern basins drain eastward and southeast toward the Jordan Valley. This basin is of great tectonic complexity and the major movement is eastwards with a southerly component near the river Jordan. The basin is subdivided into : Wadi Malih -Buquei'a, Faria, Auja Fasail, Ramallah - Jerusalem and eastern desert sub-basins. The eastern basins are draining from Neogene and Pleistocene, and lower and upper Cenomanian sub-aquifers. The Cenomanian - Turonian aquifer system in the eastern basin can be divided into two sub units: the shallow and relatively thin upper Cenomanian - Turonian sub-aquifers and the deep lower Cenomanian sub-aquifer. The Faria sub-basin represent 61% of the eastern basin.

4.3 Aquifer systems

A series of aquifers and aquicludes in the West Bank are as follows (Table 2.1): Kurnub (Kurnov) group aquiclude, Ajlun series (Judean group) aquifer, Belqa series (Mount Scoupes group) aquiclude, Jenin sub-series aquifer to aquitard and Beide and Lisan aquifer. The eastern aquifer system in the West Bank is heterogeneous and its parameters are varying from point to point (TAHAL 1966). The study area includes one upper phreatic and two lower confined aquifer systems. Groundwater is found in formations of Pleistocene to lower Cenomanian age, at depth ranging from several hundred of meters to many meters. In the area under investigation, five sub-aquifers are located within unconfined and confined strata. These aquifers are the unconfined Pleistocene, Neogene and Eocene and the confined upper and lower Cenomanian sub-aquifers

The upper, unconfined aquifer system includes the sub-aquifers of Quaternary, Neogene and Eocene formations. The E-W geographic locations of these aquifers as indicated from groundwater wells in the area of study are Faria of Eocene (642), Al Aqrabanieh of Neogene (653), Froush Biet Dajan of Eocene (673) and Jiftlik area of Pleistocene (670) and Eocene (671) (Fig.4.1). These numbers of sub-aquifers are named according to the HYDROLOGICAL SERVICE (1997). The natural groundwater flow in this system starts from Faria area of Eocene western sub-aquifer (642), reaching Al Aqrabanieh of Neogene sub-aquifer (653) then to Froush Biet Dajan of Eocene eastern sub-aquifer (673) till Jiftlik of Pleistocene sub-aquifer (670) before reaching the Jordan River. This covers the formations of Jenin sub series (Eocene), Beida & Lisan (Neogene & Pleistocene) as well as alluvium (Holocene); in some formations basalt with alluvium. These sub-aquifers are described as follows:

1. Pleistocene sub-aquifer: The Pleistocene sub-aquifer consists of unconsolidated sand, gravel, cobbles, and boulders of different sizes separated by impermeable layers of saline lacustrine marl deposits. These deposits are composed of limestone, dolomite, chert, gravel with sand and clay fillings and forming alluvial fans. The groundwater occurring in the alluvial fans differs quantitatively and qualitatively according to it's location within the fan. Fresh water occurs around the apex of the fan, whereas saline water occurs at the fringes. Very steep deep faults in the Jordan Rift valley may cause deep circulation of the groundwater bringing it into contact with salt formations, then appearing as brackish springs near the river. This aquifer is composed of Lisan, Alluvium and gravel fan formations. Lisan formation (Pleistocene sub-aquifer) as well as Alluvial and gravel fans (Holocene) extends along the Jordan Valley. The alluvium is unconsolidated in the Rift Valley, where it is formed of laminated marls with occasional sands. However, the Pleistocene sub-aquifer is composed of basalt in some places as well.

2. Neogene sub-aquifer: Neogene sub-aquifer consists of well cemented conglomerates and contains a small amount of fresh water. It is composed of Beida formation and conglomerate lenses, marl and clay of the Lower Tertiary. The natural outlets of the aquifer are springs of Abu Saleh, Miska and Shibli. These springs discharge into the Wadi Faria with a current outflow of about 1.8 Mill. m³.

3. Eocene sub-aquifer: The Eocene sub-aquifer consists mainly of nummulitic limestone with chalks, chert bands and marl. The limestone is thin bedded with chalk, chert and marl intercalation. This aquifer is utilized by 28 pumping wells in the Faria area. Natural outlets are the springs Faria, Duleib, Hamad & Beida and Qudiera. The Eocene formations in the Faria basin cover an area of 150 km² with an average rainfall of 500 mm/year, which represent a volume of 75 Mill. m³ per year. The amount of recharge is calculated to be 27 Mill. m³ yearly, which represent 36% of the total volume of rainfall (DROR et al. 1971).
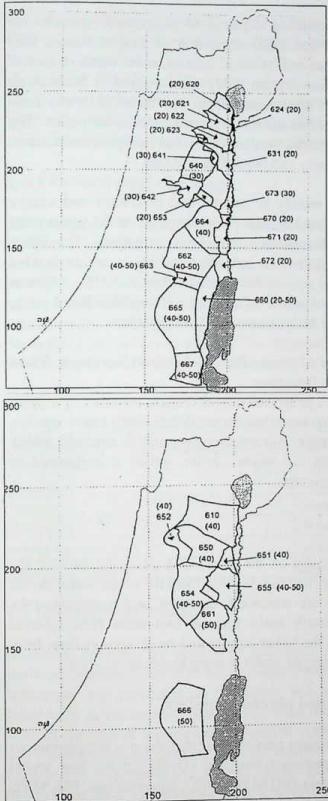
Fig. 4.1: A: The geographic locations of the phreatic (upper) sub-aquifers in the
           Faria basin modified after HYDROLOGICAL SERVICE (1997).
        B: The geographic locations of the confined (lower) sub-aquifers in the
           Faria basin modified after HYDROLOGICAL SERVICE (1997)
           (Notice: The numbers represent the sub-aquifers according
           to the HYDROLOGICAL SERVICE (1997)).

Confined aquifer system (lower1) occurs in the lower and upper Cenomanian formations
(Ajlun group). The findings of the groundwater wells indicate that there is no hydraulic

61

separation between the lower and upper Cenomanian. Three E-W geographic locations are located in the Faria basin (Fig.4.1); Faria -Badan (654) and Jiftlik as well as Froush Biet Dajan area (655). There is only one groundwater well (Gitit 3) located in the southern part of the study area discharging from the lower Cenomanian (661). This aquifer is build from formations of upper Lower Biet Kahel (Jiv't Ye'arin), upper Upper Biet Kahel & Lower Yatta (Keslan + Beit Meir), Lower Beithlehem (Kefar Sha'al) and Jerusalem (Bin'a) formation. The outlets of this aquifer are through lateral flow to the Jordan Valley and pumping from wells. This aquifer is divided into two sub-aquifers upper and lower Cenomanian.

The upper Cenomanian sub-aquifer consists mainly of interbedded dolomites and chalky limestones. This aquifer is classified as fairly good aquifer. It is composed of the upper parts of Ajlun series that include the Bethlehem, Jerusalem and Hebron formations. The lower Cenomanian sub-aquifer consists mainly of dolomitic limestone and thick to thin bedded marly limestones. It is classified as an excellent aquifer due to it's thickness of 800 - 850m in Faria area (GUTTMAN 1995). It is composed of Lower Ajlun group; Lower Beit Kahil (early lower Cenomanian) and Upper Beit Kahil (Late lower Cenomanian) formations.

Confined aquifer system (lower2) is composed of Lower Ramali (Kurnov) formation. There are no wells in the study area that penetrate this formation.

Generally, the aquifer systems in the area under investigation are divided into lower aquifer, which is composed of limestone of lower and upper Cenomanian age, middle aquitard, which consists of chalky limestone of Senonian age and upper aquifer, which is composed of limestones of Eocene and Neogene to Pleistocene age.

4.4 Groundwater flow and discharge

Groundwater flow is probably affected by the dip on the flanks and along the axes of the plunging synclines. Therefore, the groundwater direction is away from the major water divide of the West Bank. The main flow directions are westward, eastward, and northeastwards. Geochemical and isotopic studies in the eastern basin indicate two main flow systems (GUTTMAN 1995). Most wells are located in the lower aquifer and most springs flow from the upper aquifer. Geologic structure and topography result in steep hydraulic gradient.

4.4.1 Connection between the confined and phreatic aquifers

The outcrops along the creeks in the Al Aqrabania area suggest that there is no continuous thick impermeable layer within the Quaternary and Neogene (Q+N) rift-fill that would effectively separate the lower and upper aquifers (SHALIV 1972). Nevertheless, Ein Miski issues at a slightly higher level than the groundwater table in the neighboring boreholes which penetrate the Q+N. SHALIV (1972) concluded that the contribution from the lower and upper Cenomanian sub-aquifers to the Pleistocene sub-aquifer caused the raise of the water table within the Pleistocene sub-aquifer a small difference.

4.4.2 Connection between the upper and lower Cenomanian aquifers

Head differences suggest that the lower aquifer may be divided into two sub-aquifers in the western drainage basins of Judean mountains, as well as in the Phasael area where the water

level in well Phasayel 1 was found to be 9 m higher than in the upper part of the aquifer. These two sub-aquifers are interconnected hydraulically in parts of the study area, due to the lenticular distribution of the aquiclude (Deir Hana). The Faria area borehole data of GUTTMAN (1995) indicated that there was no separation between the upper and lower Cenomanian sub-aquifers. Moreover, in places where the aquiclude is present, minor thin faults may result in a connection between these sub-aquifers. The lower sub aquifer receives recharge from both it's own exposures and by the leakage from the upper aquifer.

4.4.3 Groundwater discharge

The pumpage of groundwater wells of the eastern aquifers, that are extracted from Pleistocene to upper Cenomanian sub-aquifers is varying from 7 to 14 Mill. m³ per year according to the varieties of their thickness (Table 4.1). In the Faria area, the total pumpage of Eocene wells is estimated to be 2.8 Mill. m³, representing 7.3% of the total pumpage of the basin (18 Mill. m³ yearly). The Jordan Valley is the only distinct groundwater discharge zone. Discharge from the upper aquifer is controlled by the topography, dip of rock formations and discharge from the lower aquifer. The relationship between the Jordan River & groundwater flow in the Alluvium sediment of the Jordan Valley is not well understood.

Table 4.1: Total pumpage from the eastern aquifers in Mill. m³, thickness in meters,
            utilization and the average Cl⁻ content in mg/l.

Sub-aquifer	pumpage (Mill. m³)	utilization	thickness (m)	Cl-content (mg/l)
Pleistocene	9.2	Agriculture	-	100-2000
Neogene	7	Agriculture	100	72
Eocene	7-9	domestic	130	110
Turonian	9-10	domestic	130	27-189
lower Cenomanian	8	domestic	-	30-149
upper Cenomanian	13-14	domestic	1260	27-30

4.5 Groundwater recharge

Recharge volumes are related to quantities of precipitation and surface geology of the drainage catchment. Most of the recharge comes directly from the rainfall that falls on karstic limestone and dolomites of the upper and lower aquifer, as well as in Wadies. Other potentially significant recharge components include return flows from domestic & industrial sources (sewage & wastewater), irrigation water, spring flows and leakage from stream beds and channels that are flowing into this aquifer. The effective recharge in semi arid regions is expected to range from 5 to 20% of rainfall (CDM 1997). The average groundwater recharge in the West Bank is calculated to be 836 Mill. m³ (HYDROLOGICAL SERVICE 1997). The annual average recharge to the lower aquifer in the confined aquifer of the eastern basins is about 118.5 Mill. m³ (GUTTMAN 1995). The recharge is estimated to be around 60 Mill. m³ in the whole Faria basin (chapter 3).

The lower aquifer is a major water resource in the Faria area. The Ajlun group (Judea), which is mainly karstic and composed of dolomites interbedded with beds of lower permeability is exposed in the western, south - northwestern, and northeastern of the area. These outcrops act

as replenishment areas to the lower aquifer. The outcrop area is in the western part of this basin. This aquifer is naturally replenished by rainfall on exposures covering an area of 100 km^2. Impermeable beds separate the upper and lower parts of the sequence, creating two sub-aquifers; lower and upper Cenomanian sub-aquifers. In the Faria basin, these two sub-aquifers are hydraulically connected due to a huge faulting system. The dense clustering of faults along the borders of the Faria graben probably enables groundwater of sandstone aquifer (lower aquifer 2) to pass into the Ajlun aquifer (lower aquifer 1) and the phreatic aquifer to the Jordan Valley (SHALIV 1972).

4.6 Natural springs

The discharge rate and the chemical composition of the spring water vary continuously and are dependent on the area contributing recharge to the aquifer and the rate of recharge. The recharge areas for the springs are hydrologically separated from the recharge areas, which feed the lower aquifer, from which the wells produce (GUTTMAN 1995). Generally it can be said that most of the springs are affected by changes in the amount of precipitation (GUTTMAN 1995). Four groups of springs are located in this basin, Nablus (partly), Faria, Beida and Miska (ROFE and RAFFETY 1965) (Fig. 4.2). Three groups of springs are discharging in Wadi Faria and are classified according to their geographic locations into upper and lower springs. Badan series springs are located at the eastern margin of the Jenin limestone outcrop on the eastern flank of the Nablus- Beit Qad syncline. The NW-SE faulting in the northern margin of Faria graben permits the movement of the groundwater from the syncline to the springs. Two major spring groups, at Beidan and Faria, occur as a result of faulting at right angles to the axes of a syncline. Ein Miska is the largest spring within the lower springs and the water emerges through a thin alluvial cover resting upper Beida formation and marls of Wadi Faria. The nature of the Faria graben and the complexity of the faulting, make it very difficult to relate these springs to more than one aquifer.

4.7 Groundwater wells

There are 314 pumping wells in the West Bank, out of over 720 wells drilled before 1967 (AWARTANI 1992). There are 70 wells in the Faria basin, 61 wells are recently used for supply. Many wells had been drilled in the study area, located mainly in the areas of Faria, Al Aqrabanieh, Al Nasaria, Froush Biet Dajen and Jiftlik along the flexure of the Wadi Faria (Fig. 4.3). Most of the wells were drilled in the upper aquifer. Data about these wells were collected and filtered from different resources. The data were correlated to each other and all of them were checked during field surveys and water sampling campaigns, that were conducted during this study. The well names, - numbers, coordinates (x,y,z), pumpage, aquifer, depth of the well and the year of drilling are listed in the Appendix 4.1.
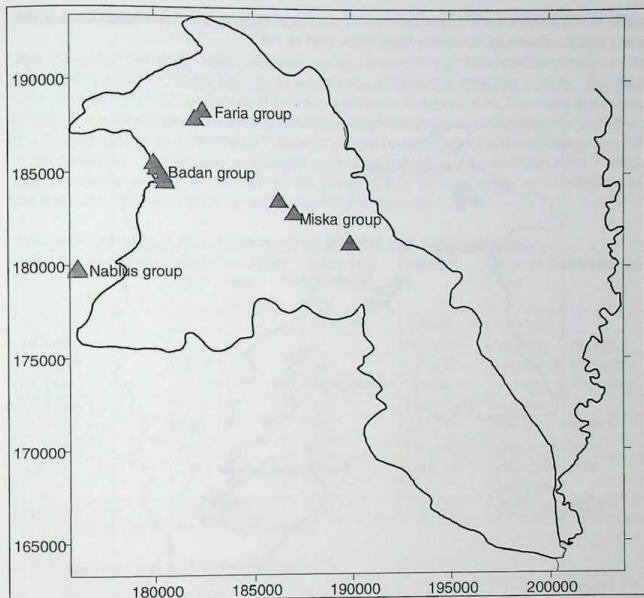
Fig. 4.2: The location of Faria group springs.

All groundwater wells in the Faria basin are in operation, except nine wells which went dry because of overpumping. The majority of wells were drilled in the period of 1960 to 1967. Seven Israeli wells were drilled after 1967 and are penetrating all sub-aquifers. All groundwater wells are located along the Wadi Faria. The deepest groundwater well in the area is Bathan No.2 (18-18/38), which penetrates the lower Cenomanian and has a depth of 748m. 56 wells were drilled in the upper aquifer (phreatic) and 14 wells in the lower aquifer (confined). Thirty six wells withdraw water from the Q+N sub-aquifer and 20 wells from the Eocene sub-aquifer. Fifty wells are in operation in the former; while 11 wells are in the latter. The depth range of wells of the lower aquifer is between 125 and 748m; while the maximum depth of the wells in the upper aquifer reach 160m (well no.19-19/56).

All wells that were drilled within the lower aquifer, except one (Gitit 3) are within the lower and upper Cenomanian sub-aquifer. This well is pumping from the lower Cenomanian sub-aquifer. An average of 62 Mill. m³ were pumped from all wells in the West Bank in the year 1993 (HYDROLOGICAL DEP. 1994). The average discharge of all groundwater wells in the Faria basin is calculated to be 18 Mill. m³. The discharge of phreatic aquifer in the Faria area (Eocene western sub-aquifer) is smaller than in Al Qurabania area (Neogene sub-aquifer);

65

while in the eastern parts larger amounts of discharge were recorded. Pumpage from of the lower aquifer shows an increasing trend from 1986 to 1987.
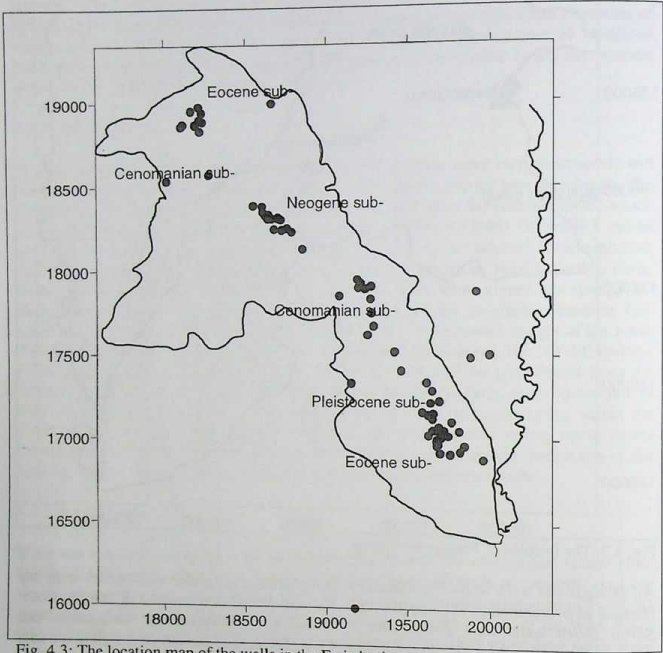
Fig. 4.3: The location map of the wells in the Faria basin.

4.8 Hydraulic characteristics of the aquifers through pumping tests

4.8.1 Pumping tests

Four pumping tests at constant rates were conducted during the field work in this study area for the wells: 18-18/23, 19-17/1, 19-17/44 and 19-17/2 (Table 4.2). An electrical sounder was used to measure the water level. Because no observation wells were located in the area, observations of the drawdown were made in the pumped wells. Constant rate tests as well as recovery and step - drawdown tests were conducted for the wells: 19-17/52, Atara1, Maasu'a1, 18-18/17 and 19-17/37.

66

4.8.2 Analyses of the pumping test data

The pumping test data were analysed using the software GROUNDWATER FOR
WINDOWS (GWW), which was developed by the UNITED NATIONS (1994). The data
were displayed and plotted for Jacob or Theis methods (Appendix 4.2). Recovery data were
plotted in similar manners as constant rate test or step drawdown test, but using the equation:
T = 2.3Q/(4πΔS) or T= 0.3665Q/ΔS ; where T is the transmissivity, Q is the discharge and ΔS
is the drawdown. A slight error is recorded ranging from 0.01 to 2.98 % (Table 4.3). For the
step drawdown tests, only one part of the pumping test or an average of two phases of
constant rates was used for the determination of transmissivity.

Table 4.2: The wells in the study area , where pumping tests were conducted.

Well No.	depth(m)	s.w.l. (m)	pumping rate (m³/hr)	saturated thickness (m)	aquifer	type of the pumping test
18-18/17	79	35	67	45,4	Eocene	constant
18-18/23	50	15,1	90	40	Neogene	constant
18-18/37	413	90.53	222	320	L&U.Ce *	constant & Recovery
19-17/1	77	29,3	120	47,7	Eocene	constant & Recovery
19-17/44	105	97,3	87	7,7	L&U.Ce	constant
19-17/2	60	31,3	70	28,7	L&U.Ce	constant
19-17/52	75	30,8	162	49,2	Pleistocene	step-draw down
Atara1	520	100,1	447	350	L&U.Ce	step-drawdown-recovery
Maasua1	600	90,02	550	255	L&U.Ce	step-draw down

* L& U. Ce means lower and upper Cenomanian

4.8.3 Aquifer type and transmissivity (T)

The saturated thickness ranges from 3 to 82.9 m for the phreatic aquifer and from 131 to 440
m for the confined aquifer. The data of the drawdown were taken from the pumped wells
themselves for the reason of the absence of observation wells in the area. The transmissivity
of the upper phreatic aquifer (Table 4.3 and 4.4): Well 19-17/2 shows some difficulties of the
transmissivity interpretation, therefore T is estimated from T = 0.124 Q/ΔS. The unfitted
points to the drawdown - time display curves (Appendix 4.2) are due to the well capacity
effect and to the failure of the drawdown measurements during the pumping test. It's T is
estimated to be 5600 m²/day; while the extracted T from the curve is 5503 m²/day. The
Pleistocene ranges between 126 and 10000 m²/d and the Eocene ranges between 158 and
1960 m²/d. The Neogene sub-aquifer shows a range of 12 to 1137.5 m²/d and shows a trend
of decreasing towards the east (Fig. 4.4). Pleistocene sub-aquifer shows a large range of T in
a small area, which is due to the fracturing, that are caused by the complex structure in the
area that were formed during the formations of the Jordan Rift valley. The T of Eocene sub-
aquifer in the Faria area (western) is of slightly larger values than the Eocene in eastern areas.

The Eocene well 18-18/17 shows a change of T towards depth (Fig.4.5), reaching different
fracture zones as a result to a specific degree of fracturing. Three transmissivities are recorded

67

with T1= 1781.1; T2= 475.2 and T3 = 200. Two fracture set systems are at a depth of 60.5 and 77.7 m cause this variable of transmissivities. The eastern Eocene shows values of T between 1960 and 158 m²/day. The transmissivity of the lower aquifer shows a range of 81.1 to 9610.9 m²/d . The largest values of T are recorded in the eastern parts of the study area. A trend of increasing T towards eastern was observed, due to the fracturing and the hydraulic connection between the lower and upper Cenomanian sub-aquifers. According to the quantitative appraisal of the aquifer production after KRANSY (1993) shows that the class of the upper and the lower aquifer are ranging between very high to intermediate class of the groundwater supply potential (class I to III). This indicates, that the withdrawals from the wells of class I and II are of great to less regional importance, respectively and the withdrawals from the wells of class III might be used for local water supply (KRANSY 1993). Transmissivity contour maps for phreatic and confined aquifers (Fig. 4.6 and Fig. 4.7) were drawn with the program Surfer using the method of kriging . All values were treated with the program Variowin to create a suitable variodiagram for each aquifer system. The contour maps are drawn after the best fit of variogramm using spherical method for the purpose of calculating a sill and range for each group of data.

4.8.4 Hydraulic conductivity (K)

The hydraulic conductivity of the sub-aquifers were estimated according to the equation : T = B K , where B is the saturated thickness of the aquifer. All K values are listed in Table 4.4 (SHALIV 1972) and Table 4.6. The hydraulic conductivity of the Eocene sub-aquifer is increasing toward the east for the reason of faulting. Neogene shows a value of 28.4 m/day and Pleistocene shows values smaller than Neogene (8 m/day). The lower aquifer shows a range from 0.3 to 25.7 m/day. In general, the hydraulic conductivity of the lower aquifer shows small values in comparing to those of the upper aquifer.

4.8.5 Storativity (S) and productivity

A storativity (S) represents the volume of water that an aquifer releases from or takes into storage per unit surface area of aquifer per unit change in the head normal to the surface. Storativity varies directly with the thickness of the aquifer according to this equation: $S = 3* 10^{-6}B$ (TODD 1980), where B is the saturated thickness of the aquifer. Because of the difficulties of calculating S from the current pumping tests for the reason of no observation wells in the area of study, it was calculated as an approximation from the equation: $S=S_0*B$, where S_0 is the storage coefficient; which lies within values of : $10^{-5}>S_0>10^{-6}$ and B is the saturated thickness. The storativity of the confined aquifer has a range of 10^{-5} to $1.1. 10^{-3}$ (Table 4.6).
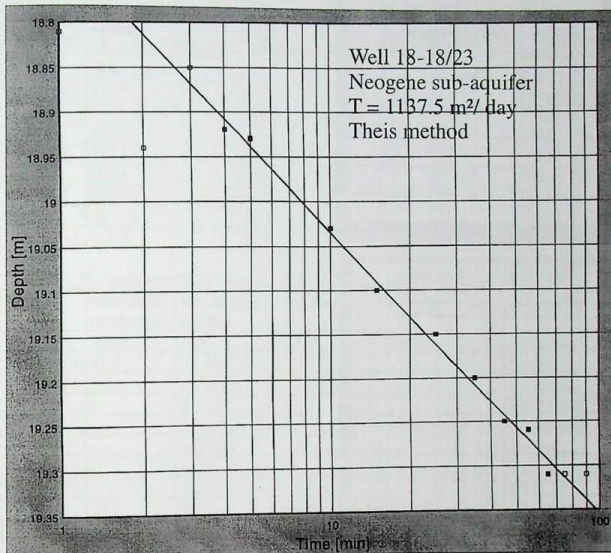
Fig. 4.4: The display of the draw down - time pumping test data of the
well 18-18/23 (Neogene sub-aquifer) and its transmissivity
(Notice: The unfitted points are due to the well capacity effect)

The productivity is an effective measure of the volume of water that a well yields when
compared to the drawdown in the well itself, and is defined according to the equation:
productivity = Q/S (where S is the drawdown). The productivity of each well is listed in
Table 4.5. A logarithmic relationship between T and productivity in the study area (Fig. 4.8)
shows, that high values of T imply high values of productivity. Values of T and productivity
can be used quantitatively to asses the potential of aquifers (KRUSEMAN and RIDDER
1994).
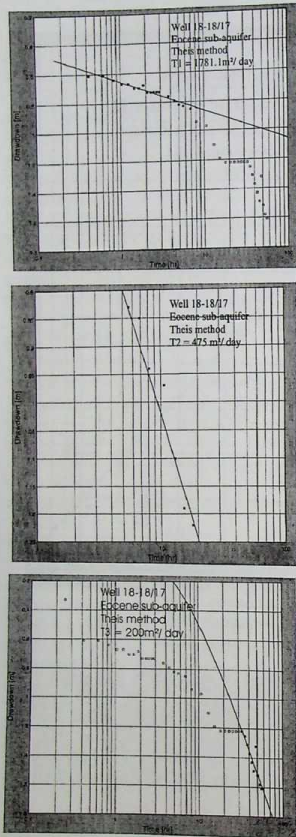
Fig. 4.5: The display pumping test data of the well 18-18/17 (Eocene western sub-
aquifer) showing three different transmissivities.

70

Table 4.3.: The transmissivities of all the sub-aquifers in the area of study and their classification after KRASNY (1993).

Well No.	transmissivity (T) m²/day	estimated error (%)	class after KRASNY (1993)	utilized sub-aquifer
18-18/17	(T1)1781.1;(T2)475; (T3) 200	0.06;0.03;0.05	I; II; II	Eocene
18-18/23	1137.5	0.01	I	Neogene
19-17/1	9599.4	0.02	I	Eocene
18-18/37	81.1	1.36	III	L&U. Ce
19-17/44	197.8	0.03	II	L&U. Ce
19-17/2	5600	0.07	I	L&U. Ce
19-17/52	391.9	0.06	II	Pleistocene
Atara1	9610.9	0.18	I	L&U. Ce
Maasua'a1	116.4	2.98	II	L&U. Ce

Table 4.4.: The transmissivities of some wells in the area of study after SHALIV (1972).

Well No.	saturated thickness	transmissivity m²/day	K m/day	storativity	class	sub-aquifer
18-18/19	106.8	380	3.6	-	II	Neogene
18-18/19A	81.2	12-33	0.1-0.4	-	III	Neogene
18-18/13	37.5	158-398	4.2-10.6	-	II	Neogene
19-17/8	-	10.000	-	-	I	Pleistocene
19-17/53	-	126-160	-	-	II	Pleistocene
19-17/5	-	158-204	-	-	II	Eocene
19-17/33	-	1960	-	-	II	Eocene
19-17/46	-	1175	-	-	I	L&U. Ce
19-17/51	37.2	200	5.3	$1.1 . 10^{-4}$	II	L&U. Ce
19-17/50	45.9	2700	58.8	$1.3 . 10^{-4}$	I	L&U. Ce

4.8.6 Permeability of the lower and upper Cenomanian

The permeability of the lower Cenomanian sub-aquifer is better parallel to the horizontal bedding planes than vertical. This is due to the well developed beddings and the abundant alternating thin marl beds (KAFRI 1970). The upper Cenomanian sub-aquifer is characterized by a high initial porosity as well as high permeability. The effect of the secondary porosity confirms the high transmissivity of the aquifer. The effective porosity, is marked by limestone and dolomite aquifers of low values and range between 2 to 8 % (TAHAL 1963). Secondary porosity (e.g., solution channels) can affect local groundwater flow patterns and in some cases, karst drainage systems may be superimposed on regional aquifer flow system.
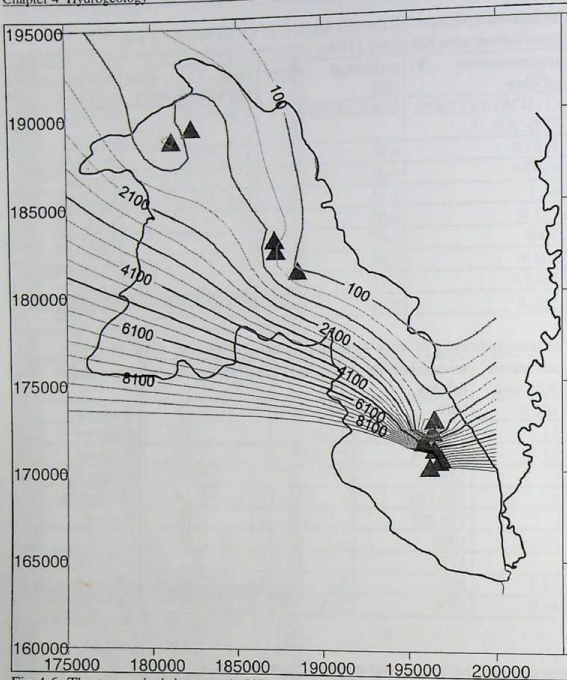
Fig.4.6: The transmissivity map (m²/day) of the upper aquifer of an interval of 500m.

Table 4.5: The productivity of wells in the area of study.

Well No.	productivity m²/day	cumulative drawdown (S)	sub-aquifer
18-18/17	68.6	28	Eocene
18-18/23	457.1	4.2	Neogene
19-17/1	3933	1.62	Eocene
18-18/37	21.1	134.6	L. & U. Ce
19-17/44	711	2.7	L. & U. Ce
19-17/2	5115	1.7	L. & U. Ce
19-17/52	241.2	9.95	Pleistocene
Atara1	109.2	186.8	L. & U. Ce
Maasua'a1	30.1	264.4	L. & U. Ce

72
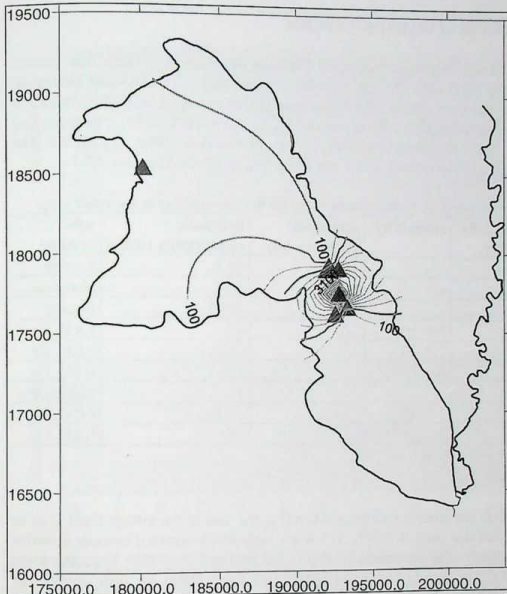
Fig.4.7: The transmissivity map (m²/day) of the lower aquifer of an interval of 500m.
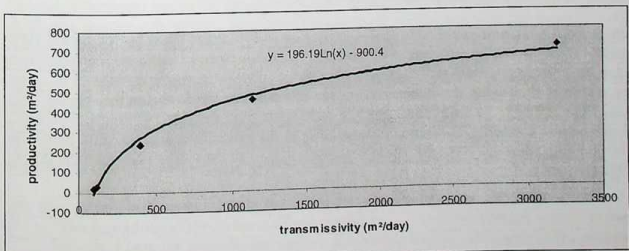
Fig. 4.8: T versus productivity for both lower and upper aquifer.

4.9 Saturated thickness of the utilized aquifers

The upper aquifer has a wide range of saturated thickness from 3 m to 106.8 m. The Eocene ranges in the western parts from 23.1 m (18-18/1) to 82.9 m (18-18/25A) and having an average of 83.4m in the eastern part. The Pleistocene has an average saturated thickness of 11.5m; while the Neogene ranges from 3m (18-18/11A) to 106.8m (18-18/19). The lower and upper Cenomanian has a thickness range of 71.3m (19-17/34) to 440m (18-18/38). The saturated thickness of all sub-aquifers in the area of study is shown in Appendix 4.3.

Table 4.6: The storativity and hydraulic conductivity for the sub-aquifers in the study area.

Well No.	transmissivity (T) m²/day	storativity	saturated thickness (m)	hydraulic conductivity m/day	sub-aquifer
18-18/17	1781.1	-	45.4	39.2	Eocene
18-18/23	1137.5	-	40	28.4	Neogene
19-17/1	9599.4	-	47.7	201.2	Eocene
18-18/37	81.1	$9.6.10^{-4}$	320	0.3	L&U. Ce
19-17/44	197.8	$2.3.10^{-5}$	7.7	25.7	L&U. Ce
19-17/2	5600	$8.6.10^{-5}$	28.7	195.1	L&U. Ce
19-17/52	391.9	-	49.2	8	Pleistocene
Atara1	9610.9	$1.1.10^{-3}$	350	27.5	L&U. Ce
Maasua1	116.4	$7.6.10^{-3}$	255	0.5	L&U. Ce

4.10 Groundwater heads

The groundwater heads (in reference to the sea level) at the area of the village Faria is at an elevation of about +166.4m (well 8-18/33). The water table drops eastward towards a Jordan Valley, down to the water table elevations of about -288.5m (well 19-17/20). Thus, the water table drops about 454.9m over a horizontal distance of about 30km for flow gradient of 15m/km (Δ= 0.015). This hydraulic gradient is an evidence of the geologic structure, which influences the direction of groundwater flow. The groundwater flow is affected by the geological formations and structure of the area.

The average of groundwater levels in all sub-aquifers in the area of study for the period 1968 to 1993 are illustrated in Appendix 4.3. These levels are transformed using the transformation equation $X_i' = (X_i - Min(X)) / (Max(X) - Min(X))$ in order to be within a range of 0 - 1 for the reason of displaying the fluctuations of the groundwater levels during this period (Fig. 4.9). There seems to be a significant drop of water table from the year 1974 until 1991 and a sharp increase in 1992. The dropping water table in the unconfined aquifer could be due to overpumping while the recharge in the year 1992 is may be caused by high rainfalls during 1991 (Fig. 3.4).

The water table fluctuations in the phreatic sub-aquifers

The groundwater level fluctuations in the confined sub-aquifers
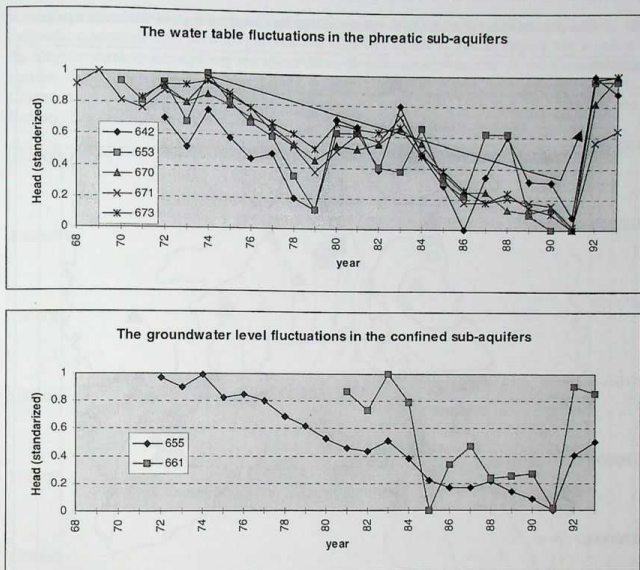
Fig. 4.9: The water table fluctuations in the phreatic aquifer and the groundwater level fluctuations in the confined aquifer for the period 1968 to 1993.

The water table in the Eocene sub-aquifer is between +166.4m to +150.7 above sea level in Faria area (western) and in the eastern between -285.6m (19-17/14) and -264.6m (19-17/23). In Eocene western sub-aquifer, water levels are between +272.1 m to +10.2m in some wells. Neogene sub-aquifer has a range of -21.4m (18-18/27) and -92.9m (18-18/19A). Pleistocene has a range of -229.2m (19-17/52) to -288.5m (19-17/20). In the confined aquifer, the elevation of groundwater levels ranges from -294.8 (19-17/34) to -178.3m (Atara2) in the eastern parts and being ~ -0.53m (18-18/37) in the western part. The difference between these elevations in the eastern and western is 294.3m. The contour maps of the static water level of phreatic and confined aquifer are shown in Fig. 4.10 and Fig. 4.11, respectively. These maps were drawn based on Kriging interpolation using spherical and linear variogramms.

The flow system in the two aquifer systems in the study area can be summarized as follows:

I-   The groundwater flow in the confined aquifer as well as in the phreatic aquifer is west to east, where the groundwater outlet is the Jordan Valley, especially for the phreatic aquifer.

II-   The groundwater flow in the upper aquifer has a steep gradient of 454m in 30 km long (15m/km).

75

III-   The groundwater gradient in the phreatic aquifer is steeper than of the lower aquifer.
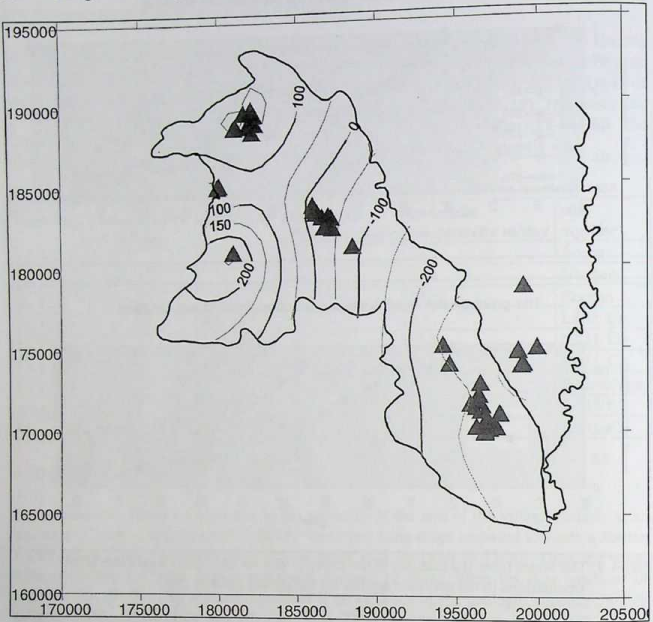
Fig. 4.10: The water table (m in reference to sea level) contour map of the phreatic aquifer.

4.12 Groundwater flow direction

The groundwater flow is affected by the geological formations, structure of the area, the transmissivity, natural hydrogeologic conditions and pumping from wells. A generalized groundwater level map of the Faria basin is given in Figures 4.10 and 4.11. In the western part of the phreatic aquifer, a high elevation of groundwater level was observed than the eastern part.

According to groundwater levels, the general direction of the groundwater flow is parallel to the Faria graben in the east and to the southeast. In the western part of the Faria basin, groundwater flows in the upper Cenomanian sub-aquifer are descending into the lower Cenomanian and moves southeastward. Where the Faria graben joins the Jordan Rift, the flow is again in the upper Cenomanian with part of the groundwater flowing riftward through the Quaternary and Pleistocene sub-aquifers. The differences in water levels between the

76

sub-aquifers in the western part of the basin are not sufficient for the establishment of hydraulic communication between phreatic and confined aquifers. The average water levels in the eastern phreatic sub-aquifers are about 20 m in difference, than that of the Cenomanian eastern sub-aquifers. This settings permit leakage from the Pleistocene sub-aquifer into Cenomanian sub-aquifers. This was recorded in two wells (19-17/46 and 19-17/56) of the Cenomanian eastern sub-aquifers which is due to the fractured nature of rocks.
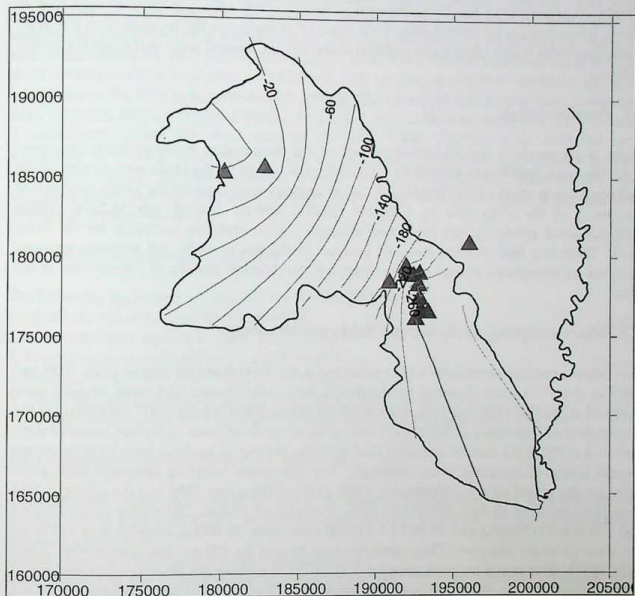
Fig. 4.11: The groundwater level (m in reference to sea level) contour map of the confined aquifer.

Static water levels are about 0.5 m above sea level near the western sides and 294.3 m below sea level near the Jordan Valley. The water table differs between the west region of the area and the aquifer outlets in the east reaches about 300 m over a horizontal distance of only 25 - 30 km. This results is a steep flow gradient which is not uniform. It is influenced by the tectonics, that are affecting the aquifer properties (GUTTMAN and ZUKERMAN 1995). In some places, the gradient is very steep (up to 5%).

77

5 HYDROCHEMISTRY

5.1 Introduction

The infiltrating rain water collects CO_2 in the soil zone, attacks the rocks and dissolves soluble constituents. In the Lisan formation, easily soluble salts like gypsum may lead to higher concentration of constituents. Four types of groundwater are recognised in the West Bank: limestone water, organically polluted water, hot and mineral water and Lisan Formation waters.

5.2 Previous work

There is no previous water chemistry study of the project area, however some data were available from ROFE and RAFFETY (1965) for the springs in the study area as part of the hydrogeological study of the West Bank. Some analyses were done for the major springs and few wells in the study area by SHALIV (1972). ABDUL JABER and ALIEWI (1996) analysed some springs in the study area through a water sampling campaign for the West Bank. There is a lack of trace elements analyses in the area of study. All available previous analyses are interpreted and are used to determine the chemical changes of groundwater in the area.

5.3 Water sampling, analyses and field measurements

Two water sampling campaigns were carried out in the Faria Basin during the years 1996 and 1997 to study the hydrochemical parameters of the aquifer system. The water samples were analysed at the WATER and SOIL ENVIRONMENTAL RESEARCH UNIT (WSERU) of the Department of Chemistry at Bethlehem University in the West Bank. Sixty-two analyses were included in the first round of sampling (before recharge) and 42 analyses were included in the second round of sampling (after recharge). The first water sampling campaign took place between the period of the 1 September 1996 to the 4 December 1996 and the second round took place between 10 June and 16 July 1997. During these periods, 20 samples were collected for: ^{18}O and ^2H (50 mL) and ^3H (0.5 L). For the same sites, 20 100mL samples were collected for trace elements analyses. These samples were filtered by 450 nm and treated with Super Pure HNO_3 (five drops for each sample) in the field to prevent any possible reactions and to prepare them for the determination of heavy metals. Two samples were collected from the lower Cenomanian aquifer to predict the age of the water using ^{14}C. These two samples (each 40 L) were treated with $Ba(OH)_2$ to precipitate carbonate for the analysis.

The purpose of the water sampling campaign and water analyses was to determine the physical properties (temperature and EC), chemical properties (pH, dissolved oxygen, major ions, trace elements) and microbiological properties (the presence of coliforms). The water sampling campaign covered all springs as well as major groundwater wells and surface water (wadi) in the area. All of these springs (13) are discharging from unconfined aquifers and are subject to direct pollution due to human activities (municipal waste water and agricultural return flow). Surface water (wadi) samples were taken to determine the deterioration of aquifers in the area that is caused by Nablus effluent sewage and industrial liquid waste, especially in wadi Faria and Bathan areas.

For all collected samples, the following parameters were measured during fieldwork at the site itself: temperature in °C, electrical conductivity (EC) in mS/cm, dissolved oxygen (DO) in mg/L, pH - value and redox potential (Eh) in mV. Alkalinity and acidity tests were done for selected samples.

The pH and temperature were measured with a pH-meter (microprocessor pH-meter, pH 320 set), which is equipped with temperature-sensitive sensors. Redox potential (Eh) was measured in the field, using the Platinum (Pt) electrode and a pH-meter and corrected for temperature. It is a function of temperature, which means that a certain value must be added to each measurement for each temperature measurement. The DO was measured using a Oxi-meter (microprocessor Oxi-meter, Oxi 320 set), with an oxygen-sensitive electrode. EC was carried out in the field using portable EC meters. The alkalinity and acidity were measured using alkalinity and acidity tests (Merck). All devices were calibrated, using relevant methods of calibration, before they were used in the field. Water samples were collected and transported to WSERU lab within 24 hours for chemical analyses. 1-L Polyethylene bottles were used for the analyses of major cations and anions, 100-mL glass sample for microbiological analyses. The water samples were cooled during transport to prevent any changes of the constituents.

5.4 Methods of laboratory analysis

The following parameters are measured at the WSERU laboratory:
1. Alkalinity and total dissolved solids (TDS)
2. Major cations in mg/L: Ca^{2+}, Mg^{2+}, Na^{1+} and K^{1+}.
3. Major anions in mg/L: HCO_3^-, Cl^-, SO_4^{2-} and NO_3^-.
4. Minor constituents: Silica (SiO_2), F, Br^- and $PO4^{3-}$
5. Trace inorganic constituents in µg/L : Fe, Mn, Pb, Zn, Cd and Cu
6. Microbiological parameters colonies / 100 mL: fecal coliforms and total coliforms

5.4.1 Laboratory measurements of major ions

Total alkalinit: Total alkalinity of a water is its capacity to neutralise acid. It is determined through the titration with H_2SO_4 or HCl-standard solution to the pH for 4.3, indicated by means of a pH-meter.
Acidity: Acidity is the capacity to neutralise alkalines.
Bicarbonate (HCO_3^-): Bicarbonate is directly calculated from the m-value assuming that humical acid does not influence the alkalinity determination.
Total Hardness (TH) (CaCO_3): The TH is defined as the sum of the calcium and magnesium concentrations, expressed in mmol/L. The TH is measured by EDTA titrimetric method at pH≤10, using indicators.
Calcium and Magnesium (Ca^{2+}, Mg^{2+}): Calcium and Magnesium are determined using the EDTA Titrimetric method. When EDTA or it's salts is added to the water containing both calcium and magnesium, it combines first with calcium. Calcium can be determined directly when pH is sufficiently high (about 12). The magnesium is largely precipitated as its hydroxide, using the Murexid as indicator. Magnesium is determined mathematically based on a mean assumption using the following equation: TH = 2.497 [Ca^{2+}] + 4.118 [Mg^{2+}].
Total dissolved solids (TDS): The TDS is referred to the portion of total solids that passes a 2.0 µm pore size under specific conditions (APHA et al. 1995). It is measured by gravimetric method. A sample is filtered through a standard glass fiber filter (2.0 µm) and the filtrate is

79

evaporated to dryness in a weighted dish and dried to a constant weight at 180 °C.

Sodium and Potassium (Na^+ and K^+): Sodium and Potassium were measured using flame emission photometric method. This method is based on converting the investigated sample to atomic vapour using flame. It is determined at a wavelength of 589 nm for Na^+ and 766.5 nm for K^+. The concentration of Na^+ and K^+ were determined through a comparison with a curve of potassium and natrium standard solution.

Chloride Cl^- : Cl^- was measured by Argentometric (Mohr) method, in which potassium chromate can indicate the end point of silver nitrate titration of chloride. In this method, the sample is titrated against $AgNO_3$ standard solution, while potassium dichromate is used as indicator.

Sulfate (SO_4^{2-}): SO_4^{2-} was precipitated in an acetic acid medium with Barium chloride ($BaCl_2$) to form Barium Sulphate ($BaSO_4$) crystals. Light absorbance of $BaSO_4$ suspension was measured by a photometer and SO_4^{2-} concentration is determined by comparison of the reading with the standard curve (Sulfate Test of Turbidimetric Method) at a wave length of 420 nm.

Nitrate (NO_3^-): The ultraviolet (UV) spectrophotometric screening technique was used for screening water samples that have low organic matter. The UV absorption at 220 nm enables rapid determination of NO_3^-. A standard curve is used to determine the concentration of the nitrate in the different samples.

5.4.2 Laboratory measurements of minor and trace inorganic constituents

Fluoride (F^-) : Colourmetric method was used. The concentation of F^- is determined using a spectrophotometer at a wave length of 570 nm. A curve developed from standard fluoride solutions is used for determining the fluoride concentration of a sample. The colorimetric method is based on the reaction between Fluoride and Zirconium - dye lake. Fluoride reacts with the lake, dissociating a portion of it into a colourless complex anion (ZnF_6^{2-}).

Bromide (Br^{-1}): The Curcumin method is used for this analysis. The water samples are acidified and evaporated in the presence of Curcumin (red colour) and then Resocyanine is formed (WSERU, 1996). The Resocyanine is compared with standards photometrically.

Silica (SiO_2): Silica is determined using Molybdosilicate methode, using spectophotometer method at a wave length of 700 nm.

Phosphate ($PO4^{3-}$): It is determined using Stanous Chloride method, using a spectrophotometer at 700 nm.

Trace inorganic constituents: All the measured trace elements (Fe, Mn, Pb, Zn, Cd and Cu) were measured by the Graphite furnace AAS, each of them having a specific wave length.

5.4.3 Laboratory measurements of microbiological analyses

Coliform bacteria are the principal biological indicator for fecal water contamination. The density of fecal and total coliform (Fc and Tc) was determined by using the membrane filter (MF) technique, in which an enriched lactose medium and incubation temperature of 44.5 +/- 0.2 °C are used. This give 93% accuracy in differentiating coliform from warm-blooded animals and from other sources (FRESENIUS et. al. 1988). Owing to incubation temperature being critical, MF cultures are submerged in a water bath for incubation at ovulate temperature or an appropriate accurate solid heat sink incubator. The total coliform is defined as comprising all aerobic and facultative anaerobic, gram negative, non-spore-forming, rod-shaped bacteria that produce a dark colony within 24 hours at 35 °C on Endo-type medium

containing lactose. Fc and Tc are expressed as colonies numbers per 100 ml sample.

5.4.4 Validation and quality control

The electrical balance of the chemical analyses of water samples was calculated following the equation:

Electrical balance = ((total cations - total anions) / (total cations + total anions)) * 100 %.

The electrical balance error for all samples ranges between 0.12 and 1.56, which indicates a good accuracy. The detection limit of the measured parameters at the lab of the WSERU / West Bank are summerized in Table 5.1.

Table 5.1: The detection limit of the measured parameters (WSERU 1996).

Chemical parameter	detection limit	Chemical parameter	detection limit
Ca^{2+}	1 mg/L	I^-	0.2 mg/L
Mg^{2+}	0.5 mg/L	Br^-	0.5 mg/L
K^+	0.4 mg/L	Fe	0.5 µg/L
Na^+	0.5 mg/L	Mn	0.05 µg/L
Cl^-	1 mg/L	Zn	30 µg/L
HCO_3^-	10 mg/L	Cd	0.5 µg/L
NO_3^-	0.7 mg/L	Cu	0.2 µg/L
SO_4^{2-}	0.13 mg/L	Pb	0.1 µg/L
SiO_2	1 mg/L	PO_4^{3-}	0.1 µg/L
F^-	0.1 mg/L		

5.5 Statistics of hydrochemical parameters

Statistical analyses of all hydrochemical parameters were done using SPSS (SPSS FOR WINDOWS 1997). The following statistical parameters were calculated for each hydrochemical element: mean, median, minimum, maximum, range, variance and standard deviation. Appendix 5.1 shows all of these statistical parameters for each sub-aquifer within phreatic and confined aquifers and for the whole aquifer system. Frequency histograms were calculated for all parameters; they vary between normal and asymmetrical frequencies. Normal frequency is shown for the distribution histograms of HCO_3, pH, SiO_2, Zn and F parameters (Fig. 5.1); while asymmetrical distribution frequencies are shown by histograms of Ca, Cl, K, Mg, Na, NO_3, SO_4, Cd, Cu, Fe, Mn and EC. Other hydrochemical parameters show weakly skewed frequency histograms like Br, DO, Pb, PO_4. The bivariate correlation procedure of SPSS computes the correlation coefficient (r), which requires normal distribution. Pearson correlation requires normal distribution and internal scaling. Since most of the variables are not normal distributed, Spearman correlation coefficient is suggested to be used (Appendix 5.1a, 5.1b, 5.1c, 5.1d, 5.1e).

Correlation coefficients of Spearman type using the significance level of 0.01 were taken into consideration (Appendix 5.2). The correlation is significant positively at the level 0.01 between the following parameters: (Mg, Cd), (Na, Pb), (Na with Fe and Pb), (K, Cu), (Fe with Ph and Na), (Cu with Na, K and NO_3), (Pb, DO), (Mn with NO_3 and F) and (Pb, Mn). It is significant negatively at the same level between the following parameters: (DO, SO_4), (Ph, Cl) and (PO_3, NO_3). Correlation is significant at the level 0.05 is found positively between the following parameters: (Ca, Na), (K, Na), (HCO_3, Mg), (Cl with Ca, Mg, Na, K, HCO_3 and

81

EC), (Cd with Ca and SO_4), (Mn, Cl). It was found that SiO_2 at the same level of 0.05 correlates negatively significant with the Ca, Mg, Na, K, Cl, HCO_3 and SO_4.

T - Test were carried out to check whether there are significant differences in the mean concentrations of the confined compared to the unconfined aquifer. Table 5.2 shows those parameters with significant ($P<0.05$) differences.

Table 5.2: The results of the T - Test analyses ((0) is the phreatic aquifer and (1) is the confined aquifer).

Parameter		number of samples	mean	standard deviation	standard error of the mean	F_{err}	significance
HCO_3	(0)	80	301.4	47.2	5.2	4.7	0.033
	(1)	16	316.4	31.6	7.9		
Na	(0)	80	82.4	93.8	10.5	5.1	0.026
	(1)	16	55.4	61.1	15.3		
K	(0)	80	6.1	7.5	0.8	9.1	0.003
	(1)	16	3.4	4.4	1.1		
Cl	(0)	80	257.9	385.8	43.1	5.8	0.018
	(1)	16	146.7	206.9	51.7		
NO_3	(0)	80	43.5	40.2	4.5	8.9	0.004
	(1)	16	21.7	10.2	2.5		
Cd	(0)	80	99.1	327.4	36.6	4.3	0.04
	(1)	16	9.4	16.8	4.4		

The analysis of variance (ANOVA) is carried out to compare the variances of the chemical parameters in the phreatic and confined aquifers (Table 5.3). The result of the ANOVA is also a F_{err} - value. However, this F_{err} - value is compared to another F_{tab} value than in the T-Test. The F_{tab} - value for the ANOVA depends on the number of groups NK (NK= 2) compared to each other and the sample size. According to the F-distribution table for the statistical confidence of 95%, the F_{tab} is about 3.92. The ANOVA has shown that the parameters of NO_3 and SiO_2 have an important difference (not random) between the variances in the different aquifers.

Table 5.3: The results of the analyses of variance (ANOVA).

Parameter	F_{err}	significance
NO_3	4.57	0.035
SiO_2	4.6	0.035

5.6 Interpretation of the analysed parameters

The chemical composition of water samples from the lower (confined) and upper (phreatic) aquifer is given in Appendix 5.3.

5.6.1 Electrical conductivity

Electrical conductivity (EC) is a numerical expression of the ability of an aqueous solution to carry electrons. It is a function of the presence of ions and their total concentration, temperature of the solution and the valence of ions and their mobilities. The EC is the

reciprocal of resistivity (R): EC = 1/R and is reported in millisiemens/cm (mS/cm) or μS/cm. Dissolved solids concentration compared with specific conductance shows a strong correlation between conductance and mineral content of water. An approximate correlation between an EC and TDS can be used for the fact that EC is dependent on the valence of the elements soluted: TDS (mg/L) = K * EC (μS/cm at 25 °C) , where K is the conversion factor and ranges between 0.55 and 0.8 .
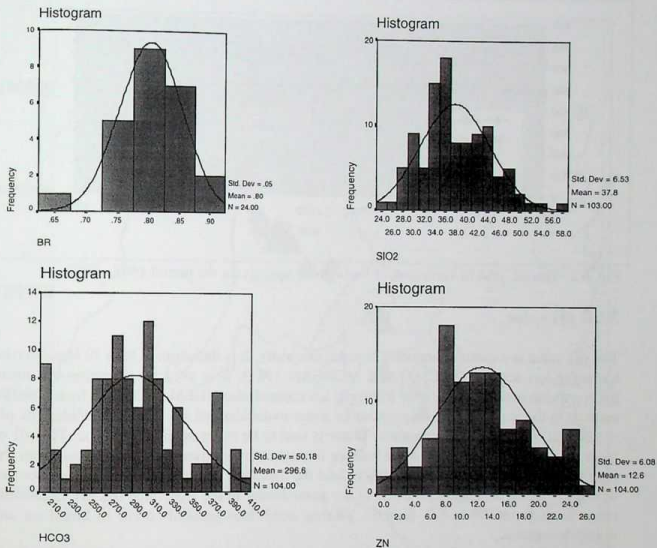
Fig. 5.1: The normal frequency histograms of Br, SiO$_2$, HCO$_3$ and Zn

EC as measured in the field is considered to be an excellent monitoring parameter on an spatial and time basis. EC is a very helpful lumped parameter to characterise the sum of inorganic constituents. The Eocene western sub-aquifer has an EC average of 752 μS and the Neogene sub-aquifer has an average of 725 μS/cm. The median of the Cenomanian sub-aquifer is found to be 726 and 899 μS/cm for the western and eastern parts, respectively. The Eocene eastern sub-aquifer as well as Pleistocene show an average of 2843 to 3386 μS/cm, respectively. The maximum EC is found in the Eocene eastern sub-aquifer to be 5300 μS/cm in the well 19-17/6. The Eocene springs show less value of EC than those of Neogene springs and Hamad and Beida spring shows the lowest EC values in the whole area (503 μS/cm). According to these EC values, the area can be subdivided into two main regions: Western phreatic and confined aquifers have low EC, and the eastern phreatic aquifer has very high

83

EC. According to this, the eastern phreatic aquifers are unusable for both drinking and agricultural purposes. The EC for the Faria group springs had a slight variation within the period 1967/68 to 1976/77 (Fig.5.2) and it agrees with the EC average of each group for the year 1996/97.
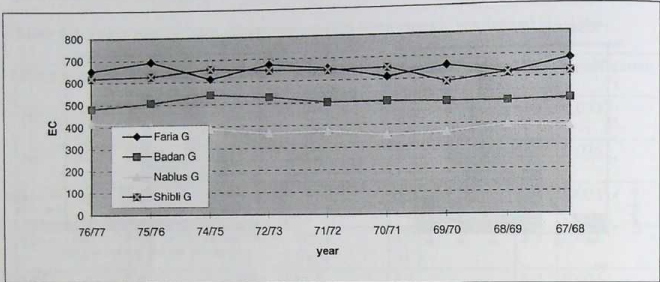
Fig. 5.2: The EC μS/cm variations of Faria group springs for the period 1967 - 1977.

5.6.2 pH value

The pH value is a master parameter in water chemistry. It is the negative base 10 logarithm of hydrogen-ion activity (STUMM and MORGAN 1981). It is used to determine the mean hydrogen-ion activity rather than hydrogen ion concentration (HEM 1985). The hydrogen ion sources in the water are the dissociation of water molecules and the dissolved solids. The pH is affected inversely by temperature. Water is said to be either acidic or alkaline. The pH of most groundwater results from the balance between the dissolved CO_2 gas derived from the atmosphere as well as biological activity and the dissolved carbonate as well as bicarbonates derived from carbonate rocks. Most of the groundwater in the study area has pH values that range from about 7.4 to 8.2. Slightly, alkaline conditions generally occur in limestone and dolomite terrains.

The average pH value is found to be 7.5 and 7.6 for the phreatic aquifer and the confined aquifer, respectively. The Eocene western sub-aquifer have an average of 7.5 and the Eocene eastern has an average of 7.4 pH. The Pleistocene as well as Cenomanian has the same average pH value of 7.6. Springs in the study area as well as some wells of the phreatic sub-aquifers have pH values different from average, which is due to water pollution. This pollution is caused by cesspools and septic tanks, which are spreaded over the whole area. The pH value of the Wadi Faria surface water was measured between 8.2 and 8.4. This surface water infiltrate through fractured outcrops into the Eocene eastern and Pleistocene sub-aquifers causing the increasing of pH for some wells and springs. The contour map of the pH in the Faria basin is illustrated in Fig.5.3.

The measured pH values in the field are smaller that those measured at the laboratory. For the Eocene western sub-aquifer, it ranges between 0.1 and 0.4 after groundwater recharge and

84

from 0.1 to 0.7 before groundwater recharge. Large differences are shown in springs of the study area. Phreatic sub-aquifers show a range between 0.1 to 0.5 (after groundwater recharge) and 0.3 to 0.4 (before groundwater recharge) for Neogene sub-aquifer, and 0.4 for the Pleistocene sub-aquifer. Cenomanian sub-aquifers show a range between 0.2 and 0.5 (after groundwater recharge) and -0.2 to 0.6 (before groundwater recharge).
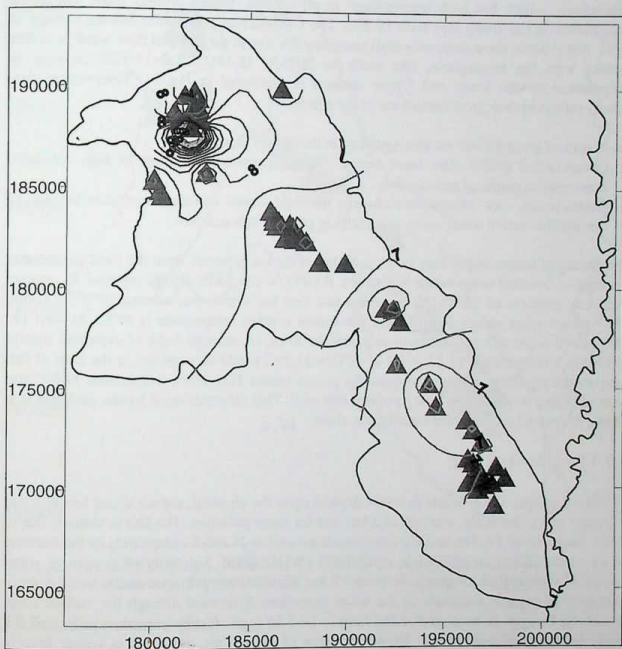
Fig. 5.3 : The contour map of the pH in the Faria basin.

5.6.3 Temperature

Temperature values are important for calculating the saturation indices with respect to mineral phases. The temperature measurements are used as well to identify deep wells and thermal water. Temperature measurements are recorded in degrees Celsius (°C). Temperature affects all physical and chemical characteristics of groundwater, such as EC, pH and DO.

85

The average temperature of the whole aquifer system is 23.3°C and its average for the phreatic and confined aquifers are 23.2°C and 23.6°C, respectively. The temperature of all phreatic sub-aquifers shows an increasing trend from west to east; 21.7°C for the Eocene western sub-aquifer, 24.5°C for the Eocene eastern sub-aquifer and 25.5°C for the Pleistocene sub-aquifer. This is due to the phreatic nature of sub-aquifers that have a free contact with the atmosphere, which has high temperatures in all seasons. Badan Springs show the lowest temperature in the study area with 19.3°C. The Cenomanian sub-aquifer has an average of 24°C. Some wells show extremely high temperatures, due to the fact that their water is in free contact with the atmosphere, like wells 18-18/25A, 18-18/35 and 19-17/8. A map of temperature for the lower and Upper aquifers is illustrated in Fig.5.4. Temperature data closely reflect hydrological conditions of the aquifer.

Two types of groundwater are distinguished in the area of study:
1. Groundwater colder than local annual surface temperature occurs in high altitudes, especially in confined sub-aquifers.
2. Groundwater with temperature close to the local annual surface temperature belongs to the shallow active water cycle, especially in phreatic sub-aquifers.

The observed temperatures may be close to temperatures expected from the local geothermal gradient or detected temperature anomalies. BARTOV and BEIN (1977) reported an average local heat gradient of 1.8°C/100 m, which less than the world wide average of 3°C / 100m. The average rainy season is 10°C and the annual average temperature is 18°C. At well 18-18/37 (well depth 413 m, depth to water table 90.53 m, i.e. average depth of exploited aquifer is 320m), a temperature of $1.8 * 3.2 + 18°C = 23.7°C$ would be expected in the case of full temperature equilibrium, for slow intake in porous media. However a temperature 24.9°C has been obtained for the water pumped from this well. This indicates rapid karstic recharge that allows for partial temperature equilibrium alone. 26,4

5.6.4 Dissolved oxygen

Dissolved oxygen (DO) levels in water depend upon the physical, chemical and biochemical activities in a water body, and acts as a key test for water pollution. The DO in water is due to redox reactions of Fe, Mn and Cu compounds as well as N and S compounds or the bacteria effect of the oxidation of organic compounds (WHO 1989). Solubility of oxygen in water decreases with higher temperature. Most of the dissolved oxygen presumably is used up in oxidation of organic materials as the water percolates downward through the vadose zone. Dissolved Oxygen is measured at the field to be 5.24 mg/L for the phreatic aquifer and 2.7 mg/L for the confined aquifer. Higher contents of oxygen are measured in winter than in summer, because of infiltration processes occurs in winter.

laboratory measurements found DO to be 5.3 mg/L for the phreatic aquifer and 5.4 mg/L for the confined aquifer. A trend of decreasing DO is shown towards the east within the phreatic sub-aquifers (5.7 to 3.7 mg/L). The Pleistocene sub-aquifer have less oxygen than the Eocene western sub-aquifer (5.7 mg/L). The confined aquifer shows identical amounts of DO in its western and eastern parts. A slight range of DO varieties between sub-aquifers are recorded, except for the Eocene western sub-aquifer. The Eocene western sub-aquifer shows

86

an extreme amounts of DO of 6.5 mg/L in wells 18-18/32 and 18-18/33.
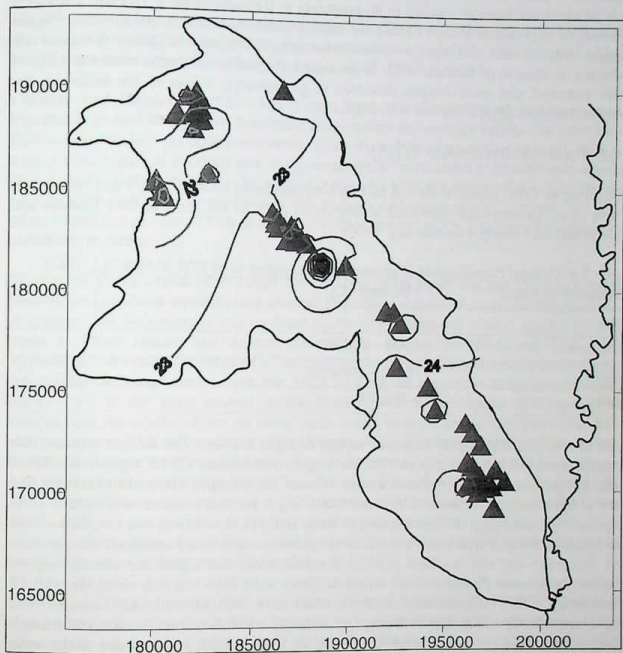
Fig.5.4: The contour map of temperature (°C) of the groundwater in the Faria basin (°C)

5.6.5 Redox potential (Eh)

The oxidation reduction potential is the key factor for mobility of some important elements in water such as Fe, Mn, S and N. The mean Eh is measured to be 553.3 mV for the Eocene western sub-aquifer, 534 mV for the Neogene sub-aquifer, 570 mV for the Pleistocene sub-aquifer, and 601 mV for the Eocene eastern sub-aquifer. The Eh of the confined aquifer is measured to be 609 mV. The smallest value is seen in the springs of the study area.

Redox potential for equilibrium processes in the groundwater is expressed in terms of pE (dimensionless) or Eh (volts). Eh measures the tendency of the water to oxidize or to reduce

87

dissolved constituents. Redox potential is defined as the energy gained in the transfer of 1 mole of electrons from an oxidant to H_2 according to the equation $pE = 16.9$ Eh. The redox potential is a potential that is caused by various redox reactions in groundwater. Higher oxygen supplies and recharge of groundwater occur in winter. Oxidation processes are preferred, leading to an increase of Eh in groundwater, because infiltration water has a higher redox potential and more oxygen dissolved in groundwater. Values of Eh decline as the dissolved oxygen (DO) decreases with depth.

5.6.6 Total dissolved solids (TDS)

According to TDS, groundwater can be classified into fresh, brackish, saline and brine water (Table 5.4). Groundwater dissolved solids (salts) exist in the form of ions (cations and anions) and zero charged species (e.g. SiO_2).

Table 5.4: General classification of groundwater according to its TDS (CARROLL 1962).

Category of water	TDS (mg / L)
Fresh	0 - 1,000
Brackish	1,000 - 10,000
Saline	10,000 - 100,000
Brine	> 100,000

TDS of the phreatic aquifer increases rapidly towards the east. The Eocene western sub-aquifer shows the lowest value of TDS (402 mg/L) and reaches 1551.5 mg/L in its eastern parts. Pleistocene sub-aquifer shows a mean value of 1608.4 mg/L. The confined sub-aquifers have a TDS ranging between 636.8 and 608.6 mg/L for their western and eastern parts, respectively. According to TDS, the area of study could be divided into two categories: fresh and brackish water. Fresh water lies within the phreatic western sub-aquifer (Eocene western and Neogene) and the confined aquifer. Brackish water lies within the phreatic eastern (Eocene eastern and Pleistocene sub-aquifers). Some wells show brackish water like well 19-17/46 and 19-17/53 (Cenomanian eastern), which show TDS values of 1203.2 and 1695.2 mg/L, respectively. That means leakage of brackish water from the phreatic eastern sub-aquifers into the Cenomanian eastern sub-aquifer has occurred, which is due to the semi-confined nature of this reservoir. A relationship between TDS and EC is shown to be :
TDS = 0.54 * EC for the whole system. A constant factor of 0.55 for the phreatic and 0.53 for the confined aquifer was calculated.

A calculated TDS for samples of the study area indicates that the water is fresh for the sub-aquifers of phreatic western and the confined aquifer. The water has a composition of $Ca^{2+} > Mg^{2+} > Na^+$ and $HCO_3^- > Cl^- > SO_4^{2-}$. Repeatedly collected samples show a slight variation in the ionic composition. The increase of TDS in springs from Nablus to Faria probably results from longer contact with rock. The vertically and laterally increased TDS is due to dissolved gypsum and halite.

5.6.7 Major ions

Major ions occur in concentrations ranging from 5 to 1000 mg/L. They form the bulk of the dissolved constituents in water and are divided into cations (positively charged): Ca^{2+}, Mg^{2+}, Na^+, K^+ and anions (negatively charged): HCO_3^-, SO_4^{2-}, CO_3^{2-}, Cl^-, NO_3^-

Calcium and Magnesium (Ca^{2+}, Mg^{2+}) stem from the dissolution of carbonate rocks. Calcium is derived from calcite dissolution and therefore balanced by HCO_3^-. An increase of Ca^{2+} concentration is the enrichment factor, which exceeds in all cases that of Mg^{2+}. Ca^{2+} has a mean of 128 mg/L in the study area. A big range of Ca^{2+} is recorded in phreatic sub-aquifers (479.6 mg/L) with a mean of 134.7 mg/L, compared with the range of the sub-confined aquifers (218 mg/L) that have a mean of 109 mg/L. A wide range of Ca^{2+} contents is a result of the increasing amount of CO_2 in the aquifer. This amount of Ca^{2+} defines the aquifers as carbonatic in nature.

Magnesium shows a mean of 35.2 mg/L for the whole system and 38.8 and 28.9 mg/L for the phreatic and confined aquifers, respectively. There is a variety of range in the amount of magnesium for both phreatic and confined aquifers. The confined aquifer shows the same mean for both eastern and western Cenomanian sub-aquifer (28.4 and 27.2 mg/L, respectively). A trend of increasing Ca^{2+} towards the east is recorded, especially in the Eocene sub-aquifer (88.3 mg/L in the west and 257.8 mg/L in the east). The Neogene sub-aquifer shows Ca^{2+} of the same amount as the Eocene western sub-aquifer (90 mg/L). The Cenomanian sub-aquifer shows the same mean in the western and eastern parts, due to its confined nature. This is also due to slight changes of CO_2 in the groundwater. The rocks of the phreatic aquifer are highly fractured, causing CO_2 to enter the groundwater from the soils that cover the rocks of the phreatic aquifers. The second round of water sampling (July 1997, after recharge) shows greater amounts of Ca^{2+}, especially for Eocene springs, which show double Ca^{2+} contents than that of the first round of water sampling (September 1996, before recharge). The springs of both Eocene and Neogene sub-aquifers show less amounts of Ca^{2+} compared to those of the groundwater wells.

The Mg^{2+} increases from the western Eocene (20 mg/L) towards the eastern Eocene (73 mg/L) sub-aquifer. The Mg^{2+} of the Neogene sub-aquifer shows the same as the Eocene western sub-aquifer (21.1 mg/L). Mg^{2+} of the Pleistocene sub-aquifer shows an extreme amount (102.6 mg/L), due to the volcanic nature of the sub-aquifer. The amount of Mg^{2+} and Ca^{2+} in both phreatic western and confined aquifers reflects the limestone nature in the western phreatic and confined aquifers and limestone to dolomite nature for the eastern phreatic aquifer. Some of the wells and springs of the phreatic aquifer show a large amount of Mg^{2+}, which reflects the dolomitic strata within the limestone sub-aquifer, especially for the Eocene and Neogene sub-aquifers. There is a large range in Mg^{2+} (51.8 to 384.3 mg/L) in the Pleistocene sub-aquifer.

Towards the Jordan Rift, an increase in Mg^{2+} is observed (from 1.6 to 8.4 meq/L). This increase in Mg^{2+} can be attributed to water-rock interactions with the aquifer rocks which change in composition from limestones to dolomites eastwards. The higher total dissolved ions TDI content along with the rise in Mg^{2+} values is attributed to contribution by local

89

shallow aquifers that have flushed the salts from the nearby outcropping lisan formations.

Sodium and potassium (Na⁺ and K⁺): Sodium in groundwater stems from rain waters and is derived from rock weathering. A decrease of K is observed for groundwater at the outlets of basalt aquifers and a sharp increase is observed in values of the ratio Na / K.

The mean of Sodium shows the same value in the Eocene western and Neogene sub-aquifers (32.4 and 34.4 mg/L , respectively). Sodium in the eastern Eocene sub-aquifer shows a large range of distribution, between 58.5 and 269.1 mg/L . That means, it is six times greater than the western sub-aquifer. Na^+ of the Pleistocene sub-aquifer shows a mean of 249.1 mg/L. A decreasing trend of Na^+ is shown towards the east (59.3 to 40.5 mg/L) in the confined aquifer. Otherwise, the mean of the phreatic aquifer is greater than that of the confined aquifer (55.4 mg/L). The mean of Na^+ for the whole system is 74.4 mg/L. The Faria group springs, as well as the Shibli group springs, show greater values (double) than that of the Badan group springs.

Potassium shows a mean of 3.4 mg/L for the confined aquifer and 6.1 mg/L for the phreatic aquifer. K^+ of the Eocene western and Neogene sub-aquifers has a small mean of 11.9 to 2.4 mg/L, in contrast to the Eocene western and Pleistocene sub-aquifers, which are of 13.5 to 20.1 mg/L, respectively. A small trend of increasing K^+ is shown in the Cenomanian aquifers towards eastern sub-aquifers. Phreatic western sub-aquifers as well as the Cenomanian western sub-aquifer show a little variety in contrast to those in eastern parts of the Faria basin.

Potassium is a potential indicator of anthropogenic effects on groundwater, namely agriculture use in the recharge area of the aquifer. In the study area, high contents of potassium (> 6 mg/L) in the groundwater result from fertilising with KNH_4 near the wells. Higher concentrations of K^+ below the water table indicate a relatively short residence time in unsaturated zone.

Na^+ and K^+ of the Eocene western and Neogene sub-aquifers differ from those of the Eocene eastern and Pleistocene sub-aquifers. The latter shows a large amount, which reflects the basalt origin of Pleistocene, while the Eocene consists of evaporates and gypsum. The confined aquifer as well as phreatic western sub-aquifers consists of limestone and dolomite.

Bicarbonate (HCO₃⁻), m- and p-Value (HCO₃⁻ and CO₃²⁻): The amount of HCO_3^- in both phreatic and confined aquifers (301.4 and 316.4 mg/L), reflects the carbonate nature of the aquifer systems in the area. Both of them range between 209.9 and 405 mg/L. They have the same amount of median and mean values, which reflects their normal frequency distribution. The western part of the Faria basin shows larger varieties of HCO_3^- than those of the eastern (double), with an obvious trend of increasing towards the east. The confined aquifer shows identical amounts in both eastern and western parts.

The p-value is measured to be 2.9 mmol /L for the Eocene western and 2.3 mmol /L for the Neogene sub-aquifer and shows an increasing trend towards the east, reaching a value of 5.4 mmol /L. In the confined aquifer, p-value is measured to be 2.2 mmol /L for Cenomanian sub-aquifers. The m-value is found to be 5.25 mmol /L for the Eocene eastern and 5 mmol /L

for the Neogene sub-aquifers. It is found to be 5.25 5 mmol /L for the confined aquifers.

Sulfate (SO_4^{2-}): Often sulphate contents increase with chlorine contents. The phreatic western sub-aquifers as well as the confined aquifer show a range of SO_4^{2-} between 18.4 to 36.4 mg/L; the latter shows smaller amounts of SO_4^{2-} than those of the former. The increasing trend of SO_4^{2-} towards the east is recorded, as the followings profile of sub-aquifers: Eocene western 18.4 mg/L; Neogene 24.1 mg/L; Cenomanian western 26.5 mg/L and Cenomanian eastern 36.4 mg/L. All sub-aquifers show a wide range of varieties between 7.8 mg/L in the Hamad and Badan spring (Eocene western) to 121.3 mg/L in the well 19-17/6 (Eocene eastern). Phreatic and confined aquifers show the mean of 33.6 mg/L and 32.3 mg/L, respectively. The increasing of SO_4^{2-} in the eastern outcrops is due to anhydrite rocks in the Lisan formation. The amount of SO_4^{2-} in both phreatic western and confined sub-aquifers reflects the nature of carbonate rocks.

Evaporates occur as independent rocks, such as gypsum, but are common also as veins in marine sedimentary rocks, mainly clay, or as secondary minerals in soils, mainly in arid zones (MAZOR 1985). Furthermore, sulphur is enriched in the soil by fertilising and by release of sulphur during decomposition of organic material (MATTHESS 1990)

Chloride (Cl^{-1}): Chloride content was found to be increased in the east and southeast provinces, especially in Pleistocene and Eocene eastern sub-aquifers. Low Cl⁻ content was recorded in the phreatic western sub-aquifers. The mean of the eastern phreatic sub-aquifers are found to be 10 times greater than those of the western phreatic sub-aquifers. The Eocene western sub-aquifer shows an average of 62.9 mg/L and increasing slightly towards the Neogene sub-aquifers (67.3 mg/L). Pleistocene shows extreme values of Cl⁻ (908.9 mg/L). The wells 18-18/17 of the Eocene western and 18-18/19A of the Neogene sub-aquifers show Cl⁻ amounts of twice times the average in both sub-aquifers. The springs of the Badan group are of lesser Cl⁻ than those of the Faria group. The Cenomanian sub-aquifer in the eastern parts has a slightly higher amount compared to those of the western parts. An extreme value of 504.7 mg/L is recorded in well 19-17/46 of the Cenomanian eastern sub-aquifer. The Pleistocene sub-aquifer shows an extreme amount up to 2108.7 mg/L in well 19-17/28. The high amount of Cl⁻ in the Eocene (east) and Pleistocene is due to chlorine-bearing rocks in the alluvium as well as Lisan formation, which contains a high amount of NaCl. The intensive use of fertilizers in the agricultural area is an additional source, which causes this increase of chloride content. The water of the eastern phreatic sub-aquifers is not potable for drinking and is used for agriculture. All springs in the Faria basin show a slight variability of Cl⁻ in mg/L within the period 1967/68 to 1991/92 (Fig.5.5).

Nitrate NO$_3^-$: The sources of NO$_3^-$ are input through precipitation and the decomposition of plant debris, animal waste and nitrate fertilizers. The cause of high amounts of NO$_3^-$ are the return flows from irrigation, disposal of industrial and urban waste and wastewater. Industrial waste chemicals may contain high concentrations of nitrogen. This will cause nitrification phenomena (oxidation and reduction). NO$_3^-$ is significantly enriched in waters of the populated and cultivated areas as a result of the intensive use of fertilizers and contamination by sewage.
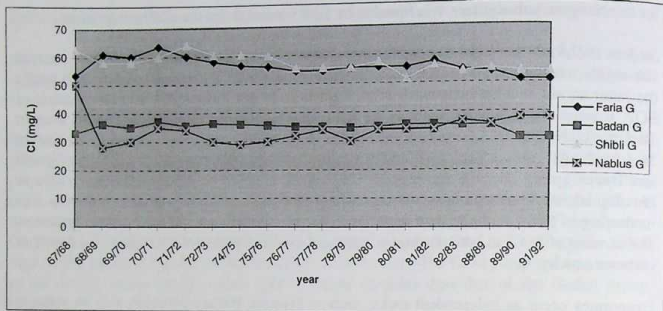
Fig. 5.5: The trends of chloride content in mg/L of the Faria group springs for the
period 1967- 1992

The NO_3^- has a mean of 43.5 mg/L for the phreatic aquifer and 21.8 mg/L for the confined aquifer. NO_3^- concentrations are higher in the Eocene western and Neogene sub-aquifers (45.4 and 52.6 mg/L respectively). The eastern phreatic aquifer shows less amounts of NO_3^- (22.2 to 31 mg/L). The Cenomanian sub-aquifer shows less amounts in the western parts (15.5 mg/L) and increases towards the east (24.5 mg/L). The Neogene sub-aquifer shows a large NO_3^- value 190.8 mg/L in well 18-18/31. The Eocene wells in the western sub-aquifers: 18-18/ 17, 16, 25A, 32 are polluted with NO_3^-, with extreme amounts reaching 182.5 mg/L. The pollution of the Eocene western sub-aquifers is due to leakage from septic tanks and cesspools in the area. The pollution of the Neogene sub-aquifer is due to the wastewater from the Nablus municipality. Agricultural fertilizers in both the Eocene and Neogene sub-aquifers are also cause an increase in the amounts of NO_3^- in the groundwater. The confined aquifer is not yet polluted with NO_3^- due to its confined nature and greater mean residence time.

Silica SiO_2: The presence of silica in groundwater is attributed to the chemical weathering of silicate minerals. Temperature and the rate of water movement through the rock affect the weathering and the degree to which silica dissolves in water. The mean of SiO_2 in the phreatic aquifer is found to be 38 mg/L, while it is found to be 34.2 mg/L in the confined aquifer. The Eocene western sub-aquifer shows the greatest amount of SiO_2 (43 mg/L). It decreases in the Eocene sub-aquifers, reaching 32 mg/L in the eastern parts. A maximum value of SiO_2 is found in Ein Dulieb spring (Eocene western), which ranges between 58 and 49 mg/L, after and before recharge, respectively. This is due to silisified limestone with chert laminations in the Eocene sub-aquifers. An increase in SiO_2 towards the east in the confined aquifer is also observed. It shows a mean of 39 mg/L for the western Cenomanian and 29 mg/L for the eastern Cenomanian sub-aquifers.

5.6.8 Minor ions and trace elements

Trace constituents occur in low concentration of less than 0.1 mg/L. They are important,

92

because they limit the use of water for certain purposes. Examples are heavy metals like Cu, Cd, Mn, Cr, Co, Pb and pesticides.

Iron (Fe): Iron values are higher in the phreatic sub-aquifers, especially the Eocene eastern sub-aquifer, which is due somewhat to the ferrygenous lithology of the aquifer. Water may dissolve iron upon contact with metal well casing, pump parts and piping. Iron is common in many igneous rocks and is found as trace amounts in all sediments and sedimentary rocks. The average concentration of Fe is found to be 22.1 and 17.8 μg/L in the phreatic and confined aquifers, respectively. A big difference in Fe is found between the phreatic sub-aquifers (105.8 μg/L) comparing to the confined aquifer (46.6 μg/L). The average concentration of Fe in the whole aquifer system ranges between 17.5 μg/L (Eocene eastern) and 24.7 μg/L (Eocene western). A trend of decreasing Fe towards the east is recorded. The springs show the lowest concentration of Fe (10 μg/L) in the area. Some wells such as 18-18/11A (105.8 μg/L) and 18-18/4 (88.5 μg/L), show extreme values of Fe, due to the corrosion of well screens in the study area. The confined aquifer shows identical values in both eastern and western directions.

Manganese (Mn^{2+}): Manganese is less abundant in the groundwater than iron (KEMMER 1977 in ARAD et al. (1984)). It acts as soluble manganous bicarbonate, which changes to insoluble manganese hydroxide when it reacts with atmospheric oxygen. Manganese is enriched in the eastern sub-aquifers, which are known for their manganese mineralization. The mean of Mn^{2+} for the phreatic aquifer is found to be 1.4 and 1.8 μg/L for the confined aquifer. The average of Mn^{2+} for the Eocene sub-aquifer increases from 0.4 μg/L (western) to 9.1 μg/L (eastern). The Pleistocene sub-aquifer shows a greater average value (3.2 μg/L) than those of the Cenomanian sub-aquifer (2.2 μg/L for the western and 1.5 μg/L for the eastern). In the Faria and Badan group springs, a very small amount of Mn^{2+} is recorded with respect to other springs of the same group. Abnormal values of 20.8 and 14.14 μg/L may be due to the Mn^{2+} ores in the alluvium rocks of the alluvium formation.

Flouride (F$^-$), Iodine (I$^-$) and Bromide (Br$^-$): Flouride is mainly enriched in waters of the southeastern parts of the Faria basin reflecting the close association with phosphorites and the effects of desert dust. The F$^-$ is enriched in southeastern and eastern parts. In the Pleistocene sub-aquifer it is associated with phosphoritic formations, which contain clastics of magmatic rock origin (KAFRI et al. 1988). The western phreatic and the confined aquifers show an F$^-$ average of 0.2 mg/L. This average increases rapidly, reaching 0.6 mg/L towards the Eocene eastern and Pleistocene sub-aquifers (0.4). This increase is also due to the intensive use of fertilizers in agriculture, as well as to the Lisan formation.

The I$^-$ is found to be less than the detection limit of 0.2 mg/L in the whole aquifer system. Bromide is often determined in arid and semi-arid regions, where the water is used for irrigation. It is necessary in very small quantities for normal growth of all plants. The average concentration of Br$^-$ is found to be 0.8 mg/L in sub-aquifers of the study area.

Phosphate (PO$_4^{3-}$): Dissolved phosphorous in the water occurs as phosphoric acid (H$_3$PO$_4$) and its dissociation products. The phosphate is released to the environment from animal fertilizers, animal wastes, sewage and detergents. Phosphate ranges between 0 and 0.5 mg/L

for the whole aquifer system with an average of 0.2 mg/L. The average concentration in the phreatic sub-aquifers is found to be 0.2 (western) and 0.3 mg/L (eastern). The PO_4^{3-} average for the water of the Wadi Faria with the mixed wastewater (8 samples) shows an average of 0.3 mg/L; one extreme value of 3.38 mg/L was found. After the percolation and infiltration of this water to the groundwater, the PO_4^{3-} value in the eastern sub-aquifers may increases. The PO_4^{3-} of the Eocene western sub-aquifer was found to be 0.08 mg/L after the recharge period, which has a lesser amount than that before the recharge period, 0.2 mg/L. Springs in the eastern parts show higher values of PO_4^{3-} than those in the western parts, and this can be explained by the presence of phosphate formations within the Lisan and alluvium formations.

Cadmium (Cd): The western phreatic and the confined sub-aquifers show average concentration of Cd 4.5 µg/L and 9.4 µg/L, respectively. The Eocene western sub-aquifer shows the lowest amount of 6.1 µg/L, while the Eocene eastern sub-aquifer shows a very high average amount of 477.3 µg/L. A large range of Cd is found in the Pleistocene sub-aquifer, which has a maximum amount of 1,600 µg/L in well 19-16/1.

Copper (Cu): Copper shows an average of 4 µg/L for the whole aquifer system. The Eocene sub-aquifer as well as Cenomanian western sub-aquifers show a slight increase of Cu towards the east, ranging from 4.9 to 2.6 µg/L for the Eocene sub-aquifers and from 4.3 to 3.3 µg/L for the Cenomanian sub-aquifers.

Lead (Pb): Lead is found to be 3.8 µg/L for the phreatic aquifer and 2.7 µg/L for the confined aquifer. Phreatic sub-aquifers have an amount of Pb ranging from 4.2 to 5.5 µg/L, except the Neogene sub-aquifer, which has an amount of 1.3 µg/L. The confined aquifer shows a decreasing trend towards the east. The largest amount of Pb is found in the Eocene western sub-aquifer and it has a range of 0.7 to 12.7 µg/L.

Zinc (Zn): The aquifer system of the whole area has an average Zn concentration of 12.6 µg/L and it ranges between 0 and 25.4 µg/L. The confined aquifer as well as the phreatic eastern sub-aquifers show smaller values of Zn than sub-aquifers of the phreatic western sub-aquifers. The Pleistocene sub-aquifer shows the value of 10.2 µg/L which is the lowest value in the whole area.

5.6.9 Changes in trace element contents along the flow path

The concentration of the dissolved ions is increased with distance for calcium - bicarbonate water in the western parts to sodium-chloride water in the eastern parts. An increase in the chlorine content along the flowpath is found to be accompanied by a slight increase of F and B, whereas Mn shows no significant changes. As water travels down the flowpath, it increases the total dissolved solids from 15 meq/L in the Faria area of the western part to the Jordan Rift of the eastern part to 67.1 meq/L. The average mean of major ions of all sub-aquifers of the Phreatic aquifer in the Faria basin shows an increasing trend towards the east and southeast - towards the Jordan Rift valley (Fig. 5.6). Calcium, magnesium, chloride and sodium show a strong increasing trend from the Eocene western sub aquifer towards Pleistocene in the eastern part of the basin. As compared to the groundwater of the Jordanian

94

side of the Rift Valley, all ions show a progressive increase towards the Jordan Rift valley (EL-NASER 1991).
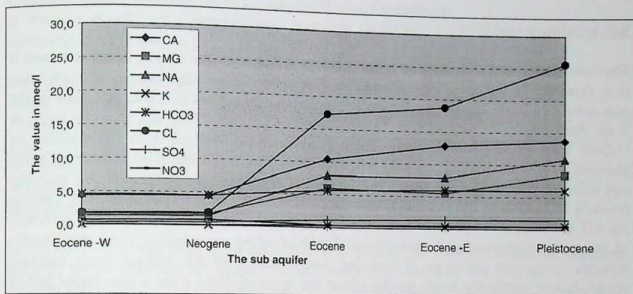
Fig. 5.6: The average mean of major ions in the W-E and NW-SE profile directions.

5.7 Microbiological analyses

Different micro-organisms can be found in natural groundwater and surface water. The most important organisms are bacteria, viruses, yeasts, algae and protozoa. Virological analyses are not carried out in natural analyses, while yeast and algae are of less importance in the groundwater (CDM 1997). The most prevalent micro-organisms in water are bacteria. Some of them can be pathogenic and cause disease to human beings, like cholera, shigella and salmonella. The presence of pathogenic bacteria in water indicates the degree of contamination in the water and is a common indicator of water polluted by human wastes. The coliform group is the principal indicator of suitability of water for domestic and other uses.

Analyses for fecal Coliform (FC) and total Coliform (TC) are carried out to determine whether a water is suitable for domestic purposes. Twenty analyses for FC and TC were conducted for the upper and lower aquifers (Appendix 5.3) and indicated that the upper aquifer is contaminated with human wastes, through septic tanks in the area and the wastewater of the Nablus municipality, which is draining into Faria Wadi. The Eocene sub-aquifer contains a wide range of FC and TC, with an increasing trend towards the east. The Neogene and Eocene eastern sub-aquifers show a high degree of contamination, because of their direct location under the influence of the Nablus wastewater. Pleistocene wells show less of FC and TC, because of their high salinity. The lower aquifer is not contaminated, reflecting its confined nature.

5.8 Indicators for water quality

Water originating from limestone formations can be regarded as naturally uncontaminated. The concentrations of Na^+ as well as Cl^- and the bacteria found in the organically polluted

95

water indicate sewage pollution (eastern Nablus sewage). Water from Lisan formation is found to be contaminated.

5.8.1 Salinity / TDS

The concentration of chloride ions is the common indicator for the salinity of aquifers and it is a function of the flow regime and the distribution of salinity sources. The chloride concentrations in the aquifers in the natural replenishment regions near the watershed of the West Bank are of 25 - 40 mg/L in Nablus as well as Jerusalem hills and 60 to 80 mg/L in Hebron hills (SCHWARTZ 1980). These concentrations originate from the washout of airborne salts by the rainfall and their levels reflect the fluctuation ratios between evaporation and infiltration from place to place. The amount of dissolved solids in the rainfall accounts for only 10 percent of the chloride concentration in the groundwater (DANIEL et al. 1982 in ARAD and BEIn (1986)). Other sources are the sea water around the Dead Sea and diffusion of brines along the Jordan Valley. A lateral shift of saline water bodies along the margins towards centres of pumpage is recorded. Intensification of the leakage from brackish aquitards that overlie the lower aquifer causes the rising of saline water bodies under part of the pumping fields (over-exploited basin).

Lower Cenomanian groundwater in the eastern aquifers is initially of low salinity. Flowing to the east of the recharge area where the aquifer formations outcrop downwards toward the deeper saline groundwater in the Jordan Valley, the aquifer's freshwater mixes with saline water and becomes brackish. According to the salinity, two groundwater bodies were identified a low salinity groundwater originating from Cenomanian as well as Eocene sub-aquifers, and a high salinity groundwater originating from Pleistocene and Basalt sub-aquifers. The changes in the chlorine composition of groundwater indicates an increasing trend toward the eastern direction of the area.

The type and concentration of salts depend on the environment, movement and the groundwater source. STARINSKY (1974) suggested that the calcium - brines, which are found in the subsurface of the Jordan Rift valley represent a residual product of the evaporated Pliocene sea water, which precipitated halite during the occurrence of its evolution in the Sdom depression, within the rift. After their partial evaporation, the Mg-rich brines interacted with sediments of this depression and carbonates along the margins of the rift thus acquiring Ca-Cl composition. These brines are diluted by fresh water. Below the fresh-water body, there is a body of salt water (in the lower aquifer). Uncontrolled pumping in the fresh-water body could cause a upconing salt water towards the fresh water. This will enlarge the transition zone between the salt and fresh waters in the area. The source of salt water in the area is brine water captured within the layer of the Lisan in the period when the level of the Dead Sea was high at an elevation of - 180 m (in the last rainy period 6,000 - 15,000 years ago) and which spread westward into the layers of the Ajlun (Judean) group (confined aquifer) in some places where a contact between them is taking place. A certain washing of brine water by fresh water occurs towards the Jordan Valley.

96

5.8.2 Soluble sodium percentage (SSP) or % Na

Soluble Sodium Percentage (% Na) is calculated using the equation:
% Na = (Na+K) / (Ca+Mg+Na+K) in meq/L. WILCOX (1955) classified the water according to his % Na and EC (mS/ cm) from excellent to unsuitable water (Table 5.5).

Table 5.5: The classification of water according to WILCOX (1955).

Class	% Na	EC µS/cm
excellent	< 20	< 250
good	20 - 40	250 - 750
permissible	40 - 60	750 - 2000
doubtful	60 -80	2000 - 3000
unsuitable	> 80	> 3000

The % Na is calculated to be in the range of 0.01 to 0.02 for the western Phreatic sub-aquifers and 0.01 for the confined sub-aquifers, while it ranges between 0.11 and 0.28 for the eastern phreatic sub-aquifers. The Pleistocene sub-aquifer shows extreme values and an average of 0.25, thus leading to the conclusion that the western phreatic sub-aquifers as well as the confined aquifer have excellent to good classes of water, while the eastern phreatic sub-aquifers have a permissible class of water.

5.9 Graphical presentation of results

Graphs are useful for display purposes, for comparing analyses and for emphasizing similarities and differences. They can also aid in detecting the mixing of water of different compositions and in identifying chemical processes occurring as groundwater moves.

5.9.1 Ion distribution and the chemical composition

The Total dissolved ions (TDI) for major ions in the area of study is calculated to be 15 to 15.6 meq/L for the Eocene western and Neogene sub-aquifers, respectively, and ranging between 20.9 to 20.5 meq/L for the confined sub-aquifers. TDI is calculated to be 67.1 meq/L for the Pleistocene sub-aquifer and 53.4 meq/L for the Eocene eastern sub-aquifer. The increasing trend is seen towards the east. Several sub-aquifers have relatively high Na contents and their Na/Cl molar ratios approach and exceed 1. The highest ratios are found in basaltic aquifers and in aquifers rich in basaltic clastic material.

The following hydrochemical parameters in meq/l are plotted against each other (Fig. 5.7): (Ca+Mg) vs. (K+Na), (Ca+Mg)/ (HCO₃) vs. ((K+Na)/Cl), Mg vs. Ca, SO₄ vs. HCO₃, Ca vs. (SO₄+ HCO₃), HCO₃ vs. Cl and SO₄ vs. Cl. They form two clusters. Variations of both Ca^{2+} and Mg^{2+} (Fig. 5.7) is an indication of different recharge areas to the aquifer system. The comparison between water samples of different sites while addressing regional changes of the water chemistry is illustrated graphically on maps of important chemical parameters (Fig.- 5.8, - 5.9, - 5.10).

97
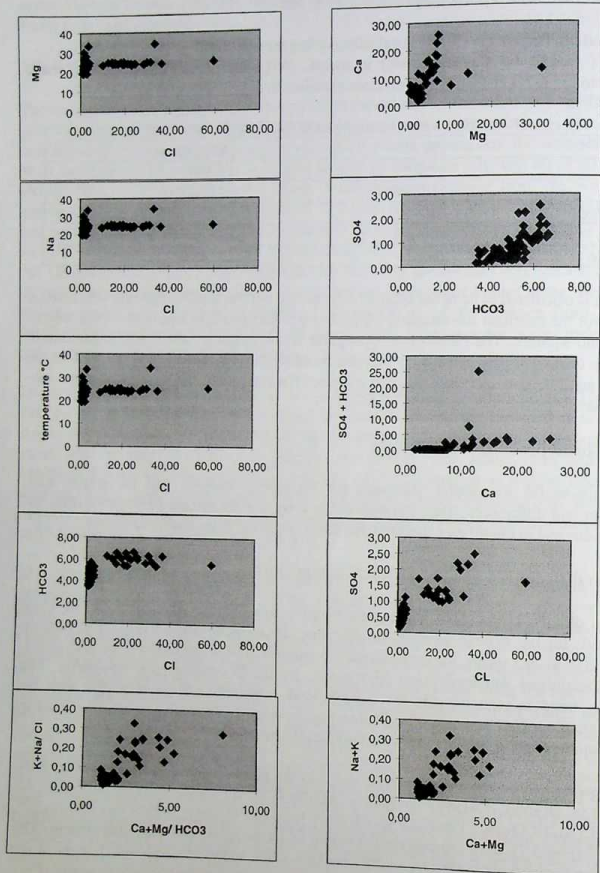
Fig. 5.7: The clustering and correlation as a result of plotting different hydrochemical parameters (meq/L).

98

Water sample concentrations are converted to meq/L for graphical representations. The Surfer was used for plotting maps of water chemistry after identifying the variogram function with Variowin. A spherical method is used after the best fit of data within a diagram of a suitable sill and range values. Groundwater for Windows (GWW)(1994) and Hydrowin software were used to represent graphs of water chemistry data. Schoeller diagrams, trilinear plots (Piper diagrams(1944)), and Durov diagrams were used to represent chemical data and to understand water type bodies (Fig. 5.11).
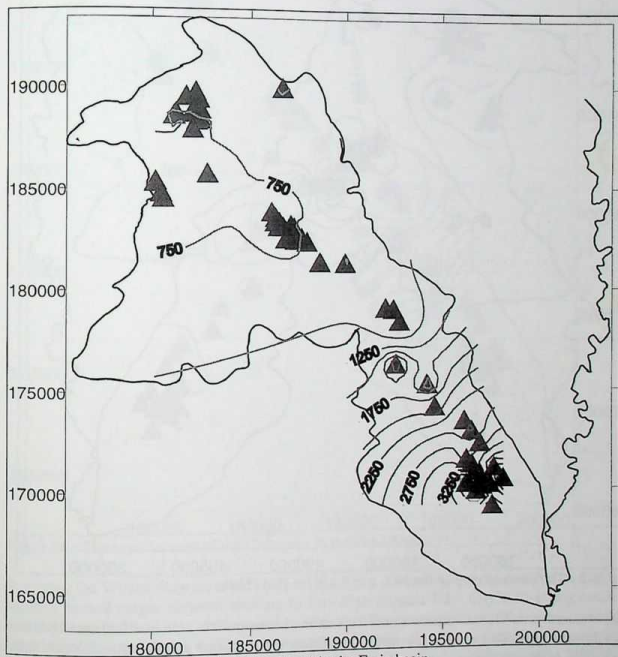
Fig. 5.8 : The contour map of the EC (μS/cm) in the Faria basin.

Piper diagrams were illustrated (Fig. 5.12, Fig. 5.13 and Fig. 5.14) for classifying the groundwater and defining a pathway of chemical evolution. The illustration of all water samples of the Faria basin for both sampling rounds before and after recharge indicates there

99

are very few chemical changes within the aquifer. The majority of the groundwater are found within calcium sodium cation types. Two anion types are found: chloride-sulphate-bicarbonate for the eastern phreatic sub-aquifers and bicarbonate-chloride-sulphate type for the western phreatic sub-aquifer as well as the confined aquifer.
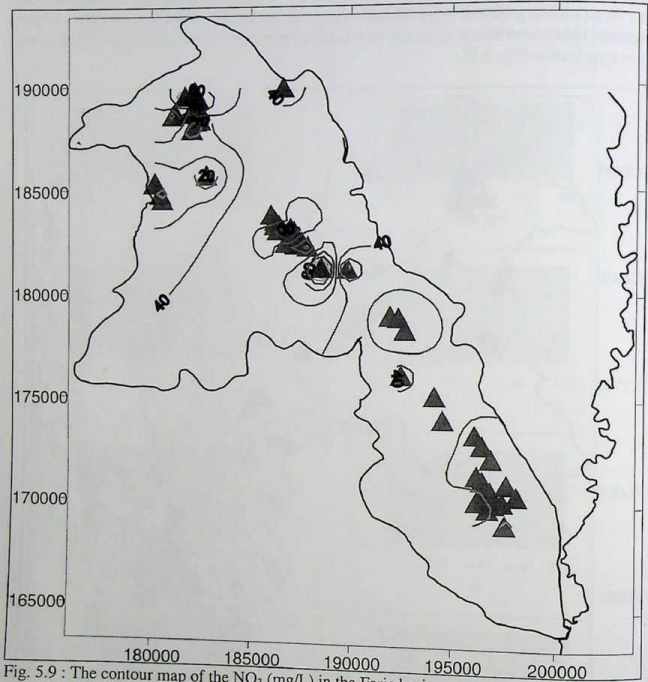
Fig. 5.9 : The contour map of the NO_3 (mg/L) in the Faria basin.

The western phreatic sub-aquifers and the confined sub-aquifers are classified as calcium - bicarbonate type. The eastern phreatic sub-aquifers are classified as calcium - chloride type and some of them as calcium-magnesium-chloride type.

Interpretation of the few historic analyses and comparison with the actual interpretations to yield the conclusion that a very slight chemical change occurred during the last 35 years. A Schoeller diagram of all data indicates that two groundwater bodies are present. They are Ca-

100

HCO$_3$ and Ca-Chloride for the phreatic western and eastern sub-aquifers, respectively. The confined aquifer has a Ca-HCO$_3$ classification.
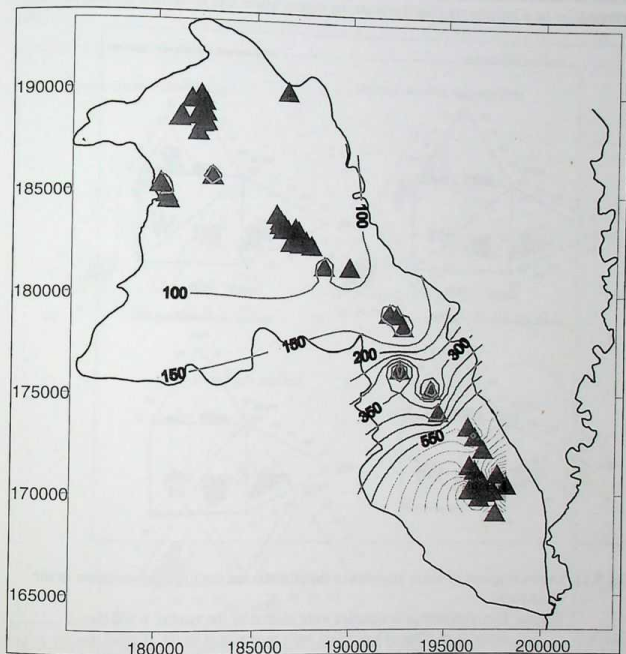
Fig. 5.10 : The contour map of the Cl (mg/L) in the Faria basin.

Applying the Wilcox diagram (1955) (Fig.5.15 and Fig. 5.16) yields to the conclusion that the salinity hazard ranges between medium to very high (classes C2 - C4) with a low sodium (alkali) hazard (class S1). Few samples from the Pleistocene sub-aquifer show medium alkalinity (class S2) and a very high salinity hazard. Thus, the water of medium salinity and low sodium (class C2-S1) can be used for irrigation on all soils (LLOYD and HEATHCOTE 1985). Durov diagram of water analyses (Fig.5.11) reveals that two groundwater bodies are allocated in the Faria basin. Calcium-magnesium-bicarbonate type is in the western phreatic sub-aquifers and in the confined aquifer and calcium-magnesium-choride type in the eastern phreatic sub-aquifers. Durov diagram shows that the calcium-magnesium-choride type lies

101

within the area of ion exchange; while the calcium-magnesium-bicarbonate type lies within the area of reverse ion exchange. Both of them are not lying on the line of simple dissolution or mixing.
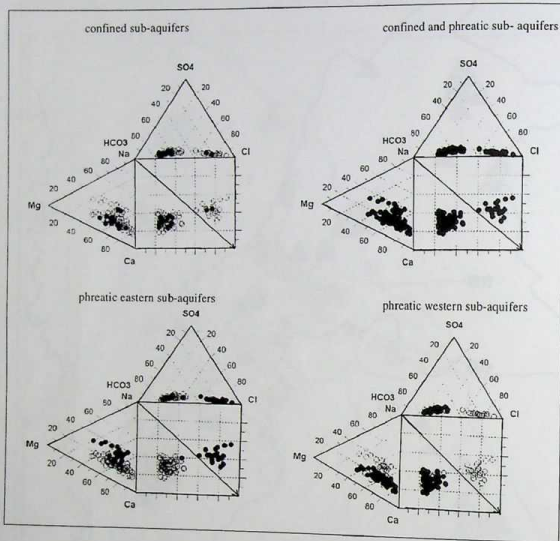
Fig. 5.11: Durov diagram of water analyses of the phreatic and confined sub-aquifers in the Faria basin.

Notice: The representative samples were plotted by the symbol ● and the samples of other sub-aquifers were represented by the symbol o.

5.9.2 Compositional diagrams

Compositional diagrams between major ions as well as temperature and TDI were drawn (Fig. 5.17). The data plot on straight lines, revealing correlation between Ca^{2+}, Mg^{2+}, Na^+, K^+ and Cl^- with TDI. The major pattern of these compositional diagrams indicate that two clusters are existed. This yields to the conclusion, that two groups of groundwater are located in the study area. Diagrams of temperature, NO_3^-, HCO_3^-, Na^+, Mg^{2+} vs. TDI show two clusters. The TDI diagram, a randomly distribution is seen around first cluster, due to the pollution, that occurs in the western phreatic sub-aquifers. Two clusters indicate that two separate hydraulic systems are involved, having two distinct water types. Data plotting on

lines TDI with Cl⁻, Na⁺, K⁺ indicate the mixing of two groups. The straight line of plotting indicates the occurrence of mixing. The extrapolation of the straight line towards the Y-axis indicates that the mixing of two water groups are occurred with significant load of dissolved ions.
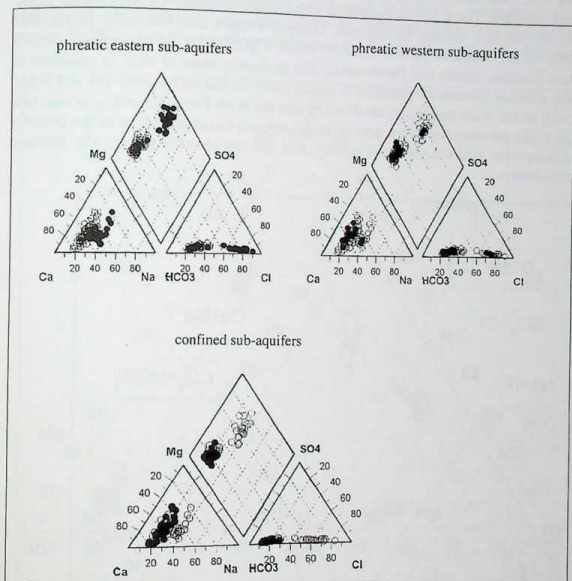
Fig. 5.12: Piper diagram illustrates chemical analyses of water samples
of the phreatic eastern and western as well as confined sub-
aquifers of the Faria basin.
Notice: The representative samples were plotted by the symbol ● and the
samples of other sub-aquifers were represented by the symbol o.

The groundwater chemistry of the confined aquifer is similar to that of the phreatic - western sub-aquifers. Thus there is no indications during the flow from recharge areas to the aquifers. In the phreatic eastern sub-aquifers a mixing process is proposed that the flash flood waters from the mountain areas, recharging the graben fill lisan aquifers, dissolve salts during their flow in these formations (RONEN and REBHUN 1974). The salinity of these waters range from 25.6 to 18.8 meq/L of Cl⁻.

5.9.3 Water types

The phreatic western sub-aquifers and the confined aquifer show an increasing trend of Ca^{2+}> Mg^{2+} > Na^{+}+ K^{+}. An increasing trend of Ca^{2+}> Na^{+} + K^{+} > Mg^{2+} is shown for the eastern phreatic sub-aquifers. Three anions increasing trend orders are observed: HCO_3^->CL^->NO_3^- >SO_4^{2-} in the phreatic western sub-aquifers (Eocene western and Neogene), HCO_3^->CL^- >SO_4^{2-}>NO_3^- in the confined aquifer and CL^->HCO_3^-> SO_4^{2-}>NO_3^- in the phreatic eastern sub-aquifers (Eocene eastern and Pleistocene). The increasing trend of NO_3^- in reference to SO_4^{2-} in the phreatic western sub-aquifers is due to pollution caused by cesspools and septic tanks, as well as the wastewater, that are draining into the Wadi Faria. According to this, two main water types are recorded in the area of study: calcium-bicarbonate type in the phreatic western sub-aquifers and the confined aquifer, and calcium-chloride type in the phreatic eastern sub-aquifers.

Fig. 5.13: Piper diagram illustrates chemical analyses of water samples of the Faria basin (before recharge)

The phreatic western sub-aquifers and the confined aquifer are composed of carbonate rocks (limestone and in some places dolomitic limestone) with low salinity (< 800 mg/L). Otherwise, the phreatic eastern sub-aquifers consist of alluvium and lisan formations (gypsum-marl-lisan) with high salinity (> 1000 mg/L). Thus, the composition of rocks and soils has a direct influence on water quality. In carbonate rocks, total dissolved salts are mainly $Ca(HCO_3)_2$ in the case of limestone and $(Ca, Mg)(HCO_3)_2$ in the case of dolomite.
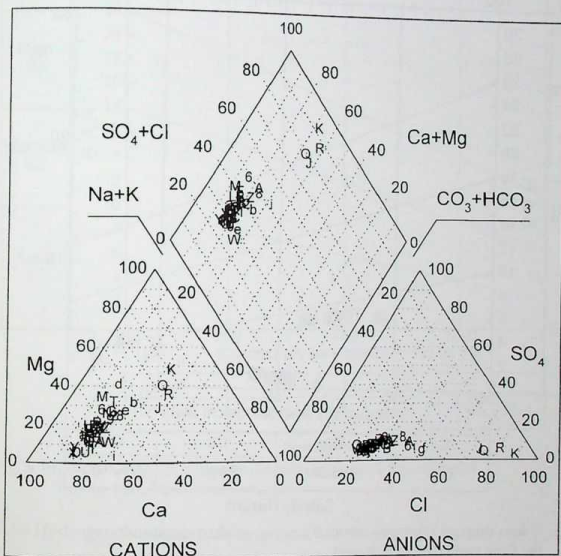
Fig. 5.14: Piper diagram illustrates chemical analyses of water samples of the Faria basin (after recharge).

The chemical composition of the confined aquifer is homogeneous in comparison with the phreatic aquifer. The latter shows trends of chemical constituents toward the east. Salinity and chlorinity tend to increase in the flow direction. The waters are divided into two groups: Calcium-bicarbonate group and chloride-bicarbonate group. Calcium carbonate aquifers are characterized by the ion relationships: $Ca^{2+} > Na^+ > K^+ > Mg^{2+}$ and $HCO_3^- > CL^- > SO_4^{2-}$. The ion concentration is relatively low, varying between 15 and 15.6 meq/L, especially for western phreatic sub-aquifers, while it is higher in the eastern phreatic sub-aquifers, varying

105

between 49.3 and 67.1 meq/L. The ionic relationship varies to $Ca^{2+} > Mg^{2+} > Na^+ + K^+$ and $CL^- > HCO_3^- > SO_4^{2-}$ for the phreatic eastern sub-aquifers. The ration Mg/Ca is between 0.3 and 0.8, within the same ration of rainfall, which indicates aquifers of limestone and dolomitic nature.
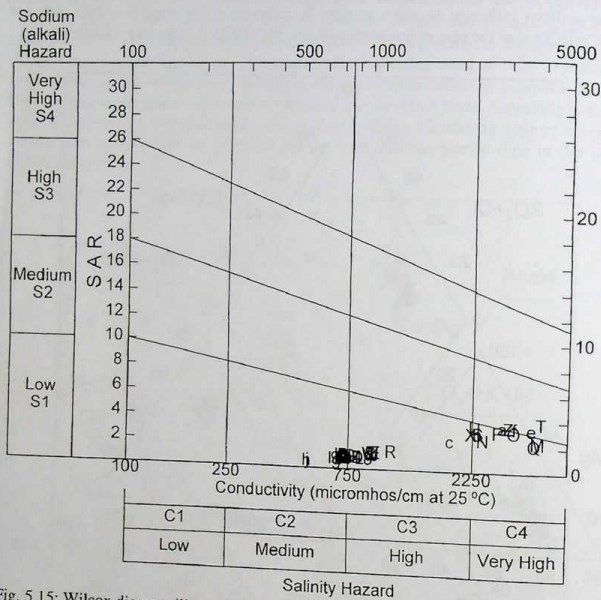
Fig. 5.15: Wilcox diagram illustrates chemical analyses of water samples of the Faria basin (before recharge)

Chloride type is generally characterized by ion relations: $Ca^{2+} > Mg^{2+} > Na^+ + K^+$ and $CL^- > HCO_3^- > SO_4^{2-}$. The ration Mg/Ca is high, varying between 1.3 and 2.4. According to LERMAN (1970) and LEVY (1972), Ca-chloride waters are defined by Na/Cl<1 and Ca/(HCO_3^- +SO_4^{2-}) >1.

Limestone water can be divided into calcium-bicarbonate type and calcium-magnesium-bicarbonate type. Calcium is predominant in both but with more magnesium in the former, while the ratios of Ca/Mg and Na vary around a unity in the latter. Bicarbonate is dominant in the latter and the chloride and sulphide are of double times greater than the former. Calcium-

106

carbonate type appear in Jenin sub-series, while the Ca-Mg-HCO$_3$ type appear in Bethlehem, Jerusalem and Hebron formations and others in Beida formations.
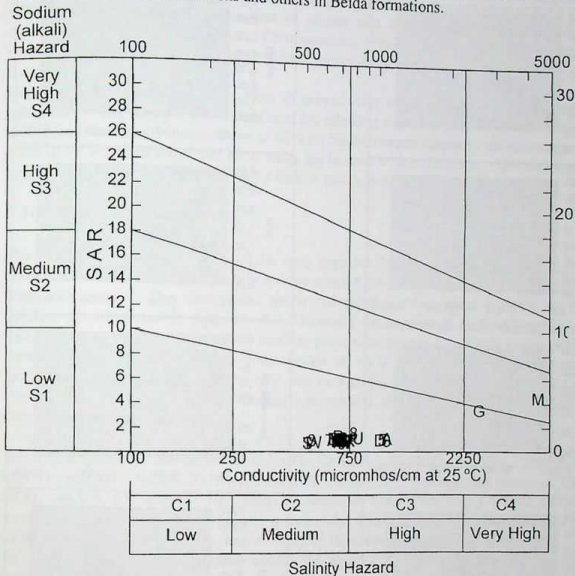
Fig. 5.16: Wilcox diagram illustrates chemical analyses of water samples of the Faria basin (after recharge)

5.10 Hydrogeochemical model

Water composition changes through reactions with the environment and water quality yields information about the environment, through which the water has circulated (APPELO 1996). In this study, the computer program PhreeqC (PARKHURST et al. 1980) was used to calculate the equilibrium speciation and saturation indices. To ease the use of PhreeqC the windows interface Phredit (MERKEL and MERKEL 1997) was used. PhreeqC is a geochemical program and is capable of simulating a wide range of geochemical reactions including mixing of water, dissolving and precipitating phases to achieve equilibrium with the aqueous phase and effects of changing temperatures. It is also used to indicate mineral species and to provide estimates of element concentrations that had not been determined analytically.

107
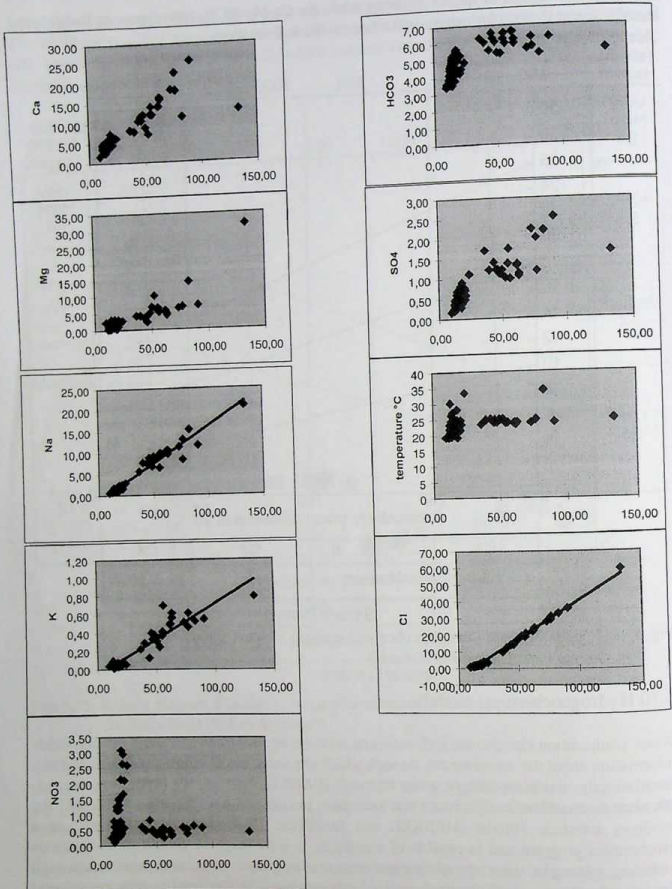
Fig. 5.17: Compositional diagrams of Ca, Mg, Na, K, HCO3, SO4, Cl, NO3 and Temperature against TDI

Hydrogeochemical modeling is of importance in identifying a single set of phases that account for the observed water chemistry and in simulating the possible mixing ratios of different water bodies. The selection of phases that control these mixing, is based on mineralogical and geological data. Compositional relations among dissolved species can reveal the origin of solutes and the generated processes of water composition.

Representative chemical analyses from all groundwater wells and springs were taken for the simulation with PhreeqC. The criteria used for selecting these representative analyses are well distributed locations, representative to all well fields, representative to all water type. All of them show very less errors and all of them are located within the same chloride content and don't showing extreme values of major ions or trace elements.

5.10.1 Distribution of species

The data base phreeqc and wateq4f.dat were used for determining the distribution of major species for each water analyses. Only species which have the minimum molality of 10^{-8} mol/L were interpretated. The distribution species of representative water samples of all sub-aquifers are illustrated in Appendix 5.4. Generally the species of each sub-aquifer are the same, but their molality differs from place to place according to the chemical composition of each sample. The major two to four species of each element have the same series of molalities in each sub-aquifer. Generally, the western phreatic sub-aquifers and the confined sub-aquifers show the same distribution species and slightly different from those of the phreatic eastern sub-aquifers.

The major species of carbon are HCO_3^-, CO_2, $CaHCO_3^+$, $MgHCO_3$, $CaCO_3$, $CaHCO_3$, CO_3^{2-}, $MgCO_3$, $NaCO_3^-$, $ZnCO_3$, $ZnHCO_3^+$, $FeHCO_3^+$, $CdHCO_3^+$. The molality mean of CO_2 and HCO_3^- are $2.8. 10^{-4}$ and $4.9. 10^{-3}$ mol/L, respectively. $CaCO_3$ and $MgCO_3$ have the molality mean of $1.7. 10^{-5}$ and $4.3. 10^{-6}$ mol/L, respectively. Calcium form the major species of Ca^+, $CaHCO_3^+$, $CaSO_4$, and $CaCO_3$. The molality of these species range from $1.9. 10^{-3}$ to $1.4. 10^{-5}$ mol/L. Calcium of the phreatic eastern sub-aquifer have the species $CaOH^+$ of a molality mean $1.4. 10^{-8}$ mol/L. Cadmium has the major species of Cd^{2+}, it ranges in molality between $2.4. 10^{-7}$ and $5.2. 10^{-9}$ mol/L for the springs and wells, respectively. The eastern phreatic sub-aquifers have the species of $CdCl_2$ with a molality mean of $1.3. 10^{-8}$ mol/L. Chloride has the major species of Cl^- of $1.4. 10^{-3}$ mol/L and has the minor species $CdCl^+$ and $ZnCl^+$ of $1.3. 10^{-10}$ mol/L molality. Copper has the major species of $Cu(OH)_2$ of $1.03. 10^{-7}$ mol/L molality. Minor species Cu^+, Cu^{2+} and $CuOH^+$ of less than $1.4. 10^{-9}$ mol/L molality are observed. Iron (2) has the major species of Fe^{2+}, $FeOHCO_3^+$ and it ranges between $2.7. 10^{-8}$ and $1.2. 10^{-8}$ mol/L, respectively. Iron (3) has the major species $Fe(OH)^{2+}$ and its molalility ranges between $1.9. 10^{-7}$ and $5.1. 10^{-8}$ mol/L molality, respectively. Iron of the phreatic western sub-aquifers has the species $Fe(OH)_4^-$ of a molality mean $1.3. 10^{-8}$ mol/L. Potassium has the major species of K^+ and it ranges in molality between $3.3. 10^{-5}$ and $4.6. 10^{-5}$ mol/L. Minor species are observed KSO_4^- of a molality range $1.8. 10^{-8}$ to $5.1. 10^{-8}$ mol/L. Magnesium has the major species of Mg^{2+}, $MgHCO_3^+$, $MgSO_4$ and $MgCO_3$ with a molality range of $1.3. 10^{-3} - 4.9. 10^{-4}$, $1.8. 10^{-5} - 8. 10^{-5}$, $6.1. 10^{-5} - 7.4. 10^{-5}$ and $2.1. 10^{-6} - 6.5. 10^{-6}$ mol/L, respectively. The major species of N(5) is NO_3^- and its molality ranges between $2.3. 10^{-4}$ to $4.3. 10^{-4}$ mol/L. Sodium has the species of Na^+, $NaHCO_3$, $NaSO_4^-$, $NaCO_3^-$ and it ranges in

109

molality between $7.3. 10^{-3}$ to $6. 10^{-7}$ mol/L. Oxygen $O(0)$ has the major species of O_2 of a molality mean $1.6. 10^{-4}$ mol/L. Lead (Pb) has the major species of $PbCO_3$ and it ranges between $1.3. 10^{-8}$ to $8.4. 10^{-8}$ mol/L in molality. Sulfer has the species of SO_4^{2-}, $CaSO_4$, $MgSO_4$, $NaSO_4^-$ and KSO_4^- and its molality ranges between $1.3. 10^{-4}$ to $2.7. 10^{-8}$ mol/L. Silica has the major species H_4SiO_4 and $H_3SiO_4^-$. The molality of these species range between 5.6. 10^{-4} - $7.8. 10^{-4}$ and $1.8. 10^{-6}$-$6.3. 10^{-6}$ mol/L for the former and latter, respectively. Zinc has the major species of $ZnCO_3$, Zn^{2+}, $Zn(CO_3)_2^{2-}$ and $ZnHCO_3$. Zinc in the western phreatic sub-aquifers and the confined aquifer have the species $Zn(CO_3)_2^{2-}$, of the molality range between of $1.4. 10^{-8}$ and $4.3. 10^{-8}$ mol/L, respectively.

5.10.2 Saturation indices (SI)

The SI indicates whether a water is saturated or not saturated regarding to a certain mineral. It is calculated using this equation: SI = Log (IAP / K_{sp}) where, IAP is the Ion Active Product and K_{sp} is the solubility product. The solution is considered to be in equilibrium regarding particular minerals if SI equals zero. It is considered to be undersaturated if the SI is less than 0 and oversaturated if SI > 0. Saturation index is used to define the amounts of an assemblage of pure phases that can react reversibly with the aqueous phase. As groundwater moves underground it tends to develop a chemical equilibrium by chemical reactions with its environment.

The saturation indices of all water samples are determined using the PhreeqC programme (Table 5.6). The following phases are found to be in the trend of equilibrium with the solution: Calcite, Dolomite, Aragonite, Fe(OH)$_3$, Chalcedony, Quartz and SiO$_2$. The phases Calcite (CaCO$_3$), Dolomite (CaMgCO$_3$) and Aragonite (CaCO$_3$) represent the limestone-dolomitic origin of major sub-aquifers in the area. The Silica phases Chalcedony, Quartz and SiO$_2$ agree with the SiO$_2$ high content in the chemistry of the water samples. Oversaturated phases were Goethite (FeOOH) and Hematite (Fe$_2$O$_3$) which represent the high quantity of iron in the chemistry of water samples.

The following phases were found to be undersaturated Anhydrite (CaSO$_4$), Cd(OH)$_2$, CdSiO$_3$, Chrysotile (Mg$_3$Si$_2$O$_5$(OH)$_4$), Gypsum (CaSO$_4$.2H$_2$O), H$_2$, Manganite (MnOOH), Siderite (FeCO$_3$) and Otavite (CdCO$_3$). Resulting computations show all waters to be highly saturated with Calcite and Dolomite, whereas water from the eastern phreatic sub-aquifers are slightly saturated with these two minerals.

5.10.3 Ionic strength and electrical balance

The lowest and highest ionic strength values are found in the Eocene western sub-aquifer and the Neogene sub-aquifer, respectively. A trend of decreasing ionic strength is found to be toward eastern. The confined sub-aquifers have the same ionic strength ($1.1. 10^{-2}$ mol/L). The electrical balance of all water samples is ranging between -5.2. 10^{-5} and +8.4. 10^{-6}. The error is calculated according to the equation: error = (electrical balance (eq)/ ionic strength(IS))* 100. This error for all samples are ranging between $1.2. 10^{-2}$ and $8.6. 10^{-4}$. The ionic strength, electrical balance and electrical error of selected water samples are illustrated in Table 5.7.

Table 5.6: The average of saturation indices (SI) of all sub-aquifers in Faria basin.

Phase	chemical composition	SI of phreatic western	SI of phreatic eastern	SI of confined aquifer	SI of all sub-aquifers
Anglesite	$PbSO_4$	-6.4	-5.8	-6.5	-6.2
Anhydrite	$CaSO_4$	-2.6	-1.8	-2.5	-2.3
Aragonite	$CaCO_3$	0.1	0.5	0.3	0.3
$CO_2(g)$	CO_2	-2.1	-1.8	-2.1	-2.0
Calcite	$CaCO_3$	0.2	0.6	0.5	0.4
$Cd(OH)_3$	$Cd(OH)_3$	-7.5	-6.2	-7.0	-6.8
$CdSO_5$	$CdSO_5$	-12.9	-10.8	-12.3	-11.8
$CdSiO_4$	$CdSiO_4$	-6.2	-4.9	-5.8	-5.5
Cerrusite	$PbCO_3$	-2.3	-2.0	-2.3	-2.2
Chalcedony	SiO_2	0.4	0.3	0.3	0.3
Chrysotile	$Mg_3Si_2O_5(OH)_4$	-3.7	-3.8	-3.0	-3.5
Dolomite	$CaMg(CO_3)_2$	0.3	0.9	0.8	0.7
$Fe(OH)_3$	$Fe(OH)_3$	0.8	0.8	0.9	0.8
Goethite	$FeOOH$	6.6	6.7	6.8	6.7
Gypsum	$CaSO_4:2H_2O$	-2.4	-1.6	-2.2	-2.1
$H_2(g)$	H_2	-23.0	-22.7	-23.2	-22.9
Hausmannite	Mn_3O_4	-20.6	-19.0	-18.9	-19.3
Hematite	Fe_2O_3	15.1	15.3	15.5	15.3
Jarosite-K	$KFe_3(SO_4)_2(OH)_6$	-8.9	-6.6	-8.5	-7.9
Manganite	$MnOOH$	-7.8	-7.5	-7.3	-7.4
Melanterite	$FeSO_4:7H_2O$	-9.5	-8.7	-9.6	-9.3
$O_2(g)$	O_2	-0.8	-0.9	-1.3	-1.0
Otavite	$CdCO_3$	-2.0	-0.4	-1.5	-1.2
$Pb(OH)_2$	$Pb(OH)_2$	-3.5	-3.4	-3.4	-3.4
Pyrochroite	$Mn(OH)_2$	-9.1	-8.7	-8.7	-8.8
Pyrolusite	MnO_2	-12.9	-12.3	-12.0	-12.3
Quartz	SiO_2	0.8	0.7	0.8	0.8
Rhodochrosite	$MnCO_3$	-3.0	-2.3	-2.7	-2.6
Sepiolite	$Mg_2Si_3O_7.5OH:3H_2O$	-1.9	-2.2	-1.6	-1.9
Sepiolite	$Mg_2Si_3O_7.5OH:3H_2O$	-4.8	-5.1	-4.4	-4.8
$SiO_2(a)$	SiO_2	-0.5	-0.5	-0.5	-0.5
Siderite	$FeCO_3$	-2.1	-1.7	-2.1	-2.0
Smithsonite	$ZnCO_3$	-2.6	-2.7	-2.8	-2.7
Talc	$Mg_3Si_4O_{10}(OH)_2$	0.7	0.5	1.4	0.8
Willemite	Zn_2SiO_4	-3.4	-4.1	-3.8	-3.7
$Zn(OH)_2$	$Zn(OH)_2$	-3.8	-4.2	-4.0	-4.0

Table 5.7: The ionic strength, electrical balance and error of selected water samples from
Faria basin after using PhreeqC programme.

Water sample	sub-aquifer	ionic strength (IS)	electrical balance (eq)	error ((eq /IS) * 100)
18-18/1	Eocene western	$9.913. 10^{-3}$	$-5.266.10^{-5}$	0.53
E.Hamad & Beida	Eocene western	$6.689. 10^{-3}$	$-3.496.10^{-5}$	0.52
Ein Fariaa	Eocene western	$9.072. 10^{-3}$	$-5.898.10^{-5}$	0.65
Ein Miska	Neogene	$1.017. 10^{-2}$	$-2.165.10^{-5}$	0.21
18-18/11A	Neogene	$9.719. 10^{-3}$	$8.402.10^{-6}$	0.086
18-18/36	Neogene	$1.007. 10^{-2}$	$8.553.10^{-5}$	0.85
18-18/37	Cenomanian western	$1.000. 10^{-2}$	$2.075.10^{-5}$	0.21
18-18/38	Cenomanian western	$8.633. 10^{-3}$	$-5.222.10^{-5}$	0.06
19-17/44	Cenomanian eastern	$1.215. 10^{-2}$	$-2.651.10^{-5}$	0.22
19-17/34	Cenomanian eastern	$1.153. 10^{-2}$	$-9.070.10^{-5}$	0.78
19-17/27	Pleistocene	$3.028. 10^{-2}$	$-7.124.10^{-5}$	0.24
19-17/10	Pleistocene	$4.133. 10^{-2}$	$-1.532.10^{-4}$	0.37
19-17/1	Eocene Eastern	$3.201. 10^{-2}$	$1.289.10^{-4}$	0.41
19-17/33	Eocene Eastern	$2.923. 10^{-2}$	$3.484.10^{-4}$	1.2
19-17/55	Eocene Eastern	$3.025. 10^{-2}$	$-3.178.10^{-5}$	0.11

6 ENVIRONMENTAL ISOTOPES ANALYSES

6.1 Introduction

Environmental isotopes contribute to investigations of groundwater routinely. Since meteoric processes modify the stable isotope composition of the infiltrating water, the recharge water will have a characteristic isotopic signature. Both ^2H and ^{18}O were used in this study. Radioisotopes e.g. ^3H provide due to the decay with time information and thus the mean residence time of groundwater.

6.2 Sampling methods and isotope analyses

Samples of groundwater were obtained from shallow and deep wells in phreatic and confined aquifers. The 50 ml glass bottles for ^2H and ^{18}O were obtained from pumping wells. The complete analyses and separation of stable isotopes were carried out in the laboratory of GSF-institute for Hydrology in Neuherberg. The relative ratio of $^{18}O/^{16}O$ and $^2H/^1H$ is expressed in delta (δ) notation according to the equation:

δ $^0/_{00}$ = ((R_x / R_{SMOW}) - 1) * 1000 (promille) , where R_x is the isotopic ratio $^{18}O/^{16}O$ or $^2H/^1H$ in the substance x; δ is expressed in parts per thousand (permils or $^0/_{00}$), which could be compared with isotopic ratios of the Standard Mean Ocean Water (SMOW). The instrumental error is 0.1 $^0/_{00}$ for ^{18}O and 1% for ^2H. Larger 500 ml ^3H samples were stored in a sealed polyethylene bottles. The ^3H analyses were carried out in the lab of Institute for Angewande Physik of the TU Bergakademie Freiberg.

6.3 Deuterium and ^{18}O

The isotopic composition ^2H and ^{18}O of phreatic and confined groundwater in the Faria basin are listed in Table 6.1.

6.3.1 Deuterium

The highest Deuterium values were found in the phreatic aquifers, ranging between -27.5 and -22 $^0/_{00}$ with a mean of -24.3 $^0/_{00}$. The confined sub-aquifers of lower and upper Cenomanian have a range from -27.3 to 24.1 $^0/_{00}$ and a mean of -25.45 $^0/_{00}$. The mean is -24.4 $^0/_{00}$ for all groundwater wells with a large variability in ^{18}O, especially for the Eocene sub-aquifers. The variability of both ^2H and ^{18}O shows a strong trend towards east (Fig.6.1).

6.3.2 Oxygen - 18

Delta ^{18}O values in the study are spread between -5.72 $^0/_{00}$ to -4.56 $^0/_{00}$ in the phreatic aquifers with a mean of -5.15$^0/_{00}$. The confined sub-aquifers of lower and upper Cenomanian has a range of -5.57 to -5.27 $^0/_{00}$ with a mean of -5.4 $^0/_{00}$. The mean is -5.21 $^0/_{00}$ for all groundwater wells with small variations in Deuterium (Fig.6.1). The δ ^{18}O was plotted against altitude (NW-SE profile) (Fig.6.2). The stable isotopes are good tracers for determining the origin of groundwater in hilly areas because of the altitude effect (ERIKSSON 1985). However in this case no altitude effect could be shown. The isotopic composition in wells of the phreatic aquifer has larger variability than the confined aquifer. The ^{18}O values are found to be high in

113

Neogene and Eocene sub- aquifers (Fig.6.1).
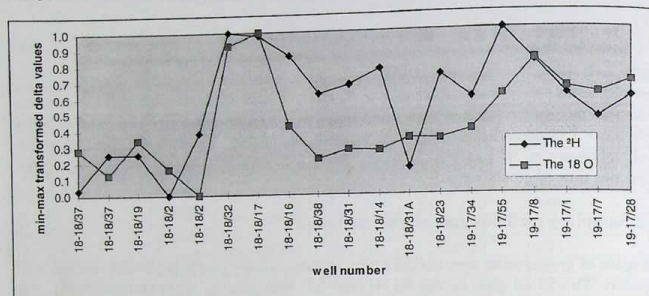
Fig.6.1 : The variation profile of ^{2}H and ^{18}O fractionation (NW - SE).

Table 6.1: The isotopic composition of the water samples for the phreatic and confined sub-
aquifers and the sampling sites.

Well ident.	x	y	z	^{2}H [$^o/_{oo}$]	^{18}O [$^o/_{oo}$]	^{3}H [TU]	sub-aquifer	datum
18-18/2	182200	188350	177	-27.5	-5.53	2,6 +/- 0,5	Eocene	17/06/97
18-18/32	182170	189000	197,2	-22	-4.65	4,6 +/- 0,6	Eocene	17/06/97
18-18/17	182310	189420	196,5	-22.1	-4.56	3,7 +/- 0,6	Eocene	17/06/97
18-18/16	182370	188890	170,5	-22.8	-5.23	3,2 +/- 0,5	Eocene	02/11/96
18-18/2D	182200	188350	177	-25.4	-5.72	2,8 +/- 0,5	Eocene	02/11/96
18-18/31A	186650	183120	-29	-26.6	-5.32	1,6 +/- 0,5	Neogene	18/06/97
18-18/19	181150	188730	-46,6	-26.1	-5.32	1,7 +/- 0,5	Neogene	18/06/97
19-17/1	196900	170740	-250	-24.2	-4.98	7,6 +/- 0,5	Pleistocene	02/11/96
19-17/7	196940	172290	-243,4	-25	-5.02	19,3 +/- 1,8	Eocene	29/06/97
19-17/28	198150	170500	-267,9	-24.3	-4.93	2,9 +/- 0,5	Pleistocene	29/06/97
19-17/8	196250	170260	-250,6	-23.1	-4.78	3,3 +/- 0,5	Pleistocene	02/07/97
18-18/14	186610	189950	-30,2	-23.3	-5.41	8,3 +/- 0,9	Neogene	29/10/96
18-18/31	186410	183120	-29,2	-23.8	-5.4	1,2 +/- 0,4	Neogene	29/10/96
18-18/23	187210	183070	-28,8	-23.5	-5.33	1,0 +/- 0,4	Neogene	29/10/96
19-17/55	196150	173400		-22	-5.03	3,0 +/- 0,5	Eocene	02/11/96
19-17/1D	196900	170740	-250	-22.1	-4.56	5,2 +/- 0,7	Eocene	29/06/97
Rainfall						6,8 +/- 0,8	Rainfall Ramallah	30/07/97
19-17/34	192740	178370	-148,9	-24,3	-5.27	1,3 +/- 0,4	Cenomanian	29/10/96
18-18/37	180150	185400	210,9	-26.1	-5.57	1,8 +/- 0,5	Cenomanian	02/11/96
18-18/38	182750	185750	90	-24.1	-5.46	2,2 +/- 0,5	Cenomanian	02/11/96
18-18/37D	180150	185400	210,9	-27.3	-5.39	1,3 +/- 0,5	Cenomanian	17/06/97

6.3.3 Comparison between ^{2}H with ^{18}O

Delta ^{2}H with ^{18}O could be used to identify water bodies that are affected by rapid evaporation. A linear relationship is found, after plotting δ ^{2}H as a function of ^{18}O for the water in continental precipitation (MAYO, MULLER and RALSTON 1985): δ ^{2}H = 8 δ ^{18}O +

114

d (meteoric water line MWL) where d is constant and the results are given in terms of permills deviations from SMOW ($\delta^0/_{00}$) (CRAIG 1961). Deviation from the MWL may caused by precipitation that occurred during warmer and colder climate than at present or by subsurface changes. Delta ^2H values of phreatic and confined aquifers were plotted as a function of ^{18}O forming a straight line that is parallel to, but below the meteoric water line. This is interpreted as a local meteoric water line of the precipitation in the area for the period 1950 - 1990 (Fig.6.3).
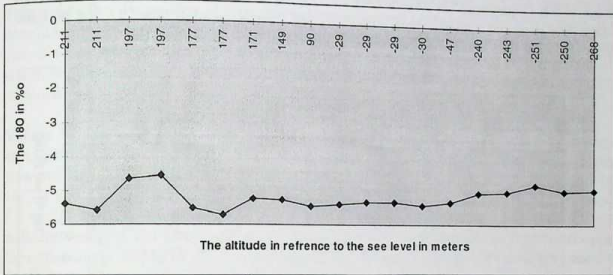
Fig.6.2: The relationship between ^{18}O and altitude of the sampling point (NW-SE).

Most of the samples for the two aquifer systems are grouped at the meteoric water line and deviations occurred as a result of evaporation. These values lie on the local meteoric water line as defined by GAT & DANSGAARD (1972). The samples of a confined aquifer have relatively low ^2H and ^{18}O concentrations. The samples of Eocene sub-aquifer show high ^2H and ^{18}O. The samples of Neogene sub-aquifer show high ^2H and relatively low ^{18}O.
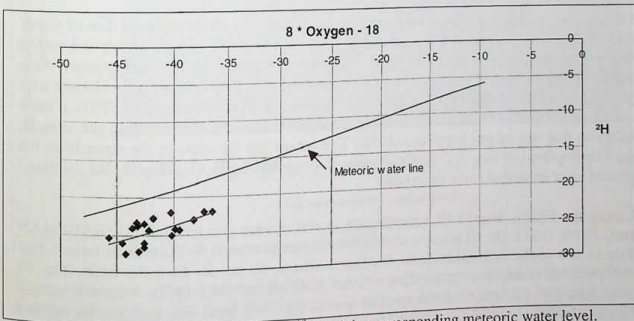
Fig.6.3: The relationship between ^2H and ^{18}O and the corresponding meteoric water level.

The most depleted isotope content is found in springs, close to the mountain crest , such as Ein Faria, which has $\delta\ ^{18}O$ of -6.42 $^0/_{00}$ and $\delta\ ^2H$ of -27.8 $^0/_{00}$ (GAT 1972). In some wells of

115

the phreatic aquifer, a large delta values of ^2H and ^{18}O are shown, due to the combined effect of rain water and accompanying flood flows.

6.3.4 The ^2H and ^{18}O isotope composition of precipitation

The precipitation in Israel and indeed throughout the eastern Mediterranean sea area, is characterized by a relatively large Deuterium excess over ^{18}O (GAT 1972). The long term average at Bet Dagan near Tel Aviv is $\delta\ ^2H = -22.8\ ^0/_{00}$ and $\delta\ ^{18}O = -5.29\ ^0/_{00}$ (Fig.6.4). Both phreatic and confined aquifers show a mean ^2H less than of rainfall. For ^{18}O, the phreatic aquifer is greater than that of rain; while the confined aquifer is lesser than that of rain.
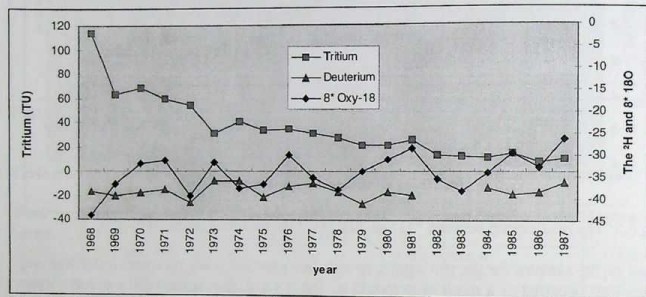
Fig.6.4: The variability of ^3H, ^2H and ^{18}O in $^0/_{00}$ in the rainfall for the period 1968 to 1987.

6.4 Tritium (^3H)

Tritium concentrations in groundwater provide an indication to mean residence time of water. Prior to 1953, rainwater had less than 10 TU, starting in 1953, the manufacturing and testing of nuclear weapons have increased Tritium in rainfall and consequently, groundwater. As a result, ^3H can be used in quantitative manner to date groundwater because groundwater with less than 2 to 4 TU is dated prior to 1953. If the amount of ^3H is between 10 to 20 TU, it must have been in contact with the atmosphere since 1953. The absence of ^3H in the sample, indicates that it is of pre bomb age (1952). This means low ^3H refers to the water from the pre-bomb period. Table 6.1 lists the isotopic composition ^3H of phreatic and confined groundwater measured in the Faria basin.

During the 1950's, Israel's ^3H concentration in precipitation was about 5 TU (KAUFMAN and LIBBY 1954). The ^3H concentration in present precipitation is 10 TU or less. Tritium rain data in this study were taken from Bet Dagan station, 50 km far from the basin. The ^3H concentration is similar for the whole of Israel (CARMI and GAT 1973). A rainfall sample from Ramallah (70 km from the southern part of the study area) was analyzed for ^3H and found to be 6.8 +/- 0.8 TU.

6.4.1 Discussion

The high values of ^{3}H in some samples are due to the fact that the aquifer is directly recharged from rainfall. The Eocene eastern sub-aquifer has values ranging between 2.6 to 7.6 TU. Pleistocene sub-aquifer has an average ^{3}H value of 3.1 TU. Values of two samples 18-18/14 and 19-17/1 of Eocene eastern and Neogene sub-aquifers have nearly the same amount as natural rainfall. Two highest values of ^{3}H are recorded in the wells 18-18/14 from Neogene sub-aquifer and 19-17/7 from eastern Eocene sub-aquifer to be 8.3 and 19.3 TU, respectively. This means that the aquifers of these two wells have a direct contact with the atmosphere. It is concluded that water samples of Eocene, Pleistocene and partly Neogene of the Table 6.1 are classified as younger than 1953 or contain younger components (mixing of young and old water, recharge according to expontential model. This suggests recent recharge and tritium of meteoric origin.

Values of less than 1 TU may be interpreted as water from 1953 when the natural atmosphere was around 10 TU (IAEA 1988). However, this is true only assuming a piston flow recharge system. The samples of the lower and upper Cenomanian (19-17/34 and 18-18/37) and Neogene sub-aquifers (18-18/31 and 18-18/23) contain tritium ranging between 1.3 to 2.2 TU. The samples of Neogene show low values ranging between 1 to 1.7 TU and indicate that it is not recharging directly from rainfall. In the samples of lower and upper Cenomanian as well as of Neogene sub-aquifer, the tritium concentration is low compared to the tritium content of precipitation. The low levels of tritium ($<1.0\,^0/_{00}$) indicate that there was little recharge by flood or rain water in the last 44 years. A very low value indicates that the groundwater is not diluted by young freshwater and / or it takes more than 44 years for the groundwater travel from the area of recharge.
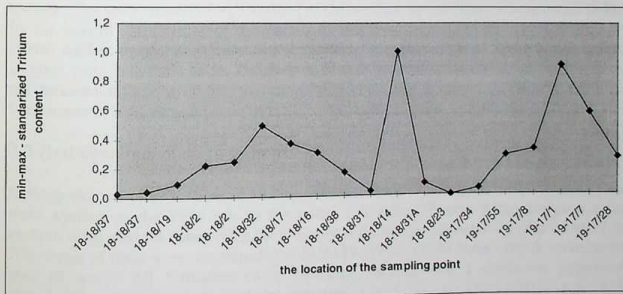
Fig.6.5: The variation of ^{3}H content as a profile NW-SE.

Three groundwater samples were taken before and after recharge, indicate ^{3}H is depleted after recharge (18-18/2, 18-18/31 and 18-18/37). The ^{3}H difference is found to be 0.2 to 1.9 TU in the well 18-18/2 and 18-18/31 of the Eocene western and eastern sub-aquifers, respectively. It is found to be 0.4 and 0.5 TU difference of Neogene and Cenomanian sub-aquifers. High tritium content in groundwater suggests a similar rapid flow regime, where the water is assumed to flow in karstic features (KROITORU 1987). The ^{3}H content is highly variable in

117

the area from the west to the east (Fig.6.5). Eocene well samples in the eastern part of the basin have higher ^{3}H content than in the western part.

Recharge in the eastern part of the basin is a result of lateral flow from western to the eastern sub-aquifers. Groundwater penetrates the Eocene and Neogene sub-aquifers through the contact zone between the them; a process that takes more than 40 years. The average Tritium content of various water resources in the limestone aquifers is considered to be a function of the water table depth (ISSAR and GAT (1982). Tritium contents were plotted against static water levels in the basin in Fig. 6.6 and agree with the variation of ^{3}H (Fig.6.5).
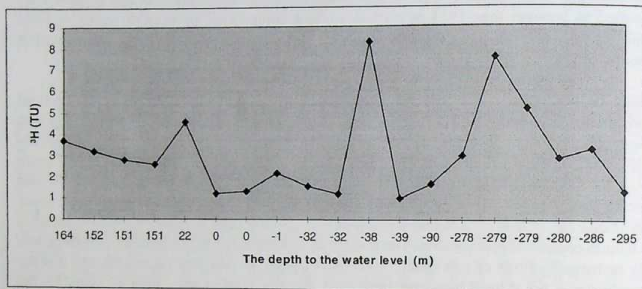
Fig. 6.6.: The relationship between ^{3}H in TU and the water level in meters (sea level).

118

7 GROUNDWATER FLOW MODELING

7.1 Introduction

The study area is part of the hydrogeological system of the eastern basin. The Faria Valley is a graben, bordered by the two NW-SE linear faults, which collects groundwater and runoff from the raised areas of it's shoulders (GUTTMAN 1985). In general, the eastern basin is located in the Judea and Samaria mountains. These mountains are a series of parallel anticlines and synclines, that treated chiefly N-S directions. Eastern from the mountains, the topography slopes is dipping steeply to the Jordan Valley, where the altitude of the land surface is about 300m below sea level. Drainage is chiefly caused by downward infiltration of rainfall and runoff through karstic features and fractures in the exposed parts of the underlying karstic limestone sub-aquifers, then eastwards by the groundwater flow to the Jordan River. The eastern basin has one phreatic and two confined aquifers. The groundwater flow regime is very complicated and is controlled by flexures (anticline and syncline), faults and fractures.

7.2 Previous studies

Few studies were conducted in the nearby area to cover the field of modeling. A study was conducted in the southern part of the area by GUTTMAN (1985) using a 2-dimensional model of the Jiftlik area. TAHAL (1995) conducted a study to apply Modflow in Cenomanian aquifers in eastern aquifers excluding Faria basin. The steady state water balance that was used by GUTTMAN (1995) suggesting that the natural recharge of the lower confined aquifer of the eastern basin is about 118.5 Mill. m³/y assuming all flows are eastward to specified springs. The study treated all sub-aquifers of Cenomanian as one layer. A conceptual model for the eastern basin excluding the Faria basin was conducted by CDM (1997). SEMHAN (1999) studied the data reconstruction for building groundwater flow model in the eastern aquifers, excluding Faria basin. The study deals with the confined aquifers only and assumes the thickness of these aquifers to be constant all over the area. It was recognized that the Wadi Faria region is a province separate from the overall eastern aquifer systems (SHALIV 1972).

7.3 Hydrogeological cross sections

Hydrogeological cross sections in all directions will bring us directly to a 3d - model of the main aquifers in the Faria area to the Jordan Rift valley. Twelve hydrogeological cross sections were used for determining the geometry of the aquifer (dimensions) (Fig.7.1 and Fig. 7.2). Some of them were developed after SHALIV (1972), GUTTMAN (1985) covering the area of study. All formations were correlated together and a consistent geological classification of aquifers and aquicludes were used.

The hydrogeological cross sections were scanned and treated with GIS-TNT mips in order to define x, y, z coordinates of the phreatic and confined aquifers. The geometry in x, y, z coordinates of the top & bottom layers for both phreatic and confined aquifers were determined. These coordinates and the coordinates from well logs were treated together with TNT-mips in order to build the conceptual model. It is concluded from these cross sections that formations of the lower aquifer is not absolutely confined but acts as semi-confined in some places, especially in the eastern parts of the Faria basin.

119
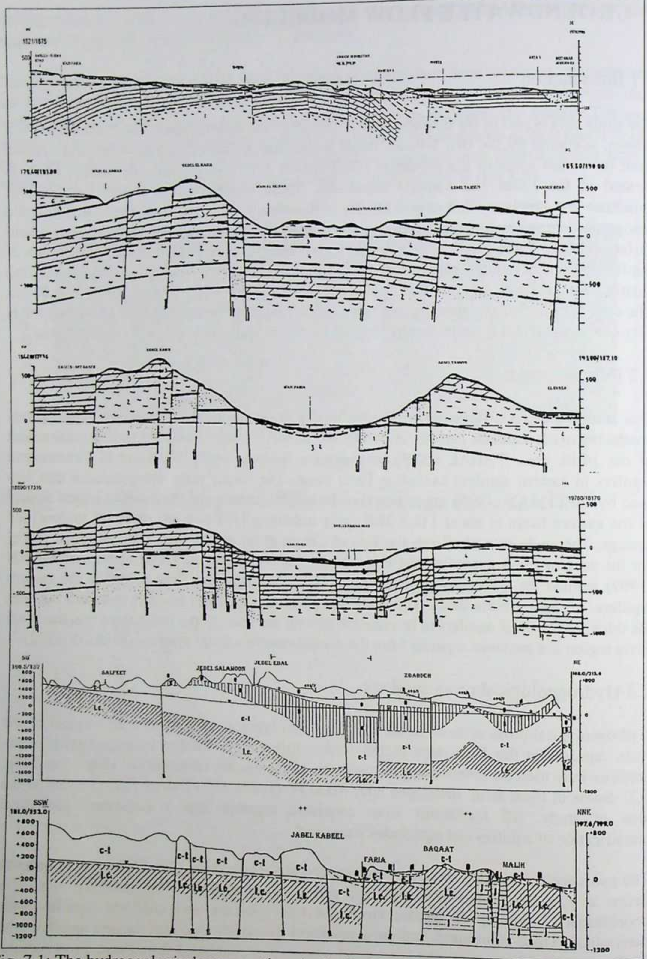
Fig. 7.1: The hydrogeological cross sections in the Faria basin modified after SHALIV (1972).
Notice: The legend is illustrated in Table 7.1.
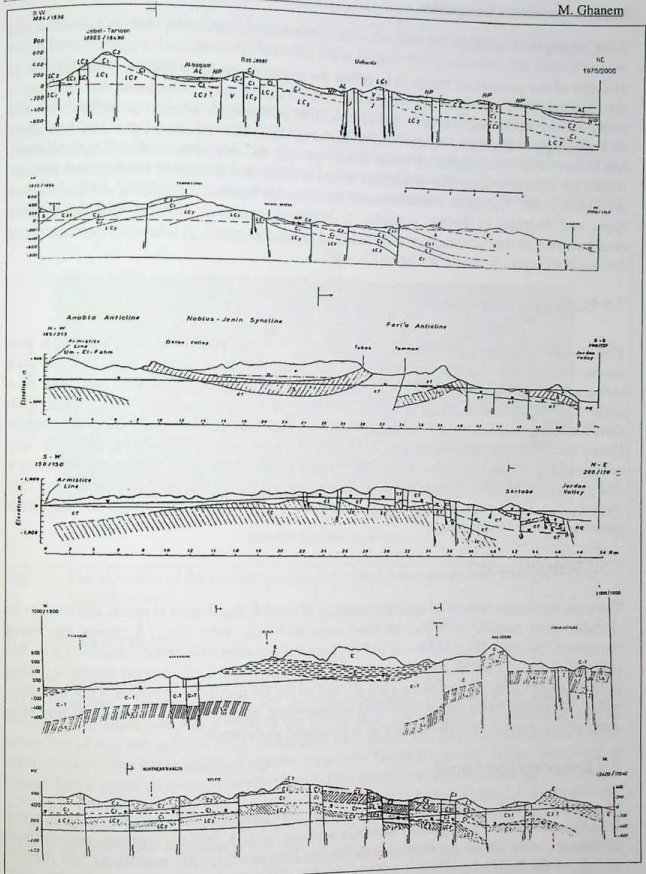
Fig. 7.2: The hydrogeological cross sections in the Faria basin modified after GUTTMAN (1985). Notice: The legend is illustrated in Table 7.1.

121

7.4 Conceptual model

The aim of the conceptual model is to define the requirements for a numerical model that is able to simulate water flow and with some restrictions transport phenomena for the region under steady state and transient conditions. The groundwater system is defined by it's hydrogeologic framework, aquifer hydraulic parameters, inflows, discharges and boundary conditions. The interrelation of these factors govern the groundwater flow characteristics within the aquifer system. The conceptual model is based on a number of fundamental aspects (MAZOR 1985): Hydraulic communication between sub-aquifers, mixtures of different water types and existing of karstic conduits. It integrates chemical, physical, geological data obtained prior to the construction of the detailed, numerical model. A schematic description of the modeled layers is shown in Tables 7.1 and 7.2.

7.5 Digital elevation model

The digital elevation model (DEM) or digital terrain model (DTM) of the Faria basin was produced using the topographic base-map, that cover the study area (Appendix 7.1). This topographic base-map was drawn after four topographic map-sheets as a mosaic map of a scale 1: 50 000 and a 50 m contouring line. This map was scanned and treated with CorelDraw version 7. Using TNT-mips, it was imported and georeferenced using the system Universal Mercator Transverse and UTM zone 36 with the ellipsoidal UGS84. It was converted from Raster into Vector in order to represent the elevation (Z-value) in addition to x and y coordinates. The Z-value for each vector line was attributed and transferred into (3d) Vector. The DEM was built using Surface fitting with a procedure minimum curvature method of 16 signed bit integer.

7.5.1 Rainfall model

The most important impact on spatial variability of rainfall distribution is due to differences in altitude: more rainfall of higher elevated areas and vice versa. Fig. 7.3 shows the linear regression (equation N` = 310.8 + 0.46 * N) between elevation and rainfall. According to this a digital model of rainfall distribution was calculated from the digital terrain model and used to calculate the distinct rainfall for each element of the finite difference model. This was done within TNT-mips using the implemented programming language SML. The rainfall model in zones of the average rainfall in mm/year is illustrated in Appendix 7.2.

7.6 Boundary conditions

The major control elements in the area are the E-W trending faults and fractures between Jehricho and Faria. These control elements serve as barriers, thus the southern and northern boundaries were set as no flow boundaries for both aquifers. All boundaries are defined mainly on the basis of geological and structural considerations and are illustrated in Fig. 7.4. The western boundary of the Faria basin was assumed along the general water divide between the western and eastern drainages. It was outlined and assumed along the groundwater divide from structural and lithological locations and can be traced by the Judean anticline, which represents the maximum uplift in the area. It was set as an no flow boundary along the Faria anticlinal axes for both aquifers.

122

The northeastern and southeastern boundaries of both the first and the third layers were set to be no flow boundary, because of the bounded faults in these two directions. The layer two was set with no flow boundaries.

The eastern boundary is the Jordan Rift valley and Jordan River. Constant-head boundaries were assumed for the confined and phreatic aquifers with a river constant head. This was considered in the numerical model by means of constant head boundary conditions (-300 m) for both the confined and unconfined aquifers. All constant head values for both aquifers were obtained by applying kriging techniques using computer code Surfer (GOLDEN SOFTWARE, INC. 1987).
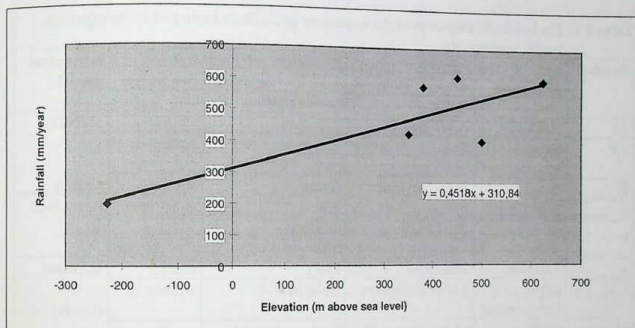
Fig. 7.3: The elevation of the rainfall stations in the Faria basin versus their average yearly rainfall in mm.

7.7 Aquifer properties

Phreatic aquifer system in the area of study consists of the following sub-aquifers: Alluvium (AL), Neogene - Pleistocene (NP) and Eocene sub-aquifers (E). They are overlying the Senonian (S) aquiclude which overlies the Cenomanian sub-aquifers. The confined aquifer composes of two sub-aquifers lower and upper Cenomanian. The following formations are the components of the lower confined aquifer: Jerusalem, Lower Bietlehem, Upper Bietlehem & Lower Yatta, upper & lower Lower Bietkahel. This confined aquifer overlies the Neocomian aquiclude (Upper Ramali); which is underlain by Albian aquifer. Table 7.1 illustrates the hydrogeological characteristics of all formations in the area of study based on the hydrogeological cross sections and well logs.

In order to run a model, values of conductivities and storativities must be assigned to each of the active cells in the model. The conductivity values were obtained from the results of the pumping tests (chapter 4). The conductivity values are subject to changes during the calibration based on matching the computed water tables to the measured. Aquifer properties are assigned to layers in order to represent hydrologic characteristics of different stratigraphic layers. The following hydraulic properties are specified for each sub-aquifer defined in the layers.

123

model: Horizontal hydraulic conductivity (K_h), vertical hydraulic conductivity (K_v), specific storativity (S_s) and specific yield (S_y), only for the confined aquifer.

The hydraulic gradient of phreatic and confined aquifers were calculated during the interpretation of pumping test data, that were conducted during this study. Initial estimates of the hydraulic conductivity for each unit in the model was based on the transmissivity that is extracted from the interpretation of the pumping tests that were carried out during fieldwork or from historic data. Data on the horizontal and vertical distribution of hydraulic conductivity are limited. The storativity in the study area was assumed to be 0.01 for the phreatic aquifer and between 0.002 and 1. 10^{-5} for the confined ones.

Table 7.1: The hydraulic properties of the formations in the Faria basin and corresponding model assumptions.

Symbol	age of the formation	formation named after Rofe & Raffety	formation referred to israelian nomenclatures	hydraulic properties	numerical model
Al	Holocene	Alluvium	Alluvium	aquifer	phreatic
NP	Neogene - Pleistocene	Beide & Lisan	Saqiye & Kurker	aquifer	
E	Eocene	Jenin Sub series	Avdat	aquifer	aquifer
S	Senonian	Belqa (chert & chalk)	Mount scops (Menuha & Mishash)	aquiclude	Aquiclude
t	Turonian	Jerusalem	Bin'a	aquifer	confined
C3t	upper Cenomanian	Lower Bietlehem	Kefar Sha'al	aquifer	(lower)
C2	upper Cenomanian	upper Upper Biet Kahel & Lower Yata	Keslan + Biet Mier	aquifer	aquifer 1
C1	lower Cenomanian	upper Lower Biet Kahel	Ji'vat Ye'arim	aquifer	
Lc1	lower Cenomanian	lower Lower Biet Kahel	Kefira	aquiclude	aquiclude
Lc2	Neocomian	Upper Ramali	Qatana	aquiclude	not considered
R	Albian	Lower Ramali	Kurnov (Tammun)	aquifer	not considered

7.8 Groundwater recharge

From the geological map and hydrogeological cross sections, it is concluded that outcrops of formations Bethlehem as well as upper Upper Beitkahil and upper Lower Beitkahil in the western parts of the basin recharge the Cenomanian sub-aquifers. In the western and northwestern sides, the outcrops of lower and upper Cenomanian play an important role in recharging the Cenomanian sub-aquifer, especially in southeastern sides of the basin. Turonian outcrops seems to be confined under Tubas area and unconfined near Tamoun area. None of the groundwater wells, that are located within the area of study are pumping from Turonian sub-aquifer.

124
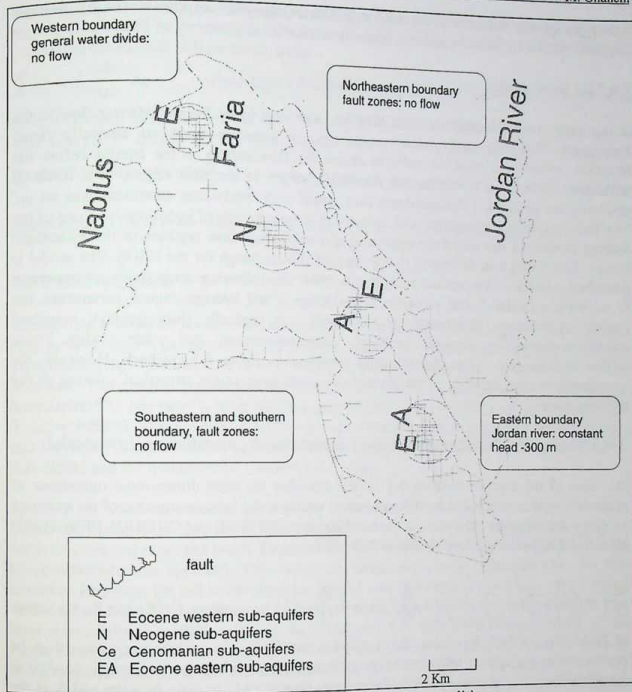
Fig. 7.4: The base map of the Faria basin showing its boundary conditions.

The recharge regions for the lower aquifer are the outcrops from lower and upper Cenomanian along the Faria anticline axis in the western parts of the basin. They are contributing water to the lower aquifer (SHALIV 1980). In these areas precipitation amounts is high and thus the recharge is high as well. In other eastern regions, in which the precipitation is lower than in the region of the anticlinal axes, lower recharge was assumed. The exposures of the western and the middle parts of the Faria basin are the recharge region of the upper aquifer. Annual average precipitation of 500 mm over the area is a dominant natural sources of replenishment to this basin. The recharge coefficient for the phreatic aquifer range from 0.1 to 0.25, according to the outcrop lithology. In the confined regions, the recharge coefficient is zero (GUTTMAN 1985). Part of the water is discharged by springs along Wadi Faria formations of the phreatic aquifer and find their way back to the aquifer, but flow in a reverse trend. The coefficient of return flow for these sections is 0.02 to 0.1, depending on the distance from the spring and lithology of the rock formation (GUTTMAN 1985). The output of the aquifer

125

system are springs and wells in the study area. The average yearly exploitation of groundwater from this aquifer by 74 wells annually sums up to 18 Mill. m³.

7.9 The flow model

In this study the finite different code Modflow was used to model groundwater flow in the Faria basin. This code accepts many various types of boundary conditions. Basically Visual Modflow model was used. In order to model the flow regime in the aquifer before the utilization started and to predict the expected changes in the flow regime as a result of operating the aquifers, a 3-dimensional flow model with steady-state conditions was set up. The Modflow code is recognized and accepted in the community of hydrologists as one of the leading models in the world for recreating and calibrating flow regimes in the hydrologic basins. The model was developed by Mc Donald and Harbaugh for the USGS. The model is described in detail in the manual published in 1994. The following components are important to establish a model: Initial estimates of hydrological and hydrogeological parameters, the model discretization horizontally (model grid) and vertically (Stratigraphy), boundary conditions (including pumpage, recharge, evapotranspiration) and water quality. Finite difference code have some disadvantages compared to finite element code. However, the advantage is easier handling of the discretization and more stable numerical solution of the flow equation.

7.9.1 Theoretical background of the 3-dimensional groundwater flow model

The base of the mathematical model, which describes the three dimensional movement of groundwater of constant density through porous media, is the balance equation of the quantity, which is described by the partial-differential equation (FREEZE and CHERRY 1979; TODD 1980 and MC DONALD and HARBAUGH 1996):

$$\frac{\delta}{\delta_x}\left(k_x\frac{\delta_h}{\delta_x}\right) + \frac{\delta}{\delta_y}\left(k_y\frac{\delta_h}{\delta_y}\right) + \frac{\delta}{\delta_z}\left(k_z\frac{\delta_h}{\delta_z}\right) - w = S_s\frac{\delta_h}{\delta_t}$$

where K_x, K_y and K_z are values of hydraulic conductivity along the x, y and z coordinate axes, which are assumed to be parallel to the major axes of hydraulic conductivity (m/day), h is the potentiometric head, w is a volumetric flux per unit volume and represents sources and / or sinks of water and S_s is the specific storage of a porous material and t is the time. This equation together with specification of flow and / or head conditions at boundaries of an aquifer system and specification of initial-head, constitutes a mathematical representation of an groundwater flow system. Finite difference method is used to solve this set of equations. The head is a function of time and space, so that discretization of the continuous time domain is also required. It derives from the continuity equation: the sum of all flows into and out of the cell must be equal to the rate of change in the storage within the cell. Outflow and loss are represented by defining outflow as a negative inflow and loss as a negative gain. These equations express inflow through a face of a cell i,j,k in terms of heads, grid dimensions and hydraulic conductivity. The differential equation that is used for the steady flow when the specific storage is set at zero is:

$$\frac{\delta}{\delta_x}\left(k_x\frac{\delta_h}{\delta_x}\right) + \frac{\delta}{\delta_y}\left(k_y\frac{\delta_h}{\delta_y}\right) + \frac{\delta}{\delta_z}\left(k_z\frac{\delta_h}{\delta_z}\right) = 0$$

To find a solution for this equation, it will be written in the finite difference form. A numerical grid will be produced for all points of the network using the continuity equation expressing the balance of flow for all nodes:

$$\sum Q_i = S_s \frac{\Delta h}{\Delta t} - \Delta v$$

where Q_i is a flow rate into the cell, S_s is the specific storage in the finite difference formulation, Δv is the volume of the cell and Δh is the change in head over a time interval of length Δt. The flow into the cells i, j, k is calculated using Darcy law

(DARCY 1856): $Q = KA \frac{\delta_h}{\delta_l}$ where Q is the discharge (L³/t), K is the hydraulic

conductivity (L/t), A is the cross-sectional area (L²) and $\frac{\delta_h}{\delta_l}$ is the hydraulic gradient

7.9.2 Discretization

A base map was drawn representing the Faria basin, its boundaries, positions of the wells and springs and their corresponding sub-aquifers (Fig. 7.4). This map was imported and georefrenced by TNT-mips. It was exported as DXF-format (vector file) to be used by Modflow. The external geometry of the system is defined by the configuration of it's natural boundaries. The geometry is lying within $X_{min} = 170000$, $X_{max} = 205000$, $Y_{min} = 160000$ and $Y_{max} = 195000$. The number of layers, that are defined for this model are three: phreatic aquifer (layer 1), aquiclude (layer 2) and confined aquifer (layer 3). The minimum elevation of Z is -850m and the maximum elevation of Z is +850m.

Modflow is used to simulate groundwater flow in three dimensions. Using the finite difference method, the domain in which the flow is simulated is divided into a rectilinear mesh of rows, columns and layers. Groundwater flow within the aquifer is simulated using a block-centered finite approach. The area of the model was divided into 100 rows by 100 columns. However, the cell width along the column was uniform grid spacing in both x and y directions of 350m. The confinement of layers were the same during all run simulations. The total active cells were 5000 cells and the model area was 320 Km². The continuity of the model is replaced by a set of discrete nodes in a grid pattern covering the modeled area. A block centered grid technique was used, where the node notes fall in the center of the grid. The bottom elevation of the three layers is imported as a Surfer grid file of minimum layer thickness of 1. The surface of the ground is imported as a surface grid file that is extracted from the DEM file. This DEM file is exported through TNT-mips as ASCII data format. The ASCII data format is filtered using Excel and the x, y coordinates are extracted as well as z-values. The x, y are extracted using the following equation:

$C = \sqrt{X^2 + Y^2} \ where X = X_1 - X_0 \text{ and } Y = Y_1 - Y_0$

$Sin\theta = \frac{Y_1 - Y_0}{C} \approx \frac{Y_i - Y_0}{C_1} \Rightarrow Y_i = \left(\frac{Y_1 - Y_0}{C}\right) * C_1 + Y_0$

Using the same equation with $Cos\theta = \left(\frac{X_1 - X_0}{C}\right) \Rightarrow X_i = \left(\frac{X_1 - X_0}{C}\right) * C_1 + C_0$

All grid Surfer files were treated using kriging and a spherical variogram function. The area around the Faria basin was digitized using a polygon inactive cells and inactive single cells. A shaded polygon appears indicating that these cells are inactive.

127

The model domain of the Faria basin is shown in Figure 7.4. The finite difference grid was created by discretizing the mode domain into rectangular cells. Model nodes, where heads and fluxes are specified or computed, are defined at the vertices of the element rectangular. Table 7.2 shows the proposed vertical discretization and stratigraphy of the model. The bottom of the lower aquifer 1, which represents the top of the aquitard Neocomian was selected as the base of the model. Hydraulically, the exchange of groundwater across the lower aquitard is unknown. Layer 3 represents the lower aquifer, which consists of lower and upper Beitkahel formations. It is anticipated that lower and upper Cenomanian sub-aquifers have similar hydraulic properties. Layer 2 represents the middle aquitard which has a low permeability and consists of chalks and marls (Mount Scoupes) formations. It represents the top of the confined aquifer. Layer 1 represents the phreatic upper aquifer, which consists the sub-aquifers of Pleistocene, Neogene and Eocene.

Table 7.2 : The proposed vertical discretization and the stratigraphy of the model.

Sub aquifer	aquifer system	no. of layer
Pleistocene	upper aquifer	1
Neogene	upper aquifer	1
Eocene	upper aquifer	1
Senonian	aquitard1	2
upper Cenomanian	lower aquifer1	3
lower Cenomanian	lower aquifer1	3
Neocomian	aquitard2	not considered
Albian	lower aquifer2	not considered

7.9.3 Additional input parameters

A unique solution of the groundwater flow differential equation requires an accurate definition of the boundary conditions, which describes the physical boundary of the hydrogeologic system. The Albian formations under the third layer is assumed to represent the impermeable base of the three dimensional model. The first and the third layer are separated from each other by the impermeable strata of Senonian formation in the western and semi permeable in the eastern parts of the basin. Therefore, downward and upward leakage from the phreatic and confined aquifer and visa versa in the vicinity of the Jordan Rift valley may occur.

A conductivity in the form of K_x , K_y and K_z was defined for each layer which appear in different colored zones of K. Since there was no information available concerning heterogeneity in any case K_x was set equal to K_y. Following the general advice of the Modflow manual K_z was set to a tenth of K_x. Initially, the first layer was defined by four different zones of k values as follows: Eocene western sub-aquifer of 21 m/day, Neogene sub-aquifer of 24 m/day, Pleistocene sub-aquifer of 8 m/day and Eocene eastern sub-aquifer of 40 m/day. The k of the second layer is given of 0.001 m/day and for the third layer of 0.3 m/day. The storage coefficient (Ss) was assumed with 0.002. The effective porosity is 0.02 and the total porosity is 0.03. The specific yield (S_y) is calculated to be 66%.

128

A recharge of the first layer was given according to Thiesen polygon method (chapter 3). Five recharge categories were given for the whole basin. The western regions are defined of higher recharge than the eastern regions.

The start and end points (N-S) of the Jordan river are -300 (x =199300, y =161300) and -311 (x =199300, y =161600) (DEM), respectively. The depth of the river is taken roughly of 1m and conductivity of bed was set of 0.01. The conductance (Modflow specific term) used to describe the ability of the river bed to conduct flow from the river to the aquifer and visa versa and was calculated according to the equation:

$$Conduc \tan ce = \frac{K_v * L * W}{B},$$ where K_v is the vertical conductance of the river bed, L is the length of the river, W is the wide of it and B is the thickness of the river bed. This conductance is calculated to be 430 for the input parameters of this model. Discharge data of springs was given as input of the inflow in this model.

7.9.4 Calibration

Different options were applied in order to select the best parameters set for this model. Different scenarios of K were taken to simulate the groundwater flow. The best option is shown for the first layer after subdividing the basin into two different zones; upper Faria in the western part with high conductivity values and lower Faria in the eastern part with low conductivity values. About 400 simulations were applied taking into consideration the conductivity of well fields, faults, constant head boundaries for the first and the third layer in the eastern part and river constant head. The values of conductivity and recharge were changed during these simulation in order to simulate the groundwater flow for the first and the third layer without generating dry cells, that had caused problems at the beginning. Some problems occurred due to dry cells in the second layer (aquiclude). This is due to the lack of data in this part, which has a large area without enough data that will cover all parts of it. Figures 7.5 and 7.6 represent the simulated steady-state water level map for the phreatic and confined aquifers. The contours are coinciding with the observed water level values (chapter 3). In the middle part of the Faria basin, there are differences due to intensive faulting. The steady state velocity field is illustrated in Fig. 5.7 and 5.8 for the phreatic and confined aquifers.

Calibration may be done by trial and error or inverse modeling (FREEZE and CHERRY 1979). This model was calibrated steady state and the objective was to represent the situation in the year 1960 (before utilization) for the whole aquifer system. The steady state calibration was based on a comparison of the measured water tables to calculated ones. The calibration was based on a comparison of the measured water tables to calculated ones. The calibration principle consists of simultaneously adjusting the permeability values of the aquifers, the vertical permeability of the aquiclude and the subsurface recharge values. Hydraulic conductivity is the most important parameter by which flow pattern and simulated water level is controlled. The calibrated hydraulic conductivities are shown in Table 7.3. The conductivity value of the aquiclude was estimated to be 0.003 m/day in the adjacent catchments of the same formations. Recharge coefficients were calibrated according to Fig. 7.9.

129
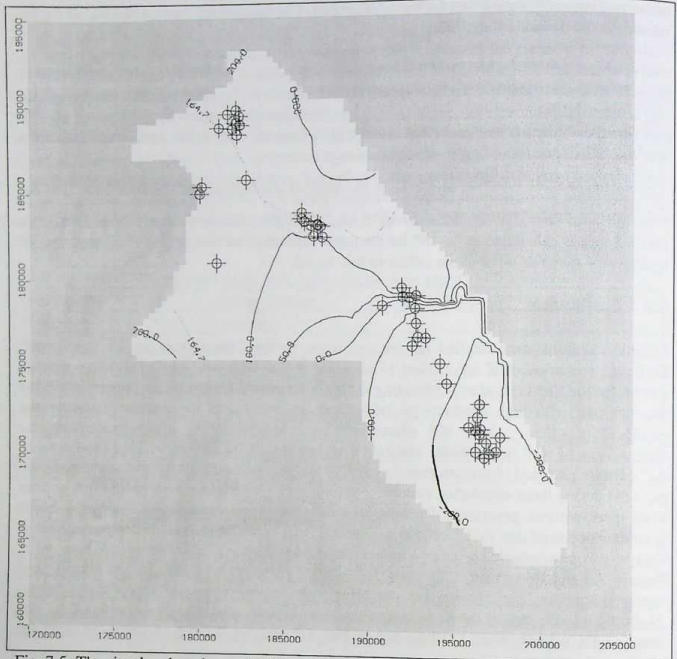
Fig. 7.5: The simulated equipotential lines of the phreatic aquifer.

7.10 Water flow budget

Considering the simulated calculations of the aquifer system, the in/out flows from the groundwater reservoir can be defined as follows: The recharge to all aquifers in this model was calculated to be 58 Mill. m³/year. The upward leakage to the Jordan river was calculated to be 0.1 Mill. m³/year. Recharge through constant head was found to be 0.4 Mill. m³/year. Water was discharged as springs from the aquifers before their utilization through wells. The discharge of springs was considered as outflow from the whole aquifer system and was calculated to be 14.1 Mill. m³/year. Table 7.4 shows the water flow budget of the whole model calculated on a yearly basis. The inflow - outflow = 44.4 Mill. m³/year which is flowing in the Jordan river. The estimated recharge of the basin in this model (58 Mill. 10³) matches the estimated one that was calculated in chapter 3 (60 Mill. 10³). The difference between the two amounts is attributed to the calibration phase of the model.

130
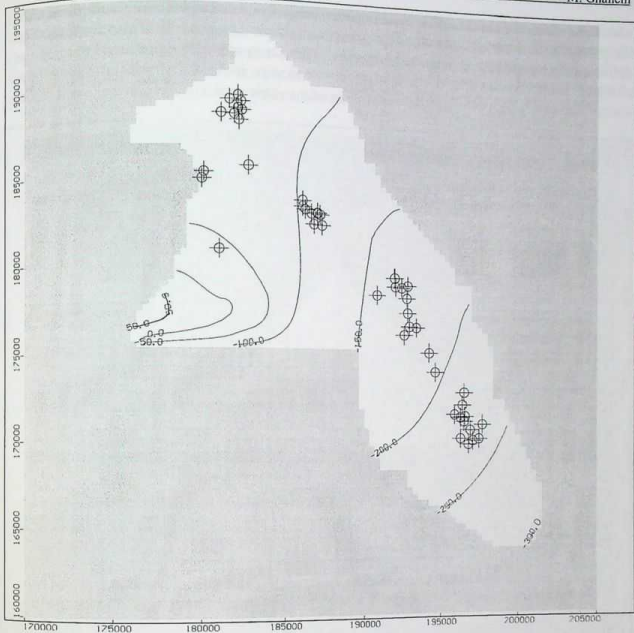
Fig.7.6: The simulated equipotential lines of the confined aquifer.

Table 7.3: The calibrated conductivity values of the phreatic and confind aquifers in m/day.

Layer	type	region	sub-aquifers	calibrated K
first	phreatic	upper Faria	Eocene western and Neogene	11
	aquifer	lower Faria	Eocene eastern and Pleistocene	0.06
second	aquiclude	upper Faria	Senonian aquiclude	0.003
		lower Faria		0.03
third	confined	upper Faria	lower and upper Cenomanian	1.5
	aquifer	lower Faria		5

7.11 Sensitivity analyses

Reliability of the predictions of a model dependent strongly on the quality of it's data and it's boundary conditions. In order to cope with the data in accuracy and in sufficient knowledge of the boundary conditions, the model has to be calibrated. During calibration, values of the various parameters are constantly changed until the calculated results are in good agreement

131

with the measured field data. The most important objective was to give a regional picture of the potentiometric surface as well as the groundwater flow directions. It is also important to delineate the hydrodynamic relationship between the two aquifers. The simulated data of the confined aquifer shows that the potentiometric surface is above the simulated data of the unconfined aquifer, especially in the eastern part of the study area.
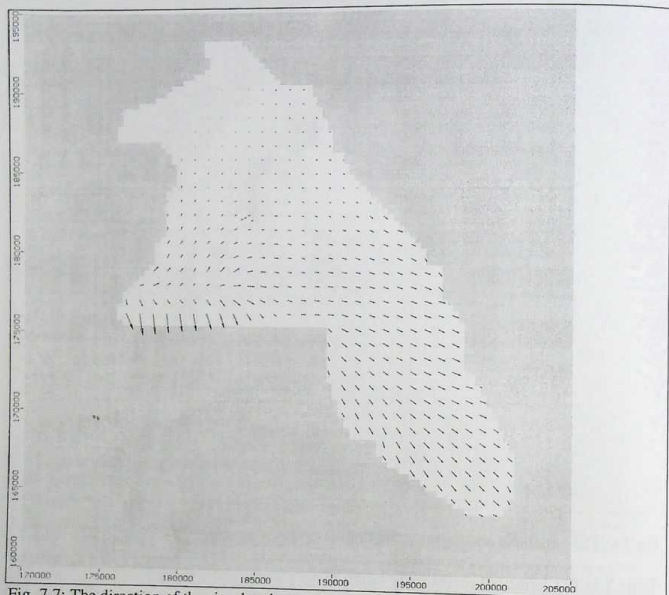
Fig. 7.7: The direction of the simulated water level of the confined aquifer.

Table 7.4: Water budget of the whole model domain (Mill. m³/year).

Flow item	In	Out	In-Out
Constant head	0.4	0	-0.4
Drains	0.0	0.0	0.0
Springs	0	14.1	-14.1
Recharge	58	0	58
River leakage	0.1	0	0.1
Sum	58.5	14.1	44.4
Discrepancy			0.0 %

Different options were taken by changing one parameter and keeping other parameter constant in order to reach the best fit of simulated values to the measured values. Recharge and conductivity parameters are the most effective parameters in the calibration phase. The simulated water level of the first layer is lower than the observed level. However in some places, there is some mismatching between the simulated and observed values.

Fig. 7.8: The direction of the simulated water level of the phreatic aquifer.

Three types of error are taken into consideration: the mean error, main observed error and root means square error (RMS). The error is found as follows: the mean error of 16.8 , the main observed error of 20.3 and the RMS of 29.1. The RMS error is the most important error which is equal to the square root of the standard deviations SD:

$$RMS = \sqrt{\sum (SD)^2}$$

The outcroppings of these aquifers are composed of fractured rocks and crossed by faults may cause the RMS to be larger than 5% of the difference between the highest and the lowest elevation points in the area (Fig. 7.10). The maximum deviation is found 70 m in the first layer of the eastern part. The mass balance which reveals to inflow - outflow to be 44.4 Mill. m³/year matches the groundwater balance of this basin that was calculated through different methodologies in chapter 3.

133

Applying this result of the steady state condition to obtain a mass balance of the unused water nowadays in this basin the following equation was used:

The unused water = (inflows-outflows) - (well discharges + runoff) = 44.4 Mill. m³/year (from the model) - (18 + 7.5 Mill. m³/year) (chapter 3) = 19.9 Mill. m³/year. This quantity of 19.9 Mill. m³/year could be exploited from the basin.
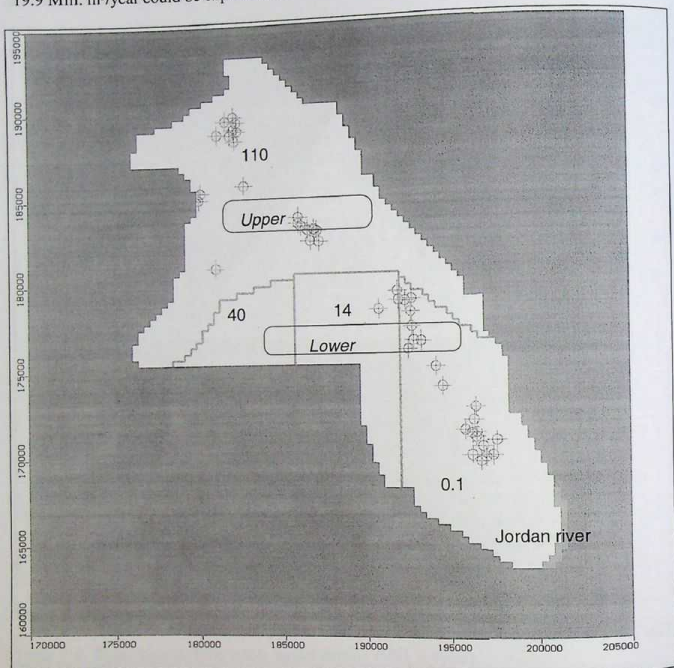
Fig. 7.9: Calibrated recharge zones for the phreatic aquifer (first layer) and the calibrated wells.

7.12 Model results and discussions

The conductivity values which were obtained at the end of the steady state calibration appear in Table 7.4. The calibrated conductivity of the second layer is 0.003 and 0.03 m/day in the western and eastern parts, respectively. The calibrated conductivity is found to be 1.5 and 5 m/day for the western and eastern of the third layer, respectively.

134

The version of the model that represents this system showed a good water balance i.e. the discrepancy in the calculations is about zero. Regarding to the model (steady state condition), the following results appeared after more than 400 run:

- The best result is taken after the subdivision of the basin into zones of conductivities.
- The calibration of the first layer shows that the observed data match the calculated data in the eastern and western parts and does not in the middle of the basin (+/- 70 m).
- The groundwater level of the third layer (confined aquifer) matches the observed data of this aquifer. The calibration of the third layer shows that the observed data match the calculated data with +/- 10m.
- The dried cells within the second layer (aquiclude) in the western part and the eastern part ($K_h = 0.003$ m/day) may be caused by the extreme thinness of this layer at some parts.
- Calibration is not easy because of the heterogeneity of the aquifer due to the faults and fractures which are spreading all over the area. These faults and fractures as well as the sharp topography affect the hydraulic properties of the aquifers to be of spatial variability.
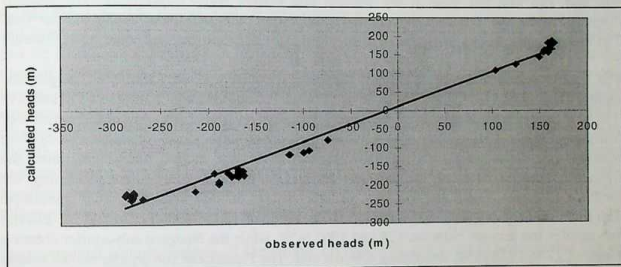
Fig. 7.10: The calculated heads against observed heads in meters in reference to sea level.

It is difficult to obtain accurate results during calibration of this model, due to the following reasons:

1- The geometry effect of the basin, which has a sharp slope (ranges from +850 ,,the highest point" to -850 ,,the lowest point"). Additional hydrogeological cross sections are necessary to cover the basin in order to avoid this effect. Modeling of small areas within the basin like the well field, which represents one sub-aquifer may give accurate modeling results.

2- The intense of faulting in the area, especially in the eastern parts and a highly jointed nature of the outcrops of both aquifers. The formations consist of limestone and dolomite (Karst), which will bring difficulties in calibrations according to the differences of conductivity within one layer.

3- Visual Modflow assumes Darcy–flow, which is not necessary by the case for karstic aquifers.

4- The data were taken from 4 wells fields along the Faria wadi, which does not make the extrapolations of data to be of a highly representative to those regions which are far away from the observed points. The scarcity and missing data will affect the model results and doesn't make it to represent the nature, especially in the places outside the well fields.

5- There is no any observation wells in the study area for the calibration phase and the data of pumping wells were used for it does not reflect very accurate calibration processes.

135

8 DISCUSSIONS AND CONCLUSIONS

Hydrogeological and hydrochemical studies were conducted in the Faria catchment area (320 km²) in the north eastern part of the West Bank. Colored stratigraphical and structural maps were done using TNT-mips in order to define the recharge zones of the aquifer system in the area.

A hydrological study was conducted to determine the volume of recharge to the groundwater. Thirty years data of precipitation, evapotranspiration, wind, humidity and runoff records were used to determine the recharge rate in these semi-arid to arid region. Using global and hydrometeorological groundwater-balance equations as well as the salt-balance method and the numerical Modflow model, the annual recharge volume was estimated to be around 60 Mill. m³. The rate of infiltration was found to be 26 % of the rainfall, which varies between 598 and 196 mm per year in the western and eastern parts, respectively. The recently discharge of the aquifers through wells and springs were calculated to be 32 Mill. 10^3 per year. The unused groundwater is estimated to be +16.6 Mill. m³ in the area and could be exploited.

The aquifer system consists of phreatic (upper) and confined (lower) aquifers. The phreatic aquifer consists of Pleistocene, Neogene and Eocene sub aquifers with a saturated thickness of 3 to 82.9 m; while the thickness of the lower aquifer ranges from 131 to 440 m and consists of lower and upper Cenomanian sub aquifers. A total of three step - drawdown tests, five constant rate - pumping tests and two recovery tests were carried out to determine the hydraulic characteristics of the sub-aquifers and to evaluate their potentials. Using the methods of Jacob, Theis and recovery, different values of transmissivities were calculated. The Pleistocene sub-aquifer has a transmissivity range of 126 to 10000 m^2/d and the Eocene sub-aquifer has a range between 158 and 1960 m^2/d; while the Neogene sub-aquifer shows a range of 12 to 1138 m^2/d, decreasing towards east. The Pleistocene sub-aquifer shows a wide range of transmissivity within a small area, due to the fracturing caused by the complex structure in the area that were formed during the formation of the Jordan Rift Valley. A trend of increasing transmissivity towards the Jordan Rift is determined, which is due to fracturing, faulting and also to the hydraulic connection of lower to upper Cenomanian as well as karstification phenomena. Values of transmissivity and specific capacity were used for evaluating the potentiality of the aquifers. The hydraulic conductivity of the Eocene sub-aquifer is increasing toward the east with the increased density of faulting. The Neogene sub-aquifer has a conductivity of 28.4 m/day ; while Pleistocene sub-aquifer shows 8 m/day. The confined aquifer shows a range of 0.23 to 25.7 m/day. The storativity of the confined aquifer shows a range from $1.1 * 10^{-3}$ to $1 * 10^{-5}$.

A hydrochemical study was conducted to define water types in the study area and to determine hydrochemical parameters of the aquifer system. More than 150 water samples were analysed within two water sampling campaigns (before and after recharge), which covered all springs and groundwater wells as well as surface water (wadies) in the area. The physical properties (temperature and EC), chemical properties (pH, dissolved oxygen, major ions, trace elements) and microbiological properties (total and fecal coliforms) were determined. The major ions are represented by four major cations (Ca^{2+}, Mg^{2+}, Na^+ and K^+) and four major anions (HCO_3^-, Cl^-, SO_4^{2-} and NO_3^-). The minor constituents are represented by SiO_2, F^-, Br^-, I^- and PO_4^{3-}. The trace elements Cu, Cd, Fe, Mn, Cr, Zn, Pb were determined. Statistical analyses of all hydrochemical elements were used and interpretated on the 0.01 significance level. Indicators for water quality were determined using salinity and soluble sodium percentage showing that

the confined aquifer is not polluted. The hydrogeochemical model PhreeqC was used to calculate distribution of species and saturation indices. Ionic Strength, Electrical balance and Electrical error were calculated.

Two categories of groundwater were recognized according to the TDS i.e. fresh water within the phreatic western sub-aquifers and the confined aquifer, and brackish water within the phreatic eastern sub-aquifers. The water has a calcium - bicarbonate type in the western parts and sodium-chloride type in the eastern parts. The ion concentrations of water show an increasing trend towards the east. Two groundwater bodies were identified: a low salinity groundwater originating from Cenomanian as well as Eocene sub-aquifers, and a high salinity groundwater originating from Pleistocene and basalt sub-aquifers. The majority of the groundwater were found to be of the calcium-sodium-cation type. Two anion types were found: chloride-sulphate-bicarbonate for the eastern phreatic sub-aquifers and bicarbonate-chloride-sulphate type for the western phreatic sub-aquifer as well as the confined aquifer. The western phreatic sub-aquifers and the confined sub-aquifers are classified as calcium - bicarbonate type. The eastern phreatic sub-aquifers are classified as calcium - chloride type and some of them as calcium-magnesium-chloride type. The phreatic western sub-aquifers and the confined aquifer show an increasing trend of $Ca^{2+} > Mg^{2+} > Na^+ > K^+$. An increasing trend of $Ca^{2+} > Na^+ + K^+ > Mg^{2+}$ is shown for the eastern phreatic sub-aquifers. Three anions increasing trends were observed $HCO_3^- > CL^- > NO_3^- > SO_4^{2-}$ (Eocene western and Neogene sub-aquifers), $HCO_3^- > CL^- > SO_4^{2-} > NO_3^-$ (the confined aquifer) and $CL^- > HCO_3^- > SO_4^{2-} > NO_3^-$ (Eocene eastern and Pleistocene sub-aquifers). The chemical composition of the confined aquifer is homogeneous in comparison with the phreatic aquifer. The latter shows increase concentration of chemical constituents toward the east. Generally, the western phreatic sub-aquifers and the confined sub-aquifers show the same distribution species and slightly different from those of the phreatic eastern sub-aquifers.

Environmental isotope analyses of Deuterium, Oxygen - 18 and Tritium were carried out in the phreatic and confined aquifers in order to determine the origin of groundwater. The mean of Deuterium values and Oxygen-18 was -24.4 $^0/_{00}$ and -5.5 $^0/_{00}$ respectively. The values of ^2H and ^{18}O were used to identify the local meteoric water line in the area. The Tritium contents show a variability of 1.3 to 2.2 TU for the lower aquifer and 2.6 to 7.6 TU for the upper aquifer. The variability of ^3H content for the upper aquifer indicates, that its recharge ranges occurs from the year 1953 onwards. The Neogene sub-aquifer in the Faria basin has a low values of ^3H (1 and 1.2 TU), this indicates that it has water older than the year 1953.

A digital elevation model was constructed for the Faria basin to be used for a rainfall distribution. It was concluded from the hydrogeological cross sections that formations of the lower aquifer are not absolutely confined but acts as semi-confined in some places, especially in the eastern parts of the Faria basin.

A 3-dimensional model of multi-layer system in the Faria basin of Modflow type was built. More than 400 simulations runs were carried out during the calibration procedure. Three layers that represent the aquifer system of phreatic and confined aquifers as well as aquiclude were assigned using steady state condition . The best result were obtained by subdividing that basin into two conductivity zones of each layer. The calibration of the third layer shows that the observed data match the calculated data and the calibration of the first layer shows that the observed data match the calculated data in the eastern and western parts and does not match too good the middle of the basin. Calibration is difficult because of the heterogeneity of the rock formations of these aquifers which is due to the faults and fractures which are spreading

137

all over the area. These structural elements as well as the sharp topography cause a high spatial variability of the hydraulic properties of the aquifers. To avoid these problems a fault model would be recommended, where all faults are represented by cells of high permeability. The reasons that this model is of fairly good agreement between the measured and calculated data may come from the geometry sharp slope effect of the basin, the intense of faults in the area, the karstic nature of rocks and the scarcity of data. This means that the model results are in a good accordance with the field investigations.

The work could be considered as the first step to model the area taking the sub-aquifers of each major aquifer into account. Additional hydrogeological cross sections are necessary to cover all the basin in order to define the geometry of each sub-aquifer in more detail. Modeling of sub-areas within the basin like the well field, which represents one sub-aquifer may give more accurate modeling results. For improving this model, more data are needed in order to refine the grid of the model and to go forward to calibrate a transient model.

9 REFERENCES

ABOU KARAKI, N. (1985): The Carmel-Wadi El Fari'a microearthquake activity.11p.

ABDUL JABER, Q. and ALIEWI, A. (1996): On the development of the Nablus area water
    resources: Water quality assessment, PHG, Jerusalem.

ABU SAFAT, M. (1990): The possibilities of building a dam on Wadi El Fari'a -
    geomorphological study. Al Najah J. for Researches 2 (5): pp. 181 - 221.

ALIEWI, A. et al. (1994): Selection of a Pilot catchment for the development of a hydrological
    monitoring system in Palestine.

AMERICAN PUBLIC HEALTH ASSOCIATION (APHA), American Water Works Association and
    Water Pollution Control Federation (1995): Standard methods for the examination of water and
    wastewater, 16th edition, American Health Association, Washington, DC, USA.

APPELO, C. and POSTMA, D. (1996): Geochemistry, groundwater and pollution, Balkema pub.,
    Retterdam , Netherlands.

ARAD, A., KAFRI, U., HALICZ, L. and BRENNER, I. (1984): Chemical composition and minor
    elements in natural groundwater in Israel. Israe. Geol. Surv., Report. GSI/29/84, 52p., & 41p. (Appen.),
    tabs.

ARAD, A., KAFRI, U. and FLEISHER, E. (1975): The Na'aman springs, northern Israel: salination
    mechanism of an irregular freshwater - sea water. Journal of hydrology, vol. 25 (81-104 p.), North
    Holland pub.com.Amesterdam.

ARAD, A. and BEIN, A. (1986): Saline - Versus freshwater contribution to the thermal waters
    of the northern Jordan Rift Valley, Israel. Journal of hydrology, vol. 83 (49-66p.), North Holland
    pub.com.Amesterdam.

ARAD, A. and MICHAELI, A. (1967): Hydrogeological investigations in the western catchment
    of the Dead Sea. Israeli journal of earth sciences, vol.16, pp. 181 - 196.

ARKIN, Y. (1980): A survey of karst phenomena - western Judean mountains. Geol.Surv. Isra.
    Rep. MM 5/80, 30p.

AWARTANI, H. (1992): Artesian wells in Palestine: Present status and future aspirations,
    Palestinian Hydrology Group, Jerusalem.

BAER, G. and MIMRAN, Y. (1993): Paleomagnetism and Structural History of the Fari'a
    Anticline, eastern Shomeron. GSI current Research 58 - 61, GIS Jerusalem.

BARTOV, Y. and BEIN, A. (1994): The geology and hydrogeology of the central Arava between
    Yotvata and Paran. Isr. Geol. Surv. Rep. GSI/5/94, 20p.

BLAKE, G.S. (1928): Geology and water resources in Palestine, Jerusalem.

BLAKE, G.S. (1939): Geological map of Palestine, scale 1:250,000 (North sheet). Jerusalem,
    printing and stationary office, 133 p.

BLAKE, G., and GOLDSCHMIDt, M., 1947. Geology and water resources of Palestine. Jerusalem,
    Dep. of land settlement and water commissioner, 412 P., maps.

BLANKENHORN, M. (1896): Entstelung und Geschichte des Toten Meers, Zeitschr, Deutsch,
    Palästina. Ver.Leipzig, XIX.

BONEH, Y. and BAIDA, U. (1978): Water resources and their utilization in Judea and Samaria,"
    Judea and Samaria studies in settlement geography, Tel -Aviv university.: Bar Ilan university, vol.1.,
    pp.34-48, 1977 (in Hebrew).

BURDON, D. (1959): Handbook of the geology of Jordan. Government of the Hashemite
    kingdom of Jordan.

CANSTANCY, G. (1967): Prospection et Exploitation des Eaux Souterrain: Dunod, Paris.

CARMI and GAT, (1973): Tritium in precipitation and freshwater sources in Israel. Isr. J. Earth
    Sci., 22: 71-92.

CARROLL, D. (1962): Rainwater as a chemical agent of geologic processes - A review, U.S.
    Geological Survey water supply paper, 1535 - Q, 18pp.

CIVIL ADMINISTRATION OF THE WEST BANK; Telecommunication and Meteorological Service: The
    regional characteristics of the climate of the West Bank. (In Hebrew).

CDM, (1997): Study of the sustainable yield of the eastern aquifer basin, Task 18.

CRAIG, H. (1961). Standards for reporting concentrations of deuterium and oxygen - 18 in
    natural waters. Science, 133: 1833.

DARCY, H. (1856): Le fontaines publiques de la ville de Dijon, V. Dalmont, Paris, 647 pp.

References

DROR, G. and RAGOUL, A. (1971): Hydrogeology of Shomroun, Hydrological Service, Jerusalem.

EL-NASER, H. (1991): Groundwater resources of deep aquifer systems in NW-Jordan: hydrogeological and hydrogeochemical quasi 3-dimensional modeling. Ph.D. thesis, Würzburg university, 144pp.

ERIKSSON E. (1985): Principles and applications of Hydrochemistry. Chapman and Hall, London.

FREEZE, R. and CHERRY, J. (1979): Groundwater, Englewood Cliffs, N.J.: Pentice Hall, 604p.

FRESENIUS, W., QUENTIN, K. and SCHNEIDER, W. (1988): Water analysis; a practical guide to physio - chemical, chemical and microbiological water examination and quality assurance. Springer - Verlag, Berlin, Heidelberg, New York.

FRUMKIN, A. (1992): Karst origin of the upper erosion surface in the northern Judean mountains, Israel.Isr.J.Earth Sci.41: 169 - 176.

GAT, J. and DANSGAARD, W. (1972): Stable isotope survey of the fresh water occurrences in Israel and the northern Jordan Rift Valley. Journal of hydrology, vol. 16 (177-212p.), North Holland pub.com.Amesterdam.

GAT, J. (1972): Local variability of the isotope composition of groundwater . IAEA - SM - 182/29.

GAT, J. (1972): Comments on the stable isotope method in regional groundwater investigations. Water resources research Jou., vol. 7, no. 4. p.980.

GEOLOGICAL SURVEY OF ISRAEL (1997): Geological map of the southern Shomroun. Scale 1: 100,000, Jerusalem.

GEOLOGICAL SURVEY OF ISRAEL (1965): Geological map: Northern Sheet. Scale 1: 250,000, Jerusalem.

GOLDEN SOFTWARE, INC. (1995): Surfer for windows, version 6, Colorado, USA.

GOLDSCHMID, D. (1974): Water quality aspects of groundwater recharge in Israel. American water works association journal, Vol. 66, no.3.

GOLDSCHMIDT, M.J., ARAD, A. and NEEV, D. (1967): The mechanism of saline springs in the lake Tiberias depression GSI, Bull. No. 45 and Hydrol. Service , Hydrol. Paper No.11.

GREITZER, Y. (1963): groundwater salinity in the Cenomanian - Touronian aquifer of central Israel. Tahal , p.12, Tel Aviv.

GTZ (1995): Middle east regional study on water supply and demand development, Water and environmental research center, Al Najah University, Nablus, (unpublished report).

GUTTMAN, Y. (1997): The hydrogeological conditions in the Cenomanian aquifer along the margins of the Jordan Valley (the Fazael - Auja - Jericho area). (in Hebrew). Tel Aviv, Tahal (01/79/26).

GUTTMAN, Y., (1985): The hydrogeology of the eastern basin and possibilities for the development of water resources from the pharaoh stream to the Judean desert: Tahal, Tel Aviv, 01/95/105.

GUTTMAN, Y. and ZUKERMAN Ch. (1995): A model of the flow in the eastern basin of the mountains of Samaria from the Far'ah stream to the Jordan desert. Tahal, Tel Aviv, 01/ 95/66.

GUTTMAN, Y. (1995): The hydrogeology of the eastern basin and possibilities for the development of water resources from the pharaoh stream to the Judean desert. Tahal, Tel Aviv, 01/95/105.

GWW, (1994): Groundwater for Windows (manual and software), United Nation, New York.

HEMM, J.D. (1985): Study and interpretation of the chemical characteristics of natural water. USGS Water Supply Paper 2254, 3. Aufl. Washington D.C. 263p.

HARPAZ, Y. and SCHWARZ, J. (1966): Operating a limestone aquifer as a reservoir for a water supply system. Tahal, water planning for Israel, Tel Aviv.

HULL, E. (1889): Mount Seir, Sinai and western Palestine, published for the committee of the Palestinian Exploration Fund.

HUSARY, S., NAJJAR, T. and ALIEWI, M. (1995): Analyses of secondary source rainfall data from the northern west Bank, PHG, Jerusalem.

HYDROLOGICAL SERVICE (1997): Data about groundwater wells, unpublished data, Jeruslaem.

HYDROLOGICAL YEAR-BOOK OF ISRAEL (1987): Ministry of Agriculture, Water Commission and Hydrological Service: Jerusalem 1967- 1994.

IAEA (1988): Guidebook on Nuclear techniques in hydrology, IAEA , Vienna.

ISSAR, A. (1978): The use of isotopes for determining the past future hydrogeological regime of fossil aquifers. Ben Gurion Unv. of the Negev .

ISSAR, A. and GAT, J. (1982): Environmental Isotopes as a tool in hydrogeological research in an arid basin.

JOFFE, S. AND GARFUNKEL, Z. (1989): Plate kinematics of the cercum Red Sea reevaluation. Tectophysica 141: pp. 5-22.

KAFRI, U. (1970): Factors controlling the location of the groundwater divide in northern Isarel. Journal of hydrology, vol. 11 (22-29p.), North Holland pub. com. Amesterdam.

KAFRI, U. (1970): The Cenomanian - Turonian calcareous aquifer of central and western Galilee, Isreal. Bulletin of International Association of Hydrology, XV, 4 12/1972.

KAFRI, U., ARAD, A. and HALICZ, L. (1989): Flourine occurrence in groundwater in Israel and its significance. J. Hydol. 106: 109-129.

KAUFMAN, S. and LIBBY, W. (1954): Natural distribution of Tritium. Phys. Rev. 93: 1337-1344.

KONIKOW, L.F. and MERCER, J.W. (1988): Groundwater flow and transport modeling. J.Hydrology, 100: pp. 379-409.

KRASNY, J. (1993): Classification of transmissivity magnitude and variation: Groundwater., Vol.31, NO.2, pp.230-236.

KRUSEMAN, G. and RIDDER, N. (1994): Analysis and evaluation of pumping test data: Int. Institute for land reclamation and improvement, Amsterdam.

KROITOTU, L. (1987): The Characterization of Flow Systems in Carbonate Rocks defined by the groundwater parameters: Central Israel, Ph.D. thesis, Weizman Institute of Science, Rehovot, Israel, p124.

KROITORU, L., MAZOR, E.and GILAD, D. (1985): Hydrological characteristics of the Wadi Kelt and Elisha springs. Scientific basis of the water resources management (proceeding of the Jerusalem Symposium.Pub.No.153.

KRONFELD, J., VOGEL, J. and ROSENTHAL, A. (1992): Natural isotopes and water stratification in the Judea group aquifer (Judean desert). Isr.J.Earth Sci.; 39: 71- 76.

KRONFELD J. and ROSENTHAL, E. (1979): Uranium isotopes as a natural tracer in the waters of the Bet Shean - Harod valleys. (Abstract) 25th Annual meeting, Isr. Geo. Soci., Jerusalem.

LARTET, L. (1869): Essai sur la geölogie de la Palesstine, Amm.Sci.Geol., Pt.I., Paris.

LERMAN, A. (1970): Chemical equilibrium and evolution of chloride brines. 50th Anniv. Symp. Miner. Soc., Spec., Pap., 3: 291-306.

LEVY, Y. (1972): Interaction between brines and sediments in the Bardawil area, Northern Sinai. Ph.D. thesis, Hebrew university, Jerusalem, 113 pp. (in Hebrew).

LLOYD, J.W. and HEATHCOTE, J.A. (1985): Natural inorganic hydrochemistry in relation to groundwater, 296p, New York (Oxford University Press).

LYAKHOVSKY, V., BEN-AVRAHAM, Z. and ACHMON, M. (1994): The origin of the Dead Sea Rift: results of computer simulations. Annual meeting, Israel Geological Society.

MC DONALD M. and HARBAUGH A. (1996). Users documentation for Modflow 96, an update to the U.S. Geological Survey.

MANDEL, S. (1957): Investigation of the geo-hydrology of Tannim River catchment area. Tel Aviv.

MATTHESS, G. (1990): Die Beschaffenheit des Grundwassers, Bornträger, Berlin, 498p.

MAZOR, E. (1991): Applied chemical and isotopic groundwater hydrology. Open university press, Buckingham, 274pp.

MAZOR, E. and MOLCHO, M. (1972): Geochemical studies on the E-Feshcha springs, Dead Sea Basin. Journal of hydrology, 15 (37-47 p.), North Holland pub. com.

MAYO, A., MULLER, A. AND RALSTON, D. (1985): Hydrogeology of the Meade Thrust Allochthon, southeastern Idaho, U.S.A., and its relevance to stratigraphic and structural groundwater flow control. Journal of Hydrology 76: 27-61.

ME'IRI, D. and GUTTMAN, J. (1984): A hydrological Model of the Wadi Faria catchment basin. (In Hebrew). Tel Aviv, Tahal, 25 p.

MERKEL, B. and MERKEL, J. (1997): PHREDIT, a windows shell for PHREEQC. Http://www.geo.tu-freiberg.de/istitut/hydro/phr.tools. phtml.

METEOROLOGICAL SERVICE (1997): Rainfall, temperature, humidity, evaporation and wind data (5 stations). Unpublished data, Bet-Dagan.

METEOROLOGICAL SERVICE (1997). Meteorological data: Rainfall, temperature, wind, humidity and evapotranspiration: Unpublished data, Rahovet - Tel Aviv.

MIMRAN, Y. and NATHAN, Y. (1985): Phosphatic rocks from a Mishash formation outcrop in the eastern flank of the Fari'a anticline. Isr.J.Earth Sci. 34: pp. 227-228.

References

MIMRAN, Y. (1984): Unconformities on the eastern flank of Fari'a Anticline and their implications on the structural evolution of Samaria.Isr.J.Earth.Sci.33: 1-11.

MIMRAN, Y. (1969): the geology of the Wadi Malih area. M.Sc. thesis, Hebrew university, Jerusalem, 68p. (in Hebrew).

MIMRAN, Y. (1972): Tayasir volcanics: a lower Cretaceous formation in the Shomeron, central Israel.Isr.Geol.sur.Bull.52, 9p.

MINISTRY OF AGRICULTURE - WATER COMMISSION, HYDROLOGICAL SERVICE (1973): Judean and Samarian Springs 1967/1968 - 1970/1971.

NISSENBAUM, A. (1978): Sulfur isotope distribution in sulfates from surface waters from the northern Jordan Valley, Israel. Environmental science and technology, vol. 12, p.962.

NUSEIBEH, M. and NASSER, T. (1995): Palestinian fresh water springs-Springs description, flow and water quality (1970-1994), PCG, Jerusalem.

PARKHURST, D. L., THORSTERNSON, D.C. and PLUMMER, L.N. (1980): Phreeqe- a computer program for geochemical calculations. U.S. geological Survey, Water Resources Invest., 80-96, NTIS Tech. Report. PB81-167801, Springfield, 210pp.

PETTIJOHN, F.J. (1957): Sedimentary rocks. Harper and Row, New York, N.Y., 2 nd ed., 718pp.

PICARD, L. (1943): Structure and evolution of Palestine, Bull Geol. Dep. Hebrew University, Jerusalem, Vol. IV, No. 2-3-4, pp. 1-134.

PIPEr, A, (1944): A graphic procedure in the geochemical interpretation of water analyses, Trans Amer. Geophys. Union 25, pp. 914-928, Washington.

RABI, A., DAIBES, F. and ALIEWI, M. (1994): Availability and reliability of secondary source hydrogeological data for the West Bank with additional reference material for Gaza Strip, PHG, Jerusalem.

ROFE and RAFFERTEY CONSULTING ENG. (1965): West Bank hydrology: Nablus district water resources survey, geological and hydrological report, 120pp.

ROFE and RAFFETY CONSULTING ENG. (1965): West Bank Hydrology, 1963 - 1965; Analysis.

RONEN, D. and REBHUN, M. (1974): Groundwater quality monitoring. Belg-Isr.Symp. Groundwater quality control manag., Brussels.

ROSENTHAL E. (1988): Hydrochemical changes induced by over exploitation of groundwater at common outlets of the Bet Shean-Harod multiple aquifer system, Israel. Journal of hydrology, 97 (107- 128 p.).

ROSENTHAL E. (1988): Ca-Chloride brines at common outlets of the Bet Shean-Harod Multiple-Aquifer system, Israel. journal of hydrology, 97 (89- 106 p.).

ROSENTHAL, A. (1978): U234/U238 Disequilibrium in Waters of the Judea group aquifer in the eastern slope of the Judean and Samarea hills. M.Sc.thesis in Tel Aviv Univ.

ROTSTEIN, Y., BARTOV, Y. and HOFSTETTER, A. (1991): Active compressional tectonics in the Jericho area, Dead sea Rift. Red Sea: Birth and early History of a new oceanic Basin. Tectonophysics, 198: 129 - 259.

SCHNEIDER, R. (1991): Geologic and hydrologic factors related to artificial recharge of the carbonate rock aquifer system of central Israel.

SCHWARZ, J. (1980): Water Resources in Judea, Samaria and Gaza Strip.

SCHWARZ, J. (1982): Water resources in Judea, Samaria and Gaza Strip; View on the present & future, ed. By D. Elazar. American Enterprise Inst. For Public Policy Res., Washington, D.C.

SEMHAN, Z. (1999): Data reconstruction and groundwater flow modeling in the eastern aquifer-the West Bank-Palestine. M.Sc. Thesis, IHE, Delft, Holland.

SHALIV G., et al. (1991): The sedimentary and structural history of the Bet Shean area and it's regional applications.

SHALIV, G. (1980): The Bet Shean and eastern Samaria basins; Updated of the hydrogeological model. (In Hebrew). Tel Aviv, Tahal, 82 p.

SHALIV, G. (1972): The hydrogeology of Wadi Faria region. Part I: Geology; part II hydrology. (In Hebrew). Tel Aviv, Tahal, 81 & 91 p., Appen. (HR/72/097). (M.sc. thesis, Heb. Univ., Jerusalem).

SHALIV, G. (1989): Stages in the tectonic and volcanic history of Neogene continental basins in northern Israel. Ph.D. thesis, Hebrew university, Jerusalem, 100pp. (in Hebrew).

SHALIV, G. (1980): The Weather model of Bet Shean area in the eastern Shomeron. (In Hebrew) report

SPSS FOR WINDOWS (1997): Statistical package for the social sciences, Chicago: SPSS Inc.

STARINSKY, A. et al. (1977): The isotopic composition of Sr in groundwater, Israel (abstract).Annual meeting, Isr. Geo. Soci., Jerusalem.

STARINSKY, A. (1974): Relationship between ca-chloride brines and sedimentary rocks in Israel. Ph.D. Thesis, Hebrew University, Jerusalem (in Hebrew).

STECKER et al. (1988): Subsidence in the Gulf of Suez: implications for rifting and plate kinematics. Tectonophysics, 153: 249-270.

STUMM, W. and MORGAN, J. (1981): Aquatic chemistry: an introduction emphasizing chemical equilibric in natural waters, John Wiley and Sons, New York, 780p.

TAHAL CONSULTING ENG. LTD. (1973): City of Nablus; Master plan for water supply. Haifa, (04/73/20),

TAHAL CONSULTING ENG. LTD. (1963): Underground water storage study. Technical report no.1.Tel Aviv.

TAHAL CONSULTING ENG. LTD. (1966): Hydrogeology of Turonian-Cenomanian aquifer, Technical report. Tel Aviv.

TAHAL CONSULTING ENG. LTD. (1975): Junction of the Bet Shean water system to the national water supply system; preliminary draft, /in Hebrew/, Technical report No.01/75/82, Tel Aviv.

TODD, D.K. (1980): Groundwater Hydrology. John Wiley and Sons, 535 pp.

TOPOGRAPHIC SURVEY OF ISRAEL (1992): Topographic map sheets: Nablus, Areil, Maalie Adumiem and Baqaaout. Scale 1: 50,000, Jerusalem.

TRISTRAM, H.B. (1865): The land of Israel, a journal of travels in Palestine undertaken with special reference to it's physical character, London Soc.Promot.Christ knowledge.

UNESCO, (1979): Aridity definition (UN documents): New York.

WAKSHAL, E. and YARON, F.(1969): 234U/238U disequilibrium in waters of the Judea group (Cenomanian - Turonian) aquifer in Galilee, northern Israel.

WARAD, I. and SHAW, S. (1946): Joint Memorandum on Surface and Underground water development schemes.

WATER DEPARTMENT (1978): A monthly pumpage of the groundwater wells in the West Bank in the year 1977 - 1978. Report (In Arabic), Ramallah.

WEINBERGER, G., ROSENTHAL, A., BEN-ZVI, A. and ZEITOUN, D. (1994): The Yarkon - Taninim groundwater basin, Israel hydrogeology: case study and critical review. Journal of hydrology, 161 (227-255 p.).

WEINBERGER, G., ROSENTHAL, E. and ZEITOUN, D. (1994): The Yarkon - Taninim groundwater basin, Israel hydrogeology: case study and critical review. Jour. of hydrology 161, p227-255.

WILCOX, L.V. (1955): Classification and use irrigation waters, US Dep. Agric. Circ. 969, Washington, D.C., 19pp.

WORLD HEALTH ORGANIZATION (WHO) (1989): Guidelines for drinking water-water quality; volume II; Health criteria and other supporting information (Arabic version). WHO regional office, Alexandria.

WATER AND SOIL ENVIRONMENTAL RESEARCH UNIT (WSERU) (1996): Instructions and standard methods for analysing major and trace elements, unpublished, Bethlehem university, Bethlehem, Palestine.

YAALON, D. (1963): On the origin and accumulation of salts in groundwater and in soils of Israel. Bulletin of the research council of Israel: section Geology, vol.11G, no.3.

YECHIELI, Y., RONEN, D., CARMI, I. and KAUFMAN, A. (1994): New tritium data in waters of the Dead sea area. Isr.J.Earth Sci.; 43: 213-220.

10 APPENDIXES

Appendix 1.1: The drainage map of the Faria basin computed with GIS
software package TNT-mips.
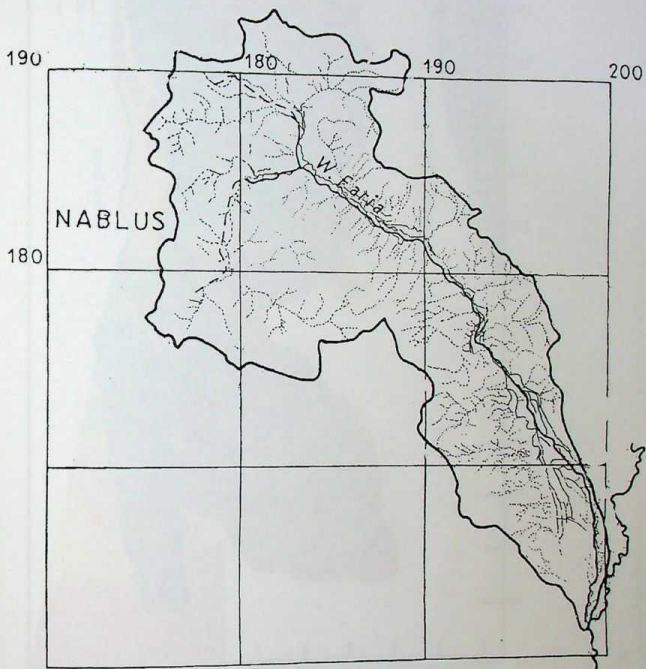
Appendix 2.1: The geological map of the West Bank modified after Rofe and Raffety (1965).

Legend:
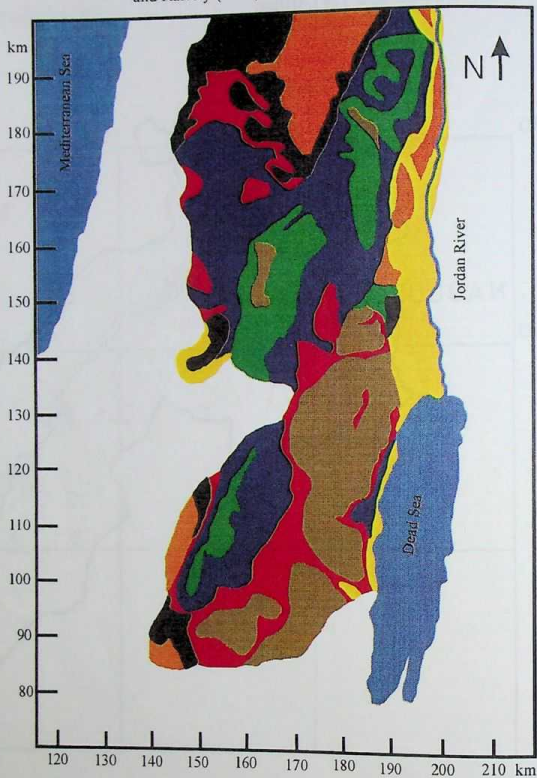
- Alluvium/Pleistocene
- Eocene
- Senonian/Paleocene undivided
- Senonian
- Turonian
- Upper Cenomanian
- Lower Cenomanian

Appendix 2.2: The geological map of the Faria basin (Stratigraphical map).

Ø   2   4 kilometers

Chalk undifferentiated

Jerusalem

Bethlehem

Hebron

Yatta

Upper Beit Kahel

Lower Beit Kahel

Ramali

Appendix 2.3: The structural map of the Faria basin (fault pattern map)
computed with GIS software package TNT-mips.
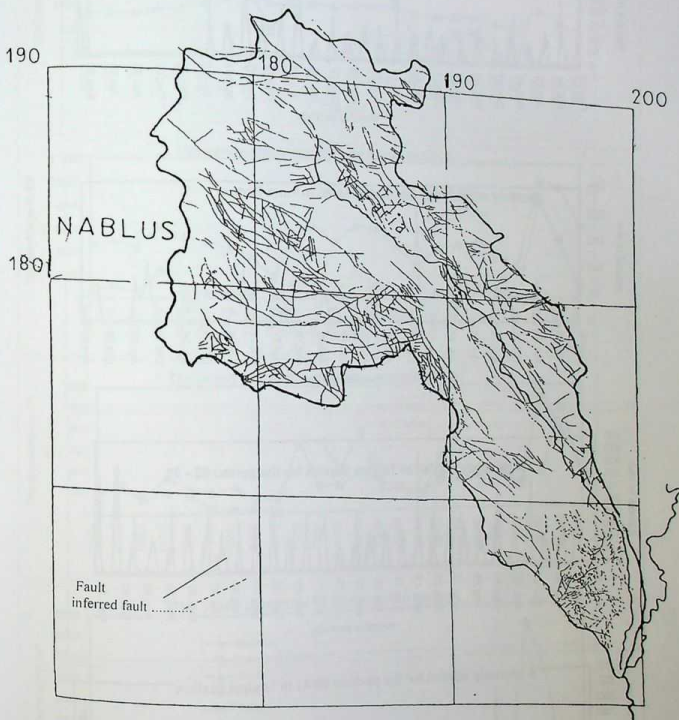
Appendix 3.1: The monthly records of rainfall in mm for the period 1962-1991 for the 4 stations in the Faria basin

Monthly records for the period 62 - 92 in Beit Dajan Station

Monthly records for the period 69-80 in Faria Station

A monthly rainfall in Talluza Station for the period 62 - 91

A monthly rainfall for the periods 69-91 in Toubas Station
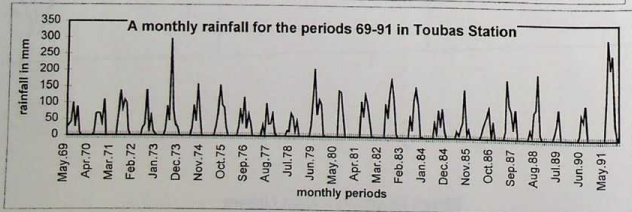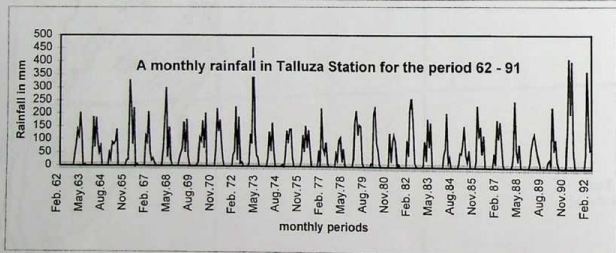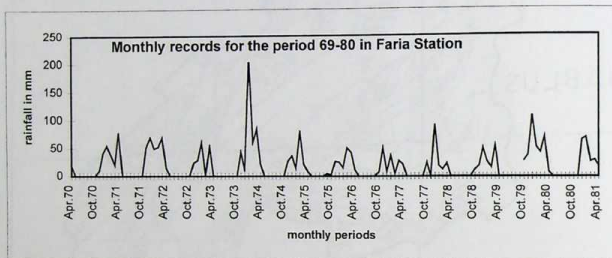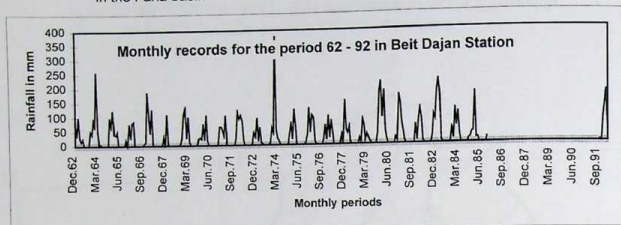
Appendix 3.2: The yearly discharge of the Miska, Faria, Nablus and Badan group springs

The yearly discharge of Miska group

The yearly discharge of Faria group springs

The yearly discharge of Nablus group springs

The yearly discharge of Badan group springs
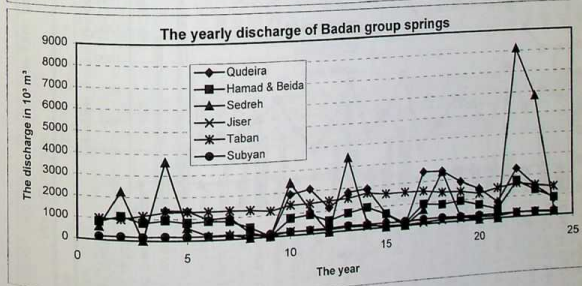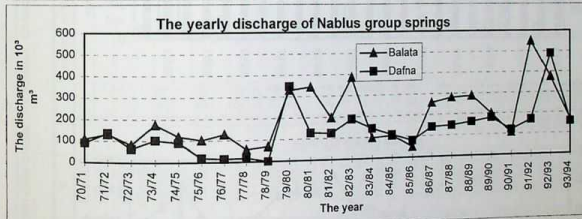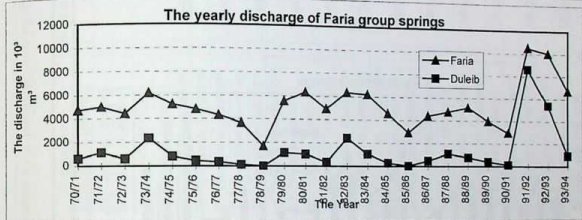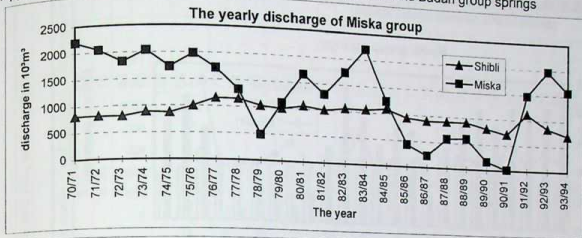
Appendix 3.3: The relationship between the yearly discharge of the Faria group springs and the rainfall in the nearest rainfall station.

Miska group springs

Legend: Miska, Shibli, Tallouza

The discharge in 10^3 m³ / The rainfall in mm in Talluza station / The year

Faria group springs

Legend: Faria, Duleib, Toubaz

discharge in 10^3 m³ / The rainfall in mm in Toubaz station / The year

Badan group springs

Legend: Qudeira, Hamad & Beida, Sedreh, Jiser

The discharge 10^3 m³ / The rainfall in mm in Tallouza station / The year
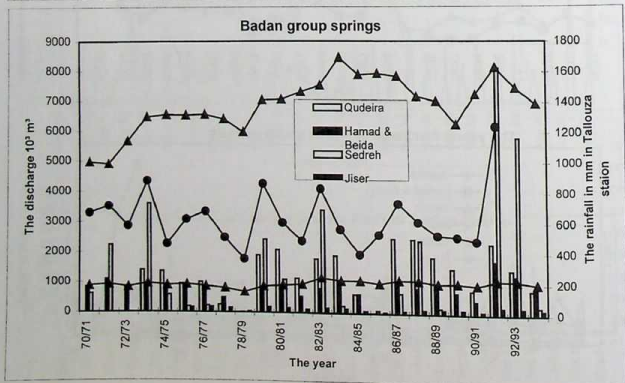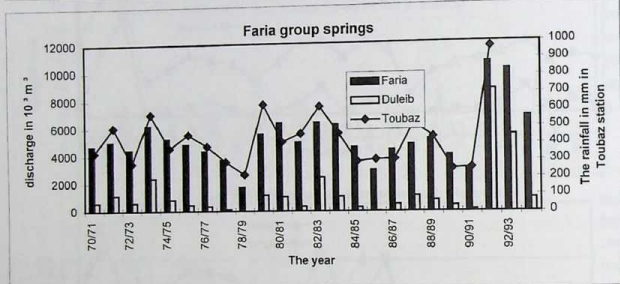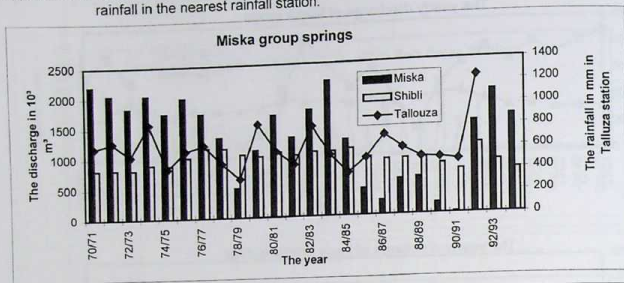
Appendix 4.1: Groundwater wells of the Faria basin (the owner, nummber, coordinates x,y,z, pumpage, sub-aquifer and No., well depth and the drilling year

Well owner	Well No.	x	Y	Z	Pumpage m³/hr	Sub Aquifer	No. of sub aquifer	well depth (m)	Drilling year
Ali Damen	19-16/1	196770	169900		90	Eocene (estern)	673	68	
Ahmed H.Izghair	19-16/3	198460	169650		42	Eocene (estern)	673	75	
Ahmed H.Izghair	19-16/4	198200	169300		36	Eocene (estern)	673	93	
Abdulaziz Sares	19-16/5	195590	188850		75	Eocene (estern)	673	68	
Samsam Nimer	19-16/6	191740	160000	-233,279	96	Eocene (estern)	673	106	
Burhan Damen	19-16/8	196780	169670		78	Neogene (eastern)	670	66	
Nawaf Damen	19-16/9	196970	169220	-272,280	70	Neogene (eastern)	670	75	
Shaher Damen	19-16/10	196850	169730		87	Neogene (eastern)	670	76	
I'nad Masri	19-17/1	196900	170740	-250	120	Neogene (eastern)	671	77	1960
Waheed Masri	19-17/2	196520	171240	-252,601	70	Neogene (eastern)	670	60	1970
Jiftlik Nursery	19-17/4	197220	170560	-260		Neogene (eastern)	670	92	1960
Tahana Haqlauat. Faria	19-17/5	196400	172200	-245	23	Eocene (estern)	673	123	1967
Adham Damen	19-17/6	196780	170000		96	Eocene (estern)	673	69	
Fathalla Masri	19-17/7	196940	172290	-243,359	50	Eocene (estern)	673	74	1968
Allan Damen	19-17/8	196250	170260	-250,645	84	Neogene (eastern)	670	72	1968
Rafiq Qamhawi	19-17/9	197470	170230	-263,850	90	Neogene (eastern)	670	91	1972
Mashu'a 1	Mashu'a 1	193380	176660	-166	550	U&l Cen. (eastern)	655	600	1975
Hamura 1 (Atara)	Atara1	192810	177530	-154	645	U&L Cen. (eastern)	655	232	1971
Hussein Drai'i	19-17/10	197060	170150	-262,618	40	Neogene (eastern)	670	77	1970
Badi' Yunis	19-17/11	198810	174870		48	Neogene (eastern)	670	72	
Argamoun 14	19-17/14	199140	178800	-248		Eocene (estern)	673	76	1968
Jamil Khamis+Part.	19-17/20	199960	175060	-267,207	72	Neogene (eastern)	670	92	1965
Mahmoud Damen	19-17/21	196520	170560	-256,162	120	Neogene (eastern)	670	73	1974
Burhan Damen	19-17/23	194200	175230	-195,937	96	Eocene (estern)	673	150	1969
Basel H. Kan'an	19-17/24	196560	171550	-250,606	30	Neogene (eastern)	670	62	1968
Hassan Simadi	19-17/27	196250	171470	-248,979	108	Neogene (eastern)	670	73	1970
Fareed Abu Shamat +Part.	19-17/28	198150	170500	-267,911	114	Neogene (eastern)	670	72	1967
Abdullatif Haider	19-17/31	197680	171060	-264,649	93	Neogene (eastern)	670	100	1970
Diya Abdo	19-17/33	196510	172910	-237,889	40	Eocene (estern)	673	57	1972
Rajeh Shak'a	19-17/34	192740	178370	-148,882	78	U&L Cen. (eastern)	655	150	1968
Abdulqader Abduljaleel	19-17/43	192920	176760	-178,629	60	U&L Cen. (eastern)	655	119	

Well owner	Well No.	x	Y	Z	Pumpage m³/hr	Sub Aquifer	No. of sub aquifer	well depth (m)	Drilling year
Moh'd Y. Shaheen	19-17/44	192000	179030	-125,555	87	U&L Cen. (eastern)	655	117	
Hassan Ibeisi	19-17/45	191940	179520	-132960	36	U&L Cen. (eastern)	655	100	
Nashat Masri	19-17/46	192560	176230	-167,021	70	U&L Cen. (eastern)	655	147	
Hassan Abduljaleel	19-17/47	192410	178970	-137,311	75	U&L Cen. (eastern)	655	147	
Moh'd Ahmed Abduljabar	19-17/50	192790	179120	-125,046	85	U&L Cen. (eastern)	655	132	1970
Tawfiq Yasidi	19-17/51	192150	179300	-127,486	90	U&L Cen. (eastern)	655	125	1970
Ari'a 1	19-17/52	195900	171650	-241	162	Neogene (eastern)	670	75	1970
Jiftlik Nursery	19-17/53	196790	170570	-258,730	56	Neogene (eastern)	670	74	1971
Ma'rouf Abu Samra	19-17/54	197600	169150		54	Neogene (eastern)	670		
Jawad R. Masri	19-17/55	196150	173400		162	Eocene (estern)	673	130	
Mahmoud Damen	19-17/56	194600	174100		90		670	160	
Atara 2	Atara 2	190840	178550	26	447	U&L Cen. (eastern)	655	520	1980
Gitit3	Gitit3	191560	173370	19		L Cenomanian	661	646	1977
Yunis Siwadi	18-18/1	181050	186620	167,218	100	Eocene (western)	642	32	1970
Abdulraouf Fares	18-18/2	182200	188350	177	78	Eocene (western)	642	57	1969
Rifat Fares	18-18/4	181910	188710	161,665	69	Eocene (western)	642	85	1967
Marwan + Amin Masri	18-18/11	187040	183140	-29,955	45	Neogene (western)	653	39	1963
Marwan + Amin Masri	18-18/11A	187040	183200	-37,048	45	Neogene (western)	653	6	1970
Abdulla Abdulhadi	18-18/13	187290	182440	-36,092	45	Neogene (western)	653	40	1970
Sukeina Abdulhadi	18-18/14	186610	189950	-30,185	120	Neogene (western)	653	18.5	1963
M. Abu Khaizaran	18-18/16	182370	188890	170,513	108	Eocene (western)	642	96	1965
Tubas Water Project	18-18/17	182310	189420	196,544	67	Eocene (western)	642	79	1969
Abdulkarim Salem	18-18/19	181150	188730	-46,643	45	Neogene (western)	653	150	1967
A. + S. Shak'a	18-18/19A	188570	181320	-47,827	45	Neogene (western)	653	125	1970
Azmi Abdulmajeed	18-18/23	187210	183070	-28,830	90	Neogene (western)	653	50	1967
Moh'd Ali Abdulla	18-18/25A	181650	189540	214,336	96	Eocene (western)	642	140	1970
Fayiz A. Issa	18-18/26	186800	182500		25	Neogene (western)	653	72	
Nadir Abdulhadi	18-18/27	186060	183850	-18,385	35	Neogene (western)	653	9	1970
Ibrahim Diyab	18-18/27A	186090	183540	-19,277	25	Neogene (western)	653	8	1970
Qasem Abdulhadi	18-18/30	186240	183350	-23,515	50	Neogene (western)	653	7	1970
Nadir Abdulhadi	18-18/31	186410	183120	-29,155	65	Neogene (western)	653	9	1970
Sameera Abdulhadi	18-18/31A	186650	183100	-29	65	Neogene (western)	653		
A.Shanti + Part.	18-18/32	182170	189000	197,283	84	Eocene (western)	642	80	1970

Well owner	Well No.	x	Y	Z	Pumpage m³/hr	Sub Aquifer	No. of sub aquifer	well depth (m)	Drilling year
Sulim Saleh	18-18/33	182140	189770	213,319	57	Eocene (western)	642	106	1971
Qasem Abdulhadi	18-18/34	185500	183900	20	25	Neogene (western)	653	7	
Hafez Abdulla	18-18/35	186450	183350	-25	45	Neogene (western)	653	33	1980
Khalil Abdulhadi	18-18/36	187600	182550	-60	72	Neogene (western)	653	21	
Bethan well No. 1	18-18/37	180150	185400	210,859	196	U&L Cen. (western)	654	748	1970
Bethan well No.2	18-18/38	182750	185750	90	264	U&L Cen. (western)	654	413	
Ibrahim M. Hamdan	18-18/39	187900	182350		36	U&L Cen. (western)	654		

Appendix 4.2: (Plate 1) The display of the draw down - time pumping test data of the groundwater and the corresponding transmissivity of the well 19-17/52 (Pleistocene sub-aquifer) and the well 19-17/1 (Eocene sub-aquifer), the unfitted points are due to the well capacity effect.

Well 19-17/52
Pleistocene sub-aquifer
Jacob method
T = 391 m² / day

Well 19-17/1
Eocene sub-aquifer
Recovery test
T = 9599 m²/ day
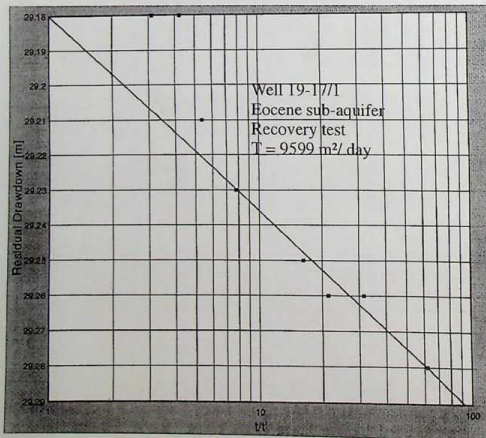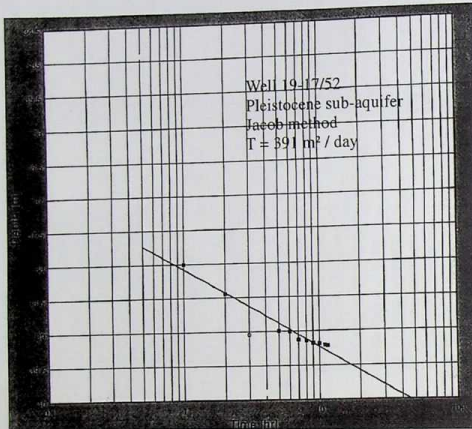
Appendix 4.2: (Plate 2) The display of the draw down - time pumping test data of the
groundwater wells of the lower and upper Cenomanian sub-aquifer and the
corresponding transmissivity of the well 18-18/37 (the first part is only
interpreted) and the well 19-17/44 , the unfitted points are due to the well
capacity effect.
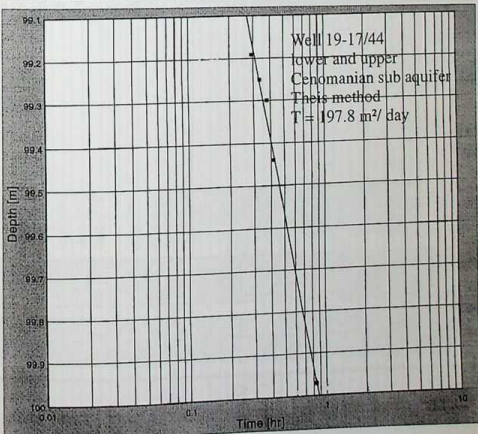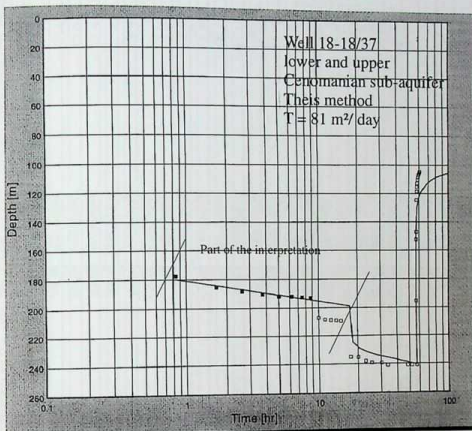
Appendix 4.3: The saturated thickness of the phreatic aquifer as well as the thickness of the confined aquifer and static water levels (swl) for all sub- aquifers in the Faria basin

Well No.	x	y	z	swl (m related to sea level)	depth to the gwl (m)	date	saturated thickness (m)	aquifer No.
18-18/16	182370	188890	170.513	151.5	19	26/09/93	75.6	642
18-18/17	182310	189420	196.544	163.6	33	26/09/93	45.5	642
M1	181000	181000		272.1	33	10/05/88		642
18-18/1	181050	188620	167.218	160	7.2	26/09/93	23.1	642
18-18/2	182200	188350	177	150.7	26.3	26/09/93	30.5	642
18-18/4	181910	188710	161.665	157.9	3.7	26/09/93	79.1	642
M2	180100	185100		146.7	3.7	20/03/93		642
M3	180000	185000		150.2	3.7	28/03/92	11.8	642
18-18/25A	181650	189540	214.336	161.6	52.8	26/09/93	82.9	642
18-18/32	182170	189000	197.283	155.8	41.5	26/09/93	37.2	642
18-18/33	182140	189770	213.319	166.4	47	26/09/93	54.2	642
18-18/11	187040	183140	-29.955	-39.9	10	27/11/80	30.2	653
18-18/11A	187040	183200	-37.048	-33.9	3.2	18/08/93	2.6	653
18-18/3	187290	182440	-36.092	-33.6	2.5	18/08/93	37.5	653
18-18/19	188150	188730	-46.643	-90.1	43.5	28/10/93	106.8	653
18-18/19A	188570	181320	-47.827	-92.6	44.8	27/11/80	81.2	653
18-18/23	187210	183070	-28.830	-38.9	10.1	18/08/93	40	653
18-18/26	186800	182500		-37.1	10.1	18/08/93		653
18-18/27	186060	183850	-18.385	-21.4	3	28/10/93	5.1	653
18-18/27A	186090	183540	-19.277	-24.8	5.5	25/09/80	3.9	653
18-18/30	186240	183350	-23.515	-26.5	3	18/08/93	3.6	653
18-18/31A	186650	183120	-29	-32	3	18/08/93	3	653
19-16/1	196770	169900		-279.3		27/10/93		673
19-17/5	196400	172200	-245	-277.6	32.6	27/10/93	85.1	673
19-17/6	196780	170000		-275.1	34.1	26/10/93		673
19-17/14	199140	178800	-248	-285.6	37.6	21/10/93		673
M4	199100	174000		-276.3	30.6	02/11/85		673
M5	199000	174000		-317.8	69.8	22/03/90		673
19-17/33	196510	172910	-237.889	-277.9	40	27/10/93	12.2	673
19-17/23	194200	175230	-195.937	-264.6	98.7	27/10/93	83.4	673
19-17/2	196520	171240	-252.601	-278.2	25.6	27/10/93	29.6	670

well No.	x	y	z	swl (m related to sea level)	depth to the gwl (m)	Date	Saturated thickness (m)	Aquifer No.
19-17/52	195900	171650	-241	-229.2	11.8	27/10/93	49.2	670
19-17/56	194600	174100		-249.3	31.6	13/10/80		670
19-17/8	196250	170260	-250,645	-285.6	30	26/11/80	37.1	670
19-17/9	197470	170230	-263,850	-279.5	15.6	27/10/93	82.6	670
19-17/10	197060	170150	-262,618	-279.4	34.8	27/10/93	56.6	670
19-17/11	198810	174870		-285.1	30.4	03/10/93		670
19-17/20	199960	175060	-267,207	-288.5	21.3	11/08/93	11.5	670
19-17/24	196560	171550	-250,606	-277.2	26.8	27/10/93	31.2	670
19-17/27	196250	171470	-248,979	-285	36	25/11/80	38.6	670
19-17/31	197680	171060	-264,649	-279.3	14.7	27/10/93	81.2	670
19-17/1	196900	170740	-250	-278.5	28.5	27/10/93	43.8	671
Mashua 1	193380	176660	-166	-268.9	2.9	10/09/93	501.2	655
Hamura 1 (At	192810	177530	-154	-268.8	114.8	21/10/93	100.1	655
19-17/34	192740	178370	-148,882	-294.8	145.9	21/10/93	71.3	655
19-17/43	192920	176760	-178,629	-276.2	97.6	07/02/73		655
19-17/44	192000	179030	-125,555	-234.6	109	28/10/93		655
19-17/45	191940	179520	-132960	-213.8	80.8	10/07/73		655
19-17/46	192560	176230	-167,021	-263.4	96.4	24/05/79		655
M6	196000	181000		-260.8	93.4	23/06/94	37.2	655
Atara 2	190840	178550	26	-178.6	204.6	06/09/93	324.6	655
19-17/47	192410	178970	-137,311	-251.1	113.8	26/10/92	52.4	655
19-17/50	192790	179120	-125,046	-227.2	101.3	07/05/75	45.9	655
18-18/37	180150	185400	210,859	0	210.8			654
18-18/38	182750	186750	90	-0.53	90.5			654

Appendix 5.1a: The univariate parameters of the hydrochemical data of all sub - aquifers; Eocene (642,671, 673), Neogene (653)Pleistocene (670) , lower and upper Cenomanian (654, 655) and surface water (333)

Aquifer	Ph	EC	DO	Ca	Mg	Na	K	Cl	HCO3	SO4	NO3	SIO2	F	Fe	Mn	Cd	Cu	Br	Pb	PO4	Zn
333 N	8.0	4.0	4.0	8.0	8.0	8.0	8.0	8.0	8.0	8.0	8.0	8.0	8.0	8.0	8.0	8.0	8.0	-	8.0	8.0	8.0
Mean	8.1	880.8	3.1	91.9	15.5	59.4	4.3	97.5	270.0	22.9	53.7	37.5	0.1	36.1	3.1	4.2	5.4	-	1.4	1.0	9.2
Median	8.2	881.5	3.2	90.4	14.8	39.3	2.5	74.0	271.5	22.9	40.0	37.6	0.1	29.9	2.0	2.6	4.1	-	1.5	0.3	8.3
Minimum	7.5	740.0	0.7	69.5	3.3	26.2	2.4	58.5	209.9	17.8	16.9	26.7	0.0	15.7	0.0	0.9	2.2	-	0.1	0.0	2.9
Maximum	8.4	1020.0	5.3	118.2	25.2	125.9	9.0	110.5	324.6	26.5	142.0	46.3	0.5	93.8	14.9	10.2	15.2	-	4.1	3.4	20.5
Range	0.9	280.0	4.6	48.7	21.9	99.7	6.6	110.4	114.7	8.7	125.1	19.6	0.5	78.1	14.9	9.3	13.0	-	4.0	3.4	17.5
Std. Deviation	0.3	155.2	2.5	20.2	7.2	39.8	2.9	44.4	41.1	2.8	45.9	7.4	0.2	24.2	4.8	3.3	4.2	-	1.3	1.4	5.2
Variance	0	24076	6	408	53	1582	8	1968	1693	8	2110	55	0	583	24	11	17	-	2	2	27
642 N	30.0	30.0	15.0	30.0	30.0	30.0	30.0	30.0	30.0	30.0	30.0	30.0	30.0	30.0	30.0	30.0	30.0	14.0	30.0	30.0	30.0
Mean	7.5	752.5	5.7	88.3	20.0	32.4	1.9	62.9	281.1	30.0	45.4	43.4	0.2	24.7	0.4	6.1	4.9	0.8	5.5	0.1	14.2
Median	7.5	727.0	5.9	88.7	19.4	31.0	1.7	56.1	284.0	16.7	27.4	42.8	0.1	17.7	0.3	1.7	3.3	0.7	5.5	0.1	12.6
Minimum	7.1	503.0	3.0	34.2	3.2	15.0	1.2	33.0	209.9	7.8	14.2	29.3	0.0	5.6	0.0	1.7	0.7	0.7	0.7	0.0	5.0
Maximum	8.0	1077.0	6.5	139.7	39.8	54.3	2.7	128.9	340.0	43.5	182.5	57.8	0.4	88.5	1.7	19.7	35.2	0.9	12.7	0.7	25.4
Range	0.8	574.0	3.5	105.5	36.6	39.3	1.5	95.9	130.1	35.7	168.3	28.5	0.4	82.9	1.7	19.7	34.5	0.2	12.0	0.7	20.4
Std. Deviation	0.2	168.3	0.9	23.9	10.1	9.1	0.5	22.4	34.0	7.6	45.0	6.1	0.1	20.4	0.5	6.5	6.2	0.1	3.7	0.1	6.1
Variance	0	28324	1	572	103	83	0	504	1158	57	2023	37	0	414	0	42	39	0	14	0	37
653 N	29.0	29.0	14.0	29.0	29.0	29.0	29.0	29.0	29.0	29.0	29.0	29.0	29.0	29.0	29.0	29.0	29.0	7.0	29.0	29.0	29.0
Mean	7.6	724.5	5.2	90.0	21.1	34.1	2.4	67.3	276.3	24.1	52.6	34.4	0.3	20.2	0.6	2.8	3.5	0.8	1.3	0.2	13.0
Median	7.7	720.0	5.2	83.1	22.3	33.3	2.3	62.1	279.8	22.3	35.1	35.1	0.2	14.7	0.0	1.5	3.1	0.8	1.1	0.2	13.7
Minimum	7.1	525.0	4.5	53.6	5.8	22.5	1.9	51.4	216.1	13.9	12.5	25.2	0.2	0.0	0.0	0.3	0.3	0.8	0.0	0.0	0.0
Maximum	8.1	921.0	6.1	149.5	35.8	66.7	3.7	125.0	309.3	53.3	190.8	39.1	0.5	105.8	9.3	22.6	13.0	0.9	5.9	0.4	23.2
Range	1.1	396.0	1.7	95.9	30.0	44.2	1.8	73.6	93.2	39.4	178.3	13.9	0.3	105.8	9.3	22.6	12.6	0.1	5.9	0.4	23.2
Std. Deviation	0.3	70.0	0.3	23.4	7.5	8.8	0.3	19.5	22.2	8.3	46.8	3.4	0.1	18.8	1.8	2.8	2.8	0.1	1.2	0.1	6.2
Variance	0	4904	0	550	56	77	0	378	492	69	2190	11	0	355	3	20	8	0	39	0	39
654 N	7.0	7.0	2.0	7.0	7.0	7.0	7.0	7.0	7.0	7.0	7.0	7.0	7.0	7.0	7.0	7.0	7.0	3.0	7.0	7.0	7.0
Mean	7.6	1058.1	5.4	108.4	28.4	59.3	4.2	163.6	308.6	26.5	15.5	38.7	0.2	17.4	2.2	15.3	4.3	3.0	4.0	0.2	11.4
Median	7.7	726.0	5.4	78.9	21.2	27.2	1.7	52.7	291.4	18.3	14.3	41.0	0.2	12.9	0.4	3.0	1.7	0.8	3.2	0.1	10.5
Minimum	7.0	630.0	4.9	64.0	8.6	22.5	0.5	42.9	270.0	15.3	6.6	29.5	0.1	7.1	0.0	0.0	0.4	0.8	0.1	0.1	1.5
Maximum	7.8	3050.0	5.9	282.7	70.0	241.5	19.7	805.6	403.8	65.0	28.4	47.0	0.6	30.2	14.1	65.5	21.3	0.8	9.5	0.5	23.7
Range	0.8	2420.0	1.0	218.7	61.4	219.0	19.2	762.7	133.8	49.7	21.8	17.4	0.5	23.1	14.1	65.5	20.9	0.1	9.5	0.4	22.2
Std. Deviation	0.3	885.5	0.7	77.6	20.4	80.7	6.9	283.8	45.6	17.6	8.3	5.7	0.2	9.5	5.3	23.4	7.5	0.0	3.4	0.2	8.0

Aquifer	Ph	EC	DO	Ca	Mg	Na	K	Cl	HCO3	SO4	NO3	SiO2	F	Fe	Mn	Cd	Cu	Br	Pb	PO4	Zn
Variance		784116.1		6028	415	6506	47	80567	2078	309	69	32		89	28	548	57		11	0	64
655 N	9.0	8.0	3.0	9.0	9.0	9.0	9.0	9.0	9.0	9.0	9.0	9.0	9.0	9.0	9.0	9.0	9.0	9.0	9.0	9.0	9.0
Mean	7.6	1011.6	5.3	109.5	29.3	52.4	2.7	133.6	322.6	36.8	26.7	30.7	0.3	18.2	1.5	4.7	3.3		1.6	0.2	13.3
Median	7.6	899.0	5.3	94.7	27.2	40.5	2.4	85.4	317.9	34.6	24.5	29.0	0.3	12.1	0.9	2.0	2.6		1.1	0.3	13.5
Minimum	7.0	650.0	5.2	79.2	20.5	23.8	2.2	81.5	298.8	25.5	19.8	24.7	0.2	5.4	0.0	0.0	1.2		0.0	0.0	3.7
Maximum	8.1	2220.0	5.5	211.6	43.1	172.8	4.9	504.7	344.9	67.1	50.2	37.6	0.5	46.6	7.6	25.2	6.9		4.3	0.4	23.2
Range	1.1	1570.0	0.2	132.4	22.6	149.0	2.7	423.2	46.1	41.6	30.4	12.9	0.4	40.6	7.6	25.2	5.7		4.3	0.4	19.5
Std. Deviation	0.4	499.5	0.2	40.5	7.1	45.8	0.8	139.3	14.9	12.5	9.4	4.3	0.1	15.3	2.4	8.0	1.9		1.4	0.4	6.6
Variance	0	249487.0		1637	51	2095	1	19409	222	156	81	18		234	6	64	4		2	0	43
670 N	12.0	12.0		12.0	12.0	12.0	12.0	12.0	12.0	2.0			12.0	12.0		12.0			12.0	12.0	12.0
Mean	7.4	3386.7	4.1	274.5	102.6	249.1	20.1	908.9	366.8	71.0	27.9	34.9	0.5	21.0	3.2	331.4	3.7		5.0	0.3	10.2
Median	7.2	3200.0	4.1	272.3	70.9	232.9	20.4	825.0	369.5	64.5	28.2	33.7	0.5	22.3	1.7	76.4	3.2		4.2	0.4	11.3
Minimum	7.2	1850.0	4.1	163.2	51.8	128.4	8.7	349.4	324.7	47.4	14.5	30.1	0.1	8.2	0.9	7.8	1.5		1.9	0.0	2.6
Maximum	7.9	5300.0	4.1	367.3	384.3	481.0	31.2	2108.7	405.0	106.9	39.0	47.6	0.8	32.6	9.4	1594.4	9.0		10.7	0.5	22.6
Range	0.8	3450.0	0.0	204.1	332.5	352.6	22.5	1759.3	80.3	59.5	24.5	17.5	0.7	24.4	8.5	1586.6	7.5		8.8	0.5	21.0
Std. Deviation	0.2	941.8	0.0	61.4	94.6	95.4	6.3	441.8	24.6	20.3	7.6	4.8	0.2	9.9	3.1	479.1	2.1		2.8	0.2	6.8
Variance	0	887042.0		3773	8944	9108	40	195218	607	410	58	23		99	9	229538	4		8	0	46
671 N	2.0	2.0	1.0	2.0	2.0	2.0	2.0	2.0	2.0	2.0	2.0	2.0	2.0	2.0	2.0	2.0	4		2.0	2.0	2.0
Mean	7.4	2525.0	3.7	209.2	73.0	182.6	13.5	614.3	348.3	55.9	22.2	32.9	0.4	17.5	9.1	171.7	2.6		4.2	0.2	12.5
Median	7.4	2525.0		209.2	73.0	182.6	13.5	614.3	348.3	55.9	22.2	32.9	0.4	17.5	9.1	171.7	2.6		4.2	0.2	12.5
Minimum	7.4	2450.0	3.7	176.6	61.7	155.7	12.1	590.1	328.4	53.8	21.4	29.7	0.4	8.9	8.8	3.1	1.9		2.9	0.0	9.4
Maximum	7.4	2600.0	3.7	241.8	84.3	209.5	14.9	638.5	368.2	58.0	22.9	36.2	0.5	26.0	9.5	340.3	3.4		5.5	0.5	15.7
Range	0.0	150.0	0.0	65.2	22.6	53.8	2.8	48.4	39.8	4.2	1.1	6.5	0.1	17.1	0.7	337.2	1.5		2.7	0.5	6.3
Std. Deviation	0.0	106.1		46.1	16.0	38.0	2.0	34.2	28.1	3.0	1.1	4.6	0.1	12.1	0.5	238.5	1.1		1.9	0.3	4.4
Variance	0.0	11250.0		2126	255	1447	7.0	1171	792	9		21		146		56862			4		20
673 N	7.0	6.0	1.0	7.0	7.0	7.0	7.0	7.0	7.0	7.0	7.0	6.0	6.0	7.0	7.0	7.0	7.0	7.0	7.0	6.0	7.0
Mean	7.4	2843.2	5.0	257.8	67.3	182.2	13.2	665.6	366.2	67.9	31.0	36.1	0.6	21.8	3.9	477.6	4.2	7.0	5.2	0.3	12.8
Median	7.4	2320.5	5.0	212.3	55.8	192.6	13.0	549.3	381.7	58.1	30.2	35.3	0.6	17.8	1.6	21.8	2.7	7.0	3.3	0.4	13.3
Minimum	7.3	1098.0	5.0	93.2	28.9	58.5	3.2	139.8	321.6	34.3	26.4	27.9	0.2	10.5	0.0	0.9	2.1	7.0	1.1	0.0	4.8
Maximum	7.6	5360.0	5.0	513.8	125.3	269.1	21.5	1281.1	400.1	121.3	35.5	45.7	0.8	47.9	20.8	1651.4	9.4	7.0	9.7	0.6	18.4
Range	0.3	4262.0	0.0	420.6	96.4	210.6	18.3	1141.3	78.5	87.0	9.1	17.8	0.6	37.4	20.8	1650.5	7.3	7.0	9.7	0.6	13.6
Std. Deviation	0.1	1527.0		161.7	33.6	62.8	6.0	385.3	30.6	30.1	3.6	5.9	0.2	12.8	7.5	784.5	2.8	8	4.1	0.2	4.2
Variance	0	2331705.0		26151	1129	3940	36	148492	934	907	13	35		164	56	615366	8		17	0	18

Aquifer	Ph	EC	DO	Ca	Mg	Na	K	Cl	HCO3	SO4	NO3	SiO2	F	Fe	Mn	Cd	Cu	Br	Pb	PO4	Zn
Total																					
N	104	98	42	104	104	104	104	104	104	104	104	103	103	104	104	104	104	24	104	103	104
Mean	7.6	1279.2	5.1	127.5	35.1	76.5	5.5	228.5	301.3	32.6	41.0	37.4	0.3	22.5	1.6	78.0	4.1	0.8	3.5	0.2	12.6
Median	7.5	760.5	5.3	94.6	24.3	35.6	2.4	70.3	299.2	23.0	25.2	36.2	0.3	17.6	0.4	2.7	3.1	0.8	2.2	0.2	11.9
Minimum	7.0	503.0	0.7	34.2	3.2	15.0	0.5	33.0	209.9	7.8	6.6	24.7	0.0	0.0	0.0	0.0	0.3	0.7	0.0	0.0	0.0
Maximum	8.4	5360.0	6.5	513.8	384.3	481.0	31.2	2108.7	405.0	121.3	190.8	57.8	0.8	105.8	20.8	1651.4	35.2	0.9	12.7	3.4	25.4
Range	1.4	4857.0	5.9	479.6	381.1	466.0	30.7	2075.7	195.1	113.5	184.2	33.0	0.8	105.8	20.8	1651.4	34.9	0.2	12.7	3.4	25.4
Std. Deviation	0.3	1106.6	1.2	86.9	43.4	86.7	6.9	351.6	45.6	22.8	38.4	6.6	0.2	17.9	3.4	289.4	4.4	0.1	3.3	0.4	6.2
Variance	0	1224536	1	7558	1886	7525	47	123599	2083	520	1477	44	0	319	12	83729	19	0	11	0	39

Appendix 5.1b:- The statistical parameters of the field measurements of all sub - aquifers

Sub - aquifer		EC	Eh	Ph	T °C
Eocene western (642)	N	27	14	27	27
	Mean	618.5	536.5	7.2	21.7
	Median	650.0	581.0	7.2	21.4
	Minimum	340.0	210.0	7.0	19.3
	Maximum	1077.0	860.0	7.7	28.2
	Range	737.0	650.0	0.6	8.9
	Std. Deviation	222.1	193.1	0.2	2.0
	Variance	49330.3	37274.3	0.0	4.0
Neogene (653)	N	25.0	13.0	25.0	25.0
	Mean	525.4	452.3	7.4	23.9
	Median	525.0	561.0	7.3	23.3
	Minimum	111.0	210.0	7.1	21.1
	Maximum	815.0	623.0	7.7	33.4
	Range	704.0	413.0	0.6	12.3
	Std. Deviation	209.3	177.0	0.1	2.7
	Variance	43819.6	31311.4	0.0	7.3
Lower and Upper Cenomanian western (654)	N	7.0	5.0	7.0	7.0
	Mean	415.3	490.4	7.3	24.0
	Median	420.0	589.0	7.2	23.7
	Minimum	100.0	210.0	6.9	23.3
	Maximum	751.0	630.0	7.5	26.4
	Range	651.0	420.0	0.6	3.1
	Std. Deviation	232.5	184.9	0.2	1.1
	Variance	54068.6	34202.3	0.0	1.2
Lower and Upper Cenomanian eastern (655)	N	6.0	6.0	6.0	6.0
	Mean	668.5	279.7	7.3	23.1
	Median	430.5	298.0	7.3	22.5
	Minimum	179.0	120.0	7.1	22.5
	Maximum	2110.0	421.0	7.4	25.1
	Range	1931.0	301.0	0.3	2.6
	Std. Deviation	739.8	146.4	0.1	1.1
	Variance	547365.9	21419.5	0.0	1.1
Pleistocene (670)	N	8.0	7.0	8.0	8.0
	Mean	3779.4	507.9	7.1	25.5
	Median	4300.0	210.0	7.1	24.1
	Minimum	135.0	210.0	6.9	23.4
	Maximum	5300.0	2060.0	7.4	34.1
	Range	5165.0	1850.0	0.5	10.7
	Std. Deviation	1588.3	686.7	0.2	3.5
	Variance	2522688.8	471615.5	0.0	12.5
Eocene eastern (671)	N	2.0	1.0	2.0	2.0
	Mean	2600.0	210.0	7.1	24.5
	Median			7.1	24.5
	Minimum	2600.0	210.0	7.1	24.0
	Maximum	2600.0	210.0	7.1	25.0
	Range	0.0	0.0	0.0	1.0
	Std. Deviation	0.0	.	0.0	0.7
	Variance	0.0	.	0.0	0.5

Appendix 5.1

Aquifer		EC	Eh	Ph	T °C
		3.0	2.0	3.0	3.0
Eocene eastern (673)	N	258.3	332.5	7.0	24.9
	Mean	132.0	332.5	7.1	24.8
	Median	113.0	323.0	6.8	24.8
	Minimum	530.0	342.0	7.2	25.1
	Maximum	417.0	19.0	0.3	0.3
	Range	235.5	13.4	0.2	0.2
	Std. Deviation	55442.3	180.5	0.0	0.0
	Variance	78.0	48.0	78.0	78.0
Total	N	935.4	457.3	7.3	23.3
	Mean	630.5	421.0	7.3	23.3
	Median	100.0	120.0	6.8	19.3
	Minimum	5300.0	2060.0	7.7	34.1
	Maximum	5200.0	1940.0	0.9	14.8
	Range	1162.3	303.4	0.2	2.6
	Std. Deviation	1350952.5	92068.6	0.0	6.6
	Variance				

Appendix 5.1c:- The statistical parameters of field measurements of the phreatic and confined aquifers

Aquifer		EC	Eh	Ph	T (°C)
Phreatic	N	65	37	65	65
	Mean	1016.1	481.6	7.3	23.2
	Median	650.0	534.0	7.2	23.1
	Minimum	111.0	210.0	6.8	19.3
	Maximum	5300.0	2060.0	7.7	34.1
	Range	5189.0	1850.0	0.9	14.8
	Std. Deviation	1238.8	327.7	0.2	2.8
	Variance	1534658.5	107405.0	0.0	7.7
Confined	N	13.0	11.0	13.0	13.0
	Mean	532.2	375.5	7.3	23.6
	Median	420.0	393.0	7.3	23.4
	Minimum	100.0	120.0	6.9	22.5
	Maximum	2110.0	630.0	7.5	26.4
	Range	2010.0	510.0	0.6	3.9
	Std. Deviation	521.9	191.1	0.2	1.1
	Variance	272365.8	36502.1	0.0	1.3
Total	N	78.0	48.0	78.0	78.0
	Mean	935.4	457.3	7.3	23.3
	Median	630.5	421.0	7.3	23.3
	Minimum	100.0	120.0	6.8	19.3
	Maximum	5300.0	2060.0	7.7	34.1
	Range	5200.0	1940.0	0.9	14.8
	Std. Deviation	1162.3	303.4	0.2	2.6
	Variance	1350952.5	92068.6	0.0	6.6

Appendix 5.1d: The statistical parameters of the hydrochemical data of the phreatic and confined aquifers

Aquifer		Ph	EC	DO	Ca	Mg	Na	K	Cl	HCO3	SO4	NO3	SiO2	F	Fe	PO4	Mn	Cd	Cu	Pb	Zn	Br
Phreatic	N	80.0	79.0	33.0	80.0	80.0	80.0	80.0	80.0	80.0	80.0	80.0	79.0	79.0	80.0	79.0	80.0	80.0	80.0	80.0	80.0	21.0
	Std. Deviation	0.2	1189.5	0.8	94.6	48.6	93.8	7.5	385.8	47.2	24.9	40.3	6.5	0.2	17.6	0.2	3.2	327.3	4.3	3.4	6.1	0.1
	Mean	7.5	1346.0	5.3	134.7	38.3	82.4	6.1	257.9	301.4	33.6	43.5	38.0	0.3	22.1	0.2	1.4	99.1	4.1	3.8	13.0	0.8
	Median	7.5	759.0	5.6	98.0	24.7	35.3	2.5	65.2	291.6	22.9	27.4	36.3	0.3	17.6	0.2	0.4	3.4	3.1	2.6	12.5	0.8
	Minimum	7.1	503.0	3.0	34.2	3.2	15.0	1.2	33.0	209.9	7.8	12.5	25.2	0.0	0.0	0.0	0.0	0.0	0.3	0.0	0.0	0.7
	Maximum	8.1	5360.0	6.5	513.8	384.3	481.0	31.2	2108.7	405.0	121.3	190.8	57.8	0.8	105.8	0.7	20.8	1651.4	35.2	12.7	25.4	0.9
	Range	1.1	4857.0	3.5	479.6	381.1	466.0	30.0	2075.7	195.1	113.5	178.3	32.6	0.8	105.8	0.7	20.8	1651.4	34.9	12.7	25.4	0.2
Confined	N	16.0	15.0	5.0	16.0	16.0	16.0	16.0	16.0	16.0	16.0	16.0	16.0	16.0	16.0	16.0	16.0	16.0	16.0	16.0	16.0	3.0
	Std. Deviation	0.3	679.2	0.4	57.3	13.9	61.1	4.4	206.9	31.6	15.3	10.2	6.3	0.1	12.7	0.2	3.8	16.8	5.0	2.7	7.0	0.0
	Mean	7.6	1033.3	5.4	109.0	28.9	55.4	3.4	146.7	316.4	32.3	21.8	34.2	0.3	17.8	0.2	1.8	9.4	3.8	2.9	12.5	0.8
	Median	7.7	883.0	5.3	92.4	27.0	36.4	2.4	83.8	315.3	28.9	24.3	34.4	0.3	5.4	0.2	0.4	2.6	2.0	1.9	11.8	0.8
	Minimum	7.0	630.0	4.9	64.0	8.6	22.5	0.5	42.9	270.0	15.3	6.6	24.7	0.1	5.4	0.0	0.0	0.0	0.4	0.0	1.5	0.8
	Maximum	8.1	3050.0	5.9	282.7	70.0	241.5	19.7	805.6	403.8	67.1	50.2	47.0	0.6	52.0	0.5	14.1	65.5	21.3	9.5	23.7	0.8
	Range	1.1	2420.0	1.0	218.7	61.4	219.0	19.2	762.7	133.8	51.8	43.6	22.2	0.5	46.6	0.5	14.1	65.5	20.9	9.5	22.2	0.1
Total	N	104	94	46	104	104	104	104	104	104	104	104	103	103	104	103	104	104	104	104	104	24
	Std. Deviation	0.3	1126.6	1.9	86.6	43.3	86.8	6.9	352.7	50.2	22.7	45.5	6.5	0.2	25.3	0.2	4.7	289.4	4.2	3.3	6.1	0.1
	Mean	7.6	1296.1	4.5	128.0	35.2	74.4	5.4	225.5	296.6	32.7	47.8	37.8	0.3	26.9	0.2	2.5	77.8	4.0	3.4	12.6	0.8
	Median	7.5	760.5	5.2	98.5	23.9	34.5	2.4	64.3	292.4	24.3	26.2	36.5	0.3	17.9	0.2	0.4	2.3	3.2	2.1	11.7	0.8
	Minimum	7.0	503.0	0.7	34.2	3.2	15.0	0.5	33.0	209.9	7.8	6.6	24.7	0.0	0.0	0.0	0.0	0.0	0.3	0.0	0.0	0.7
	Maximum	8.2	5360.0	6.5	513.8	384.3	481.0	31.2	2108.7	405.0	121.3	190.8	57.8	0.8	105.8	0.7	20.8	1651.4	35.2	12.7	25.4	0.9
	Range	1.2	4857.0	5.9	479.6	381.1	466.0	30.7	2075.7	195.1	113.5	184.2	33.0	0.8	105.8	0.7	20.8	1651.4	34.9	12.7	25.4	0.2

Appendix 5.1e:- The statistical parameters of the hydrochemical data (meq) of all sub - aquifers

Sub-aquifer		Ca	Mg	Na	K	HCO3	Cl	SO4	NO3	TDI	T °C
Eocene western (642)	N	30.0	30.0	30.0	30.0	30.0	30.0	30.0	30.0	30.0	30.0
	Mean	4.4	1.6	1.4	0.0	4.6	1.8	0.4	0.7	15.0	21.6
	Minimum	1.7	0.3	0.7	0.0	3.4	0.9	0.2	0.2	9.5	19.3
	Maximum	7.0	3.3	2.4	0.1	5.6	3.6	0.9	2.9	21.5	28.2
	Range	5.3	3.0	1.7	0.0	2.1	2.7	0.7	2.7	11.9	8.9
Neogene (653)	N	29.0	29.0	29.0	29.0	29.0	29.0	29.0	29.0	29.0	29.0
	Mean	4.5	1.7	1.5	0.1	4.5	1.9	0.5	0.8	15.6	23.6
	Minimum	2.7	0.5	1.0	0.0	3.5	1.4	0.3	0.2	12.8	21.1
	Maximum	7.5	2.9	2.9	0.1	5.1	3.5	1.1	3.1	24.2	33.4
	Range	4.8	2.5	1.9	0.0	1.5	2.1	0.8	2.9	11.4	12.3
Lower and Upper Cenomanian western (654)	N	7.0	7.0	7.0	7.0	7.0	7.0	7.0	7.0	7.0	7.0
	Mean	5.4	2.3	2.6	0.1	5.1	4.6	0.6	0.3	20.9	23.9
	Minimum	3.2	0.7	1.0	0.0	4.4	1.2	0.3	0.1	12.3	23.3
	Maximum	14.1	5.8	10.5	0.5	6.6	22.7	1.4	0.4	62.0	26.4
	Range	10.9	5.1	9.5	0.5	2.2	21.5	1.0	0.4	49.7	3.1
Lower and Upper Cenomanian eastern (655)	N	9.0	9.0	9.0	9.0	9.0	9.0	9.0	9.0	9.0	9.0
	Mean	5.5	2.4	2.3	0.1	5.3	3.8	0.8	0.3	20.5	23.3
	Minimum	4.0	1.7	1.0	0.1	4.9	2.3	0.5	0.3	17.0	22.5
	Maximum	10.6	3.5	7.5	0.1	5.7	14.2	1.4	0.8	43.7	25.1
	Range	6.6	1.9	6.5	0.1	0.8	11.9	0.9	0.5	26.8	2.6
Pleistocene 670	N	12.0	12.0	12.0	12.0	12.0	12.0	12.0	12.0	12.0	12.0
	Mean	13.7	8.4	10.8	0.5	6.0	25.6	1.5	0.5	67.1	25.0
	Minimum	8.1	4.3	5.6	0.2	5.3	9.9	1.0	0.4	36.6	23.4
	Maximum	18.3	31.6	20.9	0.8	6.6	59.5	2.2	0.6	133.5	34.1
	Range	10.2	27.4	15.3	0.6	1.3	49.6	1.2	0.4	96.9	10.7
Eocene eastern 671	N	2.0	2.0	2.0	2.0	2.0	2.0	2.0	2.0	2.0	2.0
	Mean	10.4	6.0	7.9	0.3	5.7	17.3	1.2	0.4	49.3	24.5
	Minimum	8.8	5.1	6.8	0.3	5.4	16.6	1.1	0.3	48.5	24.0
	Maximum	12.1	6.9	9.1	0.4	6.0	18.0	1.2	0.6	50.1	25.0
	Range	3.3	1.9	2.3	0.1	0.7	1.4	0.1	0.0	1.7	1.0
Eocene eastern 673	N	7.0	7.0	7.0	7.0	7.0	7.0	7.0	7.0	7.0	7.0
	Mean	12.9	5.5	7.9	0.3	6.0	18.8	1.4	0.5	53.4	24.6
	Minimum	4.7	2.4	2.5	0.1	5.3	3.9	0.7	0.4	20.9	24.0
	Maximum	25.6	10.3	11.7	0.5	6.6	36.1	2.5	0.6	90.7	25.1
	Range	21.0	7.9	9.2	0.5	1.3	32.2	1.8	0.1	69.8	1.1
Total	N	96.0	96.0	96.0	96.0	96.0	96.0	96.0	96.0	96.0	96.0
	Mean	6.5	3.0	3.4	0.1	5.0	6.8	0.7	0.6	26.1	23.2
	Minimum	1.7	0.3	0.7	0.0	3.4	0.9	0.2	0.1	9.5	19.3
	Maximum	25.6	31.6	20.9	0.8	6.6	59.5	2.5	3.1	133.5	34.1
	Range	23.9	31.3	20.3	0.8	3.2	58.6	2.4	3.0	124.0	14.8

Appendix 5.2: Correlation between hydrochemical parameters according to Spearman correlation.

** Correlation is significant at the 0.1 level (2-tailed)
* Correlation is significant at the 0.5 level (2-tailed)

Correlations

			CA	MG	NA	K	HCO3	CL
Spearman's rho	Correlation Coefficient	CA	1.000	.298**	.652**	.500**	.509**	.751**
		MG	.298**	1.000	.575**	.563**	.727**	.636**
		NA	.652**	.575**	1.000	.679**	.469**	.854**
		K	.500**	.563**	.679**	1.000	.469**	.719**
		HCO3	.509**	.727**	.469**	.469**	1.000	.629**
		CL	.751**	.636**	.854**	.719**	.629**	1.000
		NO3	.503**	-.109	.362**	.084	.567**	.395*
		SO4	.735**	.595**	.782**	.679**	-.496**	.876**
		PH	-.112	-.469**	-.311*	-.209*	-.365**	-.214*
		SIO2	-.073	-.443**	-.332**	-.404**	.444**	-.397**
		PO4	.026	.408**	.370**	.442**	-.289	.317**
		D.O	-.142	-.230	-.151	-.270	.712**	-.266
		EC	.641**	.672**	.806**	.646**	-.192	.833**
		FE	.165	-.107	.200*	.135	.472**	.144
		F	.270**	.578**	.585**	.629**	.287	.503**
		BR	.539**	-.151	.297	.147	.262**	.597**
		CD	.688**	.219*	.498**	.473**	-.107	.508**
		CU	.141	-.035	.234*	.205*	.318**	.146
		MN	.554**	.323**	.484**	.490**	.091	.586**
		PB	.341**	.104	.197*	.072	-.120	.165
		ZN	-.139	-.006	-.123	-.044		-.073
	Sig. (2-tailed)	CA		.002	.000	.000	.000	.000
		MG	.002		.000	.000	.000	.000
		NA	.000	.000		.000	.000	.000
		K	.000	.000	.000		.000	.000
		HCO3	.000	.000	.000	.000		.000
		CL	.000	.000	.000	.000	.000	
		NO3	.000	.272	.000	.398	.276	.000
		SO4	.000	.000	.000	.000	.000	.000
		PH	.256	.000	.001	.033	.000	.029
		SIO2	.462	.000	.001	.000	.000	.000
		PO4	.794	.000	.000	.000	.000	.001
		D.O	.371	.143	.341	.084	.064	.089
		EC	.000	.000	.000	.000	.000	.000
		FE	.094	.281	.042	.172	.051	.143
		F	.006	.000	.000	.000	.000	.000
		BR	.007	.480	.158	.492	.175	.002
		CD	.000	.025	.000	.000	.007	.000
		CU	.155	.722	.017	.036	.279	.139
		MN	.000	.001	.000	.000	.001	.000
		PB	.000	.293	.045	.470	.356	.093
		ZN	.159	.951	.213	.658	.225	.462

Correlations

			NO3	SO4	PH	SIO2	PO4	D.O
Spearman's rho	Correlation Coefficient	CA	.503**	.735**	-.112	-.073	.026	-.142
		MG	-.109	.595**	-.469**	-.443**	.408**	-.230
		NA	.362**	.782**	-.311**	-.332**	.370**	-.151
		K	.084	.679**	-.209	-.404**	.442**	-.270
		HCO3	-.108	.567**	-.496**	-.365**	.444**	-.289
		CL	.395**	.876**	-.214*	-.397**	.317**	-.266
		NO3	1.000	.357*	.158	.111	-.223*	.159
		SO4	.357*	1.000	-.128	-.408**	.223*	-.371**
		PH	.158	-.128	1.000	.188	-.303**	-.073
		SIO2	.111	-.408**	.188	1.000	-.558**	.153
		PO4	-.223*	.223*	-.303**	-.558**	1.000	-.156
		D.O	.159	-.371*	-.073	.153	-.156	1.000
		EC	.264**	.690**	-.447**	-.334**	.495**	-.161
		FE	.279**	.144	.200	.135	-.062	.012
		F	-.065	.571**	-.357**	-.406**	.366**	-.302
		BR	.394	.321	-.226	-.207	.168	
		CD	.262**	.576**	-.080	.090	-.032	.395**
		CU	.251*	.142	.042	.037	-.070	.148
		MN	.248*	.537**	.021	-.024	.046	-.417**
		PB	.169	.115	-.124	.419**	-.264*	.305*
		ZN	.095	-.059	-.033	.002	-.053	.190
	Sig. (2-tailed)	CA	.000	.000	.256	.462	.794	.371
		MG	.272	.000	.000	.000	.000	.143
		NA	.000	.000	.001	.001	.000	.341
		K	.398	.000	.033	.000	.000	.084
		HCO3	.276	.000	.000	.000	.000	.064
		CL	.000	.000	.029	.000	.001	.089
		NO3	.	.000	.109	.266	.023	.315
		SO4	.000	.	.194	.000	.023	.016
		PH	.109	.194	.	.057	.002	.648
		SIO2	.266	.000	.057	.	.000	.334
		PO4	.023	.016	.002	.000	.	.325
		D.O	.315	.016	.648	.334	.325	.
		EC	.009	.000	.000	.001	.000	.347
		FE	.004	.143	.042	.175	.537	.941
		F	.515	.000	.000	.000	.000	.052
		BR	.056	.126	.289	.332	.432	
		CD	.007	.000	.422	.364	.747	.010
		CU	.010	.151	.670	.711	.479	.349
		MN	.011	.000	.836	.811	.646	.006
		PB	.086	.246	.209	.000	.007	.049
		ZN	.339	.550	.738	.984	.597	.228

Correlations

			MN	PB	ZN
Spearman's rho	Correlation Coefficient	CA	.554**	.341**	-.139
		MG	.323**	.104	-.006
		NA	.484**	.197*	-.123
		K	.490**	.072	-.044
		HCO3	.318**	.091	-.120
		CL	.586**	.165	-.073
		NO3	.248*	.169	.095
		SO4	.537**	.115	-.059
		PH	.021	-.124	-.033
		SIO2	-.024	.419**	.002
		PO4	.046	-.264**	-.053
		D.O	-.417**	.305*	.190
		EC	.488**	.107	-.093
		FE	.197*	.308**	-.169
		F	.209*	.000	-.054
		BR	.184	.025	.069
		CD	.409**	.559**	-.156
		CU	.100	.322**	.118
		MN	1.000	.234*	-.090
		PB	.234*	1.000	.007
		ZN	-.090	.007	1.000
	Sig. (2-tailed)	CA	.000	.000	.159
		MG	.001	.293	.951
		NA	.000	.045	.213
		K	.000	.470	.658
		HCO3	.001	.356	.225
		CL	.000	.093	.462
		NO3	.011	.086	.339
		SO4	.000	.246	.550
		PH	.836	.209	.738
		SIO2	.811	.000	.984
		PO4	.646	.007	.597
		D.O	.006	.049	.228
		EC	.000	.294	.361
		FE	.046	.001	.085
		F	.034	.996	.586
		BR	.389	.906	.749
		CD	.000	.000	.114
		CU	.311	.001	.233
		MN	.	.017	.362
		PB	.017	.	.940
		ZN	.362	.940	.

Correlations

			EC	FE	F	BR	CD	CU
Spearman's rho	Correlation Coefficient	CA	.641**	.165	.270**	.539**	.688**	.141
		MG	.672**	-.107	.578**	-.151	.219*	-.035
		NA	.806**	.200*	.585**	.297	.498**	.234*
		K	.646**	.135	.629**	.147	.473**	.205*
		HCO3	.712**	-.192	.472**	.287	.262**	-.107
		CL	.833**	.144	.503**	.597**	.508**	.146
		NO3	.264**	.279**	-.065	.394	.262**	.251*
		SO4	.690**	.144	.571**	.321	.576**	.142
		PH	-.447**	.200*	-.357*	-.226	-.080	.042
		SIO2	-.334**	.135	-.406**	-.207	.090	.037
		PO4	.495**	-.062	.366*	.168	-.032	-.070
		D.O	-.161	.012	-.302	.	.395*	.148
		EC	1.000	.048	.475**	.565**	.417**	.067
		FE	.048	1.000	-.003	-.184	.338**	.384**
		F	.475**	-.003	1.000	.076	.300**	.014
		BR	.565**	-.184	.076	1.000	-.043	.055
		CD	.417**	.338**	.300**	-.043	1.000	.283*
		CU	.067	.384**	.014	.055	.283*	1.000
		MN	.488**	.197*	.209*	.184	.409**	.100
		PB	.107	.308**	.000	.025	.559**	.322**
		ZN	-.093	-.169	-.054	.069	-.156	.118
	Sig. (2-tailed)	CA	.000	.094	.006	.007	.000	.155
		MG	.000	.281	.000	.480	.025	.722
		NA	.000	.042	.000	.158	.000	.017
		K	.000	.172	.000	.492	.007	.036
		HCO3	.000	.051	.000	.175	.007	.279
		CL	.000	.143	.000	.002	.000	.139
		NO3	.009	.004	.515	.056	.000	.010
		SO4	.000	.143	.000	.126	.000	.151
		PH	.000	.042	.000	.289	.422	.670
		SIO2	.001	.175	.000	.332	.364	.711
		PO4	.000	.537	.000	.432	.747	.479
		D.O	.347	.941	.052	.	.010	.349
		EC	.	.641	.000	.004	.000	.513
		FE	.641	.	.975	.389	.000	.000
		F	.000	.975	.	.723	.002	.885
		BR	.004	.389	.723	.	.843	.798
		CD	.000	.000	.002	.843	.	.004
		CU	.513	.000	.885	.798	.004	.
		MN	.000	.046	.034	.906	.000	.311
		PB	.294	.001	.996	.749	.000	.001
		ZN	.361	.085	.586		.114	.233

Appendix 5.3: The chemical analyses of groundwater, springs and surface water in the Faria Basin for two water sampling rounds (G symbol for the second round 8.6-16.7.1997) after groundwater recharge and (M symbol for the first round 23.8-1.12.1996) before the groundwater recharge: major and minor ions in mg/L, Do in mg/L, EC in microseimens/cm, FC and TC numbers, trace elements in micro g/L (Notice: < d.t means lower than detection limit of the element).

Appendix 5.3a: The chemical analyses of the second round (after recharge) and the microbiological analyses

Well ident.	aquifer	No.	Ca	Mg	Na	K	HCO3	SO4	Cl	NO3	PO4	F	SiO2	EC	pH	Cation	Anion	Er %	DO	FC	TC
Ein Dulieb	642	G1	104.1	4.1	32.1	1.3	288.9	13.5	56.6	18.9	<d.t	0.14	57.77	688	7.75	7	6.9	0.52	5.9		30
18-18/2	642	G2	71.2	16.9	29.6	2.5	256.8	15.7	46.9	25.9	0.01	0.2	53.27	667	7.36	6.3	6.9	0.12	5.25	50	1000
E.Faria	642	G3	85.1	15.3	29.6	2.5	256.8	18.3	53.6	21.8	0.02	0.14	52.98	764	7.41	6.9	6.9	1.01	5.6	800	
18-18/4	642	G4	103.9	12.9	29.6	1.4	277.8	23	61.6	43.5	0.01	0.21	49.05	746	7.41	7.6	7.5	1.15	5.7		
18-18/1	642	G5	88.1	5.3	29.6	2.5	218.2	22.3	55.6	37.9	0.06	0.11	48.86	1000	7.48	6.2	6.2	0.68	6.5		
18-18/32	642	G6	139.7	21	28.6	2.5	260.5	23	89.8	182.5	0.22	0.11	40.14	1077	7.53	10.4	10.2	1.37	6.5		
18-18/25A	642	G7	113.6	19.1	39.5	1.7	260.5	18.3	82	131.9	<d.t	0.06	35.07	680	7.53	9	9.1	0.97	6.3		
18-18/33	642	G8	89.8	26.1	37	2.7	314.8	23	64.5	45	0.08	0.33	41.29	1070	7.57	8.3	8.2	0.97	6.5		
18-18/17	642	G9	122.5	35.2	37	1.5	272.9	28.1	128.9	129.7	<d.t	0.18	44.26	1030	7.47	9.9	9.8	1.01	6.1		
18-18/16	642	G10	130.2	20.6	39.5	2.5	264.2	26.6	82.1	163.3	<d.t	0.33	41.58	676	7.53	10.7	10.7	1.08	5.7		
E.Faria	642	G11	84.8	8.2	39.5	0.5	282.7	16.4	45.8	28.9	<d.t	0.33	50.97	751	7.71	9.9	9.8	0.93	4.9		
18-18/37	654	G12	78.1	21.2	29.6	1.4	291.4	18.3	52.7	15.3	0.07	0.37	41.01	654	7.84	6.7	6.8	0.45	5.9		
18-18/38	654	G13	91.2	16.3	27.2	2.5	282.7	23	42.9	11.8	0.13	0.12	46.95	503	7.77	6.9	6.5	0.64	6		
E.H&Beida	642	G14	93.2	3.2	19.8	1.6	237.1	9.9	48.8	19.3	0.11	0.1	43.88	503	7.93	5.8	6	0.92	6.3		
E.Jeser	642	G15	93.2	5.4	19.8	2.3	235.8	9.5	39.1	49	<d.t	0.14	42.73	717	7.55	6	6.3	0.57	6		
E.Abu Saleh	653	G16	83.05	30.8	33.3	4.4	281.5	26.3	62.5	81	0.07	0.41	46.28		8.39	8.2	8.3	0.85	4.95		
Waste water1	333	G17	116.1	3.3	64.3	1.9	214.8	23	113.3	106.2	0.18	0.2	36.53	640	7.67	8.9	8.9	0.65	5.25		
18-18/27	653	G18	101.5	11.6	35.7	2.6	269.2	17.5	62.5	69.9	0.12	0.2	38.32	682	7.94	7.6	7.7	0.76	5.2		
18-18/14	653	G19	125.3	12.4	33.3	2.3	258	21.5	52.7	69.9	0.13	0.24	33.82	815	7.69	7.3	7.3	0.47	6.1		
E.Miska	653	G20	99.5	17.6	40.5	2.6	232.1	31	83	90.9	0.04	0.27	38.9		7.88	8.2	8.3	0.57	5.3	TNTC	TNTC
18-18/31	653	G21	149.5	5.7	35.7	2.6	270.4	22.3	53.7	190.8	0.12	0.25	38.8	702	8.02	9.6	9.5	0.72	4.45		4
18-18/31A	653	G22	99.5	17.3	28.6	2.3	267.9	19.3	58.5	73	0.01	0.29	39.09	525	7.75	7.7	7.6	0.56	5.75	0	
18-18/13	653	G23	96.4	17	31	2.3	254.3	23	62.5	70.9	<d.t	0.23	34.78	780	7.68	7.6	7.6	0.22	5.65		
18-18/19A	653	G24	125.3	34.9	66.7	2.2	297.6	53.3	125	160	0.12	0.25	34.12	621	7.75	12.1	12.1	0.34	5.6		
18-18/25	653	G25	120.2	13.9	35.7	2.3	274.1	35.8	70.3	95.6	0.06	0.31	34.87	713	7.75	8.8	8.8	0.68	5.55		
18-18/11A	653	G26	78	20.9	35.7	2.2	216.1	33.2	62.5	123.9	0.07	0.24	35.64		8.13	7.3	7.3	0.68	5.2	TNTC	TNTC
18-18/23	653	G27	135.3	12.6	52.4	2.2	259.3	36.9	125	103.3	0.07	0.24	35.54		7.86	10.1	10.2	0.99	-		
E.AQ023	653	G28	113.4	12.6	33.3	2.2	281.5	27	68.3	70.9	0.07	0.21	36.79	719	7.87	8.2	8.3	0.72	4.65		
Well AQ023	653	G29	118.3	10.4	35.7	2.4	260.5	31.4	70.3	93.9	<d.t	0.3	36.69		8.4	8.4	8.4	0.76	4.7		
W.Shibli	653	G30	104.5	12.9	23.8	2.4	288.9	22.5	68.3	17	0.26	0.16	36.69	737	7.59	7.4	7.4	0.66	4.95	TNTC	TNTC

Well ident.	aquifer	No.	Ca	Mg	Na	K	HCO3	SO4	Cl	NO3	PO4	F	SiO2	EC	pH	cation	anion	Er%	DO	FC	TC
Waste water2	333	G31	105.6	9.3	31	2.4	274.1	26.5	74.2	21.3	<d.t	0.07	34.72		8.17	7.4	7.5	0.54	5.25		
19-17/44	655	G32	110.2	21.5	33.3	2.4	311.1	39.1	90.7	19.8	<d.t	0.24	37.59		8.05	8.8	8.8	0.3	5.3		
19-17/1	671	G33	176.6	84.3	209.5	12.1	328.4	58	638.5	21.4	<d.t	0.38	36.2	2600	7.42	25.2	25	0.81	3.7		
19-17/7	673	G34	144.2	125.3	197.6	9.7	325.9	48.9	689.2	27.3	<d.t	0.59	45.65		7.57	26.3	26.3	0.28	5	1750	1800
19-17/28	670	G35	262	384.3	481	31.2	338.3	79.7	2108.7	27.5	<d.t	0.64	39.91	5300	7.42	66.4	67.2	1.14	4.1	170	120
19-17/34	655	G36	122.5	20.5	28.6	2.4	337.1	39.1	85	24.2	<d.t	0.21	35.28	650	7.85	9.1	9.1	0.37	5.5		
Waste water3	333	G37	118.2	15	26.2	2.4	324.6	17.8	70.3	35.9	0.24	<d.t	45.74		8.22	8.3	8.3	0.87	1.2		
19-17/34D	655	G38	93.6	35.5	23.8	2.2	298.8	39.1	89.8	24.4	<d.t	0.16	35.09	700	7.9	8.7	8.6	0.41	5.2		
Waste water2	333	G39	98.5	17.3	33.3	2.4	209.9	24.3	58.5	142	0.21	<d.t	43.33		8.15	7.8	7.9	0.58	0.65		
19-17/8	670	G40	229.3	175	353.1	20.7	324.7	105.1	1172	39	0.02	0.77	47.59	4500	7.36	41.7	41.2	1.17	4.05	440	780
E.Taban	642	G41	77	13.5	22.2	1.65	253.1	12	43	16.8	0.03	0.18	42.96	534	7.5	6	5.9	1.15	4.25	250	950
E.Subian	642	G42	79.1	34.6	54.3	2.5	307.4	43.5	97.6	24.5	0.02	0.33	34.35		7.52	9.2	9.1	1.19	3		

Appendix 5.3

Appendix 5.3b: The chemical analyses of the second round (after recharge) and the microbiological analyses

Well ident.	aquifer	No.	Ca	Mg	Na	K	HCO3	SO4	Cl	NO3	PO4	F	SiO2	EC	pH	cation	anion	Er %	DO	FC	TC
18-18/1	642	M1	50.6	39.4	32	2	319.1	15	51.4	16.8	0.13	0.17	45.5	759	7.16	7.2	7.3	0.93			
18-18/6	642	M10	103.4	18.3	30	1.6	309.3	19.7	65.9	46.3	0.18	<d.t	40.7	833	7.38	8	8.1	1			0
E.Faria	642	M11	78.9	19.7	27.5	1.7	289.7	14.7	52.4	14.5	0.13	0.03	47.1	704	7.47	6.8	6.8	0.35		0	0
18-18/37	654	M12	64	35.3	25	1.9	313	15.3	54.4	14.3	0.15	0.1	37.8	726	7.7	7.2	7.2	0.13		TNTC	TNTC
18-18/6	642	M13	93.8	24.1	30	1.4	314.2	19.4	64.1	44.2	0.15	<d.t	40.5	812	7.55	8	8.1	0.94			
18-18/38	654	M14	78.9	14.3	25	1.7	280	17.2	43.7	7.3	0.12	0.17	41	639	7.77	6.2	6.3	1.05		0	0
18-18/38	654	M15	69.2	20.1	22.5	1.7	270	17.8	44.7	6.6	0.12	0.1	41	630	7.83	6.1	6.2	0.71			
E.Hamad & B	642	M16	34.2	28.6	15	1.5	209.9	7.8	33	15.7	0.12	0.02	40.6	517	7.86	4.8	4.8	0.87			
E.Taban	642	M17	36.5	28.6	17.5	1.7	219.7	8.4	33	14.5	0.14	0.06	39.6	523	7.95	5	4.9	0.62			
18-18/27	653	M18	75.9	23.7	35	2.4	306.8	13.9	58.2	16	0.19	0.37	35.1	729	7.23	7.3	7.2	1.07			
18-18/30	653	M19	75.9	21.5	35	2.2	289.9	16.8	59.2	17.2	0.16	0.4	36.3	720	7.14	7	7.1	1.28			
E.Dulib	642	M2	75.9	20.6	34.5	1.2	309.3	13.9	50.5	14.8	0.16	0.18	48.7	749	7.16	7	7	0.33			
E.Abu saleh	653	M20	72.9	22.4	22.5	3.7	274.9	16.4	52.4	15.6	0.26	0.4	33.9	680	7.23	6.6	6.6	0.8			
18-18/14	653	M21	83.4	26.8	32.5	2.6	309.3	22.9	70.9	21.5	0.16	0.4	37.9	820	7.41	7.8	7.9	0.92			
18-18/26	653	M22	65.5	24.1	25	2.4	247.9	18.6	58.2	18.6	0.17	0.4	31.9	671	7.56	6.4	6.4	0.29			
E.Miska	653	M23	75.9	27.7	27.5	2.5	279.8	21.8	70.9	19.2	0.18	0.4	36.5	762	7.44	7.3	7.4	0.68			
18-18/13	653	M24	74.4	21	30	2.4	261.4	18.9	62.1	18	0.16	0.4	32.1	702	7.53	6.8	6.7	0.89			
18-18/35	653	M25	65.5	25.5	25	2.7	274.9	17.5	51.4	12.5	0.4	0.4	33.4	695	7.43	6.5	6.6	0.93			
18-18/11A	653	M26	75.2	35.8	32.5	2.3	300.7	22.9	51.4	15.1	0.15	0.48	34	728	7.54	7.1	7.1	0.32			
18-18/11A	653	M27	53.6	35.8	30	2.6	279.8	29	56.3	14.5	0.25	0.47	35.1	921	7.68	7	7	0.76			
18-18/23	653	M28	90.8	28.6	45	2.7	304.4	26.1	106.8	25.1	0.26	0.49	33.6	820	7.83	8.9	9	0.83		4	20
18-18/39	654	M29	94.5	29.5	44.4	2.2	319.1	29	100.9	24.8	0.39	0.22	29.53	957	7.71	9.1	9.1	0.28			
18-18/32	642	M3	100.5	18.3	32	1.2	309.3	19.1	61.1	39.2	0.16	0.28	38.5	817	7.29	7.9	7.8	1.26			
18-18/36	653	M30	80.1	22.3	34.6	2.6	299.5	21.2	58.2	19.3	0.34	0.28	30.03	765	7.38	7.4	7.3	0.8			
E.Shibli	653	M31	68.8	25.9	29.6	2.6	280	18.3	58.2	16.4	0.41	0.24	25.2	740	7.38	6.9	6.9	0.23			
W.Faria 1	333	M32	72.5	24.5	42	2.4	305.6	20.5	62.1	16.9	0.34	0.27	26.66	740	7.45	7.5	7.5	0.51			
19-17/44	655	M33	99.8	25.9	39.5	2.4	344.9	28.4	82.5	21.5	0.36	0.27	29.84	924	7.6	8.9	8.9	0.6			
19-17/34	655	M34	86.9	26.8	42	2.5	317.6	30	81.5	24.5	0.29	0.32	28.19	900	7.33	8.4	8.6	1.4		4	3
19-17/34	655	M35	86.9	27.2	44.4	2.4	317.9	34.6	81.5	25	0.29	0.28	28.37	898	7.22	8.6	8.7	1.05			
W.Faria 2	333	M36	72.5	14.5	125.9	9	268.8	25.4	168.9	45.9	3.38	0.46	37.59	1020	8.11	10.5	10.6	0.5			
W.Faria 3	333	M37	69.5	14.5	116.1	8.6	262.6	22.8	159.2	44.1	2.96	0.24	37.53	1010	8.12	9.9	10.1	1.56			
19-17/46	655	M38	211.6	43.1	172.8	4.9	337.5	67.1	504.7	50.2	0.33	0.45	24.74	2220	7.49	21.7	22	1.21			
19-17/56	670	M39	163.2	51.8	128.4	8.7	381.7	81.5	349.4	36.8	0.28	0.06	31.19	1850	7.92	18.2	18.4	1.11			
18-18/4	642	M4	53.6	29.5	34.5	1.2	278.6	16.5	50.5	22.1	0.7	0.27	42.9	697	7.49	6.6	6.7	1.41			

Well ident.	aquifer	No.	Ca	Mg	Na	K	HCO3	SO4	Cl	NO3	PO4	F	SiO2	EC	pH	cation	anion	Er %	DO	FC	TC
19-17/55	673	M40	212.3	55.8	180.3	13	381.7	58.5	549.3	26.4	0.39	0.5	33.45	2351	7.28	18.2	18	1.11		TNTC	TNTC
19-17/27	670	M41	213.1	55.4	180.3	13	381.7	58.5	549.3	29.3	0.39	0.5	30.06	2350	7.35	23.4	23.5	0.49		TNTC	TNTC
19-17/2	670	M42	243.3	71.7	204.4	14.5	378	65.7	690.1	24.7	0.36	0.45	30.06	2790	7.18	23.7	27.5	0.6			
19-17/1	670	M43	241.8	61.7	155.7	14.9	368.2	53.8	590.1	22.9	0.47	0.48	29.66	2450	7.37	24.3	24.2	0.35		TNTC	TNTC
19-17/21	670	M44	282.6	80.8	148.2	16.2	398.9	83.3	669.7	34.2	0.34	0.6	35.94	3800	7.6	27.6	27.8	0.54			
19-17/8	670	M45	367.3	79	261.7	20.1	342.4	106.9	999.7	36	0.41	0.6	36.17	3700	7.53	36.7	36.7	0.16			
19-17/6	673	M46	513.8	88.1	269.1	21.5	382.9	121.3	1281.1	35.5	0.38	0.78	35.6	5360	7.37	45.1	45.6	0.94			
19-16/1	673	M47	453.4	83.5	192.6	18.1	384.2	96.5	1048.2	32.4	0.42	0.68	34.92	3900	7.33	38.3	38.4	0.3			
19-17/47	655	M48	94.7	29.9	46.3	2.6	325.2	25.5	100.9	25.3	0.42	0.47	28.23	918	7.85	9.3	9.2	1.22			
19-17/33	673	M49	156.1	51.8	175.6	11.3	367	58	436.8	29.8	0.39	0.58	33.49	2060	7.47	20	20.1	0.45			
Ein Fania	642	M5	81.9	12.5	34.5	1.8	289.7	15.4	50.5	14.2	0.22	0.28	47.4	701	7.57	6.7	6.7	1.23			
19-17/31	670	M50	361.9	84	300	24.1	349.8	56.5	1106.5	23.1	0.42	0.44	31.1	4000	7.16	38.6	38.5	0.26			
19-17/9	670	M51	318.4	54.1	243.9	22.1	362.1	51	863.8	21.6	0.38	0.42	33.49	3200	7.38	31.5	31.7	0.74			
19-17/10	670	M52	327.7	59.7	222	22.1	376.8	53.4	854.1	19.4	0.38	0.42	34.09	3200	7.22	31.5	31.7	0.61			
19-17/54	670	M53	242.3	65.3	226.8	27.3	362.1	47.4	747.3	14.5	0.51	0.42	31.63	2900	7.4	28	28.3	0.88			
19-17/53	670	M54	282.7	70	239	19.1	405	63.2	795.9	28.8	0.36	0.61	33.97	3050	7.29	30.7	30.9	0.53			
19-17/23	673	M55	93.2	37.8	58.5	3.2	321.6	34.3	139.8	35.5	0.56	0.17	27.87	1098	7.54	10.4	10.5	1.35			
19-17/53	664	M56	282.7	70	241.5	19.7	403.8	65	805.6	28.4	0.47	0.55	33.79	3050	7.44	30.9	31.2	1.05			
W.Fania 4	333	M57	82.3	25.2	36.6	2.6	293.3	17.6	73.8	17.1	0.46	0.12	28.52	753	8.32	7.8	7.8	1.06			
18-18/14	653	M58	68.3	25.2	35.5	2.1	299.5	16.5	58.2	16.2	0.21	0.35	27.4	729	7.38	7.1	7	0.32			
18-18/31	653	M59	68.3	27.5	28	2.3	299.5	16.5	53.4	16	0.25	0.34	30.95	730	7.68	6.9	7	1.37			
18-18/2	642	M6	86.3	11.6	27	1.6	280	13.1	46.7	15.4	0.16	0.4	45.8	708	7.67	6.5	6.4	0.51			
18-18/34	642	M60	79.2	30.3	50.5	2.5	315.4	28.7	104.8	24.3	0.31	0.4	29.26	957	7.55	9.2	9.3	0.44			
19-17/34	655	M61	79.2	33.6	40.5	2.9	313	28.7	85.4	25.3	0.23	0.4	29.03	883	7.62	8.6	8.6	0.25		123L	1328L
19-17/33	673	M62	231.4	28.9	202	15.7	400.1	58.1	514.5	30.2	0.25	0.55	38.79	2290	7.41	23.1	22.8	1.34			
18-18/25A	642	M7	227	39.8	30	1.2	340	75.7	75.7	48.6	0.12	<d.l	36.4	901	7.13	8.8	8.8	0.26			
18-18/17	642	M8	101.2	21	50	2.2	311.7	21.6	94.2	47.2	0.18	0.1	41.9	910	7.4	9	9	0.23		8	16
18-18/33	642	M9	102.7	17	30	1.5	321.6	16.9	58	44.2	0.12	<d.l	39	839	7.51	7.9	8	1.38			
18-18/16																					
	642																			92	TNTC

Appendix 5.3c: The minor and trace elements of water samples and TDS of the second round (after recharge)

Well Ident.	aquifer	No.	Br	Fe	Cu	Mn	Pb	Cd	Zn	date	TDS cal.	TDS/EC
Ein Dulieb	642	1	-	24	4.41	0.14	8.71	16.82	7.21	17/06/97		
18-18/2	642	2	-	76.5	8.61	0.04	8.59	12.64	11.68	17/06/97		
E.Faria	642	3	-	40.4	6.02	0.69	7.82	12.2	16.68	17/06/97		
18-18/4	642	4	-	17.4	3.36	0.48	8.32	12.2	10.79	17/06/97		
18-18/1	642	5	-	39.7	5.43	0.3	12.71	19.71	24.39	17/06/97		
18-18/32	642	6	-	51.1	7.18	<d.t	8.17	14.64	7.21	17/06/97		
18-18/25A	642	7	-	26.7	8.02	0.74	11.29	16.82	23.48	17/06/97		
18-18/33	642	8	-	7.1	2.54	1.22	6.89	10.16	11.698	17/06/97		
18-18/17	642	9	-	19.7	4.83	0.48	7.04	14.64	13.48	17/06/97		
18-18/16	642	10	-	23.5	2.72	0.85	11.17	8.71	11.68	17/06/97		
E.Faria	642	11	-	18.9	6.37	<d.t	6.45	12.64	7.94	17/06/97		
18-18/37	654	12	-	22.9	1.68	<d.t	7.49	20.12	1.47	17/06/97		
18-18/38	654	13	-	28.1	21.27	<d.t	9.48	14.64	20	18/06/97		
E.H&Beida	642	14	-	17.9	1.4	<d.t	2.7	8.93	13.48	19/06/97		
E.Jeser	642	15	-	10.1	5.36	0.3	6.36	7.6	12.57	20/06/97		
E.Abu Saleh	653	16	-	12.8	2.07	<d.t	1.9	<d.t	<d.t	18/06/97	632.2	0.9
Waste water1	333	17	-	15.7	4.17	2.7	1.69	8.26	10.79	18/06/97	688.0	0.9
18-18/27	653	18	-	27.8	8.76	0.6	2.97	0.67	15.54	18/06/97	603.8	0.9
18-18/14	653	19	-	24	1.61	0.23	0.15	0.67	7.94	18/06/97	574.6	0.8
E.Miska	653	20	-	14.7	4.13	2.47	1.66	8.26	11.68	18/06/97	631.8	0.8
18-18/31	653	21	-	18.7	4.65	9.32	1.48	1.95	22.57	18/06/97	765.2	
18-18/31A	653	22	-	32.6	3.09	<d.t	1.19	3.69	13.48	18/06/97	601.2	0.9
18-18/13	653	23	-	26.1	9.27	<d.t	5.91	22.63	15.54	18/06/97	587.7	1.1
18-18/19A	653	24	-	29.4	3.31	1.94	2.05	5.86	16.6	18/06/97	896.2	1.1
18-18/19	653	25	-	23.1	3.97	<d.t	1.22	4.13	22.57	18/06/97	678.3	1.1
18-18/11A	653	26	-	105.8	2.33	<d.t	1.81	1.51	16.68	18/06/97	558.7	0.8
18-18/23	653	27	-	39.9	4.04	0.46	0.71	8.71	<d.t	18/06/97	758.3	
E.AQ023	653	28	-	22.5	2.11	<d.t	2.23	3.91	6.47	18/06/97	641.3	0.9
Well AQ023	653	29	-	14.7	5.51	0.07	0.8	1.95	10.79	18/06/97	655.4	
E.Shibli	653	30	-	15.5	3.53	<d.t	0.41	2.4	11.68	29/06/97	565.5	0.8

Well ident.	aquifer	No.	Br	Fe	Cu	Mn	Pb	Cd	Zn	date	TDS cal.	TDS/EC
Waste water2	333	31	-	28.8	5.74	1.73	4.1	10.16	2.94	29/06/97	574.5	
19-17/44	655	32	-	34.5	1.54	7.64	<d.t	6.97	3.68	29/06/97	660.6	0.6
19-17/1	671	33	-	8.9	3.4	8.78	2.88	3.06	9.41	29/06/97	1559.7	
19-17/7	673	34	-	20.4	6.71	20.76	10.81	12.28	14.41	29/06/97	1608.7	0.7
19-17/28	670	35	-	30.7	8.96	7.85	10.66	786.36	22.57	29/06/97	3747.4	1.1
19-17/34	655	36	-	11.5	1.15	1.62	4.31	3.34	15.54	29/06/97	689.1	
Waste water3	333	37	-	22.3	2.21	2.18	1.8	2.35	7.94	29/06/97	650.5	0.9
19-17/34D	655	38	-	9.4	2.47	1.17	2.77	1.96	13.48	29/06/97	637.3	
Waste water2	333	39	-	93.8	3.99	14.87	0.09	2.1	8.68	29/06/97	625.9	
19-17/8	670	40	-	32.2	2.47	9.44	4.19	79.89	2.21	30/06/97		
E.Taban	642	41	-	10	1.4	1.25	3.68	0.57	20	01/07/97		
E.Subian	642	42	-	40.8	7.42	1.7	11.72	1.67	8.68	02/07/97		

Appendix 5.3d: The minor and trace elements of water samples and TDS of the first round (before recharge)

Well ident.	Aquifer	No.	Br	Fe	Cu	Mn	Pb	Cd	Zn	date	TDS cal.	TDS/EC
18-18/1	642	1	0.79		1.55	<d.t	1.6	1.01	10	08-Sep-96	369.8	0.5
18-18/6	642	10	0.83	5.6	1.11	0.47	0.88	0.86	13.67	10-Sep-96	439.2	0.5
E.Faria	642	11	0.79	9.7	3.21	0.32	0.71	0.42	12.66	10-Sep-96	362.8	0.5
18-18/37	654	12	0.79	10.1	1.25	0.35	3.19	<d.t	10.46	10-Sep-96	362.8	0.5
18-18/6	642	13	0.67	11	2.07	<d.t	1.31	1.16	14.96	10-Sep-96	432.6	0.5
18-18/38	654	14	0.75	10.5	0.41	0.37	1.4	3.03	8.66	10-Sep-96	331.8	0.5
18-18/38	654	15	0.83	7.1	1.22	<d.t	2.48	2.73	11.54	10-Sep-96	322.6	0.5
E.Hamad & B	642	16	0.75	15.9	2.7	0.2	3.19	0.27	25.38	10-Sep-96	253.3	0.5
E.Taban	642	17	0.76	13.9	1.29	<d.t	3.65	1.3	8.66	10-Sep-96	260.3	0.5
18-18/27	653	18	-	14.4	1.07	<d.t	2.59	<d.t	10.46	10-Sep-96		
18-18/30	653	19	-	20	2.03	0.74	1.51	0.42	9.55	10-Sep-96		
E.Dulib	642	2	0.79	8.4	0.66	<d.t	1.09	<d.t	5	08/09/96	373.6	0.5
E.Abu saleh	653	20	-	4.9	3.5	0.32	0.74	0.86	10.99	17/09/96		
18-18/14	653	21	0.8	23.6	4.17	0.42	0.54	<d.t	17.11	17/09/96		
18-18/26	653	22	0.8	14.6	1.03	1.06	0.23	<d.t	17.84	17/09/96		
E.Miska	653	23	-	13.6	0.45	<d.t	0.74	<d.t	18.43	17/09/96		
18-18/13	653	24	0.83	6.7	1.22	<d.t	1.28	1.87	23.22	17/09/96		
18-18/35	653	25	0.79	9	2.47	0.08	<d.t	1.45	13.67	17/09/96		
18-18/11A	653	26	0.75	4.1	1.19	<d.t	0.32	<d.t	20	17/09/96		
18-18/11A	653	27	0.83	6.2	3.8	0.3	0.43	4.33	18.43	17/09/96		
18-18/23	653	28	0.89	11.6	1.84	<d.t	0.37	<d.t	7.86	17/09/96		
18-18/39	654			12.9	1.7	0.35	<d.t	1.3	23.67	15-Oct-96	471.9	0.5
18-18/32	642	3	0.84	14	2.29	<d.t	1.68	1.72	21.68	08-Sep-96	423.5	0.5
18-18/36	653		-	<d.t	0.33	<d.t	0.83	1.45	2.59	15-Oct-96	377.7	0.5
E.Shibli	653		-	11.4	12.96	<d.t	1.28	<d.t	14.96	15-Oct-96	347.8	0.5
W.Faria 1	333		-	32	15.2	<d.t	0.17	2.73	6.07	15-Oct-96	379.7	0.5
19-17/44	655		-	12.1	4.05	0.32	1.14	0.86	8.66	15-Oct-96	456.5	0.5
19-17/34	655		-	17.2	4.36	0.15	0.48	0.15	12.1	15-Oct-96	439.1	0.5
19-17/34	655		-	5.4	5.42	<d.t	0.48	2.46	18.43	15-Oct-96	447.1	0.5
W.Faria 2	333		-	29.6	3.28	2.56	1.23	4.78	20.46	15-Oct-96	598.6	0.6
W.Faria 2	333		-	36.5	6.02	0.86	1.99	2.46	6.52	15-Oct-96	568.8	0.6
19-17/46	655		-	52	2.55	1.35	2.79	25.2	5.18	20-Oct-96	1203.2	0.5
19-17/56	670		-	8.2	2.1	2.21	1.86	7.8	14.24	20-Oct-96	990.9	0.5
18-18/4	642	4	0.74	88.5	35.19	<d.t	9.84	1.01	18.75	08-Sep-96	353.1	0.5

Well Ident.	Aquifer	No.	Br	Fe	Cu	Mn	Pb	Cd	Zn	date	TDS cal.	TDS/EC
19-17/55	673			12.1	3.18	0.27	1.12	51.92	18.43	08-Sep-96	1272.7	0.5
19-17/27	670			32.6	1.47	0.91	2.11	64.67	6.52	20-Oct-96	1483.4	0.5
19-17/2	670			11.4	3.5	1.47	3.75	100.63	12.1	20-Oct-96	1305.9	0.5
19-17/1	671			26	1.89	9.51	5.54	340.29	15.67	20-Oct-96	1497.7	0.4
19-17/21	670			9.9	3.36	0.94	3.71	424.07	10.99	20-Oct-96	2032.9	0.5
19-17/8	670			30.1	3.11	1.18	5.86	1594.4	20	20-Oct-96	2507.0	0.5
19-17/6	673			27.5	9.41	2.26	7.57	1651.4	14.96	20-Oct-96	2101.0	0.5
19-16/1	673			17.8	2.13	1.6	9.86	1599.5	4.82	20-Oct-96	473.0	0.5
19-17/47	655			6.7	1.71	< d.t	1.12	1.33	19.17	23-Oct-96	1087.9	0.5
19-17/33	673			10.5	2.52	1.64	1.09	5.42	10.99	23-Oct-96	364.6	0.5
Ein Fania	642	5	0.82	17.2	6.97	< d.t	6.67	0.71	10	08-Sep-96	2115.8	0.5
19-17/31	670			13	5.49	1.43	9.86	683.74	2.181	23-Oct-96	1741.5	0.5
19-17/9	670			25.9	2.48	1.94	5.7	59.57	12.1	23-Oct-96	1732.9	0.5
19-17/10	670			10.5	2.07	1.52	3.11	50.31	6.72	23-Oct-96	1535.6	0.5
19-17/54	670			29.2	5.53	7.25	4.23	52.19	1.55	23-Oct-96	1681.6	0.6
19-17/53	673			18.7	3.67	2.52	4.39	72.95	11.68	23-Oct-96	548.1	0.5
19-17/23	654			47.9	2.7	1.04	2.56	0.89	12.49	23-Oct-96	1695.2	0.6
19-17/53	333			30.2	2.38	14.14	4.2	65.54	4.14	23-Oct-96	398.5	0.5
W.Faria 4	653			30.2	2.8	0.23	0.45	0.89	10	23-Oct-96	539.1	0.7
18-18/14	653			14.3	1.89	< d.t	1.06	2.4	14.14	29-Oct-96	537.6	0.7
18-18/31	642			22.7	6.27	0.2	< d.t	0.89	6.72	29-Oct-96	350.3	0.5
18-18/2	642	6	0.82	51.3	0.85	0.4	2.94	1.45	9.11	08-Sep-96	675.0	0.7
18-18/33	655			20.2	3.36	0.41	1.15	1.73	18.55	29-Oct-96	632.6	0.7
19-17/34	673			14.9	6.86	0.92	1.21	< d.t	23.15	29-Oct-96	1513.3	0.7
19-17/33	642			16.2	2.62	< d.t	3.33	21.75	13.31	29-Oct-96	454.1	0.5
18-18/25A	642	7	0.87	10.5	6.24	< d.t	3.71	< d.t	24.24	10-Sep-96	493.6	0.5
18-18/17	642	8	0.89	8.6	1.59	0.66	4.62	0.42	24.54	10-Sep-96	427.1	0.5
18-18/33	642	9	0.85	11.8	1.4	0.94	1.62	0.27	8.66	10-Sep-96		
18-18/16	642											

Appendix 5.3e: The field measurements of groundwater, springs and surface water in the Faria Basin for the second round (8.6-16.7.1997) after groundwater recharge

Well ident	aquifer	sample No.	Ph	T (°C)	EC in microS/cm
Ein Dulieb	642	G1	7.66	21.3	688
18-18/2	642	G2	7.23	20.9	667
E.Faria	642	G3	7.21	20	677
18-18/4	642	G4	7.22	21.4	764
18-18/1	642	G5	7.22	21.9	746
18-18/32	642	G6	7.33	21.7	1000
18-18/25A	642	G7	7.36	28.2	1077
18-18/33	642	G8	7.24	22.4	680
18-18/17	642	G9	7.2	23.5	1070
18-18/16	642	G10	7.17	23	1030
E.Faria	642	G11	7.21	20	677
18-18/37	654	G12	7.48	26.4	751
18-18/38	654	G13	7.44	23.5	654
E.H&Beida	642	G14	7.42	19.3	503
E.Jeser	642	G15	7.5	19.3	503
E.Abu Saleh	653	G16	7.36	22.2	717
18-18/27	653	G18	7.42	22.3	640
18-18/14	653	G19	7.45	22.7	682
E.Miska	653	G20	7.35	21.5	815
18-18/31A	653	G22	7.61	22.1	702
18-18/13	653	G23	7.53	23.9	525
18-18/19A	653	G24	7.33	33.4	780
18-18/19	653	G25	7.34	22.5	621
18-18/11A	653	G26	7.36	22.9	713
18-18/23	653	G27	7.7	23.3	111
E.AQ023	653	G28	7.41	21.1	719
E.Shibli	653	G30	7.47	23.9	737
19-17/1	671	G33	7.12	25	2600
19-17/7	673	G34	7.16	25.1	530
19-17/28	670	G35	7.01	25	5300
19-17/34	655	G36	7.39	22.5	650
19-17/34D	655	G38	7.39	22.5	650
19-17/8	670	G40	7.4	34.1	4500
E.Taban	642	G41	7.47	19.5	534

Appendix 5.3f: The field measurements of groundwater, springs and surface water in the Faria Basin for the first round (23.8-1.12.1996) before groundwater recharge

Well ident	aquifer no.	EC	O2	p-value	m-value	corrected Eh
18-18/1	642	598	5.08	1.9		581
18-18/6	642	790	5.57	4.5		644
E.Faria	642	692	3.92	4.7		210
18-18/37	654	718	3.81	2.8		589
18-18/6	642	598	5.08	1.9		581
18-18/38	654	661	1.55	0.5		630
18-18/38	654	661	1.55	0.5	5,25mmol	630
E.Hamad & B	642	533				210
E.Taban	642	534				641
18-18/27	653	649	4.84	2.1		623
18-18/30	653	735	7.35	2.5		622
E.Dulib	642	480				210
E.Abu saleh_	653	660				210
18-18/14	653	765	8.09	2.3		572
18-18/26	653	720				596
E.Miska	653	780				210
18-18/13	653	731	6.31	2.6		561
18-18/35	653	757				210
18-18/11A	653	700	4.83	2.3		581
18-18/11A	653	700	4.83	2.3		581
18-18/23	653	920	7.54	2.2		491
18-18/39	654	928	3.8	5	5mmol	393
18-18/32	642	880	5.3	3		550
18-18/36	653	935				210
E.Shibli	653	732	4.9			413
W.Faria 1	333					210
19-17/44	655					421
19-17/34	655	863	6.5			421
19-17/34	655	863	6.5			210
W.Faria 2	333					210
W.Faria 3	333					386
19-17/46	655	2510	4.9			210
19-17/56	670	2060	5			570
18-18/4	642	718	5.66	2.5		323
19-17/55	673	2650	6.7	6.5		210
19-17/27	670	2600				210
19-17/2	670	3000	6.7			210
19-17/1	671	3110	4.9			210
19-17/21	670					210
19-17/8	670					210
19-17/6	673					342
19-16/1	673	5100	5.3	4.8		210
19-17/47	655	874				210
19-17/33	673					860
Ein Faria	642	693	4.8	2.1		345
19-17/31	670	4600	4.3			210
19-17/9	670	3600				210
19-17/10	670					210
19-17/54	670					310
19-17/53	670	3900	4.3	6.5		

Well ident	aquifer no.	EC	O2	p-value	m-value	corrected Eh
19-17/23	673					210
19-17/53	654	3900	4.3	6.5		310
W.Faria 4	333					210
18-18/14	653					210
18-18/31	653					210
18-18/2	642					210
18-18/33	642					210
19-17/34	655					210
19-17/33	673					210
18-18/25A	642	908	6.12	2.2		651
18-18/17	642	954	4.3	3.1		639
18-18/33	642	835	5.3	1.9		630

Appendix 5.4:- Distribution of species and saturation indicies calculated by means of PHREEQC

Appendix 5.4a:- Distribution of species and saturation indicies in Eocene sub-aquifer western 642 in the well 18-18/1

	Species	Molality	Activity
	OH-	2.23E-07	1.88E-07
	H+	6.01E-08	5.25E-08
	H2O	5.55E+01	9.99E-01
C(4)		6.82E-03	
	HCO3-	5.90E-03	5.04E-03
	CO2	5.93E-04	5.97E-04
	CaHCO3+	2.00E-04	1.71E-04
	MgHCO3+	8.13E-05	6.90E-05
	CaCO3	1.98E-05	2.00E-05
	NaHCO3	1.88E-05	1.89E-05
	CO3-2	8.39E-06	4.49E-06
	MgCO3	4.96E-06	5.00E-06
	NaCO3-	6.49E-07	5.51E-07
	ZnCO3	6.57E-08	6.62E-08
	ZnHCO3+	5.53E-08	4.69E-08
	FeHCO3+	2.47E-08	2.10E-08
	CdHCO3+	2.33E-08	1.98E-08
Ca		5.31E-03	
	Ca+2	4.97E-03	2.66E-03
	CaHCO3+	2.00E-04	1.71E-04
	CaSO4	1.17E-04	1.18E-04
	CaCO3	1.98E-05	2.00E-05
Cd		4.62E-07	
	Cd+2	2.39E-07	1.24E-07
	CdCl+	1.83E-07	1.55E-07
	CdHCO3+	2.33E-08	1.98E-08
Cl		1.55E-02	
	Cl-	1.55E-02	1.31E-02
	CdCl+	1.83E-07	1.55E-07
Cu(1)		3.24E-10	
	Cu+	3.24E-10	2.71E-10
Cu(2)		4.98E-08	
	Cu(OH)2	3.89E-08	3.92E-08
Fe(2)		1.08E-07	
	Fe+2	7.64E-08	4.16E-08
	FeHCO3+	2.47E-08	2.10E-08
Fe(3)		1.09E-07	
	Fe(OH)3	7.21E-08	7.26E-08
	Fe(OH)2+	3.51E-08	2.98E-08
H(0)		3.87E-26	
	H2	1.94E-26	1.95E-26
K		3.33E-04	
	K+	3.33E-04	2.81E-04
	KSO4-	5.16E-07	4.38E-07
Mg		2.30E-03	
	Mg+2	2.15E-03	1.17E-03
	MgHCO3+	8.13E-05	6.90E-05

	Species	Molality	Activity
	MgSO4	6.05E-05	6.09E-05
	MgCO3	4.96E-06	5.00E-06
Mn(2)	4.92E-09		
	Mn+2	3.20E-09	1.74E-09
Mn(3)	2.28E-30		
	Mn+3	2.28E-30	5.23E-31
N(5)	4.26E-04		
	NO3-	4.26E-04	3.58E-04
Na	7.86E-03		
	Na+	7.83E-03	6.66E-03
	NaHCO3	1.88E-05	1.89E-05
	NaSO4-	8.76E-06	7.44E-06
	NaCO3-	6.49E-07	5.51E-07
O(0)	3.13E-04		
	O2	1.57E-04	1.58E-04
Pb	5.41E-09		
	PbCO3	4.82E-09	4.86E-09
S(6)	6.10E-04		
	SO4-2	4.23E-04	2.23E-04
	CaSO4	1.17E-04	1.18E-04
	MgSO4	6.05E-05	6.09E-05
	NaSO4-	8.76E-06	7.44E-06
	KSO4-	5.16E-07	4.38E-07
Si	5.58E-04		
	H4SiO4	5.56E-04	5.60E-04
	H3SiO4-	1.84E-06	1.56E-06
Zn	2.82E-07		
	Zn+2	1.40E-07	7.39E-08
	ZnCO3	6.57E-08	6.62E-08
	ZnHCO3+	5.53E-08	4.69E-08

Saturation indicies

Phase	SI	log IAP	log KT	
Anglesite	-6.07	-13.86	-7.79	PbSO4
Anhydrite	-1.87	-6.23	-4.36	CaSO4
Aragonite	0.41	-7.92	-8.33	CaCO3
Calcite	0.56	-7.92	-8.48	CaCO3
Cd(OH)2	-6	7.65	13.65	Cd(OH)2
CdSiO3	-4.67	4.4	9.07	CdSiO3
CdSO4	-10.46	-10.56	-0.09	CdSO4
Cerrusite	-2.42	-15.55	-13.13	PbCO3
Chalcedony	0.3	-3.25	-3.55	SiO2
Chrysotile	-3.84	28.38	32.23	Mg3Si2O5(OH)4
CO2(g)	-1.76	-19.91	-18.15	CO2
Dolomite	0.88	-16.2	-17.09	CaMg(CO3)2
Fe(OH)3(a)	0.54	18.46	17.92	Fe(OH)3
Goethite	6.43	18.46	12.03	FeOOH
Gypsum	-1.65	-6.23	-4.58	CaSO4:2H2O
H2(g)	-22.56	-22.56	0	H2
Hausmannite	-21.12	39.96	61.08	Mn3O4
Hematite	14.86	36.92	22.06	Fe2O3
Jarosite-K	-7.2	22.68	29.88	KFe3(SO4)2(OH)6
Manganite	-8.26	17.08	25.34	MnOOH
Melanterite	-8.82	-11.03	-2.21	FeSO4:7H2O
O2(g)	-0.84	-3.8	-2.96	O2
Otavite	-0.15	-12.25	-12.1	CdCO3
Pb(OH)2	-3.8	4.35	8.16	Pb(OH)2
Pyrochroite	-9.4	5.8	15.2	Mn(OH)2
Pyrolusite	-13.05	28.36	41.41	MnO2
Quartz	0.73	-3.25	-3.98	SiO2
Rhodochrosit	-2.98	-14.11	-11.13	MnCO3
Sepiolite	-2.26	13.5	15.77	Mg2Si3O7.5OH:3H2O
Sepiolite(d)	-5.16	13.5	18.66	Mg2Si3O7.5OH:3H2O
Siderite	-1.84	-12.73	-10.89	FeCO3
SiO2(a)	-0.54	-3.25	-2.71	SiO2
Smithsonite	-2.48	-12.48	-10	ZnCO3
Talc	0.46	21.88	21.42	Mg3Si4O10(OH)2
Willemite	-3.74	11.61	15.35	Zn2SiO4
Zn(OH)2(e)	-4.07	7.43	11.5	Zn(OH)2

Appendix 5.4

Appendix 5.4b:- Distribution of species and saturation indicies in Neogene sub-aquifer western 653 in the spring Ein Miska

	Species	Molality	Activity
	OH-	2.65E-07	2.38E-07
	H+	3.98E-08	3.63E-08
	H_2O	5.55E+01	1.00E+00
C(4)		4.90E-03	
	HCO3-	4.44E-03	4.01E-03
	CO2	3.35E-04	3.36E-04
	CaHCO3+	6.58E-05	5.96E-05
	MgHCO3+	3.76E-05	3.39E-05
	CaCO3	9.65E-06	9.67E-06
	CO3-2	7.45E-06	4.99E-06
	MgCO3	3.35E-06	3.36E-06
	NaHCO3	2.43E-06	2.43E-06
	NaCO3-	1.01E-07	9.08E-08
	ZnCO3	8.51E-08	8.53E-08
	ZnHCO3+	4.81E-08	4.33E-08
	FeHCO3+	1.50E-08	1.35E-08
Ca		1.90E-03	
	Ca+2	1.79E-03	1.20E-03
	CaHCO3+	6.58E-05	5.96E-05
	CaSO4	2.79E-05	2.80E-05
	CaCO3	9.65E-06	9.67E-06
Cl		2.00E-03	
	Cl-	2.00E-03	1.80E-03
	ZnCl+	4.24E-10	3.82E-10
Cu(1)		2.31E-11	
	Cu+	2.31E-11	2.07E-11
Cu(2)		7.06E-09	
	Cu(OH)2	6.34E-09	6.35E-09
	Cu+2	5.95E-10	4.01E-10
	CuOH+	1.23E-10	1.10E-10
Fe(2)		7.01E-08	
	Fe+2	5.00E-08	3.37E-08
	FeHCO3+	1.50E-08	1.35E-08
Fe(3)		1.74E-07	
	Fe(OH)3	1.27E-07	1.27E-07
	Fe(OH)2+	4.33E-08	3.90E-08
H(0)		1.87E-26	
	H2	9.35E-27	9.38E-27
K		6.40E-05	
	K+	6.39E-05	5.75E-05
	KSO4-	5.17E-08	4.66E-08
Mg		1.14E-03	
	Mg+2	1.08E-03	7.27E-04
	MgHCO3+	3.76E-05	3.39E-05
	MgSO4	1.93E-05	1.93E-05
	MgCO3	3.35E-06	3.36E-06
	MgOH+	6.79E-08	6.12E-08
N(5)		3.10E-04	
	NO3-	3.10E-04	2.78E-04
	PbNO3+	1.74E-13	1.57E-13

	Species	Molality	Activity
Na	1.20E-03		
	Na+	1.19E-03	1.08E-03
	NaHCO3	2.43E-06	2.43E-06
	NaSO4-	7.05E-07	6.36E-07
	NaCO3-	1.01E-07	9.08E-08
O(0)	3.31E-04		
	O2	1.66E-04	1.66E-04
Pb	3.57E-09		
	PbCO3	3.29E-09	3.30E-09
	PbHCO3+	1.35E-10	1.21E-10
S(6)	2.27E-04		
	SO4-2	1.79E-04	1.19E-04
	CaSO4	2.79E-05	2.80E-05
	MgSO4	1.93E-05	1.93E-05
	NaSO4-	7.05E-07	6.36E-07
	KSO4-	5.17E-08	4.66E-08
Si	6.08E-04		
	H4SiO4	6.05E-04	6.07E-04
	H3SiO4-	2.56E-06	2.30E-06
Zn	2.82E-07		
	Zn+2	1.29E-07	8.57E-08
	ZnCO3	8.51E-08	8.53E-08
	ZnHCO3+	4.81E-08	4.33E-08

Saturation indicies

Phase	SI	log IAP	log KT	
Anglesite	-6.54	-14.34	-7.8	PbSO4
Anhydrite	-2.49	-6.85	-4.35	CaSO4
Aragonite	0.1	-8.22	-8.32	CaCO3
Calcite	0.25	-8.22	-8.47	CaCO3
Cerrusite	-2.57	-15.72	-13.15	PbCO3
Chalcedony	0.36	-3.22	-3.57	SiO2
Chrysotile	-3.65	28.79	32.44	Mg3Si2O5(OH)4
CO2(g)	-2.03	-20.18	-18.15	CO2
Dolomite	0.38	-16.66	-17.05	CaMg(CO3)2
Fe(OH)3(a)	0.89	18.85	17.96	Fe(OH)3
Goethite	6.77	18.85	12.08	FeOOH
Gypsum	-2.26	-6.85	-4.58	CaSO4:2H2O
H2(g)	-22.89	-22.88	0.01	H2
Hematite	15.43	37.69	22.27	Fe2O3
Jarosite-K	-8	22.13	30.13	KFe3(SO4)2(OH)6
Melanterite	-9.16	-11.4	-2.23	FeSO4:7H2O
O2(g)	-0.83	-3.78	-2.95	O2
Pb(OH)2	-3.76	4.46	8.22	Pb(OH)2
Quartz	0.79	-3.22	-4.01	SiO2
Sepiolite	-1.98	13.83	15.81	Mg2Si3O7.5OH:3H2O
Sepiolite(d)	-4.83	13.83	18.66	Mg2Si3O7.5OH:3H2O
Siderite	-1.9	-12.78	-10.88	FeCO3
SiO2(a)	-0.49	-3.22	-2.73	SiO2
Smithsonite	-2.39	-12.37	-9.98	ZnCO3
Talc	0.74	22.36	21.62	Mg3Si4O10(OH)2
Willemite	-3.08	12.41	15.49	Zn2SiO4
Zn(OH)2(e)	-3.69	7.81	11.5	Zn(OH)2

	Species	Molality	Activity
	OH-	5.09E-07	4.58E-07
	H+	2.19E-08	2.00E-08
	H2O	5.55E+01	1.00E+00
C(4)	5.29E-03		
	HCO3-	4.93E-03	4.46E-03
	CO2	2.03E-04	2.03E-04
	CaHCO3+	6.21E-05	5.62E-05
	MgHCO3+	5.33E-05	4.81E-05
	CaCO3	1.69E-05	1.69E-05
	CO3-2	1.52E-05	1.02E-05
	MgCO3	8.86E-06	8.88E-06
	NaHCO3	2.45E-06	2.46E-06
	NaCO3-	1.95E-07	1.76E-07
	PbCO3	1.43E-08	1.43E-08
Ca	1.60E-03		
	Ca+2	1.50E-03	1.01E-03
	CaHCO3+	6.21E-05	5.62E-05
	CaCO3	1.69E-05	1.69E-05
	CaSO4	1.65E-05	1.66E-05
Cl	1.54E-03		
	Cl-	1.54E-03	1.38E-03
	MnCl+	1.45E-11	1.30E-11
	ZnCl+	1.27E-11	1.15E-11
	FeCl+	1.12E-11	1.01E-11
Cu(1)	2.09E-11		
	Cu+	2.09E-11	1.88E-11
Cu(2)	1.97E-08		
	Cu(OH)2	1.89E-08	1.90E-08
	Cu+2	5.35E-10	3.62E-10
	CuOH+	2.01E-10	1.81E-10
Fe(2)	1.19E-08		
	Fe+2	7.80E-09	5.27E-09
	FeHCO3+	2.60E-09	2.35E-09
	FeCO3	1.29E-09	1.29E-09
Fe(3)	1.69E-07		
	Fe(OH)3	1.38E-07	1.38E-07
	Fe(OH)2+	2.50E-08	2.25E-08
H(0)	5.64E-27		
	H2	2.82E-27	2.83E-27
K	4.86E-05		
	K+	4.86E-05	4.38E-05
	KSO4-	2.78E-08	2.51E-08
Mg	1.45E-03		
	Mg+2	1.37E-03	9.27E-04
	MgHCO3+	5.33E-05	4.81E-05
	MgSO4	1.75E-05	1.76E-05
	MgCO3	8.86E-06	8.88E-06
	MgOH+	1.68E-07	1.51E-07
Mn(2)	6.37E-09		
	Mn+2	3.43E-09	2.32E-09

Appendix 5.4c:- Distribution of species and saturation indicies in L and U Cenomanian sub-aquifer western 654 in the well 18-18/37

	Species	Molality	Activity
	MnCO3	1.88E-09	1.88E-09
	MnHCO3+	1.02E-09	9.20E-10
Mn(3)	1.52E-30		
	Mn+3	1.52E-30	6.00E-31
N(5)	2.31E-04		
	NO3-	2.31E-04	2.07E-04
Na	1.09E-03		
	Na+	1.09E-03	9.80E-04
	NaHCO3	2.45E-06	2.46E-06
	NaSO4-	4.50E-07	4.06E-07
	NaCO3-	1.95E-07	1.76E-07
O(0)	9.38E-05		
	O2	4.69E-05	4.70E-05
Pb	1.54E-08		
	PbCO3	1.43E-08	1.43E-08
	Pb(CO3)2-2	5.57E-10	3.68E-10
	PbHCO3+	3.17E-10	2.86E-10
	Pb+2	1.22E-10	8.07E-11
S(6)	1.59E-04		
	SO4-2	1.25E-04	8.33E-05
	MgSO4	1.75E-05	1.76E-05
	CaSO4	1.65E-05	1.66E-05
	NaSO4-	4.50E-07	4.06E-07
	KSO4-	2.78E-08	2.51E-08
Si	6.30E-04		
	H4SiO4	6.25E-04	6.26E-04
	H3SiO4-	4.92E-06	4.44E-06
Zn	1.61E-08		
	ZnCO3	6.62E-09	6.64E-09
	Zn+2	4.87E-09	3.25E-09
	Zn(CO3)2-2	2.19E-09	1.45E-09
	ZnHCO3+	2.03E-09	1.83E-09

Saturation indicies						
Phase	SI	log IAP	log KT			
Anglesite	-6.38	-14.17	-7.8	PbSO4		
Anhydrite	-2.72	-7.08	-4.36	CaSO4		
Aragonite	0.34	-7.99	-8.33	CaCO3		
Calcite	0.49	-7.99	-8.47	CaCO3		
Cerrusite	-1.94	-15.08	-13.14	PbCO3		
Chalcedony	0.36	-3.2	-3.57	SiO2		
Chrysotile	-1.66	30.69	32.35	Mg3Si2O5(OH)4		
CO2(g)	-2.24	-20.39	-18.15	CO2		
Dolomite	1.05	-16.01	-17.06	CaMg(CO3)2		
Fe(OH)3(a)	0.88	18.82	17.94	Fe(OH)3		
Goethite	6.76	18.82	12.06	FeOOH		
Gypsum	-2.5	-7.08	-4.58	CaSO4:2H2O		
H2(g)	-23.4	-23.4	0	H2		
Hausmannite	-17.63	43.69	61.33	Mn3O4		
Hematite	15.46	37.64	22.18	Fe2O3		
Jarosite-K	-9.18	20.85	30.03	KFe3(SO4)2(OH)6		
Manganite	-6.88	18.46	25.34	MnOOH		
Melanterite	-10.13	-12.36	-2.22	FeSO4:7H2O		
O2(g)	-1.37	-4.33	-2.95	O2		
Pb(OH)2	-2.88	5.31	8.19	Pb(OH)2		
Pyrochroite	-8.44	6.76	15.2	Mn(OH)2		
Pyrolusite	-11.41	30.16	41.57	MnO2		
Quartz	0.79	-3.2	-4	SiO2		
Rhodochrosit	-2.5	-13.63	-11.13	MnCO3		
Sepiolite	-0.67	15.12	15.79	Mg2Si3O7.5OH:3H2O		
Sepiolite(d)	-3.54	15.12	18.66	Mg2Si3O7.5OH:3H2O		
Siderite	-2.39	-13.27	-10.88	FeCO3		
SiO2(a)	-0.48	-3.2	-2.72	SiO2		
Smithsonite	-3.49	-13.48	-9.99	ZnCO3		
Talc	2.75	24.29	21.54	Mg3Si4O10(OH)2		
Willemite	-4.81	10.62	15.43	Zn2SiO4		
Zn(OH)2(e)	-4.59	6.91	11.5	Zn(OH)2		

Appendix 5.4d:- Distribution of species and saturation indicies in lower and upper Cenomanian sub-aquifer eastern 655 in the well 19-17/34			
	Species	Molality	Activity
	OH-	1.98E-07	1.77E-07
	H+	5.15E-08	4.68E-08
	H2O	5.55E+01	1.00E+00
C(4)	5.68E-03		
	HCO3-	5.04E-03	4.54E-03
	CO2	4.92E-04	4.93E-04
	CaHCO3+	8.24E-05	7.42E-05
	MgHCO3+	4.01E-05	3.59E-05
	CaCO3	9.20E-06	9.22E-06
	CO3-2	6.59E-06	4.32E-06
	NaHCO3	4.16E-06	4.17E-06
	MgCO3	2.70E-06	2.71E-06
	NaCO3-	1.29E-07	1.16E-07
	ZnCO3	4.94E-08	4.95E-08
	ZnHCO3+	3.66E-08	3.28E-08
	FeHCO3+	3.49E-08	3.13E-08
Ca	2.17E-03		
	Ca+2	2.04E-03	1.33E-03
	CaHCO3+	8.24E-05	7.42E-05
	CaSO4	4.15E-05	4.16E-05
	CaCO3	9.20E-06	9.22E-06
Cd	1.34E-09		
	Cd+2	1.05E-09	6.75E-10
	CdCl+	1.47E-10	1.31E-10
Cl	2.30E-03		
	Cl-	2.30E-03	2.06E-03
	ZnCl+	3.18E-10	2.85E-10
	FeCl+	2.19E-10	1.96E-10
	CdCl+	1.47E-10	1.31E-10
Cu(1)	3.48E-10		
	Cu+	3.48E-10	3.10E-10
Cu(2)	6.83E-08		
	Cu(OH)2	5.75E-08	5.77E-08
	Cu+2	9.15E-09	6.04E-09
	CuOH+	1.44E-09	1.29E-09
Fe(2)	1.49E-07		
	Fe+2	1.05E-07	6.90E-08
	FeHCO3+	3.49E-08	3.13E-08
Fe(3)	1.59E-07		
	Fe(OH)3	1.08E-07	1.08E-07
	Fe(OH)2+	4.90E-08	4.39E-08
H(0)	3.11E-26		
	H2	1.55E-26	1.56E-26
K	6.40E-05		
	K+	6.39E-05	5.72E-05
	KSO4-	6.86E-08	6.15E-08
Mg	1.10E-03		
	Mg+2	1.04E-03	6.84E-04
	MgHCO3+	4.01E-05	3.59E-05

	Species	Molality	Activity
	MgSO4	2.40E-05	2.40E-05
	MgCO3	2.70E-06	2.71E-06
	MgOH+	4.71E-08	4.23E-08
Mn(2)	2.73E-09		
	Mn+2	1.77E-09	1.17E-09
	MnHCO3+	5.26E-10	4.71E-10
	MnCO3	3.99E-10	4.00E-10
Mn(3)	6.68E-31		
	Mn+3	6.68E-31	2.49E-31
N(5)	3.95E-04		
	NO3-	3.95E-04	3.53E-04
Na	1.83E-03		
	Na+	1.82E-03	1.64E-03
	NaHCO3	4.16E-06	4.17E-06
	NaSO4-	1.44E-06	1.29E-06
	NaCO3-	1.29E-07	1.16E-07
O(0)	1.38E-04		
	O2	6.88E-05	6.90E-05
Pb	2.32E-09		
	PbCO3	2.11E-09	2.11E-09
	PbHCO3+	1.13E-10	1.02E-10
	Pb+2	4.36E-11	2.82E-11
	Pb(CO3)2-2	3.55E-11	2.29E-11
	PbOH+	1.31E-11	1.17E-11
S(6)	3.13E-04		
	SO4-2	2.46E-04	1.60E-04
	CaSO4	4.15E-05	4.16E-05
	MgSO4	2.40E-05	2.40E-05
	NaSO4-	1.44E-06	1.29E-06
	KSO4-	6.86E-08	6.15E-08
Si	4.70E-04		
	H4SiO4	4.68E-04	4.69E-04
	H3SiO4-	1.51E-06	1.35E-06
	H2SiO4-2	2.59E-12	1.67E-12
Zn	1.85E-07		
	Zn+2	8.81E-08	5.75E-08
	ZnCO3	4.94E-08	4.95E-08
	ZnHCO3+	3.66E-08	3.28E-08

Saturation indicies

Phase	SI	log IAP	log KT	
Anglesite	-6.54	-14.35	-7.8	PbSO4
Anhydrite	-2.32	-6.67	-4.35	CaSO4
Aragonite	0.08	-8.24	-8.32	CaCO3
Calcite	0.23	-8.24	-8.47	CaCO3
Cd(OH)2	-8.16	5.49	13.65	Cd(OH)2
CdSiO3	-7	2.16	9.16	CdSiO3
CdSO4	-12.96	-12.97	-0.01	CdSO4
Cerrusite	-2.75	-15.92	-13.16	PbCO3
Chalcedony	0.25	-3.33	-3.58	SiO2
Chrysotile	-4.69	27.83	32.51	Mg3Si2O5(OH)4
CO2(g)	-1.87	-20.02	-18.16	CO2
Dolomite	0.26	-16.77	-17.03	CaMg(CO3)2
Fe(OH)3(a)	0.86	18.83	17.97	Fe(OH)3
Goethite	6.73	18.83	12.1	FeOOH
Gypsum	-2.09	-6.67	-4.58	CaSO4:2H2O
H2(g)	-22.67	-22.66	0.01	H2
Hausmannite	-21.82	39.84	61.65	Mn3O4
Hematite	15.31	37.66	22.34	Fe2O3
Jarosite-K	-7.56	22.66	30.22	KFe3(SO4)2(OH)6
Manganite	-8.28	17.06	25.34	MnOOH
Melanterite	-8.72	-10.96	-2.24	FeSO4:7H2O
O2(g)	-1.21	-4.16	-2.95	O2
Otavite	-2.44	-14.54	-12.1	CdCO3
Pb(OH)2	-4.13	4.11	8.24	Pb(OH)2
Pyrochroite	-9.47	5.73	15.2	Mn(OH)2
Pyrolusite	-13.4	28.39	41.78	MnO2
Quartz	0.69	-3.33	-4.02	SiO2
Rhodochrosit	-3.18	-14.3	-11.12	MnCO3
Sepiolite	-2.82	13	15.83	Mg2Si3O7.5OH:3H2O
Sepiolite(d)	-5.66	13	18.66	Mg2Si3O7.5OH:3H2O
Siderite	-1.65	-12.53	-10.87	FeCO3
SiO2(a)	-0.6	-3.33	-2.73	SiO2
Smithsonite	-2.63	-12.61	-9.97	ZnCO3
Talc	-0.52	21.17	21.69	Mg3Si4O10(OH)2
Willemite	-4.03	11.51	15.54	Zn2SiO4
Zn(OH)2(e)	-4.08	7.42	11.5	Zn(OH)2

Appendix 5.4e:- Distribution of species and saturation indicies in Pleistocene sub-aquifer eastern 670 in the well 19-17/27

	Species	Molality	Activity
	OH-	2.48E-07	2.09E-07
	H+	5.11E-08	4.47E-08
	H2O	5.55E+01	9.99E-01
C(4)	6.73E-03		
	HCO3-	5.89E-03	5.04E-03
	CO2	5.08E-04	5.12E-04
	CaHCO3+	1.98E-04	1.69E-04
	MgHCO3+	8.04E-05	6.83E-05
	CaCO3	2.27E-05	2.29E-05
	NaHCO3	1.87E-05	1.89E-05
	CO3-2	9.70E-06	5.19E-06
	MgCO3	5.64E-06	5.68E-06
	NaCO3-	7.25E-07	6.15E-07
	FeHCO3+	5.61E-08	4.76E-08
	CdHCO3+	2.91E-08	2.47E-08
	ZnCO3	2.55E-08	2.57E-08
	ZnHCO3+	1.85E-08	1.57E-08
	FeCO3	1.17E-08	1.18E-08
Ca	5.33E-03		
	Ca+2	4.99E-03	2.67E-03
	CaHCO3+	1.98E-04	1.69E-04
	CaSO4	1.18E-04	1.18E-04
	CaCO3	2.27E-05	2.29E-05
Cd	5.77E-07		
	Cd+2	2.98E-07	1.55E-07
	CdCl+	2.28E-07	1.93E-07
	CdHCO3+	2.91E-08	2.47E-08
	CdCl2	1.05E-08	1.05E-08
Cl	1.55E-02		
	Cl-	1.55E-02	1.31E-02
	CdCl+	2.28E-07	1.93E-07
	CdCl2	1.05E-08	1.05E-08
Cu(1)	1.15E-10		
	Cu+	1.15E-10	9.57E-11
Cu(2)	2.31E-08		
	Cu(OH)2	1.91E-08	1.92E-08
	Cu+2	3.38E-09	1.84E-09
Fe(2)	2.48E-07		
	Fe+2	1.74E-07	9.46E-08
	FeHCO3+	5.61E-08	4.76E-08
	FeCO3	1.17E-08	1.18E-08
Fe(3)	3.37E-07		
	Fe(OH)3	2.32E-07	2.34E-07
	Fe(OH)2+	9.92E-08	8.43E-08
H(0)	2.81E-26		
	H2	1.41E-26	1.42E-26
K	3.33E-04		
	K+	3.33E-04	2.81E-04
	KSO4-	5.12E-07	4.35E-07
Mg	2.28E-03		

	Species	Molality	Activity
	Mg+2	2.14E-03	1.16E-03
	MgHCO3+	8.04E-05	6.83E-05
	MgSO4	5.92E-05	5.96E-05
	MgCO3	5.64E-06	5.68E-06
	MgOH+	1.03E-07	8.71E-08
Mn(2)		1.66E-08	
	Mn+2	1.06E-08	5.76E-09
	MnHCO3+	3.05E-09	2.59E-09
	MnCO3	2.36E-09	2.38E-09
Mn(3)		6.79E-30	
	Mn+3	6.79E-30	1.56E-30
N(5)		4.73E-04	
	NO3-	4.73E-04	3.98E-04
Na		7.86E-03	
	Na+	7.83E-03	6.66E-03
	NaHCO3	1.87E-05	1.89E-05
	NaSO4-	8.75E-06	7.43E-06
	NaCO3-	7.25E-07	6.15E-07
O(0)		2.54E-04	
	O2	1.27E-04	1.28E-04
Pb		1.02E-08	
	PbCO3	9.16E-09	9.23E-09
	PbHCO3+	4.82E-10	4.09E-10
	Pb(CO3)2-2	2.31E-10	1.20E-10
	Pb+2	1.97E-10	1.02E-10
S(6)		6.10E-04	
	SO4-2	4.24E-04	2.24E-04
	CaSO4	1.18E-04	1.18E-04
	MgSO4	5.92E-05	5.96E-05
	NaSO4-	8.75E-06	7.43E-06
	KSO4-	5.12E-07	4.35E-07
Si		5.58E-04	
	H4SiO4	5.56E-04	5.59E-04
	H3SiO4-	2.11E-06	1.79E-06
Zn		9.96E-08	
	Zn+2	4.69E-08	2.48E-08
	ZnCO3	2.55E-08	2.57E-08
	ZnHCO3+	1.85E-08	1.57E-08

Appendix 5.4

| Saturation indicies				
Phase	SI	log IAP	log KT	
Anglesite	-5.85	-13.64	-7.79	PbSO4
Anhydrite	-1.87	-6.22	-4.36	CaSO4
Aragonite	0.47	-7.86	-8.33	CaCO3
Calcite	0.62	-7.86	-8.47	CaCO3
Cd(OH)2	-5.76	7.89	13.65	Cd(OH)2
CdSiO3	-4.46	4.64	9.1	CdSiO3
CdSO4	-10.39	-10.46	-0.07	CdSO4
Cerrusite	-2.13	-15.28	-13.14	PbCO3
Chalcedony	0.31	-3.25	-3.56	SiO2
Chrysotile	-3.52	28.79	32.31	Mg3Si2O5(OH)4
CO2(g)	-1.83	-19.98	-18.15	CO2
Dolomite	0.99	-16.08	-17.07	CaMg(CO3)2
Fe(OH)3(a)	1.09	19.02	17.93	Fe(OH)3
Goethite	6.98	19.03	12.05	FeOOH
Gypsum	-1.64	-6.22	-4.58	CaSO4:2H2O
H2(g)	-22.7	-22.7	0	H2
Hausmannite	-19.17	42.08	61.25	Mn3O4
Hematite	15.91	38.05	22.14	Fe2O3
Jarosite-K	-5.81	24.17	29.98	KFe3(SO4)2(OH)6
Manganite	-7.53	17.81	25.34	MnOOH
Melanterite	-8.46	-10.68	-2.22	FeSO4:7H2O
O2(g)	-0.94	-3.89	-2.96	O2
Otavite	0.01	-12.09	-12.1	CdCO3
Pb(OH)2	-3.47	4.71	8.18	Pb(OH)2
Pyrochroite	-8.74	6.46	15.2	Mn(OH)2
Pyrolusite	-12.36	29.16	41.52	MnO2
Quartz	0.74	-3.25	-3.99	SiO2
Rhodochrosit	-2.4	-13.52	-11.13	MnCO3
Sepiolite	-2.01	13.77	15.78	Mg2Si3O7.5OH:3H2O
Sepiolite(d)	-4.89	13.77	18.66	Mg2Si3O7.5OH:3H2O
Siderite	-1.42	-12.31	-10.88	FeCO3
SiO2(a)	-0.53	-3.25	-2.72	SiO2
Smithsonite	-2.9	-12.89	-9.99	ZnCO3
Talc	0.79	22.29	21.5	Mg3Si4O10(OH)2
Willemite	-4.47	10.94	15.4	Zn2SiO4
Zn(OH)2(e)	-4.41	7.09	11.5	Zn(OH)2

Appendix 5.4f:- Distribution of species and saturation indicies in Eocene sub-aquifer eastern 671 in the well 19-17/1

	Species	Molality	Activity
	OH-	2.59E-07	2.17E-07
	H+	4.89E-08	4.27E-08
	H2O	5.55E+01	9.99E-01
C(4)	6.46E-03		
	HCO3-	5.64E-03	4.81E-03
	CO2	4.64E-04	4.68E-04
	CaHCO3+	2.13E-04	1.82E-04
	MgHCO3+	8.52E-05	7.21E-05
	CaCO3	2.55E-05	2.57E-05
	NaHCO3	1.54E-05	1.55E-05
	CO3-2	9.81E-06	5.18E-06
	MgCO3	6.22E-06	6.27E-06
	NaCO3-	6.22E-07	5.26E-07
	ZnCO3	6.17E-08	6.21E-08
	ZnHCO3+	4.30E-08	3.64E-08
	FeHCO3+	4.03E-08	3.41E-08
	MnHCO3+	3.05E-08	2.58E-08
	MnCO3	2.46E-08	2.48E-08
	PbCO3	2.41E-08	2.43E-08
Ca	6.04E-03		
	Ca+2	5.69E-03	3.01E-03
	CaHCO3+	2.13E-04	1.82E-04
	CaSO4	1.17E-04	1.17E-04
	CaCO3	2.55E-05	2.57E-05
	CaOH+	1.38E-08	1.17E-08
Cd	3.03E-08		
	Cd+2	1.54E-08	7.88E-09
	CdCl+	1.24E-08	1.05E-08
	CdHCO3+	1.42E-09	1.20E-09
	Cd(OH)4-2	2.07E-26	1.06E-26
Cl	1.67E-02		
	Cl-	1.67E-02	1.40E-02
	CdCl+	1.24E-08	1.05E-08
Cu(1)	1.37E-10		
	Cu+	1.37E-10	1.14E-10
Cu(2)	2.97E-08		
	Cu(OH)2	2.49E-08	2.51E-08
	Cu+2	4.07E-09	2.19E-09
Fe(2)	1.86E-07		
	Fe+2	1.32E-07	7.08E-08
	FeHCO3+	4.03E-08	3.41E-08
Fe(3)	2.81E-07		
	Fe(OH)3	1.96E-07	1.97E-07
	Fe(OH)2+	8.06E-08	6.82E-08
H(0)	2.56E-26		
	H2	1.28E-26	1.29E-26
K	3.82E-04		
	K+	3.81E-04	3.21E-04
	KSO4-	5.17E-07	4.37E-07

	Species	Molality	Activity
Mg	2.54E-03		
	Mg+2	2.39E-03	1.29E-03
	MgHCO3+	8.52E-05	7.21E-05
	MgSO4	5.77E-05	5.81E-05
	MgCO3	6.22E-06	6.27E-06
	MgOH+	1.18E-07	1.00E-07
Mn(2)	1.73E-07		
	Mn+2	1.12E-07	6.02E-08
	MnHCO3+	3.05E-08	2.58E-08
	MnCO3	2.46E-08	2.48E-08
Mn(3)	7.22E-29		
	Mn+3	7.22E-29	1.61E-29
N(5)	3.70E-04		
	NO3-	3.70E-04	3.09E-04
Na	6.78E-03		
	Na+	6.76E-03	5.73E-03
	NaHCO3	1.54E-05	1.55E-05
	NaSO4-	6.67E-06	5.64E-06
	NaCO3-	6.22E-07	5.26E-07
O(0)	2.32E-04		
	O2	1.16E-04	1.17E-04
Pb	2.68E-08		
	PbCO3	2.41E-08	2.43E-08
	PbHCO3+	1.22E-09	1.03E-09
	Pb(CO3)2-2	6.15E-10	3.16E-10
	Pb+2	5.25E-10	2.69E-10
	PbCl+	1.73E-10	1.47E-10
	PbOH+	1.45E-10	1.23E-10
S(6)	5.61E-04		
	SO4-2	3.80E-04	1.98E-04
	CaSO4	1.17E-04	1.17E-04
	MgSO4	5.77E-05	5.81E-05
	NaSO4-	6.67E-06	5.64E-06
	KSO4-	5.17E-07	4.37E-07
Si	4.94E-04		
	H4SiO4	4.92E-04	4.96E-04
	H3SiO4-	1.96E-06	1.66E-06
Zn	2.41E-07		
	Zn+2	1.15E-07	6.01E-08
	ZnCO3	6.17E-08	6.21E-08
	ZnHCO3+	4.30E-08	3.64E-08

Saturation indicies				
Phase	SI	log IAP	log KT	
Anglesite	-5.48	-13.27	-7.8	PbSO4
Anhydrite	-1.87	-6.23	-4.36	CaSO4
Aragonite	0.52	-7.81	-8.33	CaCO3
Calcite	0.67	-7.81	-8.47	CaCO3
Cd(OH)2	-7.01	6.64	13.65	Cd(OH)2
CdSiO3	-5.77	3.33	9.1	CdSiO3
CdSO4	-11.74	-11.81	-0.06	CdSO4
Cerrusite	-1.71	-14.86	-13.14	PbCO3
Chalcedony	0.26	-3.3	-3.56	SiO2
Chrysotile	-3.39	28.94	32.33	Mg3Si2O5(OH)4
CO2(g)	-1.87	-20.03	-18.15	CO2
Dolomite	1.08	-15.98	-17.07	CaMg(CO3)2
Fe(OH)3(a)	1.02	18.96	17.93	Fe(OH)3
Goethite	6.91	18.96	12.05	FeOOH
Gypsum	-1.65	-6.23	-4.58	CaSO4:2H2O
H2(g)	-22.74	-22.74	0	H2
Hausmannite	-15.98	45.3	61.28	Mn3O4
Hematite	15.76	37.92	22.16	Fe2O3
Jarosite-K	-6.13	23.87	30	KFe3(SO4)2(OH)6
Manganite	-6.45	18.89	25.34	MnOOH
Melanterite	-8.63	-10.86	-2.22	FeSO4:7H2O
O2(g)	-0.98	-3.93	-2.96	O2
Otavite	-1.29	-13.39	-12.1	CdCO3
Pb(OH)2	-3.01	5.17	8.18	Pb(OH)2
Pyrochroite	-7.68	7.52	15.2	Mn(OH)2
Pyrolusite	-11.28	30.26	41.54	MnO2
Quartz	0.69	-3.3	-4	SiO2
Rhodochrosit	-1.38	-12.51	-11.13	MnCO3
Sepiolite	-2	13.79	15.79	Mg2Si3O7.5OH:3H2O
Sepiolite(d)	-4.87	13.79	18.66	Mg2Si3O7.5OH:3H2O
Siderite	-1.55	-12.44	-10.88	FeCO3
SiO2(a)	-0.58	-3.3	-2.72	SiO2
Smithsonite	-2.52	-12.51	-9.99	ZnCO3
Talc	0.82	22.33	21.51	Mg3Si4O10(OH)2
Willemite	-3.68	11.73	15.41	Zn2SiO4
Zn(OH)2(e)	-3.98	7.52	11.5	Zn(OH)2

Appendix 7.1: The Digital elevation model (DEM) of the Faria Basin computed with GIS software package TNT-mips.

☐	-300 - 0 m
☐	001 - 200 m
☐	201 - 400 m
☐	401 - 600 m
☐	601 m - 800 m
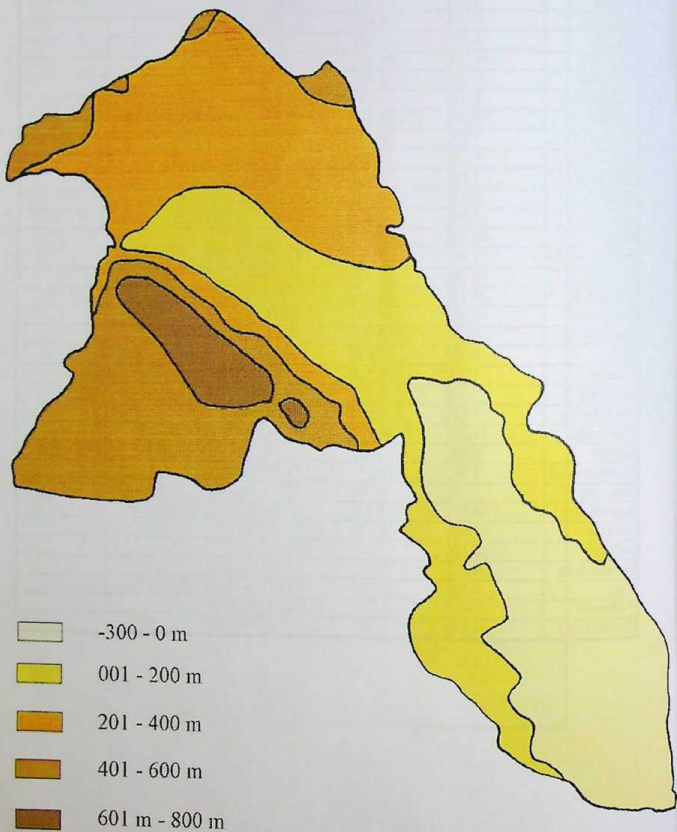
Appendix 7.2: The rainfall model of the Faria Basin computed with GIS software package TNT-mips.

0 - 150 mm/year

151 - 250 mm/year

251 - 350 mm/year

351 - 450 mm/year

451 - 600 mm/year
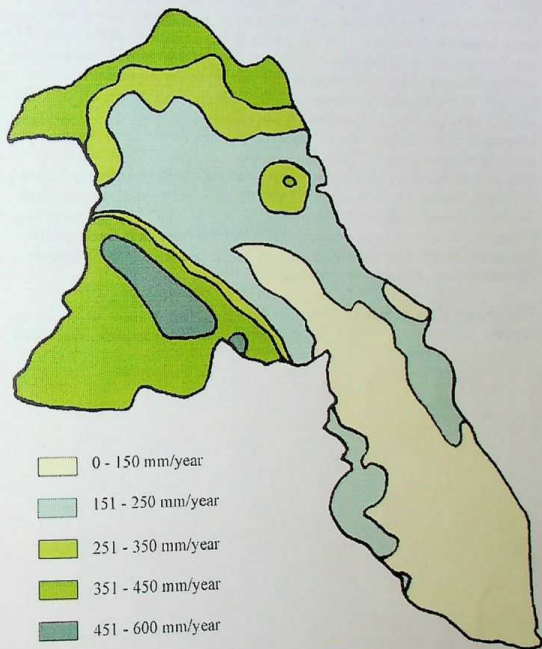
Information about the Author

Marwan Ghanem was born on the 3rd of April 1965 in Dier Ibzi, Ramallah in Palestine. Between 1971 and 1977 he visited the elementary school of Dier Ibzi and from 1977 to 1980 the preparatory school of Kufer Nima, Ramallah. From 1980 till 1982 he visited the secondary school of the catholic school, Ramallah and in the year 1983 he got his Tawjehi. After he got his B.Sc. in Geology in the year 1986 from the department of Earth and Environmental Sciences at the Yarmouk University, Irbid/Jordan, he attended his master programme at the same university. In the year 1990 he got his M.Sc. in Geology, in the fields of Geochemistry and Petrology. During the period 1987 – 1990, he worked as a scientific assistant for the undergraduate courses of Geology at Yarmouk University. He worked as a teacher of natural sciences in the Republic of Yemen (1990 – 1992). From the period of 1992 – 1994, he worked as a geologica researcher in the Palestinian Hydrology Group in Jerusalem. He attended a course on groundwater resources management in arid environments in Britain and a course on seismology in Turkey in 1994. From 1995 to 1999 he was a Ph.D. student in the field of Hydrogeology and Hydrochemistry at the TU Bergakademie Freiberg, Institut für Geologie, Lehrstuhl Hydrogeology. During this time he attended many courses: GOCAD (in France), GIS and modelling (in Germany). He is a member of the following assiciations: The International Association of Hydrogeologists IAH, the Palestinian Geological Association and European Geophysical Society. He speaks Arabic (native language), English and German. His hobbies are reading and travelling.

The address of the author is: Dier Ibzi / Ramallah, West Bank – Palestine
and/or: PHG, P.O. Box 565, Ramallah, West Bank – Palestine